Introduction

This dissertation is an amalgam of projects that have a close relationship to a much larger experiment that I have had the good fortune to be a part of. This experiment, the TransCom 3 effort, is itself the third part of a decade long effort to intercompare tracer models used in the CO_2 inversion problem. TransCom 1 compared forward transport model simulations of two key components of the global carbon cycle: fossil fuel emissions and biosphere exchange (*Rayner and Law*, 1995). TransCom 2 examined the forward simulations of SF_6, a long-lived gas with relatively well-known sources (*Denning et al.*, 1999). TransCom 3 was the undertaken to fulfill the goal of dissecting the impact and characterizing the uncertainty that different tracer transport have on the CO_2 inverse problem.

I came to the process in the latter half of the TransCom 2 phase. Therefore, I was able to evolve with the TransCom 3 phase from its earliest beginnings. In addition to assisting in the coordination and central scientific work of TransCom 3, I was a participant in the transport model simulations, contributing results from the CSU model to what became a very large group of models from around the world. Through this process I have benefited from the collective wisdom of those that envisioned the experiment and the many participants that contributed to the nuts and bolts of the science.

This dissertation therefore reflects my own evolution through the TransCom 3 process. In the early stages, I operationalized the vision that the architects had constructed. Through time, I began to contribute to the intellectual content of the experiment and have hopefully arrived at a point where I am contributing original scientific work.

Through this evolution and through the scientific results that the following pages reflect, the enormous contribution that all of the TransCom participants have made is not always obvious. Intercomparisons are fundamentally dependent upon the rigor, quality control, and scientific maturity participants bring to an experiment. Without the hard work and persistence of the TransCom participants, the results presented in this dissertation would not exist.

This introduction will serve two purposes: to introduce the reader to the TransCom 3 experiment, and to provide a roadmap through the dissertation. Because this document is a mixture of published material and new, unpublished material, this roadmap should serve to tie together the material and explain the format of presentation.

TransCom 3

Much of our understanding of the global carbon budget is derived from atmospheric observations of CO_2. Hemispheric or regional fluxes may be calculated from atmospheric concentration measurements by a numerical procedure known as an "inversion," which requires that atmospheric transport be accounted for using a Chemical Tracer Model (CTM) (*Tarantola*, 1987; *Enting et al.*, 1995; *Enting*, 2002). In the simplest sense, transport inversions for CO_2 fluxes aim to find that combination of surface fluxes that generate the best match between simulated and observed CO_2 concentrations.

As context and motivation for the TransCom 3 experiment, it is useful to review a bit of the recent history associated with CO_2 inverse research. I will begin at the onset of the 1990s with the work of Tans et al. (*Tans et al.,* 1990). In this early study, a three-dimensional tracer transport model was run with a series of prescribed fluxes in an attempt to match the meridional CO_2 gradient observed at 20 CO_2 observing locations. Though not an inversion in the formal sense used in the current study, the authors attempted a series of different hypothetical flux arrangements in an attempt to best match the meridional CO_2 concentration gradient. The conclusion was that the northern extratropical land was a sink of between 2 and 2.7 Gt C/year in the early to mid-1980s. Furthermore, the total oceanic uptake was less than 1 Gt C/year, much less than oceanographers had estimated. Though the current consensus estimates for land/ocean total flux for the 1980s has departed from this early estimate, the Tans et al. work raised an important challenge.

Using formal optimization in an inverse study, Ian Enting and colleagues in Australia followed with a series of studies aimed at carbon flux estimates using a more formal inverse approach (*Enting et al.,* 1993*; Enting et al.,* 1995). Constructing basis functions as processes or collections of surface gridcells the authors solved for the best match between observed and simulated CO_2 with the aid of prior information. The prior information, necessary to stabilize the underdetermined problem, was included with uncertainty. Combined with the uncertainty assigned to the mismatch between simulated CO_2 and measured CO_2, formal estimates of uncertainty and uncertainty reduction could be achieved. These studies utilized three-dimensional transport and included observations of $\delta^{13}C$.

With a slightly larger net ocean uptake (-1.3 Gt C/year) than found in the Tans et al. (1990) study, the authors also found a large northern land sink of roughly –2.0 Gt C/year. However, net uptake was estimated for the tropics, contrary to inventory work which suggested net release due to deforestation and biomass burning. The results presented in this study utilized data for the 1986/87 period only and therefore must be compared with that caveat in mind.

Following closely behind the Enting et al. (1995) study, another 2D mass-balance inversion was published but examining a different time period: 1990 to 1993, a period which included the June 1991 Mt. Pinatubo volcanic eruption (*Ciais et al.,* 1995). This study also performed the flux estimation in two week intervals over the full time period considered allowing for characterization of the seasonal cycle and interannual changes. This study estimated a large northern extratropical land sink of –4.2 and –3.0 Gt C/year in the years 1992 and 1993, respectively. Furthermore, the authors placed the timing of this uptake in the June to September period, implying photosynthesis in excess of respiration during those months.

By the late 1990s atmospheric CO_2 inversion research was routinely attempting to solve for fluxes with three-dimensional models solely. One of the more controversial studies in CO_2 inversion research was authored by Songmiao Fan and colleagues at Princeton University (*Fan et al.,* 1998). This study claimed that most of the northern terrestrial uptake in the 1988-1992 period was occurring in North America, and that this uptake was roughly offsetting the fossil fuel emissions in the United States.

Another 3D atmospheric CO_2 inversion from Peter Rayner and colleagues at the Australian CSIRO attempted to solve fluxes for a much longer period of time and for a much more discretized surface flux grid. When averaged over their 1980 to 1996 time period, they found that the northern terrestrial sink is distributed much more widely, with North America accounting for a portion (*Rayner et al.*, 1999). Like the results reported by Philippe Ciais and colleagues, Rayner et al. (1999) found a large increase in terrestrial uptake in the early 1990s relative to the decade of the 1980s.

Closing out the decade of the 1990s, Philippe Bousquet and colleagues published another 3D Bayesian synthesis inversion with similar spatial resolution to the Rayner et al. (1999) study but with 77 CO_2 observing stations, considerably more than utilized in the Rayner et al (1999) work (*Bousquet et al.,* 1999). In this study, Asia dominated the mean 1985-1995 northern extratropical land sink.

The discrepency among inversion studies in the 1990s over the placement of terrestrial uptake was one of the prime motivating forces behind the TransCom 3 project. By involving inverse modelers from around the world into a collaborative experiment, it was anticipated that a deeper understanding of the factors that give rise to varying regional carbon flux estimates might be achieved. Furthermore, the process could serve to improve the methods used in inverse carbon cycle modeling. At the outset, the goals of the TransCom experiment were succinctly stated as follows:

(1) To quantify the degree of uncertainty in carbon budget inverse calculations that arises from CTM transport;

(2) Analyze the mechanisms by which the models differ; and

(3) Recommend and prioritize improvements to the observing and modeling systems to produce more robust carbon budget inversions in the future.

An experimental approach was designed to meet these objectives that contained three levels of participation (*Gurney et al.,* 2000). The first level focused on annual mean carbon sources and sinks and required a limited number of tracers using supplied input fields of regional carbon exchange. The second level expanded on the first by including an inverse calculation of the strength of the seasonal cycle and interannual variations in regional fluxes, but required a much larger number of CTM tracers. The third level invited participants to perform their own inversions allowing for a comparison of different inversion methods.

Though the results of the TransCom 3 experiment continue to be analyzed, there is a general recognition within the inverse community that TransCom has met, and often surpassed, these modest initial goals. As will be shown, the carbon flux estimates generated by the TransCom experiment are robust to details of the inversion set-up and data choices. Much of this is due to the participation of nearly all the research groups engaged in carbon cycle inverse modeling allowing for the computation of model mean flux estimates. As a result, TransCom has become a benchmark for work in this field and has resulted in greater communication and collaboration among those engaged in carbon cycle inverse modeling.

Sixteen transport models or transport model variants participated in the Level 1 TransCom 3 experiment while thirteen models participated in the Level 2 experiment. The models ran forward simulations of a series of prepared regional and background global fluxes. The simulations were sampled following agreed upon protocols and deposited centrally. CO_2 observations were averaged from the Globalview dataset to serve as the observational data constraint to the inversion process (*GLOBALVIEW-CO_2*, 2002). The process employed a Bayesian synthesis approach which specified prior fluxes and prior flux uncertainties for the 11 land and 11 ocean regions (*Enting et al.*, 2002). The level 1 inversion produced annual mean flux estimates in these regions while the Level 2 produced both stationary seasonal results and interannually varying flux estimates.

A key aspect of the TransCom experiment was the goal to make both the intermediate and final products of the research available to the TransCom community and finally to the public. The individual model output, inversion code, stations lists and much more were immediately available to any member or affiliate of the TransCom 3 experiment. After publication of the cyclostationary control results, the TransCom 3 archive was made available to the public through the TransCom website (http://transcom.colostate.edu).

In addition to the generous participation by the community of inverse modelers, the success of the TransCom 3 experiment is owed largely to the support received from a few institutions. In particular, support was received from the National Science Foundation (OCE-9900310), the National Oceanic and Atmospheric Administration (NA67RJ0152, Amend 30) and the International Geosphere Biosphere Program/Global Analysis, Interpretation, and Modeling Project (IGBP/GAIM).

A Roadmap

As mentioned previously, this dissertation is a mixture of published results and new, unpublished material. The first three chapters are comprised of previously published papers in the journals *Nature*, *Tellus* and *Global Biogeochemical Cycles*, respectively. The last two chapters represent new material. This has a few implications for the flow and format of this document. First, the two chapters that represent new material (chapters 4 and 5) have been written in a format consistent with the papers constituting the first three chapters. This means, they each have an introduction and conclusions section and have separate reference sections. When referring to the published material in the first three chapters, a journal citation is used rather than referring to “chapter 1” or “chapter 2”. Chapters 4 and 5 are, in essence, proto-papers themselves.

The new material has also been written in what I hope is a more succinct and focused style, more consistent with published papers and less so with a typical dissertation. Because each paper/chapter contains introductory material pertinent to each, I have not included exhaustive introductory material about climate change, atmospheric transport or the global carbon cycle. This also means the document, in its entirety, is not voluminous. It is hopefully succinct and to the point.

With a familiarity of the TransCom 3 experiment provided in the last section, the content of the dissertation is as follows.

Chapter 1 is a paper published in 2002 in the journal Nature (*Gurney et al.*, 2002). It describes the core results from the annual mean (or Level 1) phase of TransCom 3. It only presents the model mean inverse results and highlights the most important flux results and the most important aspects of sensitivity of the model mean results. In addition to examination of the errors introduced by both the observational data and the model transport, a case is made that the model mean is relatively robust to most of the inversion details. This latter result is a theme that that will persist through all of the TransCom 3 results. Supplementary material was included with this paper which provides among other details, a careful examination of the differences between the influential results from *Fan et al.* (1998) and the TransCom 3 results.

Chapter 2 is a paper published in 2003 in the journal *Tellus* (*Gurney et al.*, 2003). This paper also presents annual mean/model mean results but goes into far more detail on the methodology, sensitivity testing, and model-specific results. The sensitivity testing for this paper is limited to the flux side of the inversion problem. A companion paper written by Rachel Law and colleagues (not included here) tackled the sensitivity of the TransCom 3 model mean results to the CO_2 observation treatment (*Law et al.*, 2003).

Chapter 3 is a paper published in 2004 in the journal *Global Biogeochemical Cycles* (*Gurney et al.*, 2004). This paper presents the model mean seasonal inversion results. In addition to characterization of the errors due to CO_2 observations and tracer transport, the potential biogeochemical drivers of the altered seasonal cycle are explored. Sensitivity tests are performed and comparison to the annual mean case is made.

Chapter 4 presents new material and is focused on the model mean interannual flux estimates. Characterization of the uncertainties associated with the model mean are explored and a number of sensitivity tests are performed including the influence of different CO_2 observing networks. As with the annual and seasonal inversion results, a case is made for the robustness of the model mean flux. Finally, an initial exploration of biogeochemical drivers is undertaken with particular emphasis on the El Niño-Southern Oscillation index.

Chapter 5 presents new material that questions one of the basic assumptions prevalent through most, if not all, CO_2 inversions. As the CO_2 inverse problem increases both the spatial and temporal resolution of the problem formulation, will the assumed fossil fuel background flux bias the results. This sensitivity test achieves some surprising and disturbing results.

There are three themes running through this mixture of material. First, the errors that arise from transport are carefully quantified and compared to other uncertainties in the CO_2 inversion problem. This includes not only description and quantification but an interpretation of what factors cause the errors that come with inverse flux estimates.

With this information in hand, a case is made for the robustness of the model mean results. This is not to say that the model mean flux estimates found in TransCom 3 come with low random error, but that the model mean estimates themselves are less sensitive than any particular transport model inversion to the particulars of the inversion set-up and CO_2 observing choices. This is a quality that "emerges" from the use of an ensemble and impossible to characterize with a single tracer transport model.

Given the importance of transport to the CO_2 inversion problem, it is tempting to conclude that the TransCom 3 inversion results represent the "best" or most accurate regional carbon exchange estimates. However, because the model mean TransCom 3 estimates are not completely immune to some aspects of the inversion set-up (just less sensitive than individual models) and are likely prey to unknown bias, the results presented here should not be viewed as the best or consensus view of the CO_2 inversion community. After all, the future may provide a transport model that is found to be perfect and arrives at carbon exchange results that do not coincide with the central estimates presented in this document. Each transport model in the TransCom experiment is viewed as equally likely to represent real transport; they do not purport to be a random sample around the truth.

The final theme that I have tried to return to throughout this document is a recognition that the model mean carbon exchange estimates should be used to understand the biogeochemistry of the carbon cycle. The temporal and spatial signatures of the fluxes themselves provide insights into mechanism that CO_2 observations themselves cannot. The results from the TransCom experiment have provided a new beginning for this aspect of CO_2 inversion research. In addition to refinement of the methodology, the next step in the "top-down" approach to characterizing the global carbon cycle is a more mechanistic connection to processes in the oceans and biosphere. This will come with greater spatial and temporal resolution but will also come with a more realistically coupled approach to the earth system which incorporates models and observations of the many aspects carbon exchange besides atmospheric CO_2.

References

Bousquet, P., P. Ciais, P. Peylin, M. Ramonet, and P. Monfrey, "Inverse modelling of annual atmospheric CO_2 sources and sinks. Part 1: method and control inversion," *Journal of Geophysical Research*, **104** (D21), November 20, 1999.

Ciais et al., "A large northern hemisphere terrestrial CO_2 sink indicated by the $^{13}C/^{12}C$ ratio of atmospheric CO_2," *Science*, **269**, pp. 1098, 1995.

Denning, S. *et al.* Three-dimensional transport and concentration of SF_6: A model intercomparison study (Transcom 2). *Tellus* **51B**, 266-297 (1999).

Enting, I.G., Trudinger, C.M., Francey, R.J., and H. Granek, "Synthesis Inversion of Atmospheric CO_2 Using the GISS Tracer Transport Model," CSIRO Division of Atmospheric Research Technical Paper No. 29, 1-44, 1993.

Enting, I.G., Trudinger, C.M., and R.J. Francey, "A synthesis inversion of the concentration and delta ^{13}C of atmospheric CO_2," *Tellus*, **47B**, 35-52, 1995.

Enting, I. 2002. *Inverse Problems in Atmospheric Constituent Transport*. Cambridge University Press: Cambridge, U.K.

Fan, S., M. Gloor, J. Mahlman, S. Pacala, J. Sarmiento, T. Takahashi, and P. Tans, A Large Terrestrial Carbon Sink in North America Implied by Atmospheric and Oceanic Carbon Dioxide Data and Models, *Science*, **282**, 442-446, 1998.

GLOBALVIEW-CO_2, Cooperative Atmospheric Data Integration Project - Carbon Dioxide, CD-ROM, NOAA CMDL, Boulder, Colorado, 2002.

Gurney, K.R., R.M. Law, A.S. Denning, P.J. Rayner, D. Baker, P. Bousquet, L. Bruhwiler, Y.H. Chen, P. Ciais, S. Fan, I.Y. Fung, M. Gloor, M. Heimann, K. Higuchi, J. John, T. Maki, S. Maksyutov, P. Peylin, M. Prather, B.C. Pak, J. Sarmiento, S. Taguchi, T. Takahashi, C.W. Yuen, Towards robust regional estimates of CO_2 sources and sinks using atmospheric transport models, *Nature,* **415**, 626-630, 2002.

Gurney, K.R., R.M. Law, A.S. Denning, P.J. Rayner, D. Baker, P. Bousquet, L. Bruhwiler, Y.H. Chen, P. Ciais, S. Fan, I.Y. Fung, M. Gloor, M. Heimann, K. Higuchi, J. John, T. Kowalczyk, E. Maki, S. Maksyutov, K. Masarie, P. Peylin, M. Prather, B.C. Pak, J. Randerson, J. Sarmiento, S. Taguchi, T. Takahashi, C.W. Yuen, Transcom 3 CO_2 Inversion Intercomparison: 1. Annual mean control results and sensitivity to transport and prior flux information, *Tellus*, **55B,** 555-579, 2003.

Gurney, K.R., R.M. Law, A.S. Denning, P.J. Rayner, B. Pak, and the TransCom 3 L2 modelers, "Transcom 3 Inversion Intercomparison: Control results for the estimation of seasonal carbon sources and sinks," *Global Biogeochemical Cycles,***18**, GB1010, doi:10.1029/2003GB002111, 2004.

Rayner, P., and R. Law, A comparison of modelled responses to prescribed CO_2 sources, CSIRO Division of Atmospheric Research, 1995.

Rayner, P. J., I.G. Enting, R.J. Francey, and R.L. Langenfelds, Reconstructing the recent carbon cycle from atmospheric CO_2, $\delta^{13}C$ and O_2/N_2 observations, *Tellus*, **51B**, 213-232, 1999.

Tans, Fung, and Takahashi, "Observational Constraints on the Global Atmospheric CO_2 Budget," *Science*, **247**, 1431-1438, March 23, 1990.

Tarantola, A. 1987. Chapter 4 in: *Inverse Problem Theory: Methods for Data Fitting and Parameter Estimation*, Elsevier, Amsterdam.

supported metal clusters from extended metal surfaces. These effects (and thus opportunities for tuning catalytic properties by choice of the support) are most pronounced for the smallest clusters, and may be negligible for large supported metal particles for which only a small fraction of the metal atoms are bonded to the support.

Purely geometric effects can also distinguish the catalytic activity seen with small metal clusters from that seen with bulk metal or larger supported particles, by limiting the structures that can bond to a very small cluster and subsequently react on it. For example, propylidyne is stable on Ir_4/γ-Al_2O_3 when treated in He or H_2 at temperatures up to 523 K (ref. 8), whereas propylidyne on extended metal surfaces[17,20] decomposes thermally under vacuum at 403–433 K and is largely hydrogenated in the presence of H_2 at room temperature. This qualitative difference in reactivity is attributed to the presence of neighbouring metal centres that facilitate reaction on the extended surfaces, and the lack of such centres on isolated Ir_4 (ref. 8). Thus, propylidyne on Pt(111) undergoes catalytic hydrogenation[15] whereas propylidyne at saturation concentration on Ir_4/γ-Al_2O_3 does not react, rendering the clusters almost inactive for propene hydrogenation (Table 1). □

Received 16 August; accepted 11 December 2001.

1. Collman, J. P., Hegedus, L. S., Norton, J. R. & Finke, R. G. *Principles and Applications of Organotransition Metal Chemistry* 2nd edn (University Science Books, Mill Valley, California, 1987).
2. Stevenson, S. A., Dumesic, J. A., Baker, R. T. K. & Ruckenstein, E. (eds) *Metal-Support Interactions in Catalysis, Sintering, and Redispersion* (van Nostrand Reinhold, New York, 1987).
3. Haller, G. L. & Resasco, D. E. Metal-support interaction: group VIII metals and reducible oxides. *Adv. Catal.* **36,** 173–235 (1989).
4. Yudanov, I. V., Vent, S., Neyman, K., Pacchioni, G. & Rösch, N. Adsorption of Pd atoms and Pd-4 clusters on the MgO(001) surface: a density functional study. *Chem. Phys. Lett.* **275,** 245–252 (1997).
5. Matveev, A. V., Neyman, K., Pacchioni, G. & Rösch, N. Density functional study of M-4 clusters (M = Cu, Ag, Ni, Pd) deposited on the regular MgO(001) surface. *Chem. Phys. Lett.* **299,** 603–612 (1999).
6. Goellner, J. V. *et al.* Ligand-free osmium clusters supported on MgO: a density functional study. *Langmuir* **16,** 2736–2743 (2000).
7. Ferrari, A. M. *et al.* Faujasite-supported Ir_4 clusters: A density functional model study of metal–zeolite interactions. *J. Phys. Chem. B.* **103,** 5311–5319 (1999).
8. Argo, A. M., Goellner, J. F., Phillips, B. L., Panjabi, G. A. & Gates, B. C. Reactivity of site-isolated metal clusters: propylidyne on γ-Al_2O_3-supported Ir_4. *J. Am. Chem. Soc.* **123,** 2275–2283 (2001).
9. McVicker, G. B. *et al.* Effect of sulfur on the performance and on the particle size and location of platinum in Pt/KL hexane aromatization catalyst. *J. Catal.* **139,** 48–61 (1993).
10. Jentoft, R. E., Tsapatsis, M., Davis, M. E. & Gates, B. C. Platinum clusters supported in zeolite LTL: influence of catalyst morphology on performance in *n*-hexane reforming. *J. Catal.* **179,** 565–580 (1998).
11. Xu, Z. *et al.* Size-dependent catalytic activity of supported metal clusters. *Nature* **372,** 346–348 (1994).
12. Gates, B. C. Supported metal clusters: synthesis, structure, and catalysis. *Chem. Rev.* **95,** 511–522 (1995).
13. Argo, A. M. *Influence of Supports, Cluster Structure, and Cluster Composition on Hydrogenation Reactions Catalyzed by Oxide-Supported Metal Clusters.* Thesis, Univ. California at Davis (2001).
14. Odzak, J. F., Argo, A. M., Lai, F. S. & Gates, B. C. A flow through X-ray absorption spectroscopy cell for characterization of powder catalysts in the working state. *Rev. Sci. Instrum.* **72,** 3943–3945 (2001).
15. Cremer, P. S., Su, X., Shen, Y. R. & Somorjai, G. A. Hydrogenation and dehydrogenation of propylene on Pt(111) studied by sum frequency generation from UHV to atmospheric pressure. *J. Phys. Chem.* **100,** 16302–16309 (1996).
16. Cremer, P. S., Su, X., Shen, Y. R. & Somorjai, G. A. Ethylene hydrogenation on Pt(111) monitored in situ at high pressure using sum frequency generation. *J. Am. Chem. Soc.* **118,** 2942–2949 (1996).
17. Shahid, G. & Sheppard, N. Infrared spectra and the structures of the chemisorbed species resulting from the adsorption of propene and propane on a Pt/SiO_2 catalyst. *Spectrochim. Acta. A* **46,** 999–1010 (1990).
18. Newell, H. E., McCoustra, M. R. S., Chesters, M. A. & De La Cruz, C. The thermal chemistry of adsorbed ethyl on the Pt(111) surface: infrared evidence for an ethylidene intermediate in the ethyl to ethylidyne conversion. *J. Chem. Soc. Faraday Trans.* **94,** 3695–3698 (1998).
19. Bent, B. E., Mate, C. M., Crowell, J. E., Koel, B. E. & Somorjai, G. A. Bonding and thermal decomposition of propylene, propadiene, and methylacetylene on the Rh(111) single crystal surface. *J. Phys. Chem.* **91,** 1493–1502 (1987).
20. Chesters, M. A. *et al.* Infrared spectroscopic comparison of the chemisorbed species from ethene, propene, but-1-ene and *cis*- and *trans*-but-2-ene on Pt(111) and on a platinum/silica catalyst. *J. Chem. Soc. Faraday Trans.* **86,** 2757–2763 (1990).
21. Neurock, M. & van Santen, R. A. A first principles analysis of C–H bond formation in ethylene hydrogenation. *J. Phys. Chem. B* **104,** 11127–11145 (2000).

Supplementary Information accompanies the paper on *Nature*'s website (http://www.nature.com).

Acknowledgements

We thank the US National Science Foundation for support and the National Synchrotron Light Source at Brookhaven National Laboratory for beam time.

Competing interests statement

The authors declare that they have no competing financial interests.

Correspondence and requests for materials should be addressed to B.C.G. (email: bcgates@ucdavis.edu).

Towards robust regional estimates of CO_2 sources and sinks using atmospheric transport models

Kevin Robert Gurney*, Rachel M. Law†, A. Scott Denning*, Peter J. Rayner†, David Baker‡, Philippe Bousquet§, Lori Bruhwiler‖, Yu-Han Chen¶, Philippe Ciais§, Songmiao Fan#, Inez Y. Fung☆, Manuel Gloor, Martin Heimann**, Kaz Higuchi††, Jasmin John☆, Takashi Maki‡‡, Shamil Maksyutov§§, Ken Masarie‖, Philippe Peylin§, Michael Prather‖‖, Bernard C. Pak‖‖, James Randerson¶¶, Jorge Sarmiento#, Shoichi Taguchi##, Taro Takahashi☆☆ & Chiu-Wai Yuen****

** Department of Atmospheric Science, Colorado State University, Fort Collins, Colorado 80523, USA*
† CSIRO Atmospheric Research, PMB 1, Aspendale, Victoria 3195, Australia
‡ National Center for Atmospheric Research (NCAR), Boulder, Colorado 80303, USA
§ Laboratoire des Sciences du Climat et de l'Environnement (LSCE), F-91198 Gif-sur-Yvette Cedex, France
‖ Climate Monitoring and Diagnostics Laboratory, National Oceanic and Atmospheric Administration (NOAA), 326 Broadway R/CG1, Boulder, Colorado 80303, USA
¶ Department of Earth, Atmospheric, and Planetary Science, Massachusetts Institute of Technology, Cambridge, Massachusetts 02141, USA
 # AOS Program, Princeton University, Sayre Hall, Forrestal Campus, PO Box CN710, Princeton, New Jersey 08544-0710, USA
☆ Center for Atmospheric Sciences, McCone Hall, University of California, Berkeley, California 94720-4767, USA
*** Max-Planck-Institut fur Biogeochemie, D-07701 Jena, Germany*
†† Meteorological Service of Canada, Environment Canada, Toronto, Ontario M3H 5T4, Canada
‡‡ Quality Assurance Section, Atmospheric Environment Division, Observations Department, Japan Meteorological Agency, 1-3-4 Otemachi, Chiyoda-ku, Tokyo 100-8122, Japan
§§ Institute for Global Change Research, Frontier Research System for Global Change, Yokohama 236-0001, Japan
‖‖ Earth System Science, University of California, Irvine, California 92697-3100, USA
¶¶ Divisions of Engineering and Applied Science and Geological and Planetary Sciences, California Institute of Technology, Mail Stop 100-23, Pasadena, California 91125, USA
National Institute of Advanced Industrial Science and Technology, 16-1 Onogawa Tsukuba, Ibaraki 305-8569, Japan
☆☆ Lamont-Doherty Earth Observatory of Columbia University, Palisades, New York 10964, USA

Information about regional carbon sources and sinks can be derived from variations in observed atmospheric CO_2 concentrations via inverse modelling with atmospheric tracer transport models. A consensus has not yet been reached regarding the size and distribution of regional carbon fluxes obtained using this approach, partly owing to the use of several different atmospheric transport models[1–9]. Here we report estimates of surface–atmosphere CO_2 fluxes from an intercomparison of atmospheric CO_2 inversion models (the TransCom 3 project), which includes 16 transport models and model variants. We find an uptake of CO_2

in the southern extratropical ocean less than that estimated from ocean measurements, a result that is not sensitive to transport models or methodological approaches. We also find a northern land carbon sink that is distributed relatively evenly among the continents of the Northern Hemisphere, but these results show some sensitivity to transport differences among models, especially in how they respond to seasonal terrestrial exchange of CO_2. Overall, carbon fluxes integrated over latitudinal zones are strongly constrained by observations in the middle to high latitudes. Further significant constraints to our understanding of regional carbon fluxes will therefore require improvements in transport models and expansion of the CO_2 observation network within the tropics.

We estimate annual average fluxes for the 1992–96 period using each transport model and a common inversion set-up (see Methods). Methodological choices for this 'control' inversion have been selected on the basis of knowledge gained from a wide range of sensitivity tests (to be reported elsewhere). Performing the inversion with multiple transport models gives mean estimated fluxes that are relatively insensitive to reasonable variations in the set-up—and estimated uncertainties that represent a more complete estimate of the true uncertainty. The maximum number of regions in our inversion and the spatial distributions of fluxes within each region are fixed, precluding sensitivity tests of these inversion components.

Figure 1 shows the mean flux estimates (left-hand cross in each box) and two uncertainty measures for the control inversion. The first uncertainty measure is the mean of the individual model flux uncertainties (circles) which we designate the 'within-model' uncertainty. For any region, this estimated flux uncertainty must be smaller than the prior flux uncertainty (outer bounds of the boxes). The magnitude of the decrease indicates the degree to which the final flux estimate is constrained by the measurements. Figure 1 shows that the northern land regions and Australia are better constrained by the measurements than are the remaining land regions. The Southern Ocean region is well constrained by the atmospheric measurements, in part because it is treated as a single large region. The Atlantic regions are constrained more by their prior flux uncertainties, which are relatively small due to better coverage of ocean measurements in these regions.

The second uncertainty measure is the standard deviation of the flux estimates over the ensemble of models (error bars in Fig. 1). We call this the 'between-model' uncertainty. This measure indicates the degree to which transport model differences contribute to the range of flux estimates. Large between-model uncertainties are found for northern Africa, tropical America, temperate Asia and boreal Asia (all greater than 0.5 Gt C yr^{-1}).

For most regions, the between-model uncertainties are of similar or smaller magnitude than the within-model uncertainties. This suggests that the choice of transport model is not the critical determinant of the inferred fluxes. Comparing the uncertainties between regions indicates where the inversion would benefit most from new observations, and where model improvements are most needed. In this particular inversion, new measurements would be most useful over tropical continents and in the South America and South Atlantic regions, while the focus for resolving transport differences would be the northern and tropical land regions.

Regarding the model mean flux estimates, two results deserve attention. First, we find consistency between the ocean fluxes predicted in this study and those based on a global database[10] of CO_2 partial pressure (p_{CO_2}), except in the Southern Ocean where the carbon uptake estimated here is roughly half that based on the p_{CO_2} database. This shift in uptake from south to north is required to match simultaneously large-scale concentration gradients (Fig. 2) and growth rates.

The mismatch between atmospheric and ocean estimates of the Southern Ocean fluxes had been noted a decade ago[11]. Our sensitivity tests find that the near-uniformity of observed concentration in the Southern Hemisphere and the small uncertainty associated with those measurements make this result robust to the choice of observing network, prior flux estimates, global ocean constraint, and transport (see Fig. 2 in Supplementary Information). The discrepancy also cannot be explained by a systematic bias in transport models, as the north–south transport has been investigated in a recent intercomparison[12] where successful simulations of the observed meridional gradient in SF_6 suggested reasonable veracity in gross interhemispheric transport.

One possible reconciliation between the p_{CO_2} database and the inverse result presented here is suggested by recent ocean measurements taken during January and August 2000 in the Indian

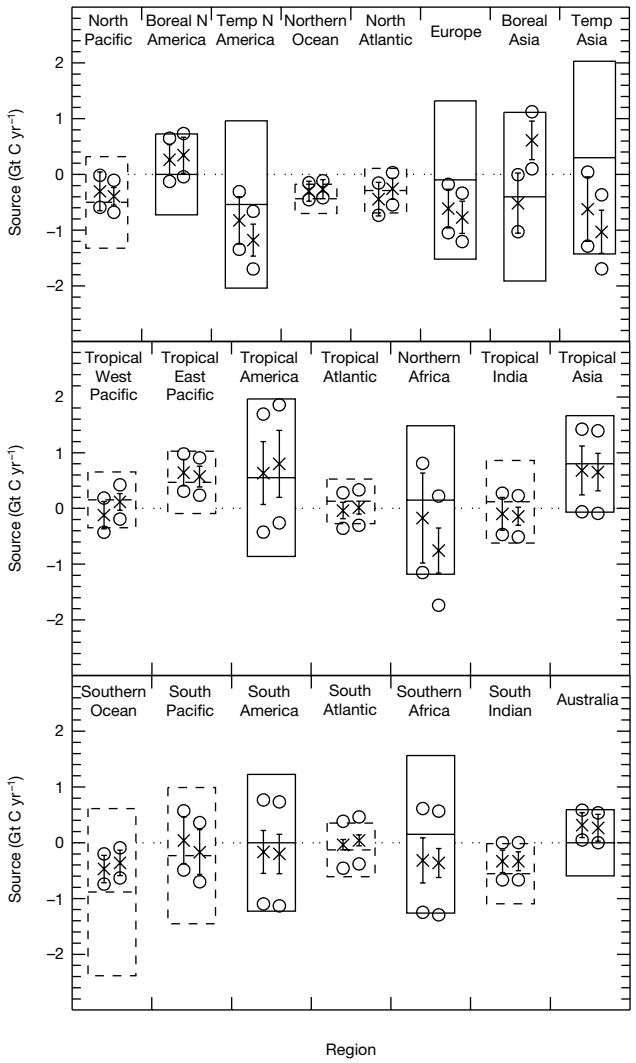

Figure 1 Mean estimated sources and uncertainties for two inversions. Left-hand symbols in each box are for the control inversion, right-hand symbols are for an inversion without the background seasonal biosphere flux. Mean estimated fluxes are shown by crosses, and include all background fluxes except fossil fuel. Positive values indicate a source to the atmosphere. The prior flux estimates and their uncertainties are indicated by the boxes (solid for land, dashed for ocean); the central horizontal bar indicates the prior flux estimate, and the top and bottom of the box give the prior flux uncertainty range. The mean estimated uncertainty across all models (the 'within-model' uncertainty) is indicated by the circles. The standard deviation of the models' estimated fluxes (the 'between-model' uncertainty) is indicated by the 'error bars'. Regions are shown in their approximate north–south and east–west relationship.

Antarctic sector of the Southern Ocean[13]. The p_{CO_2} values south of 50° S showed seasonal variations that require CO_2 uptake in summer and emission in winter. If the seasonality exhibited in this campaign is true for other parts of the Southern Ocean, this would result in a reduction of the Southern Ocean flux uptake in the database, which is currently determined predominantly by summer measurements. This seasonality-driven explanation is also consistent with forthcoming results from the second stage of the TransCom 3 comparison in which we estimate seasonal cycles (K.R.G. *et al.*, manuscript in preparation).

Second, we find carbon uptake over the continents of the Northern Hemisphere to be distributed relatively evenly across North America, Europe and Asia, in contrast to the distribution found in an earlier, widely cited inverse study[2]. We find a temperate North American sink approximately 60% of that found in the earlier study, a small boreal North American source rather than small uptake, and a large sink for Eurasia rather than an approximately neutral flux. Estimated uncertainties are moderate (0.4–0.7 Gt C yr^{-1}), indicating that regional partitioning remains difficult, but the flux differences between the two studies lie at the edge of (or outside) the uncertainty ranges.

Although previous studies have challenged the possibility of a large North American sink[3–7], little systematic exploration has been performed as to how such a result was achieved. The differences are not due to the choice of transport model, because the two models used in the earlier study are included here and lie in the middle of our range. Extensive sensitivity tests (see Tables 3 and 4 in Supplementary Information) indicate that the Eurasian flux estimate is very sensitive to the pattern of background fluxes used in the inversion, especially that representing the seasonal terrestrial biosphere. The difference in North American uptake results from a combination of methodological choices as well as differences in time period and observational stations used.

There are three methodological differences that together appear to be critical. First, recent work[14] suggests that the larger the region size in an inversion, the greater the potential for producing biased flux estimates. Second, the potential bias can be reduced by increasing the data uncertainty for sites in regions with spatially heterogeneous fluxes. The earlier study[2] inverted for larger regions than used here, and used relatively small (0.6 p.p.m.), spatially invariant uncertainties compared to the generally larger, variable uncertainties used in this study. The third factor is the uncertainty assigned to prior estimates of ocean fluxes, which were zero in the earlier study. Thus the flux adjustment required to match the atmospheric data was applied only to land regions. Together these three factors suggest that the earlier study had greater potential for biased and more sensitive flux estimates than the control results presented here.

Although transport uncertainties do not overwhelm our flux estimates, one factor appears to be responsible for a significant portion of the model spread; the 'rectifier' produced by the covariance between the seasonal biospheric background flux and atmospheric transport[15]. The effect of the rectifier can be seen by performing the inversion without the background biospheric fluxes (Fig. 1, right-hand symbols within each box). The between-model uncertainty is reduced for almost all regions, and in some regions there are substantial changes to the estimated fluxes. An increase of 1.1 Gt C yr^{-1} in boreal Asia changes it from a moderate sink to a moderate source, because rectification produces the strongest concentrations downwind of this region in many of the models. Sink strengths increase by 0.35–0.55 Gt C yr^{-1} for temperate North America, temperate Asia and northern Africa, to maintain the required global source. Measurements indicating the strength of the covariance effect in nature are needed to assess this aspect of model transport.

One way to reduce the large uncertainties in our full calculation is to aggregate our regions after performing the inversion. Figure 3 shows the flux estimates for the land and ocean separately in the southern extratropics, tropics, northern extratropics and for the

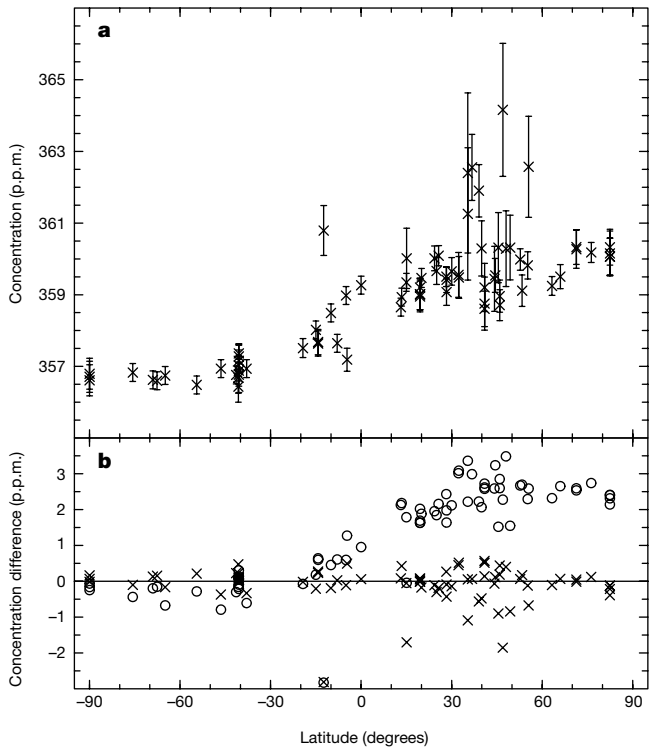

Figure 2 CO_2 concentrations input to, and as fitted by, the inversion. **a**, Meridional gradient of observational CO_2 values and the uncertainty assigned to them in the inversion. **b**, Model mean concentrations for the sum of the three background fluxes minus the observational CO_2 values (circles) and the model mean concentrations after inverting for regional fluxes minus the observational CO_2 values (crosses). Concentrations are 1992 to 1996 means. Note that the adjustment to the background fluxes requires additional uptake in the Northern Hemisphere and lessened uptake in the Southern Hemisphere for all models.

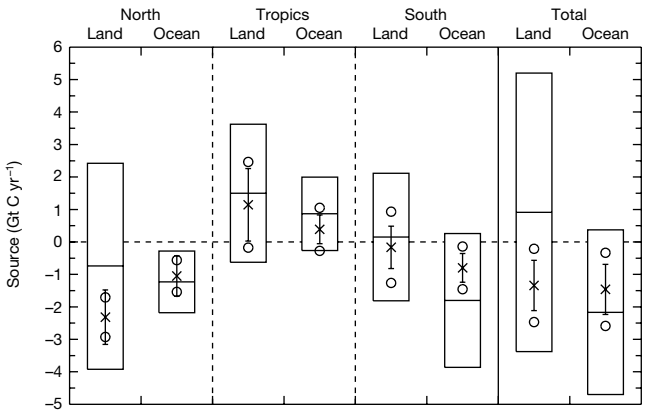

Figure 3 Mean sources and uncertainties for six aggregated regions and global land and ocean. Symbols as in Fig. 1 with the regional aggregation as follows: northern land (boreal North America, temperate North America, Europe, temperate Asia, boreal Asia), tropical land (tropical America, northern Africa, tropical Asia), southern land (South America, southern Africa, Australia), northern ocean (North Pacific, Northern Ocean, North Atlantic) tropical ocean (tropical west Pacific, tropical east Pacific, tropical Atlantic, tropical Indian), southern ocean (Southern Ocean, South Atlantic, South Indian).

globe as a whole. Within-model uncertainties are reduced relative to simply summing from constituent regions, because much of the uncertainty occurs at the scale of the original regions. There is also a reduction in the between-model uncertainty for this aggregation, as some of the model spread involves details of regional transport. At this larger scale, the decrease in the sink in the Southern Ocean and the enhanced sinks over the Northern Hemisphere appear more significant. The uncertainty on the tropical land region is large; lack of atmospheric data in this region means that inversion methods cannot reliably comment on the extent to which sources due to tropical land-use change are balanced by enhanced growth.

This first stage of the TransCom 3 intercomparison has explored many aspects of annual mean inversions more comprehensively than previous work. By incorporating a range of transport models, the fluxes and their uncertainties represent progress towards more robust inverse estimates of regional carbon exchange. Carbon exchange with the ocean is well constrained in this study and, in the case of the Southern Ocean region, is different from fluxes suggested by p_{CO_2} measurements. This result is consistent across the 16 transport models used here, and is insensitive to many aspects of the inversion set-up. Flux estimates in the northern extratropical land regions are reasonably robust as zonal means, but are difficult to distinguish in the longitudinal direction, and can be biased owing to key methodological aspects of the inversion construction. Seasonal exchange with the terrestrial biosphere is responsible for much of the model spread over these regions. Realistic characterization of this aspect of model transport is essential if this uncertainty is to be reduced in the future.

Flux estimates in the tropical land regions remain very uncertain, owing to few CO_2 observations and the limited influence of extratropical observations on the tropical land flux estimates. New observations that can be represented by global-scale transport models are needed in these regions. Future TransCom analysis will focus on the effect of transport model differences on flux estimates at seasonal and interannual timescales. □

Methods

We use a bayesian synthesis inversion formalism[16] that specifies prior estimates of both the fluxes and their uncertainty, and optimizes with respect to atmospheric observations that are also uncertain. We estimate fluxes for 11 land and 11 ocean regions (see Supplementary Information) as differences from 'background' fluxes that are run separately through each transport model and represent fossil-fuel emissions[17,18], seasonally varying air–sea gas exchange[10] and an annually balanced, seasonally varying flux due to terrestrial photosynthesis and respiration[19]. The use of seasonally varying background fluxes allows the annual mean inversion to include contributions to annual mean concentrations due to the covariance of atmospheric transport and seasonal fluxes.

We invert 5-year mean measurements for 1992–96 at 76 sites taken from the GLOBALVIEW-2000 data set[20] (see Supplementary Information). GLOBALVIEW is a data product that interpolates CO_2 measurements to a common time interval. Gaps in the data are filled by extrapolation from marine boundary layer measurements. We have chosen to use sites where the extrapolated data accounts for less than 30% of the 1992–96 period. The measurements are weighted inversely by the degree to which the predicted concentrations are required by the inverse process to match the observations, which we refer to as 'data uncertainty'. In addition to measurement precision, this uncertainty incorporates the inability of coarse-grid models to adequately represent discrete measurements. The relative uncertainty of one site to another was based on the mean residual standard deviations for 1992–96 from GLOBALVIEW. The absolute magnitudes were chosen to produce a mean square normalized residual out of the inversion of about 1.0, ensuring that the estimated fluxes were optimized to the data only to an appropriate level commensurate with our ability to model them. A minimum uncertainty was also specified. This gave uncertainties ranging from 0.25 p.p.m. for remote, 'clean air' sites to 2.2 p.p.m. for continental, 'noisy' sites (Fig. 2).

The 11 land basis region boundaries were constructed to enclose vegetation of similar seasonal structure and carbon exchange based on vegetation classification[21]. Ocean basis regions were chosen to approximate circulation features such as gyres and upwelling regions. Unit emissions of 1 Gt C yr^{-1} were specified from each region. Subregional-scale variations in emissions rates were prescribed for land regions according to simulated net primary production from the CASA model[21]. This assumes that carbon fluxes follow the distribution of vegetation productivity. Emissions from ocean regions were prescribed as spatially uniform, except that sea-ice was masked out using seasonally varying fractional ice cover distributions[22]. The inversion requires prior flux and uncertainty estimates. Our choices have been guided by ocean and terrestrial flux models and observations[10,19], and are shown in Fig. 1 (also see Table 2 in Supplementary Information). The land region prior flux estimates incorporate recent inventory estimates[23–30]. Where more than one estimate for a given region was considered, a mid-point of the estimate spread was used. The prior flux uncertainty was chosen to be large enough to encompass all estimates. Prior flux uncertainties reflect one standard deviation.

The inversion is run separately for 16 transport models or model variants. The models used (and the initials of the modellers) are CSU general circulation model (K.R.G., A.S.D.), Goddard Institute for Space Studies off-line model—UCB (I.Y.F., J.J.), UCI-CTM with GISS-II' fields (M.P., B.C.P., 3 model variants), Japan Meteorological Agency—CDTM (T.M.), MATCH/CCM3 winds (L.B.), MATCH/NCEP winds (Y.H.C.), MATCH/MACCM2 winds (R.M.L.), NIES (S.M.), National Institute for Resources and Environment (S.T.), Recherche en Prevision Numerique (C.W.Y.), SKYHI (S.F.), TM2 (P.B., P.C., P.P.), TM3 (M.H.), GCTM (D.B.). The inversion produces estimated fluxes and their uncertainties for each region individually and for some groups of regions in addition to a background concentration. Here our analysis focuses on fluxes and uncertainties that are averaged across models. We also specify two measures of uncertainty as described in the main text. We show the 'between' model uncertainty as a one standard deviation confidence interval for meaningful comparison with the within model uncertainty. The obvious alternative, showing a full range, would also produce a confidence interval that would widen as more models were included. Inspection of the individual flux estimates showed them to be close to normally distributed about the mean flux for most regions.

Received 14 June; accepted 11 December 2001.

1. Enting, I. G., Trudinger, C. M. & Francey, R. J. A synthesis inversion of the concentration and $\delta^{13}C$ of atmospheric CO_2. *Tellus B* **47,** 35–52 (1995).
2. Fan, S. *et al.* A large terrestrial carbon sink in North America implied by atmospheric and oceanic carbon dioxide data and models. *Science* **282,** 442–446 (1998).
3. Kaminski, T., Heimann, M. & Giering, R. A coarse grid three-dimensional global inverse model of the atmospheric transport, 2, inversion of the transport of CO_2 in the 1980s. *J. Geophys. Res.* **104,** 18555–18581 (1999).
4. Bousquet, P., Ciais, P., Peylin, P., Ramonet, M. & Monfrey, P. Inverse modelling of annual atmospheric CO_2 sources and sinks. Part 1: method and control inversion. *J. Geophys. Res.* **104,** 26161–26193 (1999).
5. Baker, D. F. *Sources and Sinks of Atmospheric CO_2 Estimated from Batch Least-Squares Inversions of CO_2 Concentration Measurements.* Thesis, Princeton Univ. (2001).
6. Taguchi, S. Synthesis inversion of atmospheric CO_2 using the NIRE chemical transport model. *Geophys. Monogr.* **114,** 239–254 (2000).
7. Peylin, P., Baker, D., Sarmiento, J., Ciais, P. & Bousquet, P. Influence of transport uncertainty on annual mean and seasonal inversions of atmospheric CO_2 data. *J. Geophys. Res.* (submitted).
8. Rayner, P. J., Enting, I. G., Francey, R. J. & Langenfelds, R. Reconstructing the recent carbon cycle from atmospheric CO_2, $\delta^{13}C$ and O_2/N_2 observations. *Tellus B* **51,** 213–232 (1999).
9. Bousquet, P. *et al.* Regional changes in carbon dioxide fluxes of land and ocean since 1980. *Science* **290,** 1342–1346 (2000).
10. Takahashi, T. *et al.* Global sea-air CO_2 flux based on climatological surface ocean pCO_2, and seasonal biological end temperature effects. *Deep-Sea Res. I.* (submitted).
11. Tans, P., Fung, I. & Takahashi, T. Observational constraints on the global atmospheric CO_2 budget. *Science* **247,** 1431–1438 (1990)
12. Denning, S. *et al.* Three-dimensional transport and concentration of SF_6: A model intercomparison study (Transcom 2). *Tellus B* **51,** 266–297 (1999).
13. Metzl, N., Brunet, C., Jabaud-Jan, A., Poisson, A. & Schauer, B. in *Extended Abstr. 6th Int. Carbon Dioxide Conf.* 685–688 (Organizing Committee of Sixth Carbon Dioxide Conference, Sendai, 2001).
14. Kaminski, T., Rayner, P. J., Heimann, M. & Enting, I. G. On aggregation errors in atmospheric transport inversions. *J. Geophys. Res.* **106,** 4703–4715 (2001).
15. Denning, A. S., Fung, I. Y. & Randall, D. A. Latitudinal gradient of atmospheric CO_2 due to seasonal exchange with land biota. *Nature* **376,** 240–243 (1995).
16. Tarantola, A. *Inverse Problem Theory: Methods for Data Fitting and Model Parameter Estimation* 3rd impr. (Elsevier, Amsterdam, 1998).
17. Andres, R. J., Marland, G., Fung, I. & Matthews, E. Distribution of carbon dioxide emissions from fossil fuel consumption and cement manufacture, 1950-1990. *Glob. Biogeochem. Cycles* **10,** 419–429 (1996).
18. Brenkert, A. L. Carbon dioxide emission estimates from fossil-fuel burning, hydraulic cement production, and gas flaring for 1995 on a one degree grid cell basis. ⟨http://cdiac.esd.ornl.gov/ndps/ndp058a.html⟩ (1998; accessed Oct. 1998).
19. Randerson, J. *et al.* The contribution of terrestrial sources and sinks to trends in the seasonal cycle of atmospheric carbon dioxide. *Glob. Biogeochem. Cycles* **11,** 535–560 (1997).
20. *GLOBALVIEW-CO2: Cooperative Atmospheric Data Integration Project - Carbon Dioxide* CD-ROM (NOAA CMDL, Boulder, Colorado, 2000); also available at ⟨ftp://ftp.cmdl.noaa.gov/ccg/co2/GLOBALVIEW⟩ (2000).
21. De Fries, R. S. & Townshend, J. R. G. NDVI-derived land cover classifications at a global scale. *Int. J. Remote Sensing* **15,** 3567–3586 (1994).
22. Taylor, K. E., Williamson, D. & Zwiers, F. AMIP II sea surface temperature and sea ice concentration boundary conditions. ⟨http://www–pcmdi.llnl.gov/amip/AMIP2EXPDSN/BCS/amip2bcs.html⟩ (1997).
23. Apps, M. J. & Kurz, W. A. in *Carbon Balance on World's Forested Ecosystems: Towards a Global Assessment* (ed. Kanninen, M.) 14–39 (Publications of the Academy of Finland, Helsinki, 1994).
24. Kurz, W. A. & Apps, M. J. A 70 year retrospective analysis of carbon fluxes in the Canadian forest sector. *Ecol. Applicat.* **9,** 526–547 (1999).
25. *Greenhouse Gas Inventory Data from 1990 to 1998* (Secretariat of the United Nations Framework Convention on Climate Change, National Communications from Parties Included in Annex 1 to the Convention, FCCC/SBI/2000/11, Bonn, 2000).
26. Pacala, S. *et al.* Convergence of land- and atmosphere-based U.S. carbon sink estimates. *Science* **292,** 2316–2320 (2001).
27. Houghton, R. A. The annual net flux of carbon to the atmosphere from changes in land use 1850-1990. *Tellus B* **51,** 298–313 (1999).
28. Dixon, R. K. *et al.* Carbon pools and flux of global forest ecosystems. *Science* **263,** 185–190 (1990).

29. Houghton, R. A. & Hackler, J. L. Emissions of carbon from forestry and land-use change in tropical Asia. *Glob. Change Biol.* **5,** 481–492 (1999).
30. Kauppi, P. E., Mielikainen, K. & Kuusela, K. Biomass and carbon budget of European forests, 1971 to 1990. *Science* **256,** 70–74 (1992).

Supplementary Information accompanies the paper on *Nature*'s website (http://www.nature.com).

Acknowledgements

We thank B. Stephens for comments and suggestions on earlier versions of the manuscript. This work was supported by the NSF, NOAA and the International Geosphere Biosphere Program/Global Analysis, Interpretation, and Modeling Project. S.F. and J.S. were supported by NOAA's Office of Global Programs for the Carbon Modeling Consortium.

Correspondence and requests for materials should be addressed to A.S.D. (e-mail: denning@atmos.colostate.edu).

Unsuspected diversity among marine aerobic anoxygenic phototrophs

Oded Béjà*†, Marcelino T. Suzuki*, John F. Heidelberg‡, William C. Nelson‡, Christina M. Preston*, Tohru Hamada§†, Jonathan A. Eisen‡, Claire M. Fraser‡ & Edward F. DeLong*

** Monterey Bay Aquarium Research Institute, Moss Landing, California 95039-0628, USA*
‡ The Institute for Genomic Research, Rockville, Maryland 20850, USA
§ Marine Biotechnology Institute, Kamaishi Laboratories, Kamaishi City, Iwate 026-0001, Japan

Aerobic, anoxygenic, phototrophic bacteria containing bacteriochlorophyll *a* (Bchl*a*) require oxygen for both growth and Bchl*a* synthesis[1–6]. Recent reports suggest that these bacteria are widely distributed in marine plankton, and that they may account for up to 5% of surface ocean photosynthetic electron transport[7] and 11% of the total microbial community[8]. Known planktonic anoxygenic phototrophs belong to only a few restricted groups within the Proteobacteria α-subclass. Here we report genomic analyses of the photosynthetic gene content and operon organization in naturally occurring marine bacteria. These photosynthetic gene clusters included some that most closely resembled those of Proteobacteria from the β-subclass, which have never before been observed in marine environments. Furthermore, these photosynthetic genes were broadly distributed in marine plankton, and actively expressed in neritic bacterioplankton assemblages, indicating that the newly identified phototrophs were photosynthetically competent. Our data demonstrate that planktonic bacterial assemblages are not simply composed of one uniform, widespread class of anoxygenic phototrophs, as previously proposed[8]; rather, these assemblages contain multiple, distantly related, photosynthetically active bacterial groups, including some unrelated to known and cultivated types.

Most of the genes required for the formation of bacteriochlorophyll-containing photosystems in aerobic, anoxygenic, phototrophic (AAP) bacteria are clustered in a contiguous, 45-kilobase (kb) chromosomal region (superoperon)[6]. These include *bch* and *crt* genes coding for the enzymes of the bacteriochlorophyll and carotenoid biosynthetic pathways, and the *puf* genes coding for the subunits of the light-harvesting complex (*pufB* and *pufA*) and the reaction centre complex (*pufL* and *pufM*). To better describe the nature and diversity of planktonic, anoxygenic, photosynthetic bacteria, we screened a surface-water bacterial artificial chromo-

† Present addresses: Department of Biology, Technion-Israel Institute of Technology, Haifa 32000, Israel (O.B.); Nara Institute of Science and Technology, Takayama, Ikoma 630-0101, Japan (T.H.).

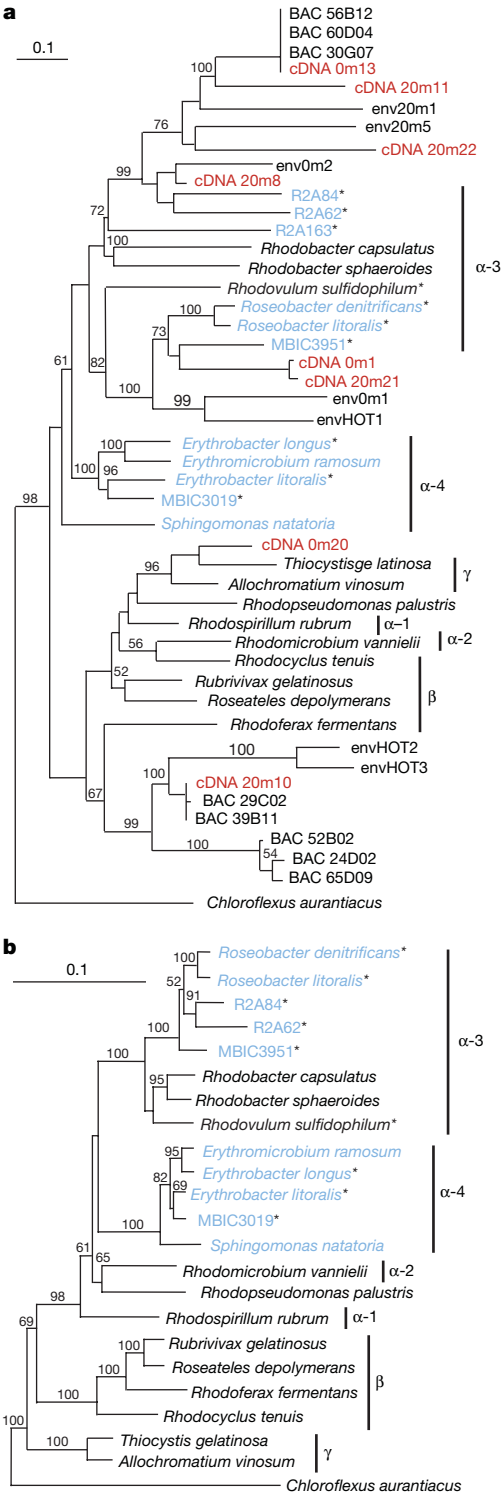

Figure 1 Phylogenetic relationships of *pufM* gene (**a**) and rRNA (**b**) sequences of AAP bacteria. **a**, **b**, Evolutionary distances for the *pufM* genes (**a**) were determined from an alignment of 600 nucleotide positions, and for rRNA genes (**b**) from an alignment of 860 nucleotide sequence positions. Evolutionary relationships were determined by neighbour-joining analysis (see Methods). The green non-sulphur bacterium *Chloroflexus aurantiacus* was used as an outgroup. *pufM* genes that were amplified by PCR in this study are indicated by the env prefix, with 'm' indicating Monterey, and HOT indicating Hawaii ocean time series. Cultivated aerobes are marked in light blue, bacteria cultured from sea water are marked with an asterisk, and environmental cDNAs are marked in red. Photosynthetic α-, β- and γ-proteobacterial groups are indicated by the vertical bars to the right of the tree. Bootstrap values greater than 50% are indicated above the branches. The scale bar represents number of substitutions per site.

Supplementary Information

Inversion input

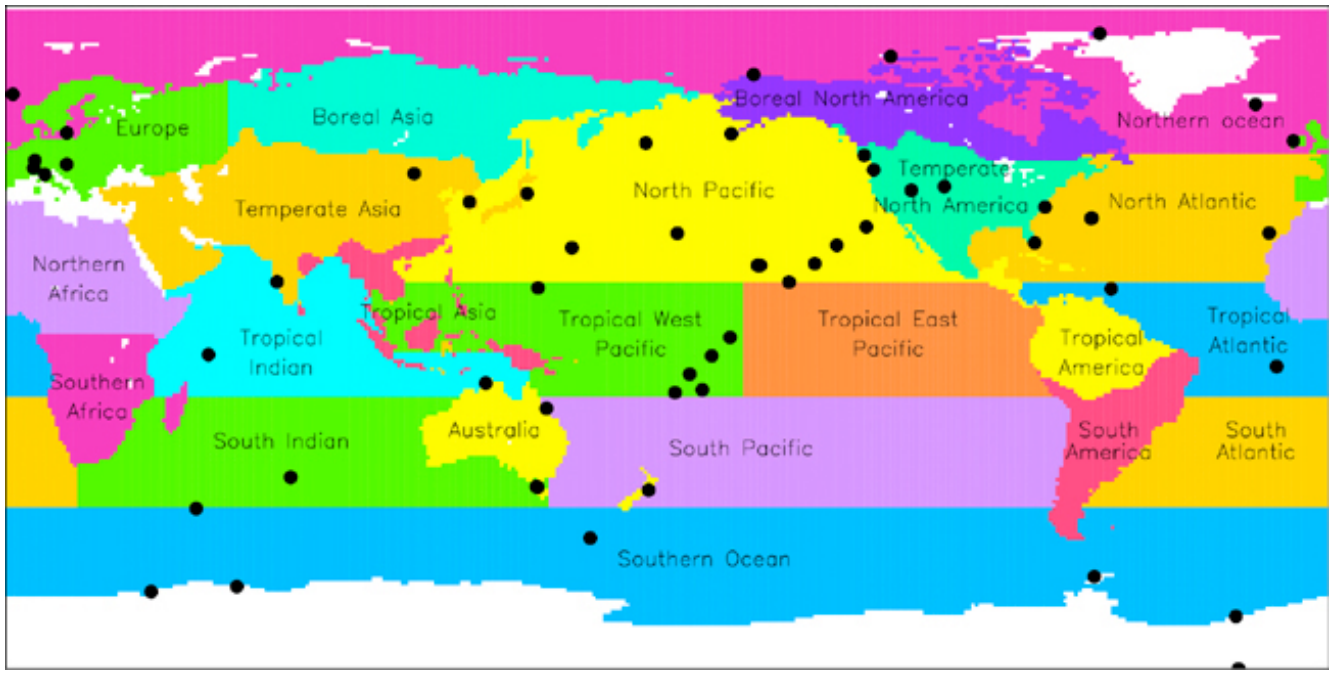

Figure 1: Regions used in the inversion and the locations of the 76 CO_2 observational records used. Multiple records exist at some locations.

Table 1: Latitude, longitude, 1992-1996 mean concentration and data uncertainty for the 76 GLOBALVIEW-CO2 (2000)[1] records used in the inversion. The uncertainty is the mean of the 1992 to 1996 residual standard deviations divided by the square root of 8, a scaling factor employed to achieve a mean square normalized residual of about 1.0 (see Methods section of main paper for elaboration). Any sites with uncertainties less than 0.25 ppm were increased to this minimum. In addition, where records were co-located, uncertainties were increased by multiplying by the square root of the number of sites within 4 degrees latitude and longitude and 1000m altitude.

Table 2: Prior and posterior fluxes and uncertainties for the land and ocean regions from the control inversion. Note that these are deviations from the global background (fossil[2,3], neutral biosphere[4] and ocean[5]) fluxes. The regional contributions of these fluxes are listed in column 5 (positive fluxes are

into the atmosphere). The main text Figure 1 shows non-fossil land fluxes (column 5) and total ocean fluxes (the sum of columns 4 and 5).

The prior flux uncertainties for land were chosen to be equivalent to the growing season net flux (the sum of carbon uptake for all months in which this is a positive number) as provided by the CASA model of net ecosystem production[4]. The prior flux uncertainties for the ocean were chosen to be proportional to the area of the region and the proportion of sample gridpoints in the region. Their magnitudes were set so that the global ocean uncertainty was 140% of the total oceanic exchange. The Southern Ocean uncertainty was capped at ± 1.5 $GtCyr^{-1}$.

Input data, the experimental protocol[6], and other information related to the TransCom 3 experiment can be found at http://dendrus.atmos.colostate.edu/transcom/TransCom_3/

Southern ocean sensitivity

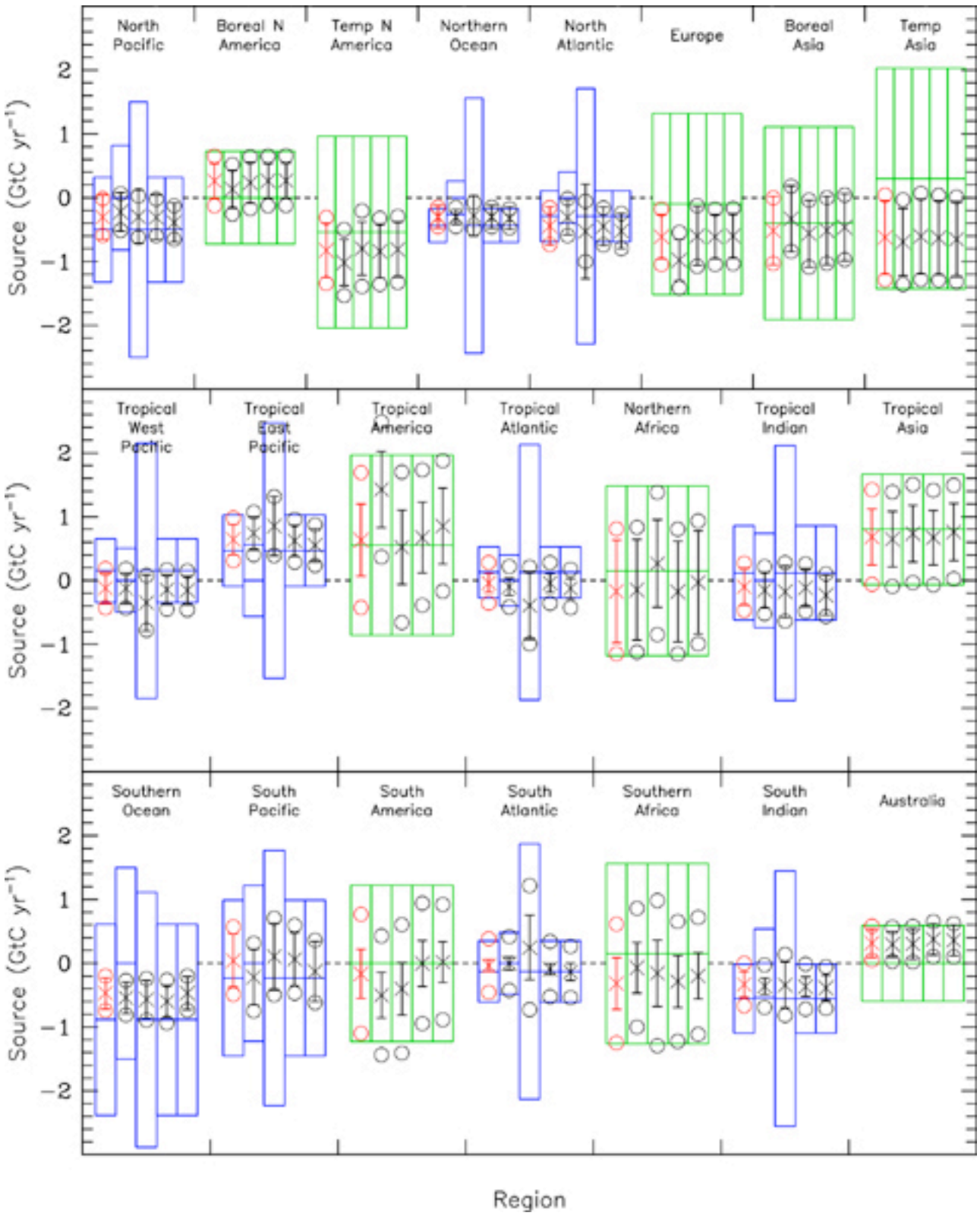

Figure 2: Prior sources and uncertainties (boxes), mean estimated sources (x), 'within-model' uncertainties (o) and 'between-model' uncertainties (error bars) for 4 example sensitivity tests. The

results from the control experiment (lefthand symbols in Figure 1, main text) are repeated in the leftmost set of symbols. Second from the left is an inversion run without the background ocean fluxes. Second from the right is an inversion run with prior source uncertainties on all ocean regions of ± 2 GtC yr^{-1}. Third from the left is an inversion run using only half the data records south of 45°S (HBA_00D0, MQA_02D0, SPO_00C0, SPO_02D0). Far right is an inversion in which the total global oceanic uptake is constrained to –2.5±0.5 GtC yr^{-1}. In each inversion there is little change to the southern ocean estimated flux.

Northern land sink sensitivity

Table 3: Summary of differences between the TransCom 3 inversion set-up and that of Fan et al., 1998 (F98)[7].

Table 4: Mean estimated sources, 'within-model' and 'between-model' uncertainties for northern extratropical land regions under different inversion conditions. The first row is the TransCom 3 control inversion, the second row is the F98 4-region inversion. The third row is an inversion using all TransCom 3 models but with the inversion set-up reconfigured as in F98, with the exception of the global background fluxes. For the reconfigured case (3rd row), the temperate North American sink is substantially larger than the TransCom 3 control inversion (1st row) and 'between-model' uncertainty is increased indicating that this set-up is more sensitive to transport differences. The Eurasian sink remains larger than F98 and again uncertainty is increased relative to the TransCom 3 control inversion. The fourth row takes the reconfigured inversion and replaces the TransCom 3 NEP and ocean background fluxes with the ocean model and earlier CASA background fluxes used in F98. These are only available for the SKYHI model version used in F98 but we have applied them to all the TransCom 3 models. While this does not provide an ideal test case, it is sufficient to indicate that the Eurasian flux estimates are sensitive to the choice of background flux. The remaining rows are for a series of inversions where each element of the reconfigured inversion was individually changed back to the control inversion. The cases are "release oceans" - TransCom 3 ocean uncertainties are used;

“tighten land” - TransCom 3 land uncertainties are used; “release SPO” - global CO_2 offset is solved for “22 region” - all TransCom regions are solved for; “time period and growth” - 1992-1996 data and growth rate are used. All but “release SPO” reduces the temperate North American sink but no single element can account for the difference between the TransCom 3 control and the reconfigured inversion. By implication a combination of factors is required as was found in a similar exploration of inversion method sensitivity[8].

Time period sensitivity

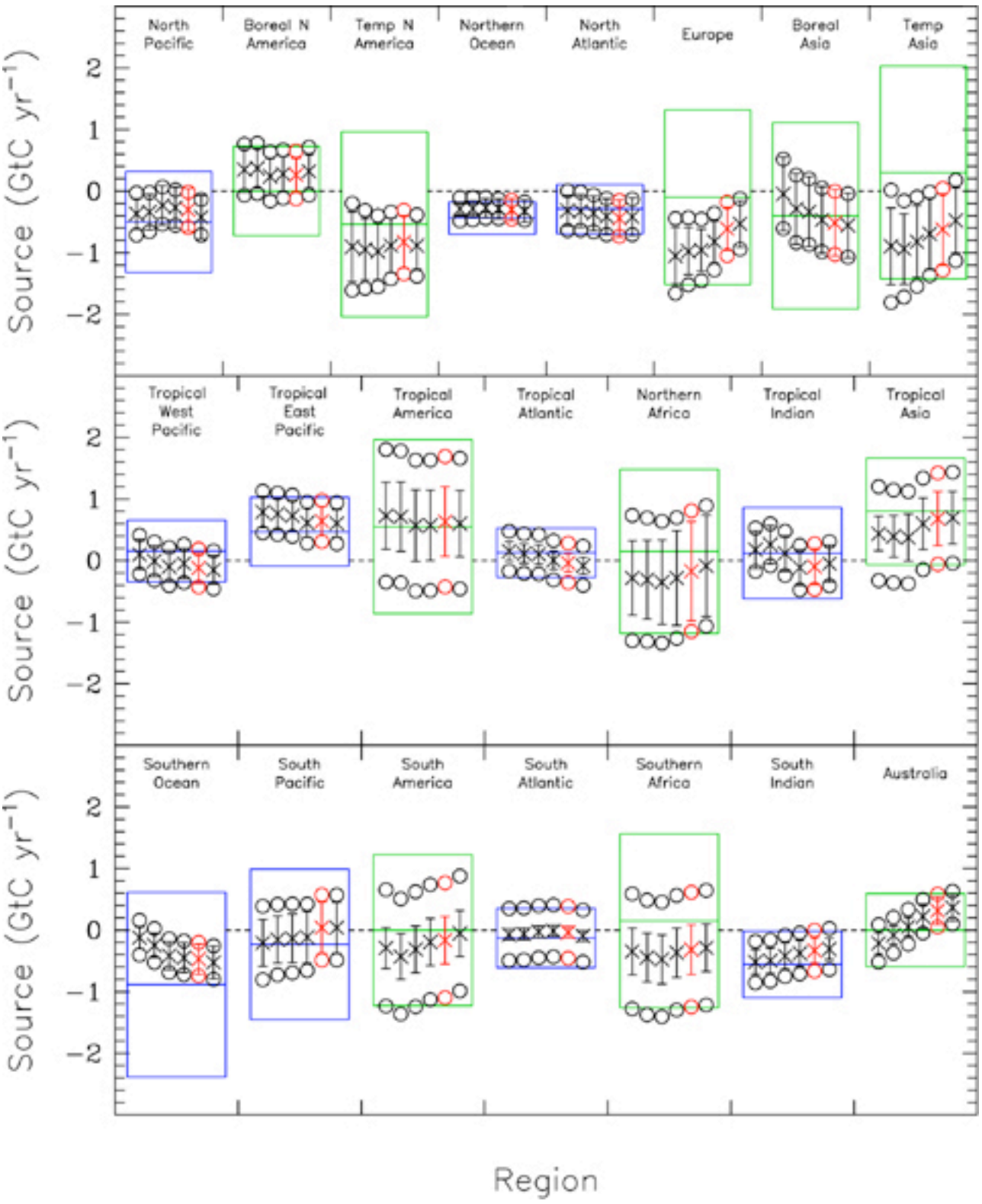

Figure 3: Prior sources and uncertainties (boxes), mean estimated sources (x), 'within-model' uncertainties (o) and 'between-model' uncertainties (error bars) for six 5-year periods. Only the CO_2

observational data is changed in each of these six periods. The time periods are displayed from left to right as: 1988-1992, 1989-1993, 1990-1994, 1991-1995, 1992-1996 (control, red symbols), and 1993-1997. The same 76 sites are used for all inversions even though this means that some sites have more than 30% extrapolated data. Growth rates and fossil emissions are adjusted to be appropriate to each period. For most regions, the change in time period does not move the mean estimated source outside the control uncertainty range.

Table 1. Station Data

Abbreviated station name	Latitude	Longitude	1992-1996 mean concentration (ppm)	1992-1996 mean "data uncertainty" (ppm)
aia005_02D2	-40.53	144.30	356.770	0.500
aia015_02D2	-40.53	144.30	356.879	0.433
aia025_02D2	-40.53	144.30	357.026	0.433
aia035_02D2	-40.53	144.30	357.156	0.433
aia045_02D2	-40.53	144.30	357.279	0.354
aia065_02D2	-40.53	144.30	357.363	0.250
alt_00D0	82.45	-62.52	360.065	0.512
alt_02D0	82.45	-62.52	360.325	0.500
alt_06C0	82.45	-62.52	360.058	0.522
alt_06D0	82.45	-62.52	360.152	0.625
ams_11C0	-37.95	77.53	356.937	0.250
asc_00D0	-7.92	-14.42	357.646	0.250
bal_00D0	55.50	16.67	362.572	1.411
bhd_15C0	-41.41	174.87	356.762	0.250
bme_00D0	32.37	-64.65	359.483	0.584
bmw_00D0	32.27	-64.88	359.554	0.626
brw_00C0	71.32	-156.6	360.271	0.535
brw_00D0	71.32	-156.6	360.330	0.484
car030_00D2	40.90	-104.8	359.204	0.671
car040_00D2	40.90	-104.8	358.752	0.741
car050_00D2	40.90	-104.8	358.607	0.495
cba_00D0	55.20	-162.72	359.818	0.381
cfa_02D0	-19.28	147.06	357.511	0.266
cgo_00D0	-40.68	144.68	356.435	0.433
cgo_02D0	-40.68	144.68	356.686	0.433
cmn_17C0	44.18	10.70	359.443	0.908
cmo_00D0	45.48	-123.97	360.313	0.978
cri_02D0	15.08	73.83	360.016	0.840
crz_00D0	-46.45	51.85	356.938	0.250
daa_02D0	-12.42	130.57	360.792	0.697
esp_06D0	49.38	-126.55	360.316	0.902
gmi_00D0	13.43	144.78	358.932	0.250
hba_00D0	-75.67	-25.50	356.828	0.250
hun_00D0	46.95	16.65	364.161	1.856
ice_00D0	63.25	-20.15	359.245	0.261
itn496_00C3	35.35	-77.38	361.257	1.846
itn_00D0	35.35	-77.38	362.399	2.232
izo_00D0	28.30	-16.48	359.416	0.354
izo_27C0	28.30	-16.48	359.076	0.370

key_00D0	25.67	-80.20	360.090	0.282
kum_00D0	19.52	-154.82	359.204	0.263
maa_02D0	-67.62	62.87	356.598	0.250
mbc_00D0	76.25	-119.35	360.180	0.280
mhd_00D0	53.33	-9.90	359.112	0.439
mid_00D0	28.22	-177.37	359.504	0.274
mlo_00C0	19.53	-155.58	358.953	0.433
mlo_00D0	19.53	-155.58	359.016	0.433
mlo_02D0	19.53	-155.58	359.010	0.433
mnm_19C0	24.30	153.97	360.016	0.347
mqa_02D0	-54.48	158.97	356.484	0.250
poc000_00D1	0.00	-163.00	359.266	0.250
pocn15_00D1	15.00	-147.00	359.345	0.250
pocn20_00D1	20.00	-140.00	359.469	0.264
pocn25_00D1	25.00	-134.00	359.662	0.376
pocn30_00D1	30.00	-126.00	359.653	0.384
pocs05_00D1	-5.00	-168.00	358.978	0.250
pocs10_00D1	-10.00	-174.00	358.491	0.250
pocs15_00D1	-15.00	-178.00	358.018	0.250
prs_21C0	45.93	7.70	358.708	0.432
prs_21D0	45.93	7.70	358.962	0.449
psa_00D0	-64.92	-64.00	356.745	0.250
rpb_00D0	13.17	-59.43	358.654	0.250
ryo_19C0	39.03	141.83	361.902	0.732
sch_23C0	48.00	8.00	360.285	1.057
sey_00D0	-4.67	55.17	357.188	0.321
shm_00D0	52.72	174.10	359.984	0.300
smo_00C0	-14.25	-170.57	357.638	0.354
smo_00D0	-14.25	-170.57	357.680	0.354
spo_00C0	-89.98	-24.80	356.795	0.433
spo_00D0	-89.98	-24.80	356.613	0.433
spo_02D0	-89.98	-24.80	356.710	0.433
stm_00D0	66.00	2.00	359.504	0.336
syo_00D0	-69.00	39.58	356.624	0.250
tap_00D0	36.73	126.13	362.555	0.921
uta_00D0	39.90	-113.72	360.292	0.769
uum_00D0	44.45	111.10	359.540	0.472

Table 2. Model mean fluxes and uncertainties

Land region	Prior Flux ($GtCyr^{-1}$)	Prior Uncertainty ($GtCyr^{-1}$)	Background Fossil Flux ($GtCyr^{-1}$)	Mean Posterior Flux ($GtCyr^{-1}$)	"Within-model" uncertainty ($GtCyr^{-1}$)	"Between-model" uncertainty ($GtCyr^{-1}$)
Boreal N America	0.00	0.73	0.01	0.26	0.39	0.33
Temp N America	-0.54	1.50	1.60	-0.83	0.52	0.44
Europe	-0.10	1.42	1.64	-0.61	0.43	0.47
Boreal Asia	-0.40	1.51	0.17	-0.52	0.51	0.52
Temperate Asia	0.30	1.73	1.80	-0.62	0.66	0.59
Tropical America	0.55	1.41	0.13	0.63	1.06	0.63
Northern Africa	0.15	1.33	0.11	-0.17	0.98	0.66
Tropical Asia	0.80	0.87	0.35	0.68	0.74	0.45
South America	0.00	1.23	0.12	-0.16	0.93	0.42
Southern Africa	0.15	1.41	0.10	-0.32	0.93	0.52
Australia	0.00	0.60	0.08	0.32	0.27	0.25
Ocean Region	**Prior Flux ($GtCyr^{-1}$)**	**Prior Uncertainty ($GtCyr^{-1}$)**	**Background Ocean Flux ($GtCyr^{-1}$)**	**Mean Posterior Flux ($GtCyr^{-1}$)**	**"Within-model" Uncertainty ($GtCyr^{-1}$)**	**"Between-model" uncertainty ($GtCyr^{-1}$)**
North Pacific	0.00	0.82	-0.51	0.20	0.29	0.42
Northern Ocean	0.00	0.26	-0.44	0.14	0.15	0.32
North Atlantic	0.00	0.40	-0.29	-0.15	0.29	0.81
Tropical W Pacific	0.00	0.50	0.15	-0.27	0.31	0.48
Tropical E Pacific	0.00	0.56	0.47	0.18	0.33	0.51
Tropical Atlantic	0.00	0.40	0.13	-0.17	0.32	0.61
Trop Indian Ocean	0.00	0.74	0.12	-0.22	0.37	0.44
South Pacific	0.00	1.22	-0.23	0.27	0.53	0.57
South Atlantic	0.00	0.48	0.13	0.09	0.42	0.74
South Indian Ocean	0.00	0.54	-0.56	0.22	0.33	0.42
Southern Ocean	0.00	1.50	-0.88	0.42	0.27	0.34

Table 3. Inversion differences between TransCom 3 control and Fan *et al.* 1998

Element of inversion	**Transcom3 control**	**Fan et al 98**
Data and data uncertainties	1992-1996 at 76 sites, 3.274 $GtCyr^{-1}$ growth rate, variable uncertainty (0.25-2.20 ppm)	1988-1992 at 63 sites, 2.8 $GtCyr^{-1}$ growth rate, constant uncertainty (0.6 ppm)
Prior sources and prior source uncertainties	Land: land-use change prior and moderate uncertainty (0.60-1.73 GtC yr^{-1}) Ocean: zero prior fluxes with moderate uncertainty (0.26-1.50 GtC yr^{-1})	Land: no prior information for regions Ocean: fixed to background fluxes
Regions solved for	11 land, 11 ocean	3 or 4 land
Global CO_2 offset	Calculated in inversion	Set using South Pole values
Global background fluxes	0.2*1990 fossil + 0.8*1995 fossil, CASA model NEP, Takahashi 99 ocean	1990 fossil, CASA model (earlier version) NEP, Takahashi 97 or ocean model (OBM)

Table 4. Methodological sensitivity under the reconfigured TransCom inverion set-up (all units: $GtCyr^{-1}$)

Inversion Case	T3 Model Mean		
	Boreal NA	**Temperate NA**	**Eurasia**
This study	**0.24** ± 0.40 ± 0.27	**-0.85** ± 0.52 ± 0.42	**-1.78** ± 0.58 ± 0.78
Fan et al., 1998	**-0.20** ± 0.4	**-1.40** ± 0.5	**-0.20** ± 0.7
T3 reconfigured	**0.61** ± 0.50 ± 0.80	**-1.85** ± 0.57 ± 0.69	**-1.56** ± 0.70 ± 1.2
Include OBM+Fan CASA	**0.33** ± 0.50 ± 0.92	**-2.23** ± 0.57 ± 0.83	**-0.69** ± 0.70 ± 1.17
Methodological adjustments			
Time period & growth	**0.61** ± 0.34 ± 0.52	**-1.32** ± 0.32 ± 0.41	**-1.62** ± 0.38 ± 0.87
Variable data unc.	**0.70** ± 0.33 ± 0.67	**-1.53** ± 0.39 ± 0.79	**-1.87** ± 0.54 ± 0.86
Release oceans	**0.81** ± 0.59 ± 0.65	**-1.77** ± 0.76 ± 0.39	**-2.51** ± 0.96 ± 1.18
Tighten land	**0.43** ± 0.38 ± 0.58	**-1.67** ± 0.51 ± 0.57	**-1.50** ± 0.60 ± 0.90
22 regions	**0.59** ± 0.81 ± 0.74	**-1.44** ± 0.82 ± 0.49	**-1.69** ± 0.99 ± 0.75
Release SPO	**0.78** ± 0.51 ± 0.77	**-2.04** ± 0.58 ± 0.58	**-1.81** ± 0.72 ± 1.18

1. GLOBALVIEW-CO2: Cooperative Atmospheric Data Integration Project - Carbon Dioxide. CD-ROM, NOAA CMDL, Boulder, Colorado [Also available on Internet via anonymous FTP to ftp.cmdl.noaa.gov, Path: ccg/co2/GLOBALVIEW], (2000).

2. Andres, R.J., Marland, G., Fung, I., & Matthews, E. distribution of carbon dioxide emissions from fossil fuel consumption and cement manufacture, 1950-1990. *Global Biogeochem. Cycles* **10**, 419-429 (1996).

3. (Brenkert: http://cdiac.esd.ornl.gov/ndps/ndp058a.html).

4. Randerson, J. *et al*. The contribution of terrestrial sources and sinks to trends in the seasonal cycle of atmospheric carbon dioxide. *Global Biogeochem. Cycles* **11**, 535-560 (1997).

5. Takahashi, T. *et al.* Net sea-air CO_2 flux over the global oceans: An improved estimate based on the sea-air pCO_2 difference. Proceedings of the 2^{nd} CO_2 in Oceans Symposium, Tsukuba, Japan (1999).

6. Gurney, K.R., Law, R.M., Rayner, P.J., & Denning, A.S. TransCom 3 experimental protocol. Colorado State University, Department of Atmospheric Science Paper no. 707 (2001).

7. Fan, S. *et al.* A Large Terrestrial carbon sink in North America implied by atmospheric and oceanic carbon dioxide data and models. *Science* **282**, 442-446 (1998).

8. Baker, D.F. *Sources and Sinks of Atmospheric CO_2 Estimated from Batch Least-Squares Inversions of CO_2 Concentration Measurements*. PhD Dissertation, Princeton University, 293 pp. (2001).

Tellus (2003), 55B, 555–579
Printed in UK. All rights reserved

TELLUS
ISSN 0280–6509

TransCom 3 CO_2 inversion intercomparison: 1. Annual mean control results and sensitivity to transport and prior flux information

By KEVIN ROBERT GURNEY[1]*, RACHEL M. LAW[2], A. SCOTT DENNING[1], PETER J. RAYNER[2], DAVID BAKER[3], PHILIPPE BOUSQUET[4], LORI BRUHWILER[5], YU-HAN CHEN[6], PHILIPPE CIAIS[4], SONGMIAO FAN[7], INEZ Y. FUNG[8], MANUEL GLOOR[9], MARTIN HEIMANN[9], KAZ HIGUCHI[10], JASMIN JOHN[8], EVA KOWALCZYK[2], TAKASHI MAKI[11], SHAMIL MAKSYUTOV[12], PHILIPPE PEYLIN[4], MICHAEL PRATHER[13], BERNARD C. PAK[13], JORGE SARMIENTO[7], SHOICHI TAGUCHI[14], TARO TAKAHASHI[15] and CHIU-WAI YUEN[10], [1]*Department of Atmospheric Science, Colorado State University, Fort Collins, CO 80523, USA;* [2]*CSIRO Atmospheric Research, PMB 1, Aspendale, Victoria 3195, Australia;* [3]*National Center for Atmospheric Research (NCAR), Boulder, CO 80303, USA;* [4]*Laboratoire des Sciences du Climat et de l'Environment (LSCE), F-91198 Gif-sur-Yvette Cedex, France;* [5]*National Oceanic and Atmospheric Administration (NOAA), Climate Monitoring and Diagnostics Laboratory, 326 Broadway R/CG1, Boulder, CO 80303, USA;* [6]*Department of Earth, Atmospheric, and Planetary Science, Massachusetts Institute of Technology (MIT), Cambridge, MA 0214, USA;* [7]*AOS Program, Princeton University, Sayre Hall, Forrestal Campus PO Box CN710 Princeton, NJ 08544-0710, USA;* [8]*Center for Atmospheric Sciences, McCone Hall, University of California, Berkeley, CA 94720-4767, USA;* [9]*Max-Planck Institute fur Biogeochemie, D-07701 Jena, Germany;* [10]*Meteorological Service of Canada, Environment Canada, Toronto, Ontario M3H 5T4, Canada;* [11]*Quality Assurance Section, Atmospheric Environment Division, Observations Department, Japan Meteorological Agency, 1-3-4 Otemachi, Chiyoda-ku, Tokyo 100-8122 Japan;* [12]*Institute for Global Change Research, Frontier Research System for Global Change, Yokohama, 236-0001 Japan;* [13]*Earth System Science, University of California, Irvine, CA 92697-3100, USA;* [14]*National Institute of Advanced Industrial Science and Technology, 16-1 Onogawa Tsukuba, Ibaraki 305-8569, Japan;* [15]*Lamont-Doherty Earth Observatory of Columbia University, Palisades, NY, USA*

(Manuscript received 22 May 2002; in final form 27 November 2002)

ABSTRACT

Spatial and temporal variations of atmospheric CO_2 concentrations contain information about surface sources and sinks, which can be quantitatively interpreted through tracer transport inversion. Previous CO_2 inversion calculations obtained differing results due to different data, methods and transport models used. To isolate the sources of uncertainty, we have conducted a set of annual mean inversion experiments in which 17 different transport models or model variants were used to calculate regional carbon sources and sinks from the same data with a standardized method. Simulated transport is a significant source of uncertainty in these calculations, particularly in the response to prescribed "background" fluxes due to fossil fuel combustion, a balanced terrestrial biosphere, and air–sea gas exchange. Individual model-estimated fluxes are often a direct reflection of their response to these background fluxes. Models that generate strong surface maxima near background exchange locations tend to require larger uptake near those locations. Models with weak surface maxima tend to have less uptake in those same regions but may infer small sources downwind. In some cases, individual model flux estimates cannot be analyzed through simple relationships to background flux responses but are

*Corresponding author.
e-mail: keving@atmos.colostate.edu

likely due to local transport differences or particular responses at individual CO_2 observing locations. The response to the background biosphere exchange generates the greatest variation in the estimated fluxes, particularly over land in the Northern Hemisphere. More observational data in the tropical regions may help in both lowering the uncertain tropical land flux uncertainties and constraining the northern land estimates because of compensation between these two broad regions in the inversion. More optimistically, examination of the model-mean retrieved fluxes indicates a general insensitivity to the prior fluxes and the prior flux uncertainties. Less uptake in the Southern Ocean than implied by oceanographic observations, and an evenly distributed northern land sink, remain in spite of changes in this aspect of the inversion setup.

1. Introduction

A quantitative understanding of the sources and sinks of atmospheric CO_2 is of vital importance for reliably predicting future CO_2 levels. The estimation of CO_2 sources and sinks can be approached in a variety of ways (Schimel et al., 2001). One approach is to use atmospheric CO_2 measurements to infer CO_2 fluxes through tracer transport inversion. This approach adjusts a series of regionally explicit "trial" fluxes to best match observed CO_2 concentrations to those simulated by an atmospheric transport model. Early inversions used two-dimensional transport models to calculate the latitudinal distribution of fluxes (e.g. Tans et al., 1990; Enting and Mansbridge, 1989; Ciais et al., 1995). Recent inversions have used three-dimensional models to estimate the longitudinal distribution of fluxes (e.g. Enting et al., 1995; Fan et al., 1998; Bousquet et al., 1999a;b; Kaminski et al., 1999). Interannual variations in fluxes have also been estimated (e.g. Rayner et al., 1999; Law, 1999; Bousquet et al., 2000; Baker, 2001).

A general concern with inversions is the sensitivity of the results to the atmospheric transport model used. This sensitivity is difficult to assess because the results to date have employed only one or two transport models in a given study. A goal of the TransCom series of experiments has been to assess the influence of different transport algorithms on the CO_2 inversion problem. The initial phases of TransCom conducted forward simulations of fossil and biospheric emissions of CO_2 (TransCom 1) (Law et al., 1996) and of SF_6 (TransCom 2) (Denning et al., 1999) to characterize model behaviour. The fossil CO_2 experiment indicated differences in simulated surface interhemispheric concentration gradients among the models of up to a factor of two. However, with no 'fossil-CO_2' observations to compare against, it was not possible to determine which simulated transport, if any, was correct. The SF_6 experiment, with relatively well known sources and observations, was intended to evaluate atmospheric transport and to identify which processes led to different model behaviour. Most of the models were reasonably successful in reproducing the marine boundary-layer observations of SF_6, but tended to overestimate the SF_6 at continental locations near sources. Those models that underestimated marine boundary-layer values due to excessive vertical convective transport tended to give better continental concentrations than the models with less convective transport.

Model differences were also large for the annual mean response to seasonal biospheric CO_2 exchange. Almost all models simulated elevated CO_2 concentrations at the surface in the northern middle latitudes due to the covariance between seasonal exchange and seasonal transport, the so-called 'seasonal rectifier effect' (e.g., Keeling et al., 1989; Denning et al., 1995), but zonal mean surface concentrations varied over 3 ppm among the models.

While these experiments provided useful insights into model behaviour, they did not directly address the sensitivity of inversion results to transport. This is the role of the current TransCom experiment (TransCom 3); the aim is to assess the contribution of uncertainties in transport to the uncertainties in flux estimates for annual mean, seasonal cycle and interannual inversions. The experiment can also contribute to our understanding of other sensitivities in the inversion process (e.g. inversion set-up, observational data choices), since more reliable results are expected by examining the sensitivity with a range of transport models than with just one or two models.

The first results from TransCom 3 were presented by Gurney et al. (2002). They showed mean inversion results for a 'control' inversion in which annual mean fluxes were estimated using 1992–1996 data. Here we present results from that same control inversion but for individual models. We also present results from a number of sensitivity tests related to the specification of prior flux information. A companion paper (Law et al., 2003) presents sensitivity tests related to CO_2 data issues including network choice, time period, data

selection and data uncertainty. Seasonal and interannual inversions will be presented elsewhere.

2. Method

2.1. Inversion formalism

The control inversion uses a Bayesian synthesis method (Enting, 2002). The first step is to choose a set of flux patterns, or basis functions ($\vec{V}_i$), from which solutions will be constructed: $\vec{V} = \sum_i s_i \vec{V}_i$. The inversion procedure reduces to solving for the scaling factor, s_i. With a set of concentration observations $\vec{D}$ the linearity of transport can be used to yield

$$\vec{D} = \sum_i s_i \mathbf{T}(\vec{V}_i) \tag{1}$$

where $\mathbf{T}$ is the atmospheric transport. If we have predefined times and places for our concentration observations (obvious in a diagnostic or inverse study) then we can repeatedly run the transport model on each basis function and sample the output at the observation locations. The concentration field generated from each basis function is referred to as its corresponding response function. If we sample the response function at our chosen observation locations, and write the result as a column vector, we produce a matrix $\mathbf{M}$ for which we can easily show

$$\vec{D} = \mathbf{M}\vec{S} \tag{2}$$

The regional fluxes, $\vec{S}$, can now be solved for using conventional least-squares techniques. These techniques rely on minimizing the mismatch between modelled concentrations, $\mathbf{M}\vec{S}$, and observed concentrations, $\vec{D}$. Adding prior information about the fluxes acknowledges the under-determinacy of the system due to the limitation of few observations to constrain fluxes from all regions. It also allows those aspects of the flux distribution that are reasonably well known to be specified.

With the addition of prior information, the solution for $\vec{S}$ now involves minimizing the difference between modelled and observed concentrations and between predicted fluxes and their prior estimates. A cost function J can be defined as

$$J = \frac{1}{2}\Big[(\mathbf{M}\vec{S} - \vec{D})^T \mathbf{C}(\vec{D})^{-1}(\mathbf{M}\vec{S} - \vec{D}) + (\vec{S} - \vec{S}_0)^T \mathbf{C}(\vec{S}_0)^{-1}(\vec{S} - \vec{S}_0)\Big] \tag{3}$$

where $\mathbf{C}(\_)$ embodies confidence in the form of an error or uncertainty covariance. Since $\mathbf{C}$ appears inverted, quantities with large uncertainty confer less influence. Deviations from this prior estimate will penalize the cost function severely, and hence be restricted. Alternatively, fluxes that are poorly understood can be assigned large uncertainties and, hence, allowed to deviate significantly from the prior estimates.

The measurements are similarly weighted inversely by the degree to which the predicted concentrations are required by the inverse process to match the observations. This weighting term, $\mathbf{C}(\vec{D})$, has traditionally been called the "data uncertainty". The name is misleading, since the term must also account for the inability of models with imperfect transport and coarse spatial and temporal resolution to match point observations. Furthermore, the chosen flux shape or "footprint" assumed for the basis functions may not represent the distribution of the true source field, and hence may add to the inability of the predicted concentrations to match observations (Kaminski et al., 2001; Engelen et al., 2002). It would be inappropriate in the inversion to attempt to fit the data better than the sum of all of these errors, yet objectively quantifying this overall model–data mismatch remains difficult.

Following Tarantola (1987) we minimize eq. (3) to yield

$$\vec{S} = \vec{S}_0 + \mathbf{M}^{(-1)}(\vec{D} - \mathbf{M}\vec{S}_0) \tag{4}$$

where $\mathbf{M}^{(-1)}$, the generalized inverse of $\mathbf{M}$, is given by

$$\mathbf{M}^{(-1)} = \Big[\mathbf{M}^T \mathbf{C}(\vec{D})^{-1}\mathbf{M} + \mathbf{C}(\vec{S}_0)^{-1}\Big]^{-1} \mathbf{M}^T \mathbf{C}(\vec{D})^{-1}. \tag{5}$$

An estimate of the uncertainty in the predicted fluxes can also be produced. This depends on the uncertainty in the prior fluxes, the data uncertainty and the response functions embodied in $\mathbf{M}$. The relation is:

$$\mathbf{C}(\vec{S}) = \Big[\mathbf{C}(\vec{S}_0)^{-1} + \mathbf{M}^T \mathbf{C}(\vec{D})^{-1}\mathbf{M}\Big]^{-1}. \tag{6}$$

This always represents a reduction in uncertainty on the prior estimate, with the amount of reduction depending on the data uncertainty and how well the

available observing locations sample the chosen flux patterns.

The mean of the individual model flux uncertainties can be computed as:

$$\overline{\mathbf{C}(\vec{S})} = \sqrt{\sum_{n=1}^{N_{\text{models}}} [\mathbf{C}(\vec{S})]^2 \Big/ N_{\text{models}}} \tag{7}$$

where the individual model posterior uncertainty estimates are taken from the diagonal of the posterior covariance matrix. We designate this mean uncertainty the 'within-model' uncertainty. The spread of flux estimates across models is represented by the standard deviation,

$$\sigma(\vec{S}) = \sqrt{\sum_{n=1}^{N_{\text{models}}} [\mathbf{C}(\vec{S}) - \overline{\mathbf{C}(\vec{S})}]^2 \Big/ N_{\text{models}}} \tag{8}$$

and designated the 'between-model' uncertainty.

The minimum value of the cost function, $J_{\min}$, describes the degree to which the inversion calculation matches the data and prior source estimates simultaneously. This is usually expressed using the reduced χ^2,

$$\chi^2 = \frac{\mathbf{J}_{\min}}{\mathbf{N}_{\text{obs}}} = \frac{\sum_{n=1}^{\mathbf{N}_{\text{obs}}} \frac{(\mathbf{M}\vec{S}-\vec{D})^2}{\mathbf{C}(\vec{D})^2} + \sum_{r=1}^{R_{\text{regions}}} \frac{(\vec{S}-\vec{S}_0)^2}{\mathbf{C}(\vec{S}_0)^2}}{\mathbf{N}_{\text{obs}}}. \tag{9}$$

Statistical consistency requires χ^2 not to be significantly greater than unity, otherwise the posterior uncertainty is inconsistent with the quality of the fit to the data. This inconsistency suggests that too much confidence has been placed in the ability of the inversion to match the data, so $\mathbf{C}(\vec{D})$ is increased accordingly. This will consequently increase $\mathbf{C}(\vec{S})$.

2.2. *Experimental design*

2.2.1. Forward simulations. Forward simulations were performed with 16 transport models (or model variants) (Gurney et al., 2000), the results of which were used to perform annual mean inversions for sources and sinks (Gurney et al., 2002). A 17th model (CSIRO) recently submitted simulations. We have not included results from this model in the calculation of mean results, in order to maintain consistency with Gurney et al. (2002), but have included it in presentations of individual model results. Details of each transport model are given in Table 1. The models vary in resolution, advection scheme, driving winds and subgrid-scale parameterizations. They include every model used in recently published CO_2 inversions. TM2 is the only model that has been used in precisely the same configuration in all the TransCom experiments, while seven of the current models performed the TransCom 2 SF_6 experiment, though some of these have been modified since that experiment.

For the annual mean experiment presented here, four-year simulations were performed by each model for each of 26 required basis functions. The 26 basis functions comprised four "background" global fluxes and 22 regional fluxes. The model output was submitted as global monthly mean distributions and as four-hourly time series at 228 specified locations. Sampling of model output was intended to mimic the sampling protocol for observations: some stations were moved offshore away from coastlines in the direction of the "clean air sector" identified for flask sampling. Full details of the experimental protocol are presented in Gurney et al. (2000). The inversions were performed on the output from each model.

The four background fluxes consisted of two fossil fuel emission fields (1990 and 1995 distributions), an annually balanced, seasonal terrestrial biosphere exchange and air–sea gas exchange. These fluxes are included in the inversion with a very small prior uncertainty so that their magnitude is effectively fixed, and the 22 regional fluxes estimated by the inversion are deviations from these global fluxes. The 1990 annual mean fossil source ($1^\circ \times 1^\circ$) is from Andres et al. (1996) and totals 5.812 Gt C yr^{-1}. The 1995 annual mean fossil source ($1^\circ \times 1^\circ$) is derived from the data prepared by Brenkert (1998) and totals 6.173 Gt C yr^{-1}. The seasonal biospheric exchange ($1^\circ \times 1^\circ$) was derived from the Carnegie Ames Stanford Approach (CASA) model (Randerson et al., 1997), and has an annual total flux of zero at every grid cell. The oceanic exchange ($4^\circ \times 5^\circ$) was produced by Taro Takahashi and colleagues and represents monthly global oceanic exchange derived from measurements of $\Delta p(CO_2)$ (Takahashi et al., 1999). The annually integrated flux is -2.19 Gt C yr^{-1} (into the ocean). The background fossil fuel emission fluxes were prescribed without seasonality. The annually balanced terrestrial fluxes were purely seasonal, and the background ocean fluxes were prescribed with both seasonal variations and annual mean uptake.

The boundaries of the 22 regional basis functions are shown in Fig. 1. In the forward simulations, each

Table 1. *Participating model description and references*

Model	Modeler	Winds	H. Res.	# Levels	Advection	Subgrid	References
CSU[a]	Gurney & Denning	Online	72 lon. × 44 lat.	17 sigma	2nd order	Cum. mass flux (Arakawa & Schubert, 1974; Randall & Pan, 1993; Ding et al., 1998), var. prog. PBL (Suarez et al., 1983; Randall et al., 1992)	Denning et al. (1996)
UCB[f]	Fung & John	1 h GISS GCM II′	72 lon. × 46 lat.	9 sigma	Slopes (Russell & Lerner, 1981)	Penetrative mass flux	Hansen et al. (1997)
UCI (s, b)[b]	Prather, Pak, Lee, & Hannegan	GISS GCM II′	72 lon. × 46 lat.	9 sigma & 23 sigma	2nd order moments (Prather, 1986)	Penetrative mass flux w/updrafts, downdrafts and entrainment; diurnally varying PBL	Prather et al. (1987); Hansen et al. (1997); Koch and Rind (1998)
JMA	Maki	6 h JMA (1997)	144 lon. × 73 lat.	32 hybrid	Hor: semi-lag., Vert: box scheme	Vert diff. (Mellor–Yamada, level 2.0), Cumulus (simple diff.), PBL (fixed layer)	Taguchi (1996)
MATCH: CCM3	Bruhwiler	NCAR CCM3	128 lon. × 64 lat.	28 sigma	Spitfire	Corrective transport, subgrid diff., PBL w/stable mixing, cloud prediction	Rasch et al. (1997)
MATCH: NCEP	Chen	6 h NCEP (1990)	128 lon. × 64 lat.	28 sigma	Spitfire	Vert. diff. w/diagnosed PBL; penetrative conv. + local conv. correction (Hack, 1994)	Rasch et al. (1997)
MATCH: MACCM2	Law	6 h MACCM2	64 lon. × 64 lat.	24 hybrid	Semi-lagrangian	Hack convection (Hack, 1994); vert. diff. with PBL (Holtslag & Boville, 1993)	Rasch et al. (1997); Law & Rayner (1999)
NIES	Maksyutov	12 h ECMWF (1997)	144 lon. × 72 lat.	15 sigma	Semi-lagrangian	Vert. diff. in troposphere (Hack, 1993); penetrative mass flux (Tiedke, 1989); vert. diff. in PBL (Schubert et al., 1993)	Maksyutov & Inoue (2000)

Table 1. *(cont'd.)*

Model	Modeler	Winds	H. Res.	# Levels	Advection	Subgrid	References
NIRE CTM-96[c]	Taguchi	6 h ECMWF (1995)	144 lon. × 73 lat.	15 hybrid	Semi-lagrangian	Vert. diff. in PBL, reduced diffusion at tropopause	Taguchi (1996)
RPN-SEF	Yuen & Higuchi	Online	128 lon. × 64 lat.	27 sigma	Semi-lag. (Richie & Beaudoin, 1994)	Vertical diffusion; PBL based on turbulent KE (Benoit et al., 1997)	D'Andrea et al. (1998)
SKYHI[d,f]	Fan	Online	100 lon. × 60 lat.	40 hybrid	2nd order	Dry/moist convective adjustment for T, q; non-local parameterization for vert. mixing in PBL	Mahlman et al. (1994); Strahan & Mahlman (1994); Hamilton et al. (1995)
TM2[e]	Bousquet & Peylin	12 h ECMWF (1990)	48 lon. × 25 lat.	9 sigma	Slopes (Russell & Lerner, 1981)	Mass flux (Tiedke, 1989); stability dependent vertical diffusion (Louis, 1979)	Heimann (1995); Bousquet et al. (1999a)
TM3[f]	Heimann	6 h ECMWF (1990)	72 lon. × 45 lat.	19 hybrid	Slopes (Russell & Lerner, 1981)	Mass flux (Tiedke, 1989); stability dependent vert. diffusion (Louis, 1979, updated)	Heimann (1995)
GCTM[e]	Baker	6 h ZODIAC GCM	256 km^2	11 sigma	2nd/4th order	Vert. diffusion, Ri number-based vert. mixing in lowest 3 layers to represent PBL.	Mahlman & Moxim (1978); Levy et al. (1982)
CSIRO-CC[g]	Kowalczyk & McGregor	Online	208 km^2	18 sigma	Hor: semi-lag (McGregor, 1996); Vert: total var diminishing	Stability dep. Vert. diff. (Louis, 1979) + non-local scheme, mass flux conv. w/downdrafts.	McGregor & Dix (2001)

[a]Participated in TransCom 1 and TransCom 2 but model differed.
[b]UCI primary model uses 3-hourly GISS II' 9-layer GCM winds and is primarily tropospheric; UCIb is a boundary-layer variant with PBL height diagnosed from Ri number, super-resolved tracer gradients using second-order moments, and non-local closure on the subgrid (Hartke and Rind, 1997); UCIs uses 6-hourly GISS II' middle atmosphere GCM winds with a well resolved stratosphere (Koch and Rind, 1998).
[c]Earlier model version participated in TransCom 1, current model version in TransCom 2.
[d]A non-local parameterization for vertical mixing in the PBL was implemented after TransCom 2 and was used in TransCom 3.
[e]Participated in TransCom 1 and TransCom 2 with current model.
[f]Participated in TransCom 2.
[g]Model output fields were interpolated from model's conformal-cubic grid to regular (2° latitude, longitude) grid before submission.

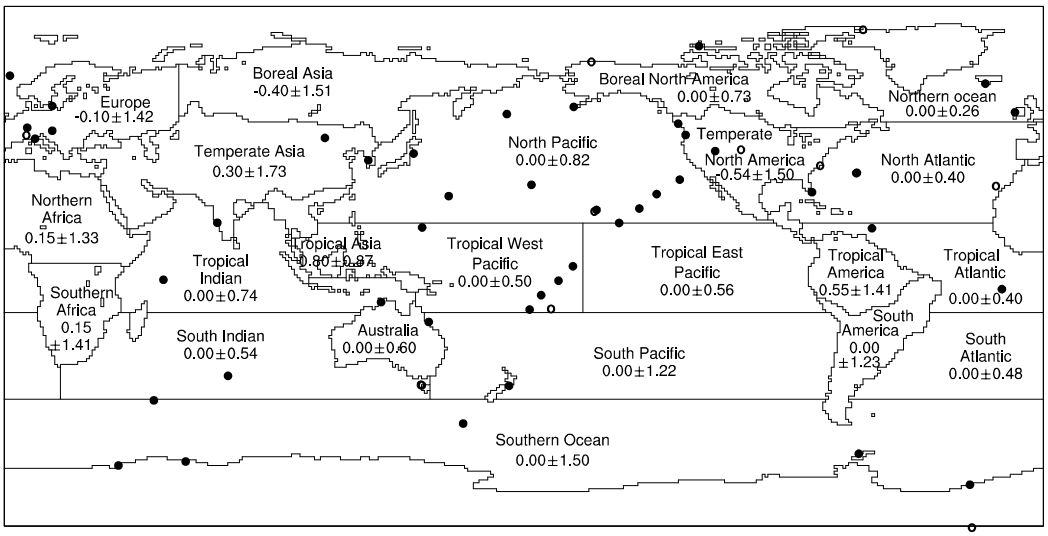

Fig. 1. Basis function regions and the locations of the 76 CO_2 observational records used in the inversion. Multiple records exist at some locations and are denoted by open circles. The prior flux and prior flux uncertainties are shown for each basis function region (Gt C yr^{-1}). The prior constraint on the atmospheric growth rate is 3.274 Gt C yr^{-1} with a prior uncertainty of 0.074 Gt C yr^{-1}. The prior global offset concentration is 355 ppm with a prior uncertainty of 100 ppm.

region emits a 1 Gt C yr^{-1} flux that is scaled independently during the inversion calculation. The regional terrestrial basis fluxes include spatial structure based on the distribution of annual mean net primary productivity (NPP), as given by a CASA model steady-state run (Randerson et al., 1997), reflecting an assumption that terrestrial exchanges are located within regions of higher biological activity. The terrestrial basis function boundaries were constructed to enclose vegetation of similar seasonal structure and carbon exchange, with some additional boundary smoothing. The starting point for the boundary construction was the $1^\circ \times 1^\circ$ land cover type classification used by the original Simple Biosphere Model (SiB) (De Fries and Townshend, 1994; Sellers et al., 1996). A uniform spatial distribution was used for the regional oceanic basis functions, with the exception of seasonal ice cover in the northern and southernmost regions. The sea-ice cover data were produced by the World Climate Research Programme, Working Group on Numerical Experimentation, Atmospheric Model Intercomparison Project (Taylor et al., 1997).

2.2.2. Inversion set-up and observational data. Prior estimates of the fluxes in each of the 22 regional basis functions were determined from independent estimates of terrestrial and oceanic exchange and are presented in Fig. 1. The land region prior flux estimates incorporate results from recent inventory studies (Apps and Kurz, 1994; Kurz and Apps, 1999; UNFCCC, 2000; Pacala et al., 2001; Houghton, 1999; Dixon et al., 1990; Houghton and Hackler, 1999; Kauppi et al., 1992). Where more than one estimate for a given region was available, a mid-point of the estimate range was used. The ocean region prior flux estimates were prescribed as zero.

The prior flux uncertainty is important for keeping the estimated fluxes within biogeochemically realistic bounds. For land regions we chose growing season net flux (GSNF, the sum of monthly mean exchange for months exhibiting net uptake) as provided by the CASA model of net ecosystem production (Randerson et al., 1997). Since it is unlikely that an annual mean residual land flux would exceed the GSNF, this provides a reasonable, ecologically relevant upper bound. The prior ocean uncertainties were guided by the aggregate estimates given in Takahashi et al. (1999), which suggest a total global oceanic uncertainty approximately 70% of the total oceanic exchange. Because this level of uncertainty tightly constrains some oceanic regions to the prior flux estimate, the aggregate uncertainty was increased to 140% of the total net oceanic exchange. The uncertainty in individual oceanic basis function regions was proportional to the

area of the region and the proportion of sampled grid points in the region.

We invert 5-yr mean measurements for 1992–1996 at 76 sites taken from the GLOBALVIEW-2000 dataset (GLOBALVIEW-CO_2, 2000). GLOBALVIEW is a data product that interpolates CO_2 measurements to a common time interval. Gaps in the data are filled by extrapolation from marine boundary-layer measurements. Sites were chosen where the extrapolated data accounts for less than 30% of total data for the 1992–1996 period. Law et al. (2003) varied this extrapolated data limit to test the sensitivity of the inversion to alternative data sets.

The uncertainty attached to each data value, *C(D)*, was derived from the residual standard deviation (RSD) of individual observations around a smoothed timeseries as given by GLOBALVIEW-CO_2 (2000). This choice was based on the assumption that the distribution of RSD (higher RSD values for northern and continental sites and lower RSD values for southern hemisphere oceanic sites) reflects the high-frequency variations in transport and regional flux that large-scale transport models are unable to accurately simulate. Direct use of the RSD values for the data uncertainty within the inversion results in a reduced χ^2 [eq. (9)] that is much smaller than unity. This indicates that the predicted concentrations fit the data much better than the uncertainty assigned to the data itself, and that the uncertainty should be reduced. Therefore, the RSD has been scaled as follows: the RSD was divided by $(8P)^{0.5}$, where P is the proportion of real data in the record and the factor 8 accomplishes the $\chi^2 \approx 1$ goal. Where this gave values less than 0.25 ppm, the uncertainty was increased to 0.25 ppm. Finally, the uncertainty was increased for those sites that are likely to occur in the same model grid cell by the square root of the number of co-located sites. This gave uncertainties ranging from 0.25 ppm for remote, "clean air" sites to 2.2 ppm for continental, "noisy" sites and a reduced χ^2 averaged across the models of 0.97, close to the desired value of one. Law et al. (2003) demonstrate the sensitivity of the inversion to the choice of C(D).

Additional prior constraints included in the inverse calculation are the global atmospheric CO_2 growth rate (3.274 ± 0.074 Gt C yr^{-1}) and a global CO_2 concentration background value (355 ± 100 ppm). The growth rate and uncertainty are the mean and standard deviation of the 1992–1996 trends at the observational stations used in this study via a fit that includes a linear trend and harmonics.

3. Results

3.1. Background simulation results

The forward simulations of the four background fluxes provide a measure of model-to-model transport differences, and explain many of the features found in the inferred regional fluxes to be discussed in Section 3.2. Figure 2 shows the surface CO_2 concentrations resulting from the sum of the background fluxes for each of the models. Maxima associated with the fossil fuel emissions and the annually balanced, seasonal biosphere exchange are evident and vary considerably from model to model. Maxima associated with the fossil fuel emissions are centered over the industrial source regions of the United States, Europe and the Asian Pacific. Maxima associated with rectification of the biosphere exchange are broadly distributed over forested areas in North America and Eurasia. Regional minima in concentration are simulated over the Southern Ocean and to a lesser extent over the North Atlantic Ocean in response to the background ocean fluxes. Surface concentration responses range from very weak (TM2 and the UCI variants) to strong but localized (GCTM) to very strong over large areas (MATCH:NCEP, UCB). As was found previously (Law et al., 1996; Denning et al., 1999), there does not appear to be a systematic difference between models driven by analyzed winds and those using GCM winds.

Figure 3 shows the zonal mean surface CO_2 concentration resulting from each of the background fluxes separately and summed. The maximum fossil fuel concentrations occur around 50 °N and vary by almost 2 ppm among the models. Southern Hemisphere concentrations also vary with CSU, MATCH:MACCM2 and NIRE producing the highest concentrations. The interhemispheric difference (IHD) (mean Northern Hemisphere surface-layer concentration minus mean Southern Hemisphere surface-layer concentration) in these simulated surface responses provides a convenient index (not always an accurate indicator; see Denning et al., 1999) to summarize both meridional and vertical model transport, and is indicated in the figure for the fossil fuel and total background responses. CSU, TM2 and JMA exhibit the smallest IHD values indicating relatively rapid mixing away from source areas (vertical or meridional or both). The ratio of largest fossil fuel IHD to smallest IHD is 1.5 compared to 2.0 for the fossil simulation results from TransCom 1, indicating a convergence of model simulations for this

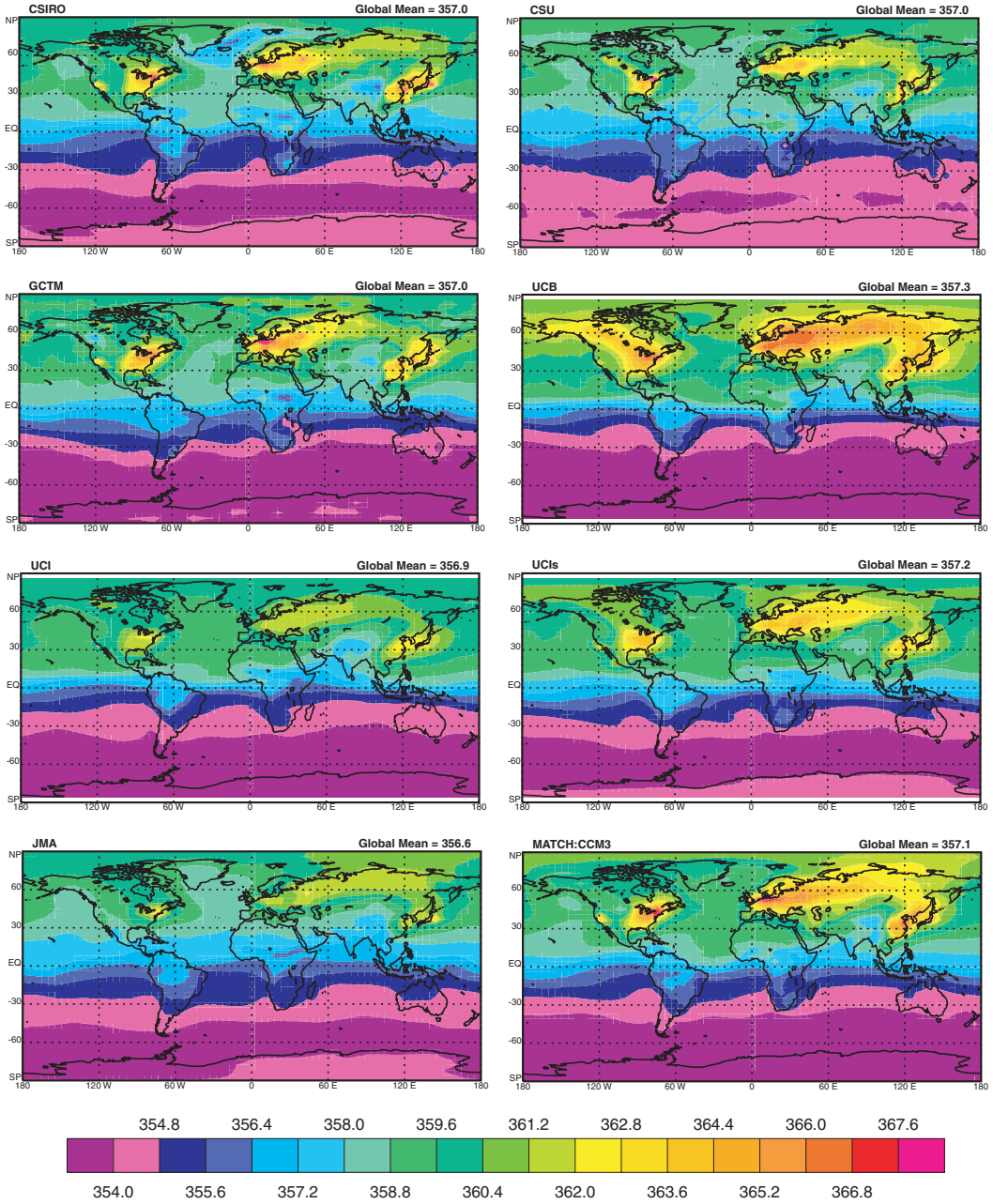

Fig. 2. Annual mean surface CO_2 concentration (ppm) resulting from the combined (relative to a background concentration of 350 ppm) background fluxes for each of the models. The UCIb model variant is not shown since its surface distribution is very similar to the UCI standard version. The global mean surface concentration is also computed for each model.

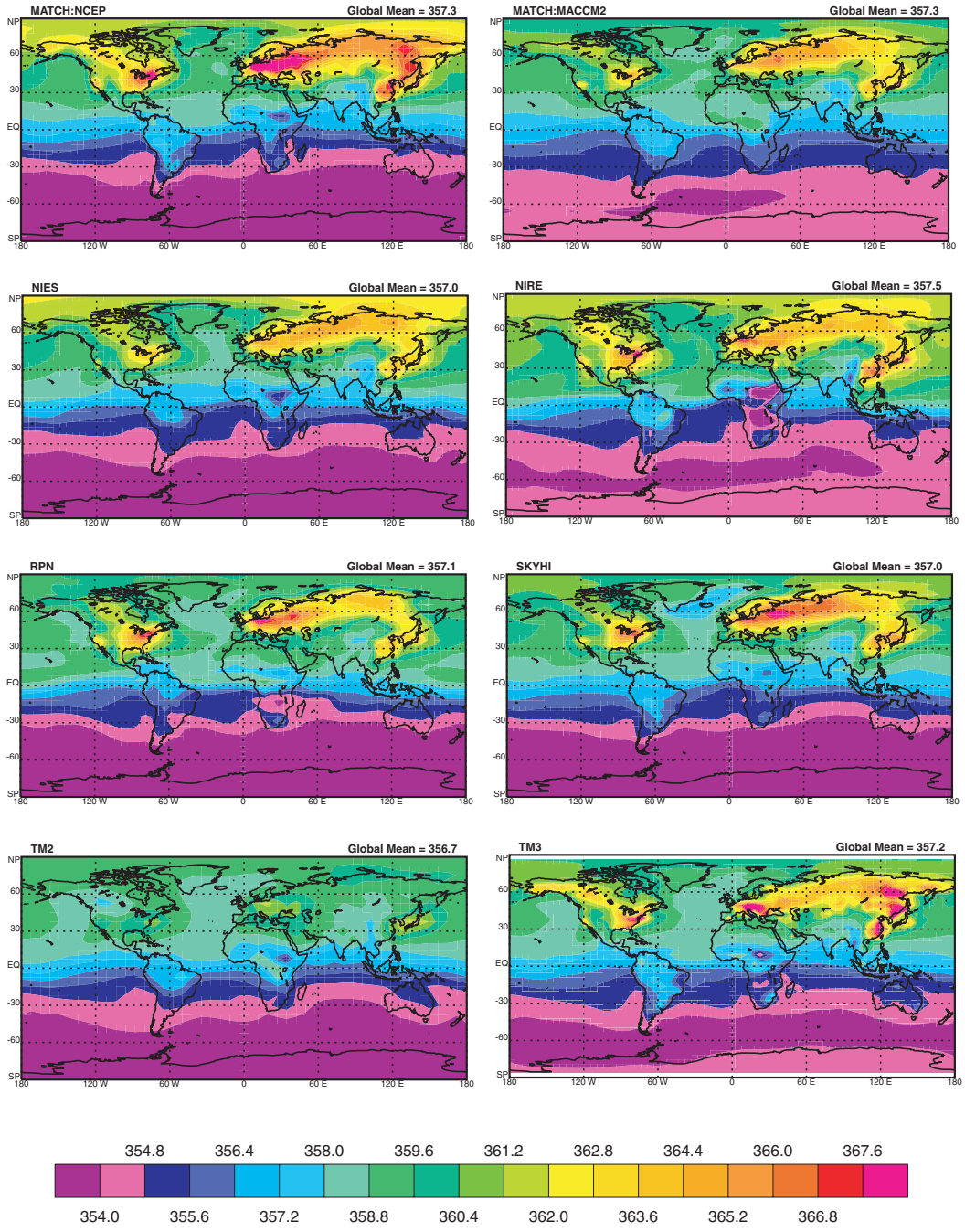
MATCH:NCEP
Global Mean = 357.3
MATCH:MACCM2
Global Mean = 357.3
NIES
Global Mean = 357.0
NIRE
Global Mean = 357.5
RPN
Global Mean = 357.1
SKYHI
Global Mean = 357.0
TM2
Global Mean = 356.7
TM3
Global Mean = 357.2
NP
60
30
EQ
-30
-60
SP
180
120 W
60 W
0
60 E
120 E
354.8
356.4
358.0
359.6
361.2
362.8
364.4
366.0
367.6
354.0
355.6
357.2
358.8
360.4
362.0
363.6
365.2
366.8

Fig. 2. (Contd.)

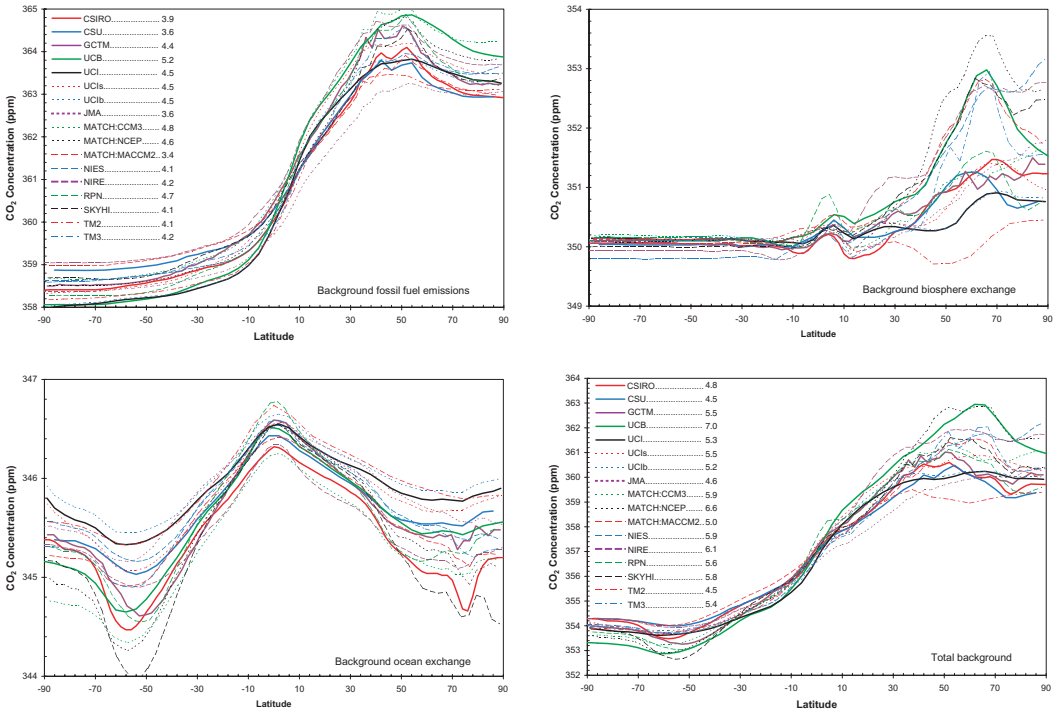

Fig. 3. Annual mean, zonal mean surface CO_2 concentration (ppm) resulting from the individual and combined (relative to a background concentration of 350 ppm) background fluxes for each of the models. The interhemispheric difference (ppm) for the background fossil and combined background CO_2 is listed in the key for each model. Note that the scale is different for each of the plots.

flux response. The 1990 fossil distribution used in this study is the same as that used in TransCom 1 but the total emission is 5.81 Gt C yr^{-1} compared to the 5.3 Gt C yr^{-1} previously used. Allowing for this difference, eight of the TransCom 1 models had IHDs below the current range (Law et al., 1996) indicating an evolution to less vigorous interhemispheric transport.

The zonal mean surface concentration for the biosphere exchange shows more spread in the northern mid- to high latitudes than for fossil fuel emissions. In TransCom 1 (using a different biosphere exchange) the model results clustered into two groups. Here, this clustering is less evident, with models spread throughout the 3.5 ppm range of concentrations around 60–70 °N. The highest concentrations (strongest rectification) are produced by MATCH:NCEP, while the weakest rectification is produced by the TM2 model. The RPN model produces relatively large equatorial concentrations, while the NIRE concentrations are greater than for other models around 20–30 °N. Besides the large variation in zonal mean response to these annually balanced fluxes, the models exhibit large variations in the spatial structure of the rectifier response within latitude zones (Fig. 2). Some strongly rectifying models (e.g., SKYHI, MATCH:MACCM2, RPN) limit concentration maxima to the immediate forcing areas over North America and Asia, where there are no stations. Others (NIES, NIRE, UCB, MATCH:NCEP) generate broad concentration maxima over the northern high latitudes and consequently have substantial impact at observing sites.

The zonal mean surface concentrations for the ocean exchange show similar structure for all models. The tropical source and extratropical uptake results in a small maximum concentration in the tropics, which varies by about 0.5 ppm across the models. Variations in the concentration minima are larger, particularly around 50–60 °S. SKYHI produces the lowest concentrations in both hemispheres, while MATCH:CCM3 exhibits low concentrations across all latitudes. RPN exhibits the largest equatorial maximum concentration. The greatest tropical/extratropical gradient is

exhibited by SKYHI, while UCI and UCIb exhibit the smallest gradients.

The zonal mean surface concentration for the total background fluxes shows how some models respond similarly to the background fluxes while others exhibit offsetting responses. For example, while responding strongly to fossil fuel fluxes over the northern extratropical source region, MATCH:CCM3 and RPN exhibit only a moderate response to the seasonal biosphere exchange. Similarly, MATCH:MACCM2 and NIES, which have a moderate fossil fuel response, show a stronger response to the seasonal biosphere exchange.

The remaining models show some similarity in their response to the background fluxes. In these cases, models that produce large surface gradients for fossil fuel also tend to produce large gradients for the background ocean exchange and exhibit a strong biospheric rectifier. This is broadly consistent with both vertical trapping of CO_2 in the lower model layers and with weaker advective mixing as compared to models exhibiting smaller gradients.

The spatial structure of surface CO_2 simulated by each model in response to the total of these background fluxes is different from the observed spatial variation of the observations. Because the background fluxes are fixed, the adjustment of the 22 regional fluxes is employed in the inversion to minimize this residual concentration response (RCR). The RCR values at all the observing stations (smoothed) is plotted for each model in Fig. 4. All models show positive RCR values in the northern mid-latitudes, implying the need for CO_2 uptake there. The greatest differences in RCR values between models are over the northern mid-latitudes (Fig. 4a). The standard deviation of these RCR values across the 17 models is less than 0.4 ppm at most stations, and greater than 1.0 ppm at 6 stations. The greatest variability is at Hungary ($\sigma = 2.4$ ppm; 47 °N, 16.7 °E).

Models with smaller background IHD values (CSU, JMA, MATCH:MACCM2) simulate higher RCR values over the southern extratropics relative to those with larger background IHD values (UCB, MATCH:NCEP, MATCH:CCM3). This suggests a potential relationship between interhemispheric transport and the magnitude of the inferred fluxes in the southern regions. Models with vigorous interhemispheric transport may require greater uptake over the southern extratropics relative to those models that exhibit weaker interhemispheric transport. Over the northern middle latitudes, where the model spread is greatest, the consistently largest RCR values are simulated by MATCH:NCEP, NIRE and UCB, and the smallest are simulated by TM2, CSU, CSIRO and JMA. These "clusters" of responses may produce similarly clustered inferred regional flux estimates.

The longitudinal distribution of the RCR values over the northern middle latitudes varied considerably among the models (Figs. 4b and 4c), particularly at continental sites near source regions (ITN, BAL, SCH and HUN). In general, RCR values increased from west to east across North America and Europe, which suggests the need for terrestrial uptake in these regions. The largest west to east gradients over North America were exhibited by NIRE and RPN, while the smallest belong to UCIb and TM2. UCIb and TM2 also had the smallest gradients over Europe while MATCH:NCEP and TM3 had the largest.

3.2. *Inversion results*

3.2.1. Model mean sensitivity. The model mean results for the control inversion were presented by Gurney et al. (2002). They found a Southern Ocean sink considerably weaker than the prior estimate of Takahashi et al. (1999). Furthermore, this result was not sensitive to the transport model used and was well constrained by observations. They also found reasonably strong data constraints over the northern continents, with uptake distributed relatively evenly across the northern land regions. Finally, they found a very weak data constraint in the tropics, with tropical flux estimates depending mostly on prior information, mass balance constraint and model transport.

To test the dependence of the model-mean inversion on the prior fluxes and their uncertainties, we performed the series of sensitivity tests described in Table 2. The first represents inversions in which the prior flux uncertainties for both land and ocean basis function regions were increased to 2, 5 and 10 Gt C yr^{-1}, bringing the inversions closer to methods that do not use prior information to constrain the flux estimates. The results of this test are presented in Fig. 5. For most regions, the mean flux estimates (X symbols) are very insensitive to the prior information, and lie within the uncertainty range of the control inversion. Exceptions are regions with few (or no) stations: the tropical and South Atlantic (all cases), northern Africa (± 5 and ± 10 Gt C yr^{-1} cases) and southern Africa and South America (± 10 Gt C yr^{-1} case).

For each model and region, the figure depicts an estimated flux and two uncertainty measures. The first

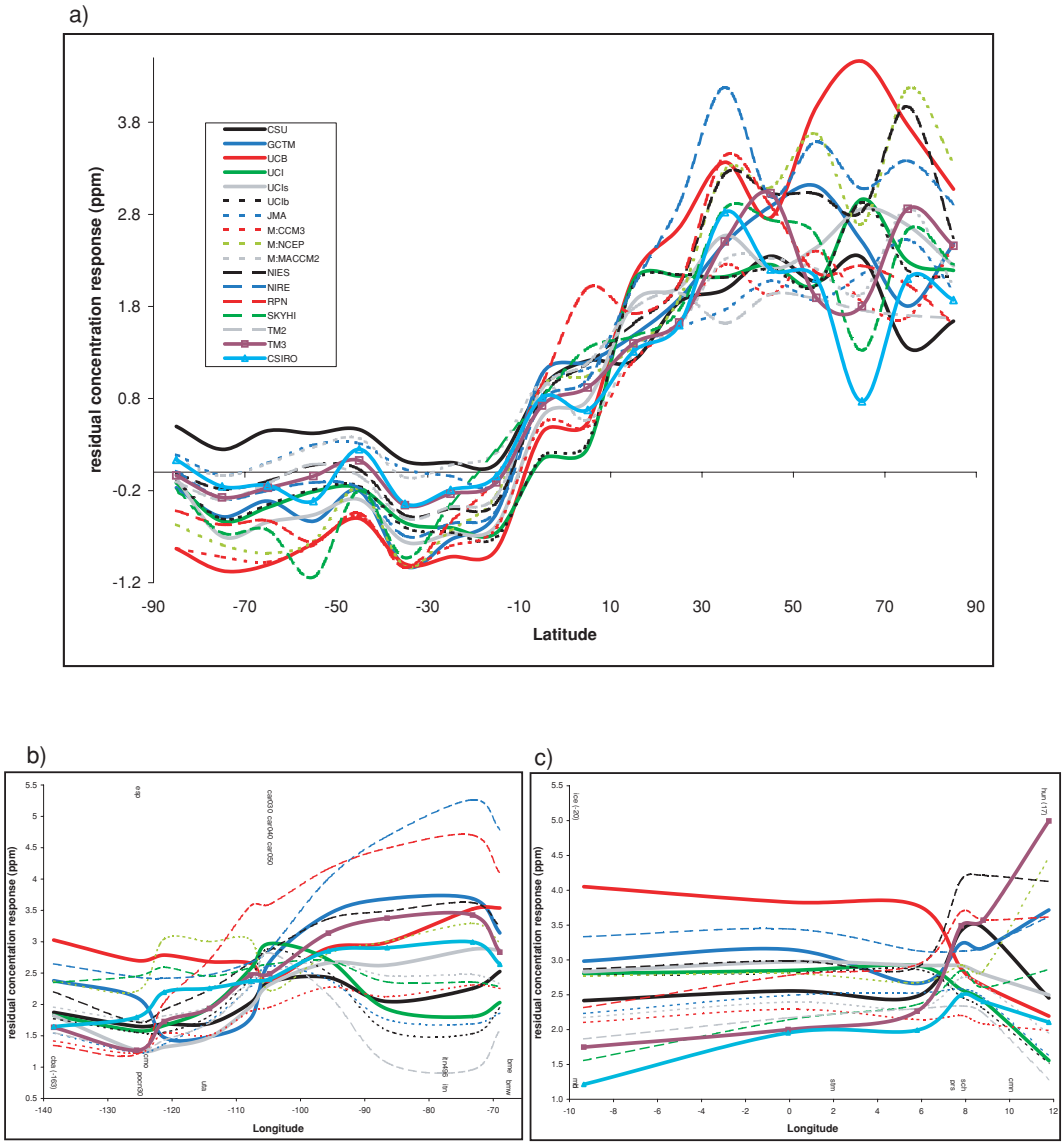

Fig. 4. (a) Smoothed (mean of 10° latitudinal bins) residual concentration response (ppm) at the 76 CO_2 observational stations for each of the models. (b) Smoothed (three station running mean) residual concentration response (ppm) at North American stations within the 30 °N to 70 °N longitudinal band. Longitudes are listed for stations located outside the center of the running mean. (c) Same as (b) but for Europe.

uncertainty measure is the within-model uncertainty (circles) defined in eq. (7). The magnitude of the decrease from the prior uncertainty indicates the degree to which the final flux estimate is constrained by the measurements. Figure 5 shows that for some regions the data constraint dominates. At the other extreme, the within-model uncertainty for some regions increases significantly as the prior flux uncertainty is increased. This indicates that these regions, for example tropical America, are poorly constrained by the CO_2 observations. Note that since the overall growth rate of CO_2 in the atmosphere is specified with small uncertainty

Table 2. *Brief description of the sensitivity tests*

Test 1 ("Loose Priors"): The prior flux uncertainties for both land and ocean basis function regions are increased to 2, 5 and 10 GtC yr^{-1}. These cases bring the inversion closer to those methods that do not use prior information to constrain the flux estimates.

Test 2 ("Zero Land Priors"): The prior basis function land fluxes are set to zero. Since many tropical regions are not well observed, it is important to check how sensitive the flux estimates are to the inclusion of land-use change information in the prior flux estimates.

Test 3 ("No Rect"): The background biospheric exchange is set to zero. This tests the sensitivity of the flux estimates to the rectifier. This case was also shown in Gurney et al. (2002) but here we also show individual model results.

Test 4 ("Adjust Rect"): The background biosphere exchange flux uncertainty is set to ±100%. This tests what rectifier magnitude the inversion estimates.

Test 5 ("Zero Ocean"): The background ocean exchange is set to zero. This tests whether the inversion is sensitive to the spatial distribution in the background ocean flux.

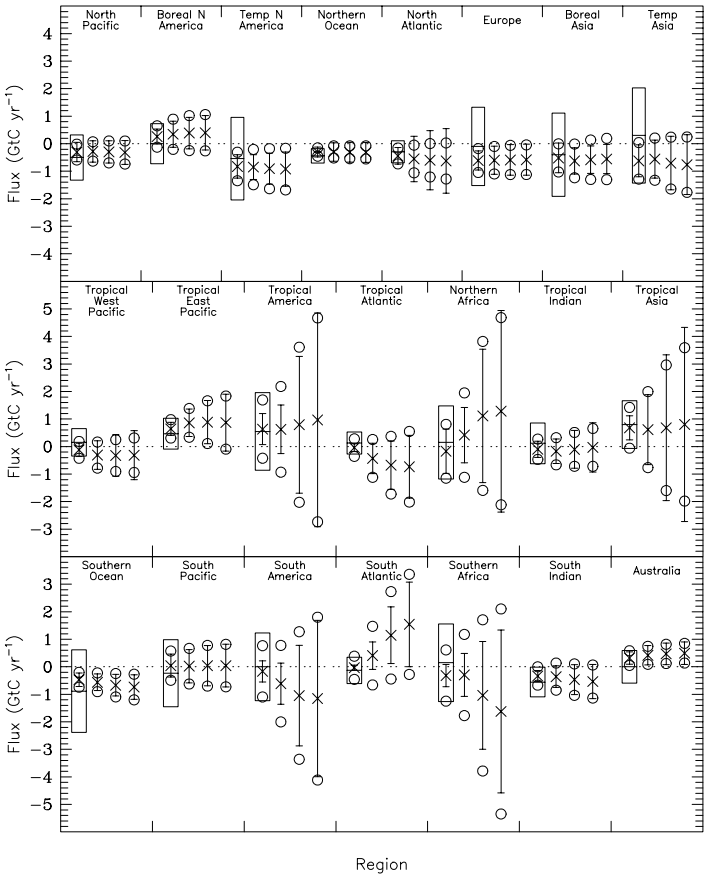

Fig. 5. Results of 'Loose Priors' case (sensitivity test 1). The control inversion is denoted by the leftmost set of symbols [crosses, posterior flux estimate (includes background ocean exchange); circles, within-model flux uncertainty; whiskers, between-model flux uncertainty; outer box, prior flux uncertainty]. The ±2 Gt, ±5 and ±10 Gt C yr^{-1} prior uncertainty cases are denoted progressively to the right of the control inversion. All uncertainties represent 1σ. Mean does not include CSIRO.

(0.074 Gt C yr^{-1}), the sum of the fluxes from the poorly constrained regions is fixed. As the priors are relaxed, dipoles of unrealistically large sources and sinks appear in these regions, but cancel each other to retain the observed mass of CO_2 in the atmosphere.

The second uncertainty measure is the standard deviation of the flux estimates across the ensemble of models (error bars) as defined in eq. (8). This measure indicates the degree to which transport model differences contribute to the range of flux estimates. Overall, the between-model uncertainty increases with the within-model uncertainty in Fig. 5. This reflects the increasing sensitivity of the inversion to differences in transport as the prior flux uncertainty is increased. As the priors are "loosened," we also obtain a somewhat closer fit to the observations: the mean data mismatch drops from 0.89 ppm for the control inversion to 0.77 ppm for ± 10 Gt C yr^{-1} case. This modest decrease in the mean data mismatch further suggests a general lack of sensitivity to the prior flux constraints chosen for the control inversion. The large between-model uncertainty in some regions means that, while the mean estimated flux can be relatively stable, individual models can give some very large fluxes. Overall, we conclude that in regions with strong data constraint, the inferred fluxes are insensitive to the prior fluxes, whereas in regions with few observations the fluxes are sensitive to both prior information and differences in model transport.

Figure 6 shows results from the other four sensitivity tests. When the land prior fluxes are set to zero only the estimated tropical Asian flux changes by greater

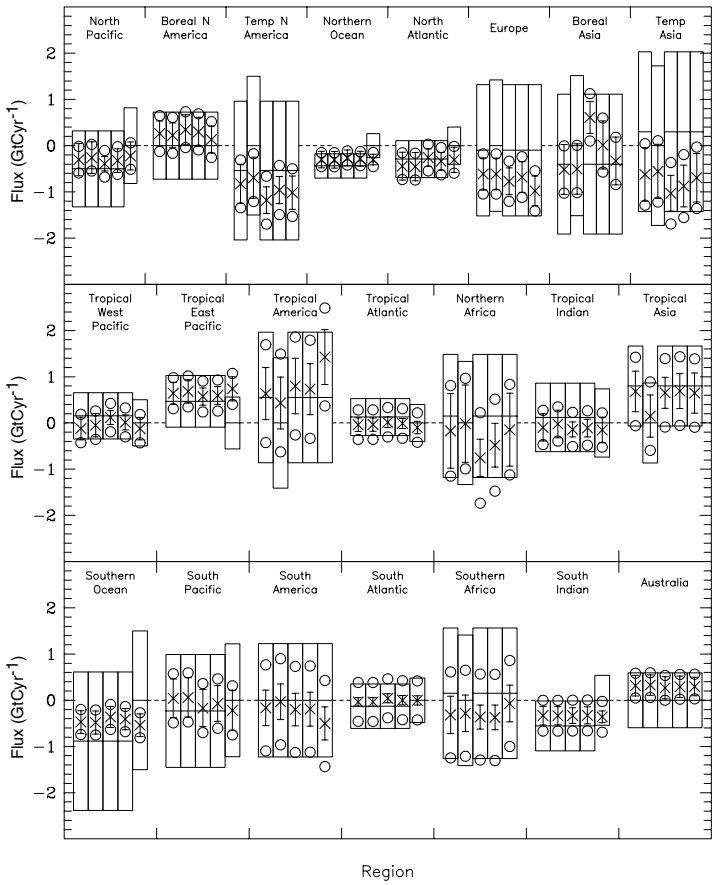

Fig. 6. Results of sensitivity tests 2–5. The control inversion is denoted by the leftmost set of symbols (as in Fig. 5). The 'Zero Land Priors' case (sensitivity test 2), 'No Rect' case (sensitivity test 3), 'Adjust Rect' case (sensitivity test 4), and 'Zero Ocean' (sensitivity test 5) are denoted progressively to the right. Mean does not include CSIRO.

than 0.2 Gt C yr^{-1}. Even for this region, the new flux estimate does not lie outside the control uncertainty range, which at 0.74 Gt C yr^{-1} is not much smaller than its prior uncertainty of 0.87 Gt C yr^{-1}. This is because none of the 76 sites used in the control inversion contributes much constraint to this region.

As described in Gurney et al. (2002), removing the background biosphere fluxes (third set of estimates in Fig. 6) has a large impact in some northern regions where rectification is pronounced; mean flux estimates change by up to 1.1 Gt C yr^{-1} and between-model uncertainty is generally reduced. For example, in almost all models, Boreal Asia changes from a moderate sink to a moderate source. In Test 4, we allow the inversion to optimize the magnitude of the seasonal rectifier by associating a large prior uncertainty ($\pm$100%) with the annually balanced biospheric flux. This tends to produce fluxes that are mid-way between the control and the 'No Rect' case, consistent with the 50% reduction in the model mean annually balanced biospheric exchange. In the final test, removing the background ocean flux had a larger impact in many of the land regions compared to oceanic regions, probably due to the generally larger prior uncertainties for land regions. However, none of the flux changes is larger than the control within-model uncertainties for the appropriate region.

3.2.2. Individual model results. Table 3 lists the control inversion flux estimates for the individual models when the land and ocean regions have been aggregated separately into the southern extratropics, tropics and northern extratropics. Figure 7 shows similar information, plotted as *differences from the model mean flux* for each region, along with flux differences for the 'No Rect' (test 3) and 'Zero Ocean' (test 5) sensitivity tests. The total land and total ocean flux estimates exhibit considerable spread and are anti-correlated since the total source is constrained. MATCH:NCEP and CSIRO produce flux estimates that lie outside the relatively large within-model uncertainties on the total land and total ocean regions. Removal of the background ocean flux reduces the extent to which these two models are outliers, with their flux estimates now inside the within-model uncertainty range. It is not clear why these two models respond in this way, since the strength of their responses to the background ocean tracer are similar to those of other models.

For the northern, tropical and southern regions, there is greater model spread for the aggregated land regions than for the oceans. This is driven by a combination of the larger variability in model response to annually balanced biospheric versus oceanic background fluxes (Figs. 2 and 3) and the larger prior flux uncertainties for land versus ocean regions. The influence of the annually balanced biospheric flux response is indicated by the considerable reduction in model spread in the 'No Rect' sensitivity test. Further evidence for this relationship is indicated by a strong correlation ($r = -0.74$) between the estimated northern land flux for each model and the annually balanced biosphere IHD values whereas there is no correlation with the fossil fuel IHD values ($r = -0.04$). Finally, the largest northern land changes between the control inversion and the 'No Rect' sensitivity test occur for those models with the largest rectifier: MATCH:NCEP, MATCH:MACCM2, NIES, UCB and TM3.

The tropical land flux estimates are negatively correlated ($r = -0.81$) with the northern land estimates. This occurs because the global growth rate is specified and with little observational constraint near the tropical continents, these tropical regions act as a repository for the flux residual remaining after optimization is made to regions with stronger observational constraints. Not surprisingly, MATCH:NCEP, with the largest rectifier, exhibits the largest tropical land flux change (2.2 Gt C yr^{-1} source to -0.1 Gt C yr^{-1} sink) when the rectifier is excluded in the 'No Rect' test.

The aggregated southern ocean flux estimates show the least amount of model spread. As suggested by the correlation ($r = 0.55$) between the total background flux IHD and the aggregated southern ocean posterior flux estimate, weaker interhemispheric transport (large background IHD values) correlates with less aggregated southern ocean uptake relative to the background ocean flux (-1.8 Gt C yr^{-1}). This lends support to our speculation that weak interhemispheric transport leads to lower southern hemisphere RCR values which, in turn, result in less uptake in the aggregated southern ocean relative to the background flux in this region. However, this relationship does not hold when the southern land and southern ocean are combined, suggesting the influence of other factors such as anomalously strong responses at particular stations or compensating tradeoffs with other regions.

Table 4 lists the individual model flux estimates and their uncertainties for all 22 land and ocean regions. Figure 8 shows similar information plotted as differences from the model mean flux for each region, for the control inversion and the 'No Rect' sensitivity test. Table 5 lists the change in individual model flux estimates when the inversion is run without the

Table 3. *Aggregated posterior fluxes and within-model uncertainties (1σ, $GtCyr^{-1}$) for individual models, control inversion*[a]

Model\Region	North land	North ocean	Tropical land	Tropical ocean	South land	South ocean	Total land	Total ocean
CSU	-2.5 ± 0.6	-1.7 ± 0.5	2.8 ± 1.4	0.9 ± 0.8	-0.7 ± 1.2	-1.6 ± 0.6	-0.5 ± 1.3	-2.4 ± 1.3
UCB	-2.9 ± 0.6	-1.1 ± 0.6	2.1 ± 1.3	0.3 ± 0.7	-0.4 ± 1.1	-0.8 ± 0.7	-1.1 ± 1.2	-1.7 ± 1.2
UCI	-1.4 ± 0.7	-1.6 ± 0.6	-0.3 ± 1.4	0.8 ± 0.7	0.7 ± 1.0	-1.0 ± 0.7	-1.1 ± 1.2	-1.7 ± 1.2
UCIs	-1.5 ± 0.7	-1.1 ± 0.6	-0.8 ± 1.3	1.1 ± 0.7	0.3 ± 1.2	-0.8 ± 0.7	$-2.0 \pm .13$	-0.8 ± 1.3
UCIb	-1.4 ± 0.7	-1.6 ± 0.6	-0.4 ± 1.4	0.9 ± 0.6	0.7 ± 1.0	-1.0 ± 0.7	-1.1 ± 1.1	-1.7 ± 1.1
JMA	-2.0 ± 0.7	-0.7 ± 0.6	0.9 ± 1.5	-0.0 ± 0.7	0.1 ± 1.2	-1.1 ± 0.8	-1.0 ± 1.3	-1.8 ± 1.3
M:CCM3	-2.5 ± 0.6	-0.7 ± 0.5	0.7 ± 1.3	0.6 ± 0.7	-0.3 ± 1.1	-0.6 ± 0.6	-2.1 ± 1.2	-0.7 ± 1.2
M:NCEP	-3.6 ± 0.5	-0.0 ± 0.4	2.2 ± 1.2	0.6 ± 0.7	-2.0 ± 1.0	0.1 ± 0.6	-3.4 ± 1.1	0.6 ± 1.1
M:MACCM2	-3.4 ± 0.6	-0.3 ± 0.5	1.8 ± 1.4	0.8 ± 0.8	-0.3 ± 1.2	-1.4 ± 0.7	-1.9 ± 1.2	-0.9 ± 1.2
NIES	-3.2 ± 0.6	-0.5 ± 0.4	2.2 ± 1.3	-0.3 ± 0.6	-0.1 ± 1.1	-0.8 ± 0.7	-1.2 ± 1.0	-1.6 ± 1.0
NIRE	-2.5 ± 0.6	-2.1 ± 0.4	1.2 ± 1.3	0.5 ± 0.5	0.4 ± 1.1	-0.4 ± 0.6	-0.8 ± 0.9	-2.0 ± 0.9
RPN	-2.0 ± 0.6	-1.3 ± 0.4	1.0 ± 1.0	-0.4 ± 0.7	-0.2 ± 0.9	0.1 ± 0.6	-1.2 ± 1.1	-1.6 ± 1.1
SKYHI	-3.2 ± 0.6	-0.9 ± 0.3	2.9 ± 1.3	-0.2 ± 0.6	-0.5 ± 1.1	-1.0 ± 0.6	-0.7 ± 1.0	-2.1 ± 1.0
TM2	-0.8 ± 0.6	-1.6 ± 0.5	-0.2 ± 1.5	-0.0 ± 0.5	0.6 ± 1.2	-0.9 ± 0.7	-0.3 ± 1.2	-2.5 ± 1.2
TM3	-3.1 ± 0.5	0.1 ± 0.4	1.4 ± 1.2	0.5 ± 0.6	-0.5 ± 1.1	-1.2 ± 0.7	-2.2 ± 1.1	-0.6 ± 1.1
GCTM	-1.2 ± 0.5	-1.6 ± 0.4	0.8 ± 1.4	0.2 ± 0.6	-0.4 ± 1.2	-0.5 ± 0.6	-0.9 ± 1.0	-1.9 ± 1.0
CSIRO	-2.7 ± 0.6	-0.1 ± 0.4	1.3 ± 1.3	0.5 ± 0.8	-1.3 ± 1.1	-0.5 ± 0.7	-2.7 ± 1.2	-0.1 ± 1.2
Mean	$\mathbf{-2.3 \pm 0.6}$	$\mathbf{-1.1 \pm 0.5}$	$\mathbf{1.1 \pm 1.3}$	$\mathbf{0.4 \pm 0.7}$	$\mathbf{-0.2 \pm 1.1}$	$\mathbf{-0.8 \pm 0.7}$	$\mathbf{-1.3 \pm 1.1}$	$\mathbf{-1.5 \pm 1.1}$

[a]The background ocean flux has been included in the oceanic fluxes. Regional aggregation is as follows: North land (Boreal North America, Temperate North America, Europe, Boreal Asia, Temperate Asia), North ocean (North Pacific, Northern Ocean, North Atlantic), Tropical land (Northern Africa, Tropical Asia, Tropical America), Tropical ocean (West Pacific, East Pacific, Tropical Atlantic, Tropical Indian), South land (Southern Africa, Australia, South America), South ocean (South Pacific, South Atlantic, South Indian, Southern Ocean). The mean sources do not include the CSIRO model. Units: GtC yr^{-1}

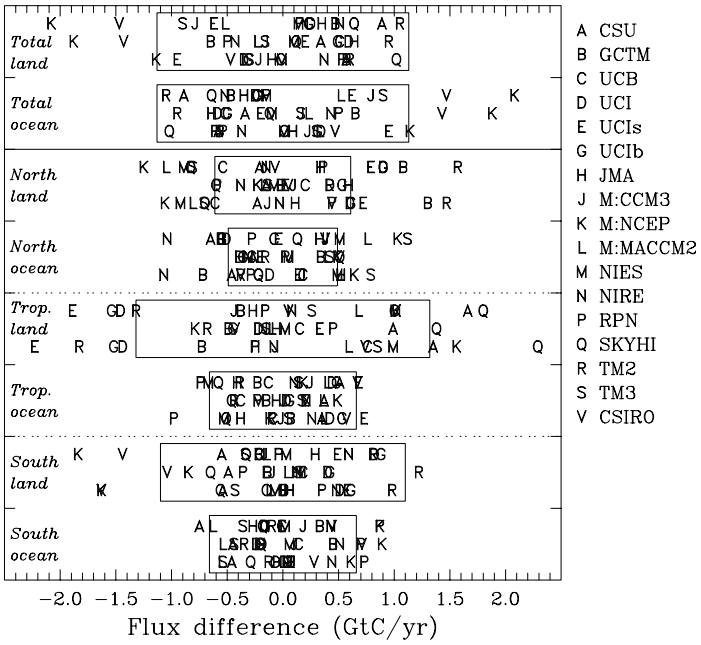

Fig. 7. Aggregated posterior flux differences from the model mean for the control inversion (top row in each box), the 'No Rect' case (sensitivity test 3, middle row in each box) and the 'Zero Ocean' case (sensitivity test 5, bottom row in each box). The box represents the within-model uncertainty (1σ). Regional aggregation is as follows: North land (Boreal N America, Temperate N America, Europe, Boreal Asia, Temperate Asia), North ocean (N Pacific, Northern Ocean, N Atlantic), Tropical land (Northern Africa, Tropical Asia, Tropical America), Tropical ocean (W Pacific, E Pacific, Tropical Atlantic, Tropical Indian), South land (Southern Africa, Australia, S America), South ocean (S Pacific, S Atlantic, S Indian, Southern Ocean).

background biospheric exchange. Most model flux estimates lie within the estimated uncertainty for the respective regions in Fig. 8. This demonstrates that the within-model uncertainty encompasses most transport differences with different models providing the extreme or outlying estimates in different regions. As was noted in the aggregated flux estimates, some of the outlying total zonal estimates can be attributed to the meridional gradient of the background fluxes. Results for the complete 22 basis function regions exhibits some longitudinal tradeoffs as well. For example, many models with large uptake in extratropical Asia such as MATCH:MACCM2. MATCH:NCEP and CSIRO show large downwind sources in the North Pacific region. Models with small combined uptake in extratropical Asia, such as TM2, show the largest uptake in the North Pacific.

The two models with the greatest combined uptake in North America, RPN (-1.11 Gt C yr^{-1}) and NIRE (-1.06 Gt C yr^{-1}), support the suggestion that large west to east declines in the RCR values are related to enhanced uptake. However, models with the smallest North American uptake (UCIb and GCTM) are not those with the smallest west to east gradient. Over Europe, the models with the smallest west to east gradient, UCIb and TM2, are among the three models with the smallest European uptake. Among those with the largest European west to east RCR gradient, both NIES and TM3 also exhibit among the greatest levels of uptake. UCB, however, has an average gradient but considerable uptake in Europe. In northern extratropical Asia, the relationship between the RCR west to east gradient and the estimated flux appears less consistent.

Another example of a relationship between the background fluxes and the model estimates of region-specific fluxes arises in the Southern Ocean region. Models that estimated the smallest uptake for the Southern Ocean region, SKYHI and MATCH:NCEP, were also models that responded most strongly to the background ocean flux (Figs. 2 and 3), particularly in the southern extratropics. They were also among the models with the lowest RCR values in the southern extratropics. Similarly, the responses of the CSIRO

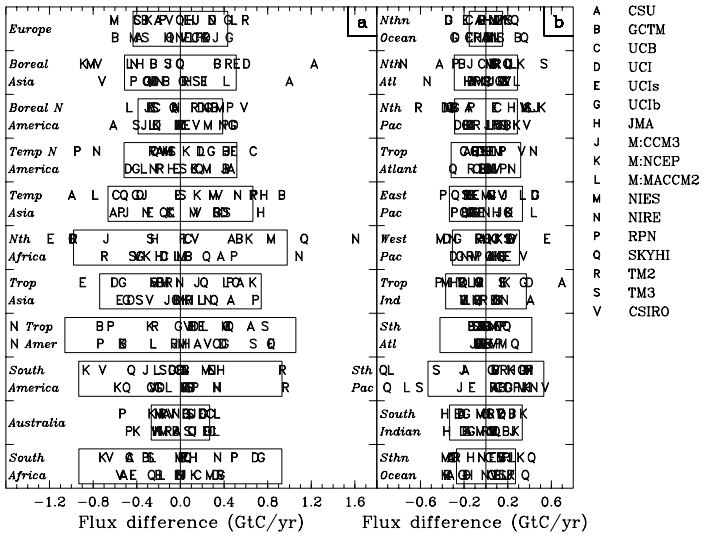

Fig. 8. Posterior flux differences from the 16 model mean for the control inversion (top row in each box) and the 'No Rect' case (sensitivity test 3, bottom row in each box). The boxes represent the 16 model mean within-model uncertainty (1σ).

and SKYHI models to the background ocean flux in the northern extratropics were the most pronounced (Fig. 3) and they also produced the least uptake in the northern ocean.

In contrast to the dependence of the estimated fluxes on the gradients in the background concentrations, there are a variety of instances in which outlying flux estimates are much more dependent on model responses at particular sites. For example, two models produce very large uptake for temperate North America, NIRE and RPN, but for different reasons. RPN is one of two models with a pronounced fossil fuel response, particularly over temperate North America. RPN also exhibits one of the weaker rectifier responses. As a result, RPN exhibits the largest uptake for the temperate North American region but shows little change in North America when the background biospheric exchange is removed. NIRE has larger responses than other models at Key Biscayne for background fossil and biospheric fluxes and for the temperate North American region. This results in significant uptake for the NIRE model in the temperate North American region, greater than all the models except RPN. This is confirmed by an inversion in which CO_2 data for Key Biscayne are excluded. The NIRE flux difference from the mean is reduced from -0.76 to -0.24 Gt C yr^{-1}.

As with the aggregated flux estimates, Table 5 shows significant changes over the northern land regions when the background biosphere exchange is removed from the inversion. In particular, large changes occur over Boreal Asia where nearly all of the models shift from uptake to emissions. The tropical land regions also exhibit shifts when inverting without the annually balanced biosphere. In particular, northern Africa becomes a sink instead of a source in many models (or in the case of NIRE, a much reduced source) when the annually balanced biosphere is removed. This apparent compensation between northern rectifier response and tropical terrestrial fluxes results from the global mass balance constraint and the relatively small ocean priors.

Models that exhibit significant surface gradients in response to the biospheric exchange are not always the models showing large shifts when the inversion excludes this background flux. This is due to the spatial pattern of the rectifier in relation to the position of the observational stations. For example, SKYHI shows one of the larger rectifiers (Figs. 2 and 3), but shows only a moderate shift in estimated flux when the background biospheric flux is removed. This is due to the somewhat limited horizontal transport of background biospheric flux near the surface over northern and eastern Asia. Since the four stations nearest to this region are located towards the eastern edge of the Asian continent, the response at these stations does not reflect the strength of the SKYHI rectification over central portions of Asia.

Table 4. *Posterior fluxes and uncertainties (1σ, $GtCyr^{-1}$) for individual models, control inversion*[a]

Region\Model	CSU	UCB	UCI	UCIs	UCIb	JMA	MATCH: CCM3	MATCH: NCEP
Boreal NA	0.21 ± 0.57	0.04 ± 0.23	0.45 ± 0.29	0.00 ± 0.37	0.51 ± 0.27	0.22 ± 0.53	−0.04 ± 0.04	−0.01 ± 0.38
Temperate NA	−1.02 ± 0.57	−0.16 ± 0.55	−0.64 ± 0.62	−0.34 ± 0.61	−0.55 ± 0.62	−0.93 ± 0.64	−0.40 ± 0.53	−0.77 ± 0.43
Trop America	1.28 ± 1.09	1.06 ± 1.06	0.76 ± 1.02	0.83 ± 1.04	0.61 ± 0.99	0.74 ± 1.13	0.72 ± 1.06	0.36 ± 1.09
South America	−0.13 ± 0.98	−0.18 ± 0.91	−0.24 ± 0.90	0.12 ± 0.96	−0.24 ± 0.90	0.20 ± 1.01	−0.48 ± 0.94	−1.03 ± 0.88
Northern Africa	0.30 ± 1.08	−0.10 ± 0.94	−1.16 ± 0.95	−1.36 ± 0.86	−1.16 ± 0.95	−0.41 ± 1.08	−0.85 ± 0.97	0.46 ± 0.91
Southern Africa	−0.78 ± 0.80	−0.79 ± 0.82	0.37 ± 0.64	−0.31 ± 1.02	0.42 ± 0.66	−0.20 ± 1.13	−0.29v0.78	−1.03 ± 0.74
Boreal Asia	0.71 ± 0.52	−0.53 ± 0.55	0.09 ± 0.58	0.00 ± 0.53	−0.18 ± 0.56	−0.89 ± 0.55	−0.63 ± 0.64	−1.41 ± 0.43
Temperate Asia	−1.62 ± 0.79	−1.21 ± 0.59	−0.99 ± 0.81	−0.64 ± 0.69	−1.03 ± 0.79	0.14 ± 0.79	−0.96 ± 0.60	−0.47 ± 0.54
Tropical Asia	1.23 ± 0.73	1.19 ± 0.79	0.08 ± 0.80	−0.22 ± 0.73	0.15 ± 0.80	0.54 ± 0.70	0.83 ± 0.78	1.34 ± 0.76
Australia	0.19 ± 0.33	0.59 ± 0.36	0.52 ± 0.34	0.51 ± 0.30	0.53 ± 0.29	0.12 ± 0.26	0.43 ± 0.30	0.05 ± 0.19
Europe	−0.82 ± 0.50	−1.01 ± 0.39	−0.32 ± 0.52	−0.55 ± 0.43	−0.18 ± 0.54	−0.52 ± 0.54	−0.47 ± 0.51	−0.90 ± 0.30
N Pacific	−0.46 ± 0.28	−0.20 ± 0.35	−0.68 ± 0.37	−0.22 ± 0.33	−0.58 ± 0.34	−0.07 ± 0.40	0.16 ± 0.31	0.21 ± 0.23
W Pacific	−0.16 ± 0.30	−0.04 ± 0.35	−0.48 ± 0.35	0.44 ± 0.31	−0.38 ± 0.29	−0.12 ± 0.37	−0.03 ± 0.32	0.00 ± 0.35
E Pacific	0.67 ± 0.45	0.70 ± 0.34	1.09 ± 0.33	0.55 ± 0.30	1.10 ± 0.33	0.49 ± 0.36	0.81 ± 0.39	0.53 ± 0.39
S Pacific	−0.15 ± 0.48	0.09 ± 0.59	0.38 ± 0.56	0.12 ± 0.63	0.37 ± 0.50	0.28 ± 0.61	−0.18 ± 0.52	0.27 ± 0.51
Northern Ocean	−0.37 ± 0.15	−0.46 ± 0.17	−0.65 ± 0.21	−0.49 ± 0.18	−0.64 ± 0.20	−0.29 ± 0.17	−0.24 ± 0.12	−0.10 ± 0.13
N Atlantic	−0.87 ± 0.35	−0.48 ± 0.29	−0.24 ± 0.32	−0.38 ± 0.32	−0.37 ± 0.29	−0.36 ± 0.33	−0.59 ± 0.30	−0.12 ± 0.28
Tropical Atlantic	−0.21 ± 0.31	−0.24 ± 0.34	−0.09 ± 0.36	0.02 ± 0.33	−0.09 ± 0.35	−0.01 ± 0.34	−0.01 ± 0.32	−0.04 ± 0.34
S Atlantic	−0.05 ± 0.44	−0.12 ± 0.44	−0.04 ± 0.46	0.08 ± 0.43	−0.03 ± 0.46	−0.03 ± 0.43	−0.10 ± 0.45	−0.05 ± 0.43
Southern Ocean	−0.79 ± 0.29	−0.44 ± 0.23	−0.75 ± 0.36	−0.41 ± 0.26	−0.79 ± 0.35	−0.61 ± 0.27	−0.25 ± 0.22	−0.15 ± 0.19
Trop Ind Ocean	0.60 ± 0.50	−0.17 ± 0.32	0.30 ± 0.40	0.06 ± 0.46	0.25 ± 0.33	−0.39 ± 0.43	−0.15 ± 0.38	0.09 ± 0.36
S Indian Ocean	−0.56 ± 0.37	−0.34 ± 0.36	−0.56 ± 0.41	−0.59 ± 0.39	−0.51 ± 0.39	−0.71 ± 0.38	−0.10 ± 0.33	0.01 ± 0.27
Glbl offset (ppm)	352.9 ± 0.2	352.6 ± 0.2	352.6 ± 0.2	352.3 ± 0.2	352.4 ± 0.2	352.9 ± 0.2	352.3 ± 0.2	352.5 ± 0.2

[a]The background ocean flux has been included in the oceanic fluxes.

Some ocean regions also show significant shifts between inversions with and without the biosphere exchange. For example, both the North Pacific and North Atlantic exhibit the largest ocean region shifts between the two cases, highlighting the downwind transport of the rectifier signal.

4. Discussion and conclusions

The TransCom 3 experiment has afforded the first thorough investigation of the extent to which transport differences among tracer models contribute to the overall uncertainty in inversion estimates of carbon sources and sinks. Fortunately, most of the models that have been used to perform carbon cycle inversions in the last decade participated in the current experiment. In addition to investigating the sensitivity of carbon inversions to transport, we have been able to compute a model mean result and test the sensitivity of the model mean to various aspects of the inversion setup. A companion paper (Law et al., 2003) extends these sensitivity tests by exploring the response of the model mean and individual model flux estimates to changes in the observation network, the observational uncertainties, baseline data selection criteria and time period.

The first and perhaps most important result of this experiment is that model transport is as large a contributor to the inversion uncertainty as the error produced by limited CO_2 observations. Some of the individual model estimated fluxes can be readily attributed to how they respond to the background flux fields. Models that exhibited large CO_2 concentration maxima near and downwind of large background fluxes estimate large uptake in those same regions in order to best match the CO_2 observations. Models with small CO_2 concentration maxima estimated less uptake near the background fluxes but compensated further downwind over ocean regions with weaker sources or small sinks. The model response to background fluxes was not always the best predictor, however. Many of the regional flux estimates for individual models were the result of strong responses at particular stations or subtle tradeoffs and compensation among regions.

The response to surface SF_6 fluxes was evaluated in the previous TransCom 2 experiment (Denning et al., 1999). Models exhibiting small surface concentration maxima like TM2 and an earlier variant of the UCB model systematically underestimated the observed meridional gradient of SF_6 in the remote marine boundary layer, so these models probably also underestimate regional fluxes in the present inversions. On the other hand, models exhibiting large surface

Table 4. *(cont'd.)*

MATCH: MACCM2	NIES	NIRE	RPN	SKYHI	TM2	TM3	GCTM	CSIRO
−0.21 ± 0.32	0.62 ± 0.44	0.49 ± 0.44	0.71 ± 0.28	0.20 ± 0.37	0.39 ± 0.51	0.03 ± 0.52	0.57 ± 0.25	0.33 ± 0.41
−0.64 ± 0.50	−0.95 ± 0.46	−1.60 ± 0.44	−1.77 ± 0.33	−1.06 ± 0.49	−1.09 ± 0.47	−0.91 ± 0.41	−0.41 ± 0.51	−0.63 ± 0.48
0.85 ± 1014	1.05 ± 10.2	−0.89 ± 1.07	−0.01 ± 0.95	1.08 ± 0.98	0.40 ± 1.18	1.41 ± 0.92	−0.11 ± 1.17	0.87 ± 1.05
−0.39 ± 1.00	0.07 ± 0.94	0.12 ± 0.91	−0.17 ± 0.85	−0.62 ± 0.85	0.77 ± 0.99	−0.33 ± 0.92	−0.12 ± 0.95	−0.85 ± 0.87
−0.12 ± 1.13	0.66 ± 0.88	1.44 ± 0.94	−0.15 ± 0.80	0.96 ± 1.06	−1.15 ± 1.08	−0.45 ± 0.95	0.37 ± 1.02	−0.05 ± 1.01
−0.58 ± 1.15	−0.33 ± 0.91	0.02 ± 0.93	0.18 ± 0.51	−0.25 ± 1.19	−0.28 ± 1.02	−0.59 ± 1.04	−0.64 ± 1.17	−0.81 ± 1.15
−0.99 ± 0.63	−1.34 ± 0.37	−0.94 ± 0.44	−0.18 ± 0.48	−0.52 ± 0.40	−0.08 ± 0.54	−0.63 ± 0.48	−0.76 ± 0.38	−1.70 ± 0.58
−1.41 ± 0.71	−0.32 ± 0.62	−0.10 ± 0.68	0.05 ± 0.67	−1.14 ± 0.62	0.04 ± 0.61	−0.61 ± 0.36	0.31 ± 0.59	−0.24 ± 0.70
1.09 ± 0.79	0.44 ± 0.72	0.67 ± 0.67	1.13 ± 0.66	0.90 ± 0.68	0.57 ± 0.79	0.44 ± 0.72	0.49 ± 0.72	0.44 ± 0.72
0.65 ± 0.35	0.12 ± 0.24	0.27 ± 0.15	−0.22 ± 0.22	0.37 ± 0.22	0.15 ± 0.14	0.41 ± 0.27	0.36 ± 0.19	0.40 ± 0.36
−0.13 ± 0.51	−1.22 ± 0.35	−0.32 ± 0.29	−0.78 ± 0.34	−0.62 ± 0.33	−0.02 ± 0.58	−1.01 ± 0.29	−0.94 ± 0.32	−0.47 ± 0.41
0.10 ± 0.33	0.06 ± 0.21	−0.66 ± 0.21	−0.44 ± 0.18	−0.63 ± 0.16	−0.92 ± 0.30	0.08 ± 0.26	−0.60 ± 0.21	0.28 ± 0.26
0.09 ± 0.38	−0.54 ± 0.30	−0.43 ± 0.21	−0.18 ± 0.18	−0.10 ± 0.34	−0.19 ± 0.28	0.08 ± 0.26	0.11 ± 0.26	−0.11 ± 0.36
0.98 ± 0.33	0.64 ± 0.33	0.69 ± 0.27	0.25 ± 0.32	0.36 ± 0.34	0.47 ± 0.20	0.46 ± 0.32	0.51 ± 0.28	0.76 ± 0.42
−0.84 ± 0.56	0.42 ± 0.43	0.44 ± 0.28	0.44 ± 0.43	−0.90 ± 0.52	0.20 ± 0.52	−0.41 ± 0.66	0.13 ± 0.57	0.02 ± 0.60
−0.19 ± 0.13	−0.19 ± 0.17	−0.23 ± 0.14	−0.17 ± 0.13	−0.04 ± 0.09	−0.34 ± 0.18	−0.09 ± 0.13	−0.34 ± 0.09	0.09 ± 0.08
−0.20 ± 0.30	−0.41 ± 0.29	−1.20 ± 0.26	−0.72 ± 0.26	−0.25 ± 0.20	−0.34 ± 0.27	0.09 ± 0.27	−0.67 ± 0.27	−0.51 ± 0.28
−0.04 ± 0.31	0.08 ± 0.34	0.40 ± 0.28	0.11 ± 0.29	−0.14 ± 0.28	−0.13 ± 0.32	−0.06 ± 0.32	−0.14 ± 0.24	0.33 ± 0.32
−0.17 ± 0.42	0.02 ± 0.37	0.03 ± 0.39	0.12 ± 0.43	0.15 ± 0.33	−0.08 ± 0.43	−0.13 ± 0.41	−0.17 ± 0.41	0.19 ± 0.37
−0.24 ± 0.27	−0.84 ± 0.30	−0.51 ± 0.29	−0.29 ± 0.24	−0.05 ± 0.16	−0.74 ± 0.35	−0.32 ± 0.25	−0.34 ± 0.22	−0.34 ± 0.16
−0.24 ± 0.44	−0.47 ± 0.34	−0.18 ± 0.26	−0.53 ± 0.39	−0.31 ± 0.31	−0.15 ± 0.25	0.05 ± 0.33	−0.32 ± 0.29	−0.44 ± 0.43
−0.19 ± 0.27	−0.38 ± 0.31	−0.33 ± 0.31	−0.20 ± 0.33	−0.19 ± 0.26	−0.29 ± 0.34	−0.29 ± 0.29	−0.09 ± 0.26	−0.34 ± 0.33
352.6 ± 0.2	352.7 ± 0.2	352.3 ± 0.2	352.5 ± 0.2	352.6 ± 0.2	352.7 ± 0.2	352.6 ± 0.2	352.5 ± 0.2	352.6 ± 0.2

concentration maxima like TM3, which performed better at marine stations, tended to overestimate continental concentrations of SF_6 near source regions, possibly reflecting excessive vertical trapping of tracer. A combination of model resolution, resolved advective transport and subgrid-scale vertical transport defines this tradeoff between meridional gradients and regional concentration extrema which produce most of the variability in model response and therefore in flux uncertainty.

When the fluxes in the current experiment are aggregated into three zonal bands for the ocean and land, they provide some instructive examples of model behaviour in estimating zonally integrated fluxes. The tight ocean constraints of the inversion setup and the greater variability in model response to the terrestrial background fluxes explain the greater model spread in the estimates for land versus ocean regions. Removal of the background biospheric exchange considerably reduces the model spread over land. Furthermore, the tropical land exchange is inversely related to the northern land uptake, highlighting the influence of the limited observational constraint in the tropical regions and the required compliance with the overall meridional gradient in the CO_2 observations. The influence of the rectifier emphasizes the need to observe and understand this phenomenon. Because incorrect spatial and temporal structure in this background flux cannot be adjusted by the inversion procedure, errors in the specification of the background flux will be aliased into errors in the regional flux estimates. Future TransCom work in which fluxes are adjusted on a monthly basis will eliminate much of the fixed temporal structure required by the current annual mean inversion.

The last conclusion that can be drawn from the aggregated flux estimates is the relationship between the Southern Ocean uptake and interhemispheric transport; models with large background flux IHDs and hence weak interhemispheric transport tend to estimate the greatest reduction in uptake when compared to the background ocean flux for this region. Like many of the other broad relationships between the background fluxes and the estimated model fluxes, this relationship is not universal to all the models and some exceptions remain.

Examination of the 22 regional flux estimates across the models further indicates some relationships to the background flux responses, though generalization is much more challenging. For example, models with a strong response to the background ocean flux estimate the least uptake in both the Southern Ocean and northern ocean regions. Models with large west to east RCR gradients across North America and Europe are among the models with the greatest uptake in these regions. However, models with small gradients are not necessarily those with little uptake in these regions.

Table 5. *Posterior flux differences in Gt C yr^{-1} for inversion performed without background biosphere flux (control case minus 'No Rect' sensitivity test)*

Region\Model	CSU	UCB	UCI	UCIs	UCIb	JMA	MATCH: CCM3	MATCH: NCEP	MATCH: MACCM2	NIES	NIRE	RPN	SKYHI	TM2	TM3	GCTM	CSIRO
Boreal NA	0.48	−0.32	−0.39	−0.41	−0.31	−0.12	−0.05	−0.14	−0.29	0.03	−0.26	−0.04	0.07	0.05	0.09	0.25	0.11
Temperate NA	−0.30	0.89	1.01	0.88	1.04	0.33	0.38	0.28	0.88	−0.01	−0.16	−0.40	−0.06	0.28	0.25	0.35	0.26
Tropical America	0.32	−0.08	−0.42	−0.80	−0.59	−0.11	−0.03	0.09	0.31	0.23	−0.17	−0.07	−0.55	−0.34	−0.06	−0.38	−0.26
South America	0.02	0.29	0.14	0.27	0.16	0.06	−0.03	−0.25	−0.07	0.22	−0.25	−0.10	0.08	0.01	−0.20	−0.02	−0.33
Northern Africa	0.68	0.80	−0.25	−0.66	−0.03	0.54	−0.12	1.52	0.67	1.41	1.09	0.12	1.48	0.30	0.75	1.05	1.02
Southern Africa	0.10	−0.58	0.41	0.49	0.41	0.17	0.05	−0.79	−0.04	−0.23	0.36	0.56	0.37	−0.28	−0.22	−0.07	0.01
Boreal Asia	−0.90	−1.15	−0.29	−0.83	−0.48	−1.57	−1.45	−1.76	−2.02	−1.69	−1.35	−0.36	−0.83	−0.73	−1.39	−1.24	−1.89
Temperate Asia	0.03	−0.09	−0.37	0.67	−0.34	0.44	0.58	0.66	−0.29	0.59	1.20	1.63	0.04	0.74	0.00	1.01	0.90
Tropical Asia	0.11	0.58	−0.12	−0.31	−0.01	−0.19	0.30	0.64	0.26	−0.20	−0.06	−0.21	−0.06	−0.15	0.17	−0.12	0.07
Australia	−0.05	0.03	0.00	0.01	0.01	0.07	0.04	0.19	0.06	0.01	−0.05	−0.01	0.00	0.00	0.07	0.14	0.13
Europe	0.33	−0.37	0.21	0.16	0.14	0.36	−0.02	−0.35	0.53	−0.02	0.46	−0.18	0.25	0.52	0.08	0.43	0.06
N Pacific	0.07	0.34	−0.03	0.35	−0.01	0.47	0.54	0.32	0.47	0.34	−0.41	−0.13	−0.41	−0.44	0.36	−0.40	0.32
W Pacific	−0.32	−0.18	−0.30	0.12	−0.26	−0.30	−0.19	−0.23	−0.16	−0.56	−0.42	−0.23	−0.35	−0.16	−0.18	−0.16	−0.41
E Pacific	0.21	0.24	0.31	0.02	0.33	−0.17	0.12	−0.26	−0.03	0.16	0.11	−0.03	−0.01	0.03	−0.03	0.12	0.05
S Pacific	−0.06	0.15	0.35	0.42	0.33	0.07	0.24	0.07	0.06	0.26	0.43	0.33	0.18	0.31	0.37	0.15	−0.04
Northern Ocean	−0.10	−0.03	−0.10	−0.07	−0.08	0.05	0.03	0.13	−0.03	0.06	−0.05	0.07	−0.12	0.01	0.04	−0.37	0.03
N Atlantic	−0.49	−0.24	−0.14	−0.26	−0.23	0.07	−0.38	−0.05	−0.22	−0.08	−0.40	−0.38	0.01	−0.09	0.17	−0.27	−0.18
Tropical Atlantic	−0.26	−0.17	−0.13	0.02	−0.12	−0.01	−0.07	−0.11	−0.03	0.01	0.17	−0.06	0.14	−0.01	−0.09	−0.12	0.20
S Atlantic	−0.05	−0.09	−0.01	0.05	−0.01	−0.01	−0.02	−0.12	−0.13	−0.17	0.00	−0.04	−0.15	−0.07	−0.14	−0.23	0.02
Southern Ocean	−0.10	−0.13	−0.22	−0.16	−0.21	−0.09	−0.11	−0.02	−0.04	−0.11	−0.01	−0.15	−0.05	−0.02	−0.11	−0.08	−0.09
Trop Indian Ocean	0.33	0.17	0.34	0.13	0.29	−0.05	0.20	0.11	0.08	−0.24	−0.13	−0.37	−0.08	0.01	0.08	−0.11	−0.07
S Indian Ocean	−0.06	−0.05	−0.02	−0.08	−0.05	−0.57	−0.01	0.07	0.04	0.00	−0.13	0.07	0.05	0.05	−0.02	0.06	0.06
Glbl offset (ppm)	0.02	−0.20	−0.21	−0.26	−0.22	−0.09	−0.80	−0.15	−0.14	−0.03	−0.10	−0.24	−0.14	−0.10	−0.09	−0.02	0.06

Furthermore, the estimated fluxes in northern extratropical Asia appear to have a limited relationship to the distribution of background flux response. Asia, however, is where the largest changes occur in individual model flux estimates when the background biosphere exchange is removed from the inversion. Most models exhibit large changes in their estimated flux when this change is made, often changing from a sink to a source.

In many instances, the model-to-model differences appear to reflect particular individual model responses at stations. Some of this is due to the coincidence of large concentration gradients and station locations, while some may be due to local transport differences at the surface, such as convective transport or the construction of the planetary boundary layer (PBL).

In contrast to the individual model flux estimates, the model mean fluxes outside of the tropical regions appear to be relatively insensitive to changes in estimates of the prior fluxes and prior flux uncertainties. Less uptake in the Southern Ocean than has been implied by oceanographic observations and a large and an evenly distributed sink over the northern continents remain despite dramatically increasing the uncertainty bounds on the prior fluxes, eliminating the prior fluxes, or eliminating the biospheric and oceanic background fluxes. In this sense the model mean estimates can be considered robust to these aspects of the inversion setup. A companion study (Law et al., 2003) finds the model mean flux estimates to be relatively insensitive to variations in the incorporation of the observational data.

A better understanding of regional carbon budgets in the middle latitudes depends on improving the simulated transport, whereas confidence in fluxes over the tropical continents is primarily limited by sparse data. The tropical land fluxes are determined primarily by global mass balance and the fluxes in better observed regions such as the northern extratropical regions. Combined with the lack of observational constraint is the tendency for deep mixing in the tropics, which leads to weak responses at the surface in these regions. The tradeoff between an uncertain rectifier in the northern extratropics and the poor tropical data constraint induces compensating fluxes. Models with strong rectifiers are able to generate large northern uptake and still maintain global mass balance by introducing large tropical sources, and vice versa. Improving the tropical observations might therefore provide a better constraint on the rectifier effect and therefore on mid-latitude fluxes. Conversely, a better understanding of northern rectifier effects would probably produce better estimates of tropical carbon budgets.

5. Acknowledgements

This work was made possible through support from the National Science Foundation (OCE-9900310), the National Oceanic and Atmospheric Administration (NA67RJ0152, Amend 30) and the International Geosphere Biosphere Program/Global Analysis, Interpretation and Modeling Project. S. Fan and J. Sarmiento acknowledge support from NOAA's Office of Global Programs for the Carbon Modeling Consortium.

REFERENCES

Andres, R. J., Marland, G., Fung, I. and Matthews, E. 1996. Distribution of carbon dioxide emissions from fossil fuel consumption and cement manufacture, 1950–1990. *Global Biogeochem. Cycles* **10**, 419–429.

Apps, M. J. and Kurz, W. A. 1994. The role of Canadian forests in the global carbon balance. In: *Carbon Balance on World's Forested Ecosystems: Towards a Global Assessment* (ed.M. Kanninen) Academy of Finland, Helsinki, 14–39.

Arakawa, A. and Schubert, W. H., 1974. Interaction of a cumulus cloud ensemble with the large-scale environment, Part I. *J. Atmos. Sci*. **31**, 674–701.

Baker, D. F. 2001. *Sources and Sinks of Atmospheric CO_2 Estimated from Batch Least-Squares Inversions of CO_2 Concentration Measurements*. Ph.D. Dissertation, Princeton University.

Benoit, B. M., Desgagné, M., Pellerin, P., Pellerin, S., Chartier, Y. and Desjardins S. 1997. The Canadian MC2: A semi-Lagrangian, semi-implicit wideband atmospheric model suited for finescale process studies and simulation. *Mon. Wea. Rev*. **125**, 2382–2415.

Bousquet, P., Ciais, P., Peylin, P., Ramonet, M. and Monfray, P. 1999a. Inverse modeling of annual atmospheric CO_2 sources and sinks 1. method and control inversion. *J. Geophys. Res*. **104**, 26161–26178.

Bousquet, P., Peylin, P., Ciais, P., Ramonet, M. and Monfray, P. 1999b. Inverse modeling of annual atmospheric CO_2 sources and sinks 2. sensitivity study. *J. Geophys. Res*. **104**, 26179–26193.

Bousquet, P., Peylin, P., Ciais, P., Le Quéré, C., Friedlingstein, P. and Tans, P. 2000. Regional changes in carbon dioxide fluxes of land and oceans since 1980. *Science*, **290**, 1342–1346.

Brenkert, A. L. 1998. Carbon dioxide emission estimates from fossil-fuel burning, hydraulic cement production,

and gas flaring for 1995 on a one degree grid cell basis. (http://cdiac.esd.ornl.gov/ndps/ndp058a.html).

Ciais, P., Tans, P., White, J. W. C., Trolier, M., Francey, R. and coauthors. 1995. Partitioning of ocean and land uptake of CO_2 as inferred by $\delta^{13}C$ measurements from the NOAA Climate Monitoring and Diagnostics Laboratory Global Air Sampling Network. *J. Geophys. Res*. **100**, 5051–5070.

D'Andrea, F. S., Tibaldi, S., Blackburn, M., Boer, G., Deque, M. and coauthors. 1998. Northern Hemisphere atmospheric blocking as simulated by 15 atmospheric general circulation models in the period 1979–1988. *Climate Dynam.* **14**, 385–407.

De Fries, R. S. and Townshend, J. R. G. 1994. NDVI-derived land cover classifications at a global scale. *Int. J. Remote Sens*. **15**, 3567–3586.

Denning, A. S., Fung, I. Y. and Randall, D. A. 1995. Latitudinal gradient of atmospheric CO_2 due to seasonal exchange with land biota. *Nature* **376**, 240–243.

Denning, A. S., Randall, D. A., Collatz, G. J. and Sellers, P. J. 1996. Simulations of terrestrial carbon metabolism and atmospheric CO_2 in a general circulation model. Part 2: Spatial and temporal variations of atmospheric CO_2. *Tellus* **48B**, 543–567.

Denning, A. S., Holzer, M., Gurney, K. R., Heimann, M., Law, R. M. and coauthors. 1999. Three-dimensional transport and concentration of SF_6: A model intercomparison study (TransCom 2). *Tellus* **51B**, 266–297.

Ding, P. and Randall, D. A. 1998. A cumulus parameterization with multiple cloud base levels. *J. Geophys. Res*. **103**, 11341–11354.

Dixon, R. K., Brown, S., Houghton, R. A., Solomon, A. M., Trexler, M. C. and Wisniewski, J. 1990. Carbon pools and flux of global forest ecosystems. *Science*, **263**, 185–190.

Engelen, R. J., Denning, A. S., Gurney, K. R. and TransCom 3 modelers. 2003. On error estimation in atmospheric CO_2 inversions. *J. Geophys. Res*. **107(02)**, 4635, doi:10.1029/2002JD002195.

Enting, I. 2002. *Inverse Problems in Atmospheric Constituent Transport*. Cambridge University Press, Cambridge, U. K.

Enting, I. G. and Mansbridge, J. V. 1989. Seasonal sources and sinks of atmospheric CO_2: Direct inversion of filtered data. *Tellus* **41B**, 111–126.

Enting, I. G., Trudinger, C. M. and Francey, R. J. 1995. A synthesis inversion of the concentration and $\delta^{13}C$ of atmospheric CO_2, *Tellus* **47B**, 35–52.

Fan, S., Gloor, M., Mahlman, J., Pacala, S., Sarmiento, J. and coauthors. 1998. A large terrestrial carbon sink in North America implied by atmospheric and oceanic CO_2 data and models. *Science* **282**, 442–446.

GLOBALVIEW-CO_2, Cooperative Atmospheric Data Integration Project - Carbon Dioxide, CD-ROM, NOAA CMDL, Boulder, Colorado, 2000.

Gurney, K., Law, R., Rayner, P. and Denning, A. S. 2000. TransCom 3 Experimental Protocol, Department of Atmospheric Science, Colorado State University, USA, Paper No. 707. http://transcom.colostate.edu/TransCom_3/transcom_3.html

Gurney, K. R., Law, R. M., Denning, A. S., Rayner, P. J., Baker, D. and coauthors. 2002. Towards robust regional estimates of CO_2 sources and sinks using atmospheric transport models. *Nature* **415**, 626–630.

Hack, J. J. 1993. Description of the NCAR community climate model (CCM2). NCAR/TN-382, 108 pp.

Hack, J. J. 1994. Parameterization of moist convection in the National Center for Atmospheric Research community climate model (CCM2). *J. Geophys. Res*. **99**, 5551–5568.

Hamilton, K., Wilson, R. J., Mahlman, J. D. and Umscheid, L. J. 1995. Climatology of the SKYHI troposphere–startosphere–mesosphere general circulation model. *J. Atmos. Sci*. **52**, 5–43.

Hansen, J., Sato, Mki., Ruedy, R., Lacis, A., Asamoah, K. and coauthors. 1997. Forcings and chaos in interannual to decadal climate change. *J. Geophys. Res*. **102**, 25679–25720.

Hartke, G. J. and Rind, D. 1997. Improved surface and boundary layer models for the Goddard Institute for Space Studies general circulation model. *J. Geophys. Res*. **102**, 16407–16422.

Heimann, M. 1995. The global atmospheric tracer model TM2, Technical Report, 10, Deutsches Klimarechenzentrum, Hamburg, Germany, 51 pp.

Holtslag, A. A. M. and Boville, B. A. 1993. Local versus nonlocal boundary-layer diffusion in a global climate model. *J. Climate* **6**, 1825–1842.

Houghton, R. A. 1999. The annual net flux of carbon to the atmosphere from changes in land use 1850–1990. *Tellus* **51B**, 298–313.

Houghton, R. A. and Hackler J. L. 1999. Emissions of carbon from forestry and land-use change in tropical Asia. *Global Change Biol*. **5**, 481–492.

Kaminski, T., Heimann, M. and Giering, R. 1999. A coarse grid three-dimensional global inverse model of the atmospheric transport, 2. Inversion of the transport of CO_2 in the 1980s. *J. Geophys. Res*. **104**, 18555–18581.

Kaminski, T., Rayner, P. J., Heimann, M. and Enting, I. G. 2001. On aggregation errors in atmospheric transport inversion. *J. Geophys. Res*. **106**, 4703–4715.

Kauppi, P. E., Mielikainen, K. and Kuusela, K. 1992. Biomass and carbon budget of European forests 1971–1990. *Science* **256**, 70–74.

Keeling, C. D., Piper, S. C. and Heimann, M. 1989. A three-dimensional model of atmospheric CO_2 transport based on observed winds: 4. Mean annual gradients and interannual variations. In: *Aspects of Climate Variability in the Pacific and the Western Americas, Geophysical Monograph 55*. (ed. D. H. Peterson), AGU, Washington, D.C., 305–363.

Koch, D. and Rind, D. 1998. 10Be/7Be as a tracer of stratospheric transport. *J. Geophys. Res*. **103**, 3907–3917.

Kurz, W. A. and Apps, M. J. 1999. A 70 year retrospective analysis of carbon fluxes in the Canadian forest sector. *Ecol. Appl.* **9**, 526–547.

Law, R. M., Rayner, P. J., Denning, A. S., Erickson, D., Heimann, M. and coauthors. 1996. Variations in modelled atmospheric transport of carbon dioxide and the consequences for CO_2 inversions. *Global Biogeochem. Cycles* **10**, 783–796.

Law, R. M. 1999. CO_2 sources from a mass-balance inversion: Sensitivity to the surface constraint. *Tellus* **51B**, 254–265.

Law, R. M. and Rayner, P. J. 1999. Impacts of seasonal covariance on CO_2 inversions. *Global Biogeochem. Cycles* **13**, 845–856.

Law, R. M., Chen, Y-H., Gurney, K. R., and TransCom 3 modelers. 2003. TransCom 3 CO_2 inversion intercomparison: 2. Sensitivity of annual mean results to data choices. *Tellus* **55B**, this issue.

Levy, H., Mahlman, J. D., and Moxim, W. J. 1982. Tropospheric N_2O Variability. *J. Geophys. Res*. **87**, C4, 3061–3080.

Louis, J. F. 1979. A parameteric model of vertical eddy fluxes in the atmosphere. *Boundary-Layer Meteord*. **17**, 187–202.

Mahlman, J. D. and Moxim, W. J. 1978. Tracer simulation using a global general circulation model: results from a midlatitude instantaneous source experiment. *J. Atmos. Sci*. **35**, 1340–1374.

Mahlman, J. D., Pinto, J. P. and Umscheid, L. J. 1994. Transport, radiative, and dynamical effects of the Antarctic ozone hole: A GFDL "SKYHI" model experiment. *J. Atmos. Sci*. **51**, 489–508.

Maksyutov, S. and Inoue, G. 2000. Vertical profiles of radon and CO_2 simulated by the global atmospheric transport model. In: CGER report, CGER-I039-2000, CGER, NIES, Japan, v.7, 39–41.

McGregor J. L. 1996. Semi-Lagrangian advection on conformal-cubic grids. *Mon. Wea. Rev*. **124**, 1311–1322.

McGregor J. L. and Dix, M. R. 2001, The CSIRO Conformal-Cubic Atmospheric GCM, *IUTAM Symposium on Advances in Mathematical Modeling of Atmosphere and Ocean Dynamics*. Kluwer Academic Publishers, Dordrecht, 197–202.

Pacala, S. W., Hurtt, G. C., Baker, D., Peylin, P., Houghton, R. A. and coauthors. 2001. Convergence of land- and atmosphere-based U. S. carbon sink estimates. *Science* **292**, 2316–2320.

Prather, M. 1986. Numerical advection by conservation of second-order moments. *J. Geophys. Res*. **91**, 6671–6681.

Prather, M., McElroy, M., Wofsy, S., Russell, G. and Rind, D. 1987. Chemistry of the global troposphere: fluorocarbons as tracers of air motion. *J. Geophys. Res*. **92**, 6579–6613.

Randall, D. A., Shao Q. and Moeng, C.-H. 1992. A second-order bulk boundary-layer model. *J. Atmos. Sci*. **49**, 1903–1923.

Randall, D. A. and Pan, D.-M. 1993. Implementation of the Arakawa-Schubert parameterization with a prognostic closure. In: *The Representation of Cumulus Convection in Numerical Models* (eds.K. Emanuel and D. Raymond). American Meteorological Society, Boston, MA, 137–144.

Randerson, J. T., Thompson, M. V., Conway, T. J., Fung, I. Y. and Field, C. B. 1997. The contribution of terrestrial sources and sinks to trends in the seasonal cycle of atmospheric carbon dioxide. *Global Biogeochem. Cycles* **11**, 535–560.

Rasch, P., Mahowald, N. M. and Eaton, B. E. 1997. Representations of transport, convection and the hydrologic cycle in chemical transport models: Implications for the modeling of short lived and soluble species. *J. Geophys. Res*. **102**, 28127–28138.

Rayner, P. J., Enting, I. G., Francey, R. J. and Langenfelds, R. L. 1999. Reconstructing the recent carbon cycle from atmospheric CO_2, $\delta^{13}C$ and O_2/N_2 observations. *Tellus* **51B**, 213–232.

Ritchie H. and Beaudoin, C. 1994. Approximations and sensitivity experiments with a baroclinic semi-Lagrangian spectral model. *Mon. Wea. Rev*. **122**, 2391–2399.

Russell, G. L. and Lerner, J. A. 1981. A new finite-differencing scheme for the tracer transport equation. *J. Appl. Meteorol*. **20**, 1483–1498.

Schimel, D. S., House, J. I., Hibbard, K. A., Bousquet, P., Ciais, P. and coauthors. 2001. Recent patterns and mechanisms of carbon exchange by terrestrial ecosystems. *Nature* **414**, 169–172.

Schubert, S., Rood, R. and Pfaendtner, J. 1993. An assimilated dataset for Earth science applications. *Bull. Am. Meteorol. Soc*. **74**, 2331–2342.

Sellers, P. J., Randall, D. A., Collatz, G. J., Berry, J. A., Field, C. B. and coauthors. 1996. A revised land surface parameterization (SiB2) for atmospheric GCMs. Part I: model formulation. *J. Climate* **9** 676–705.

Strahan, S. E. and Mahlman, J. D. 1994. Evaluation of the GFDL "SKYHI" general circulation model using aircraft N_2O measurements: 2. Tracer variability and diabatic meridional circulation. *J. Geophys. Res*. **99**, 10319–10332.

Suarez, M. J., Arakawa, A. and Randall, D. A. 1983. Parameterization of the planetary boundary layer in the UCLA general circulation model: Formulation and results. *Mon Wea. Rev*. **111**, 2224–2243.

Taguchi, S. 1996. A three-dimensional model of atmospheric CO_2 transport based on analyzed winds: Model description and simulation results for TRANSCOM. *J. Geophys. Res*. **101**, 15099–15109.

Takahashi, T., Wanninkhof, R. H., Feely, R. A., Weiss, R. F., Chipman D. W. and coauthors. 1999. Net sea–air CO_2 flux over the global oceans: An improved estimate based on the sea–air pCO_2 difference. Proceedings of the 2nd CO_2 in Oceans Symposium, Tsukuba, Japan.

Tans, P. P., Fung, I. Y. and Takahashi, T. 1990 Observational constraints on the global atmospheric CO_2 budget. *Science* **247**, 1431–1438.

Taylor, K. E., Williamson, D. and Zwiers, F. 1997. AMIP II Sea Surface Temperature and Sea Ice Concentration Boundary Conditions. (http://www-pcmdi.llnl.gov/amip/AMIP2EXPDSN/BCS/amip2bcs.html).

Tiedke, M. 1989. A comprehensive mass flux scheme for cumulus parameterization in large-scale models. *Mon. Wea. Rev*. **117**, 1779–1800.

UNFCCC. 2000. United Nations Framework Convention on Climate Change, National Communications from Parties Included in Annex 1 to the Convention: Greenhouse Gas Inventory Data from 1990 to 1998 (FCCC/SBI/2000/11).

Zhang, G. J. and McFarlane, N. A. 1995. Sensitivity of climate simulations to the parameterization of cumulus convection in the Canadian Climate Centre general circulation model. *Atmos. Ocean* **33**, 407–446.

Transcom 3 inversion intercomparison: Model mean results for the estimation of seasonal carbon sources and sinks

Kevin Robert Gurney,[1] Rachel M. Law,[2] A. Scott Denning,[1] Peter J. Rayner,[2] Bernard C. Pak,[3] David Baker,[4] Philippe Bousquet,[5] Lori Bruhwiler,[6] Yu-Han Chen,[7] Philippe Ciais,[5] Inez Y. Fung,[8] Martin Heimann,[9] Jasmin John,[8] Takashi Maki,[10] Shamil Maksyutov,[11] Philippe Peylin,[5] Michael Prather,[3] and Shoichi Taguchi[12]

Received 16 June 2003; revised 24 October 2003; accepted 19 November 2003; published XX Month 2004.

[1] The TransCom 3 experiment was begun to explore the estimation of carbon sources and sinks via the inversion of simulated tracer transport. We build upon previous TransCom work by presenting the seasonal inverse results which provide estimates of carbon flux for 11 land and 11 ocean regions using 12 atmospheric transport models. The monthly fluxes represent the mean seasonal cycle for the 1992 to 1996 time period. The spread among the model results is larger than the average of their estimated flux uncertainty in the northern extratropics and vice versa in the tropical regions. In the northern land regions, the model spread is largest during the growing season. Compared to a seasonally balanced biosphere prior flux generated by the CASA model, we find significant changes to the carbon exchange in the European region with greater growing season net uptake which persists into the fall months. Both Boreal North America and Boreal Asia show lessened net uptake at the onset of the growing season with Boreal Asia also exhibiting greater peak growing season net uptake. Temperate Asia shows a dramatic springward shift in the peak timing of growing season net uptake relative to the neutral CASA flux while Temperate North America exhibits a broad flattening of the seasonal cycle. In most of the ocean regions, the inverse fluxes exhibit much greater seasonality than that implied by the ΔpCO_2 derived fluxes though this may be due, in part, to misallocation of adjacent land flux. In the Southern Ocean, the austral spring and fall exhibits much less carbon uptake than implied by ΔpCO_2 derived fluxes. Sensitivity testing indicates that the inverse estimates are not overly influenced by the prior flux choices. Considerable agreement exists between the model mean, annual mean results of this study and that of the previously published TransCom annual mean inversion. The differences that do exist are in poorly constrained regions and tend to exhibit compensatory fluxes in order to match the global mass constraint. The differences between the estimated fluxes and the prior model over the northern land regions could be due to the prior model respiration response to temperature. Significant phase differences, such as that in the Temperate Asia region, may be due to the limited observations for that region. Finally, differences in the boreal land regions between the prior model and the estimated fluxes may be a reflection of the timing of spring thaw and an imbalance in respiration versus photosynthesis. *INDEX TERMS:* 0322 Atmospheric Composition and Structure: Constituent sources and sinks; 1615 Global Change: Biogeochemical processes (4805); 0315 Atmospheric Composition and Structure: Biosphere/atmosphere interactions; *KEYWORDS:* carbon transport, inversion

[1]Department of Atmospheric Science, Colorado State University, Fort Collins, Colorado, USA.
[2]CSIRO Atmospheric Research, Aspendale, Victoria, Australia.
[3]Earth System Science, University of California, Irvine, Irvine, California, USA.
[4]National Center for Atmospheric Research, Boulder, Colorado, USA.
[5]Laboratoire des Sciences du Climate et de l'Environment, Gif-sur-Yvette, France.
[6]Climate Monitoring and Diagnostics Laboratory, NOAA, Boulder, Colorado, USA.
[7]Department of Earth, Atmospheric, and Planetary Science, Massachusetts Institute of Technology, Cambridge, Massachusetts, USA.
[8]Center for Atmospheric Sciences, University of California, Berkeley, Berkeley, California, USA.
[9]Max-Planck-Institute fur Biogeochemie, Jena, Germany.
[10]Quality Assurance Section, Atmospheric Environment Division, Observations Department, Japan Meteorological Agency, Tokyo, Japan.
[11]Institute for Global Change Research, Frontier Research System for Global Change, Yokohama, Japan.
[12]National Institute of Advanced Industrial Science and Technology, Ibaraki, Japan.

0886-6236/04/2003GB002111$12.00

Citation: Gurney, K. R., et al. (2004), Transcom 3 inversion intercomparison: Model mean results for the estimation of seasonal carbon sources and sinks, *Global Biogeochem. Cycles*, *18*, XXXXXX, doi:10.1029/2003GB002111.

1. Introduction

[2] The spatial and temporal pattern of atmospheric CO_2 can be used to infer sources and sinks of carbon through the inversion of atmospheric tracer transport. A quantitative understanding of sources and sinks in both space and time is an essential ingredient to reliably predicting future levels of atmospheric CO_2. The use of the inversion technique has been employed at a variety of temporal and spatial scales. With the increase in spatial coverage of CO_2 observations and the development of 3D tracer transport models, recent inversions have been performed at the continental scale and have explored both the seasonal cycle of carbon sources and sinks and their interannual variability [*Enting et al.*, 1995; *Fan et al.*, 1998; *Rayner et al.*, 1999; *Bousquet et al.*, 1999, 2000; *Baker*, 2001; *Gurney et al.*, 2002; *Peylin et al.*, 2002; *Gurney et al.*, 2003]. Further reductions in spatial scale have been attempted through the use of adjoint transport models though the current global CO_2 observational network poses a constraint on the reliability of fluxes estimated at subcontinental scales [*Kaminski et al.*, 1999; *Rödenbeck et al.*, 2003].

[3] Estimates of continental carbon sources and sinks in the last decade have shown considerable disagreement. Though many aspects of these studies share common elements, different tracer transport models were often used. The primary goal of the TransCom 3 experiment was to assess the contribution of tracer transport to the spread of atmospheric CO_2 inverse results and builds on the earlier TransCom work [*Law et al.*, 1996; *Denning et al.*, 1999]. The experiment can also test other sensitivities in the inversion process (e.g., inversion set-up, observational data choices) since more reliable results are expected by examining sensitivities with a range of transport models than with just one or two.

[4] TransCom 3 was designed to estimate carbon sources and sinks at annual, seasonal, and interannual timescales. Annual mean results have already been published elsewhere and have reported on the model mean results of the control or "base case" inversion, the sensitivity of this control case to inversion set-up/observational network choices, and model-to-model differences [*Gurney et al.*, 2002, 2003; *Law et al.*, 2003]. Analysis of the interannual results are currently underway.

[5] Here we present an average seasonal inversion result. In this experiment, we estimate fluxes for each month of an average year determined as the mean of the 1992 to 1996 period. Section 2 provides a description of the methods employed including the choices involved in creating the control inversion set-up. Section 3 presents the model mean results of the control inversion including sensitivity to aspects of the inversion set-up. Section 4 contrasts the current results to the annual mean control inversion and discusses possible mechanisms responsible for the estimated regional fluxes. This paper focuses on the model average results. Future work will explore the model-to-model differences. While the model average is not presented as the mean of a randomly varying statistical ensemble, it does represent a compact representation of the tendencies inherent in the majority of models used in inverse work in recent years. It is important to note that individual model estimates cannot be judged by their proximity to the model mean.

2. Methods

[6] The inversion approach used in this study follows the Bayesian synthesis method [*Tarantola*, 1987; *Enting*, 2002] A detailed description of the formalism employed and references to source material is given in previous work for the annual mean TransCom inversion [*Gurney et al.*, 2003]. The method used here is the same except that monthly mean CO_2 observations are used rather than the annual mean values.

[7] Because results from a group of transport models will be presented, two different measures of uncertainty will be computed in the present work. The RMS of the individual model flux uncertainties can be calculated as

$$\overline{\mathbf{C}\left(\vec{S}\right)} = \sqrt{\sum_{n=1}^{N_{\text{models}}} \left(\mathbf{C}\left(\vec{S}\right)_n\right)^2 \Big/ N_{\text{models}}}, \qquad (1)$$

where S is a model flux estimate and $\boldsymbol{C}\ (S)_n$ represents the monthly posterior uncertainty estimates for each model. We designate this mean uncertainty the "within-model" uncertainty. The spread of flux estimates across models is represented by the standard deviation,

$$\sigma\left(\vec{S}\right) = \sqrt{\sum_{n=1}^{N_{\text{models}}} \left(\vec{S}\left(\vec{S}\right)_n\right)^2 \Big/ N_{\text{models}}}, \qquad (2)$$

and designated the "between-model" uncertainty. Unless specifically noted, all uncertainties quoted in the text represent the total uncertainty which are the within- and between-model combined in quadrature.

2.1. Experimental Design

2.1.1. Forward Simulations

[8] Twelve transport models (or model variants) ran a series of forward CO_2 tracer simulations [*Gurney et al.*, 2000] in order to construct model-specific response functions used to perform the inversion for seasonal carbon sources and sinks. Though monthly fluxes are resolved in the current study, the same 12 transport models were also included in an annual mean inversion and are described in detail in previous work [*Gurney et al.*, 2003].

[9] For the seasonal experiment presented here, the forward simulations were run as greens functions. A total of 268 tracers were simulated by each model, four of which were "background" global fluxes and 264 of which were region/month fluxes representing a combination of

12 months and the 22 land and ocean regions described in the annual mean inversion experiment [*Gurney et al.*, 2002]. The background fluxes were emitted for a single year, then discontinued, allowing the CO_2 concentration field to decay for the following 2 years of simulation. The region/month flux combinations were emitted for a single month then discontinued for the remainder of the 3-year simulation. These responses were converted to a single 12-month stationary response by compositing like months (summing all Januaries, all Februaries, etc., in the 3-year span) and detrending (removing the concentration trend resulting from the constant emissions in the forward simulations).

[10] The four background fluxes consisted of 1990 and 1995 fossil fuel emission fields, an annually balanced, seasonal biosphere exchange and air-sea gas exchange [*Andres et al.*, 1996; *Randerson et al.*, 1997; *Takahashi et al.*, 1999; A. L. Brenkert, Carbon dioxide emission estimates from fossil-fuel burning, hydraulic cement production, and gas flaring for 1995 on a one degree grid cell basis, available at http://cdiac.esd.ornl.gov/ndps/ndp058a.html]. These fluxes are included in the inversion with a small prior uncertainty so that their magnitude is effectively fixed. The 264 region/month fluxes estimated by the inversion are deviations from these global background fluxes for each month in a climatological year. The background fossil fuel emission fluxes were prescribed without seasonality. The neutral terrestrial fluxes were purely seasonal, and the background ocean fluxes were prescribed with both seasonal variations and annual mean uptake.

[11] Further details and references for the forward fluxes are given by *Gurney et al.* [2002]. Full details of the experimental protocol are presented by *Gurney et al.* [2000].

2.1.2. Inversion Set-Up and Observational Data

[12] Prior estimates of the fluxes in each of the 264 region/month flux combinations were determined from independent estimates of terrestrial and oceanic exchange. The land region prior flux estimates incorporate results from recent inventory studies and are identical to the annual mean values used in the annual mean inversion [*Gurney et al.*, 2003]. Where more than one estimate for a given region was considered, a midpoint of the estimate spread was used. Because the land region prior fluxes are only available as annual mean values, these were distributed evenly over those months considered the most likely to capture the emission or uptake implied by the prior flux. The ocean region prior flux estimates were prescribed as zero for each month.

[13] The prior flux uncertainty is important for keeping the estimated fluxes within biogeochemically realistic bounds. For land regions in a given month, we chose the combination of the uncertainties employed in our annual mean control case [*Gurney et al.*, 2002], and 30% each of NPP and respiration provided by the CASA model of net ecosystem production [*Randerson et al.*, 1997]. Since it is unlikely that a given region/month flux adjustment would exceed these values, this provides a reasonable, ecologically relevant upper bound. The prior ocean uncertainties were twice the annual mean uncertainty values used in the annual mean control inversion.

[14] We invert 5-year (1992–1996) mean measurements for each month at 75 sites taken from the GLOBALVIEW-2000 data set [*GLOBALVIEW-CO2*, 2000]. GLOBALVIEW is a data product that interpolates CO_2 measurements to a common time interval. Gaps in the data are filled by extrapolation from marine boundary layer measurements. Sites were chosen where the extrapolated data accounts for less than 30% of the 1992–1996 period. This station set is identical to that used in the annual mean inversion published previously except in the current experiment, the station in Darwin, Australia, was removed due to recent work showing Darwin as unrepresentative of the region [*Law et al.*, 2003]. The uncertainty attached to each data value, *C(D)*, was derived from the monthly residual standard deviation (RSD) of individual observations around a smoothed time series as given by GLOBALVIEW. This choice was based on the assumption that the distribution of RSD (higher RSD values for northern and continental sites and lower RSD values for Southern Hemisphere oceanic sites) reflects the high-frequency variations in transport and regional flux that large-scale transport models are unable to accurately simulate. *GLOBALVIEW-CO2* [2000] provides monthly RSD values averaged over 1979–1996 and annual RSD values for each separate year. To obtain monthly values for 1992–1996, we scale the 1979–1996 monthly values by the ratio of the 1992–1996 mean annual RSD to the 1979–1996 mean annual RSD.

[15] Direct use of the RSD values for the data uncertainty results in a total reduced χ^2 that is much smaller than unity [*Tarantola*, 1987, p. 212]. This indicates that the predicted concentrations fit the data much better than the uncertainty assigned to the data itself and that the uncertainty should be reduced. The aim is to scale the RSD such that the inversion produces a total χ^2 of 1.0. When making this adjustment, we limit the reduction such that the minimum uncertainty at any site is equivalent to 0.25 ppm on the annual mean concentration and we also adjust the uncertainty for data records that are co-located. The details are as follows: the RSD was divided by $(3.6*P)^{0.5}$ where P is the proportion of real data in the record and 3.6 is chosen to satisfy our total χ^2 criteria. These monthly uncertainties were converted to equivalent annual uncertainties with the following expression:

$$\sigma_a = \frac{\sqrt{\sum_{m=1}^{12} \sigma_m^2}}{A}, \tag{3}$$

where σ_a is the equivalent annual uncertainty, σ_m is the monthly uncertainty, and A represents the autocorrelation timescale for the specific station (typically around 4 months). If the annualized uncertainty was less than the minimum uncertainty used in the annual mean control inversion of 0.25 ppm, the monthly uncertainty values were increased to an uncertainty given by

$$\sigma_m^{\min} = 0.25*\sqrt{A}. \tag{4}$$

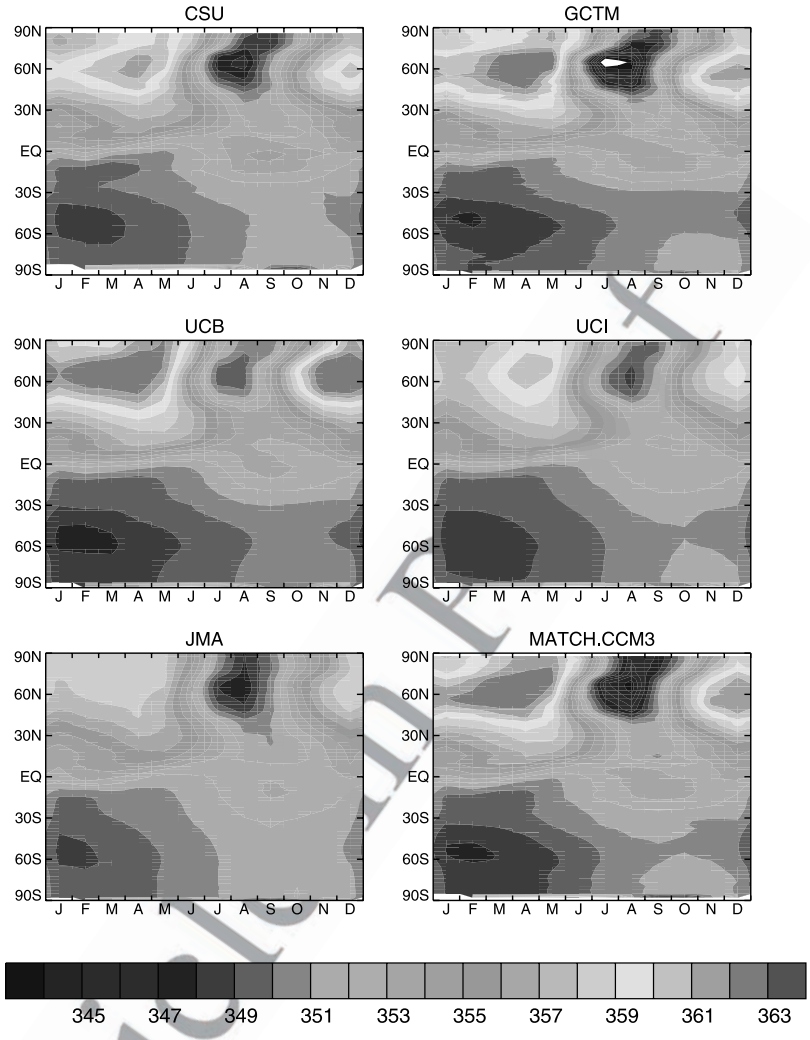

Figure 1. Zonal mean monthly predicted concentration driven by the background fluxes (fossil fuel, seasonally balanced biosphere exchange, ocean exchange) for each of the participating tracer transport models. See color version of this figure at back of this issue.

Finally, the uncertainty was increased for those sites that are likely to occur in the same model grid-cell. These adjustments gave values ranging from 0.17 ppm for a given month at remote, "clean air" sites to 4.8 ppm for continental, "noisy" sites and a mean total χ^2 averaged across the models of 1.0.

3. Results

3.1. Background Simulation Results

[16] The forward simulations of the four background fluxes provide a measure of model-to-model transport differences. Figure 1 shows the zonal mean seasonality of the model response to the background fluxes at the surface. The seasonality for each of the models reflect both the seasonality in the surface forcing and transport.

[17] A strong seasonal response is evident in the Northern Hemisphere for the MATCH variants, NIES, NIRE, and TM3 while CSU, JMA, UCI, and TM2 exhibit weak northern seasonality. The response of the GCTM model shows a winter maximum that places it in the middle of the participating models but exhibits a strong summer concentration minimum.

[18] The spatial extent of the maxima is also variable among the models. Of those models with a pronounced seasonal response, MATCH:NCEP and NIES show winter maxima that stretch almost evenly from 45°N to the pole whereas the other strongly seasonal models exhibit less extensive winter maxima.

[19] Though the full latitudinal distribution of the background simulation provides a useful overview of the different model responses, the inversion results are driven by CO_2 observations at the stations only. Figure 2 shows the simulated background seasonal amplitude at stations north of 35°N latitude plotted against the observed seasonal amplitude. In this figure, the seasonal amplitude is defined as the background response difference between the average of October through March (maximum) and the average of June through August (minimum) at the stations. The figure also provides the average amplitude value across all the stations north of 35°N for each of the models and a one-to-one line.

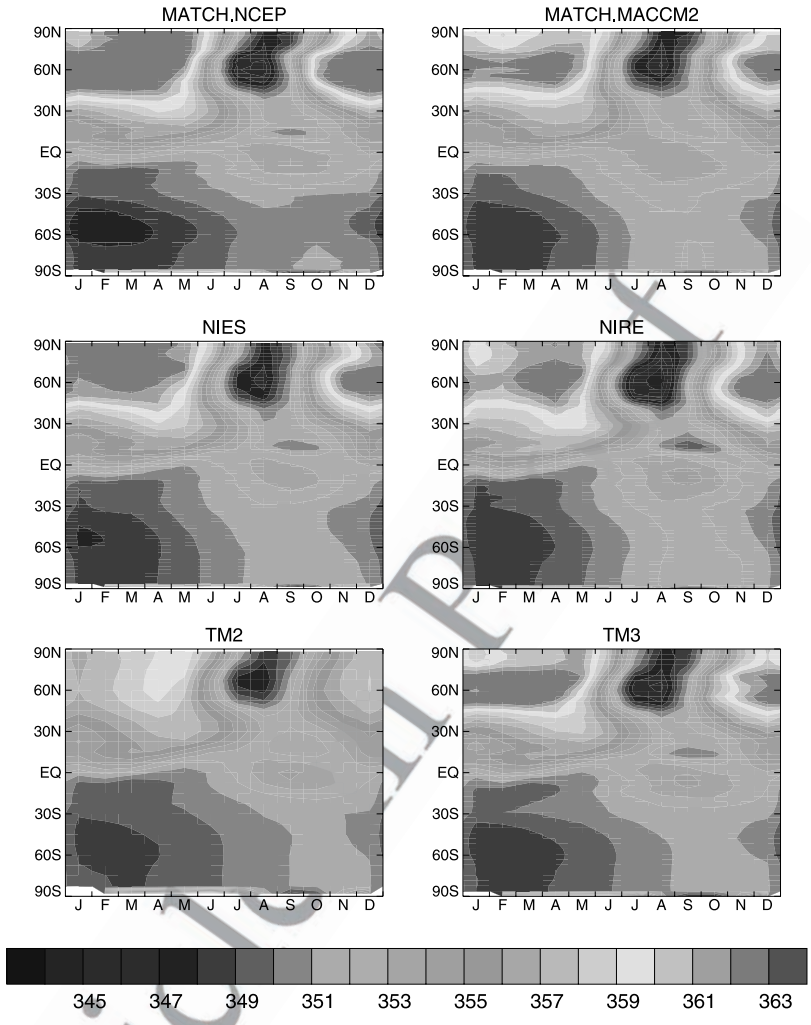

Figure 1. (continued)

[20] Consistent with Figure 1, some of the models exhibit weak northern seasonality (CSU, TM2, UCI, and JMA) while others produce greater seasonality (NIRE, NIES, and M:NCEP). This spread in model behavior has been previously noted for both biosphere CO_2 and the SF_6 tracer and tends to relate to the vigor of vertical transport [*Gurney et al.*, 2003; *Denning et al.*, 1999]. Both the magnitude and the model spread evident in the seasonal response to the background fluxes are dominated by the background biosphere exchange. Through the inversion process, in which mismatches between the background response and the observed concentration are minimized (modulated by the station uncertainty), models that underestimate the background seasonality must construct sources and sinks in order to amplify the seasonal exchange with the surface and vice versa.

[21] Previous TransCom work with a different neutral biosphere exchange and a somewhat different group of tracer transport models showed consistent overestimation of the seasonal amplitude in the Northern Hemisphere [*Law et al.*, 1996, Figure 10]. Since the biospheric exchange dominates the seasonality of the background flux, this suggests that the current CASA neutral biosphere fluxes are much more consistent with the CO_2 observations than fluxes used in the past.

3.2. Inversion Results

3.2.1. Model Mean Results

[22] Figure 3 shows the control case estimated seasonal fluxes, prior fluxes, and uncertainties for the ocean and land regions combined into north, tropical, and south aggregates. The estimated fluxes do not include fossil fuel and represent the average across the 12 models.

[23] Two measures of uncertainty are presented in Figure 3 (see section 2). For any region, the ''within uncertainty'' (distance from posterior flux to circles) must be smaller than the prior flux uncertainty (distance from prior flux to heavy dashed lines). The magnitude of the decrease indicates the degree to which the final flux estimate is constrained by the measurements. The northern extratropics and the southern extratropical oceans exhibit the greatest reduction in uncertainty due to the greater number of observing sites and sites with relatively small data uncertainty.

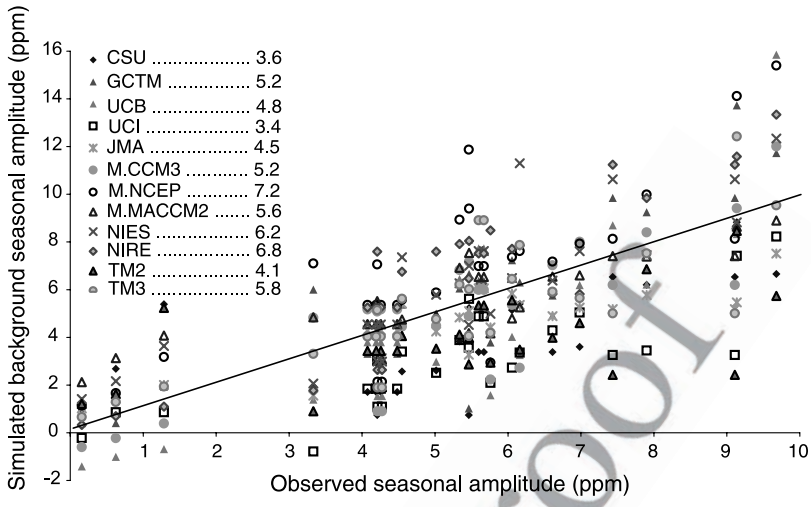

Figure 2. Simulated background seasonal amplitude versus the observed amplitude at stations north of 35°N. Amplitude is defined as the mean October-March concentration minus the mean June-August concentration. The station average simulated values are provided in the legend. The observed station average is 5.6 ppm. A one-to-one line is included. See color version of this figure at back of this issue.

[24] The "between uncertainty" (error bars) indicates the degree to which transport model differences contribute to the range of flux estimates. On land, between uncertainties are largest in the tropical region. The ocean regions exhibit between uncertainties that are largest over the tropics and southern latitudes. The uncertainty also varies over the course of the year. For example, the northern land region exhibits the largest between uncertainty during the northern growing season.

[25] The relative magnitude of these two uncertainty measures provides a reflection of the extent to which the flux estimates are limited by uncertainty associated with the observational data versus the uncertainty associated with transport differences. As can be seen in Figure 3, the northern extratropical regions where more observing stations are available show between uncertainty values that are larger than the within values. In those regions where observations are limited, such as the tropical regions and the southern land regions, the opposite occurs. In some regions such as the southern extratropical oceans, the dominance of simple advective flow and the relative availability of observations with small variability combine to provide between and within uncertainties that are of similar magnitude and represent a significant reduction of uncertainty from the prior.

[26] In the Northern Hemisphere land region, the estimated fluxes in Figure 3 show less emission during March, April, and September and greater uptake during July relative to the prior flux. Significant monthly departures from the prior oceanic flux occur in all of the aggregated ocean regions showing greater seasonality in all instances. However, the correlation (0.66) in the estimated seasonality between the ocean and land for the northern latitudes suggests the possibility that some of the land seasonality is being misallocated to the neighboring ocean region. This is further explored in section 3.2.2 where the sensitivity to prior uncertainties is tested.

[27] Disaggregation of the land regions is shown in Figure 4. Tropical and Southern America are not shown as very few significant departures from the prior flux occur in any months. In addition to the total prior flux shown in Figure 4 for each of the land regions, the portion of the prior flux associated with the neutral biosphere exchange is shown. The difference between these two priors is the flux derived from inventory studies as discussed in section 2.1.2.

[28] In Boreal North America there are deviations outside of the uncertainty range from the prior model in April, June, and August. The departures in June and August suggest a phase shift in the growing season with the estimated uptake occurring later in the year. Model spread is largest in the summer months and is primarily due to discrepancy among the models concerning the timing of the maximum seasonal uptake.

[29] Europe shows significant deviations from the peak of the growing season in June through September with greater net uptake during these months. This increased net uptake relative to the prior is exhibited by every model.

[30] Boreal Asia shows results similar to the boreal region of North America. Small but significant adjustments to the prior flux occurs in March and April indicating a reduction in early spring emissions. Less net uptake is indicated in June and more net uptake is indicated in July. In Temperate North America, the estimated fluxes exhibit a lessened seasonal amplitude relative to the prior estimates with significant deviations occurring in spring and late fall months.

[31] Temperate Asia exhibits a large deviation from the prior flux in the month of June with model mean uptake estimated at -5.1 ± 2.6 Gt C/year as opposed to -1.2 Gt C/year for the prior estimate. As a result, the overall timing of the summer uptake maximum is shifted (June/July) toward the spring relative to the prior seasonality (August). This could be due to an error in the timing of the prior seasonality (CASA model output) or a real advance of

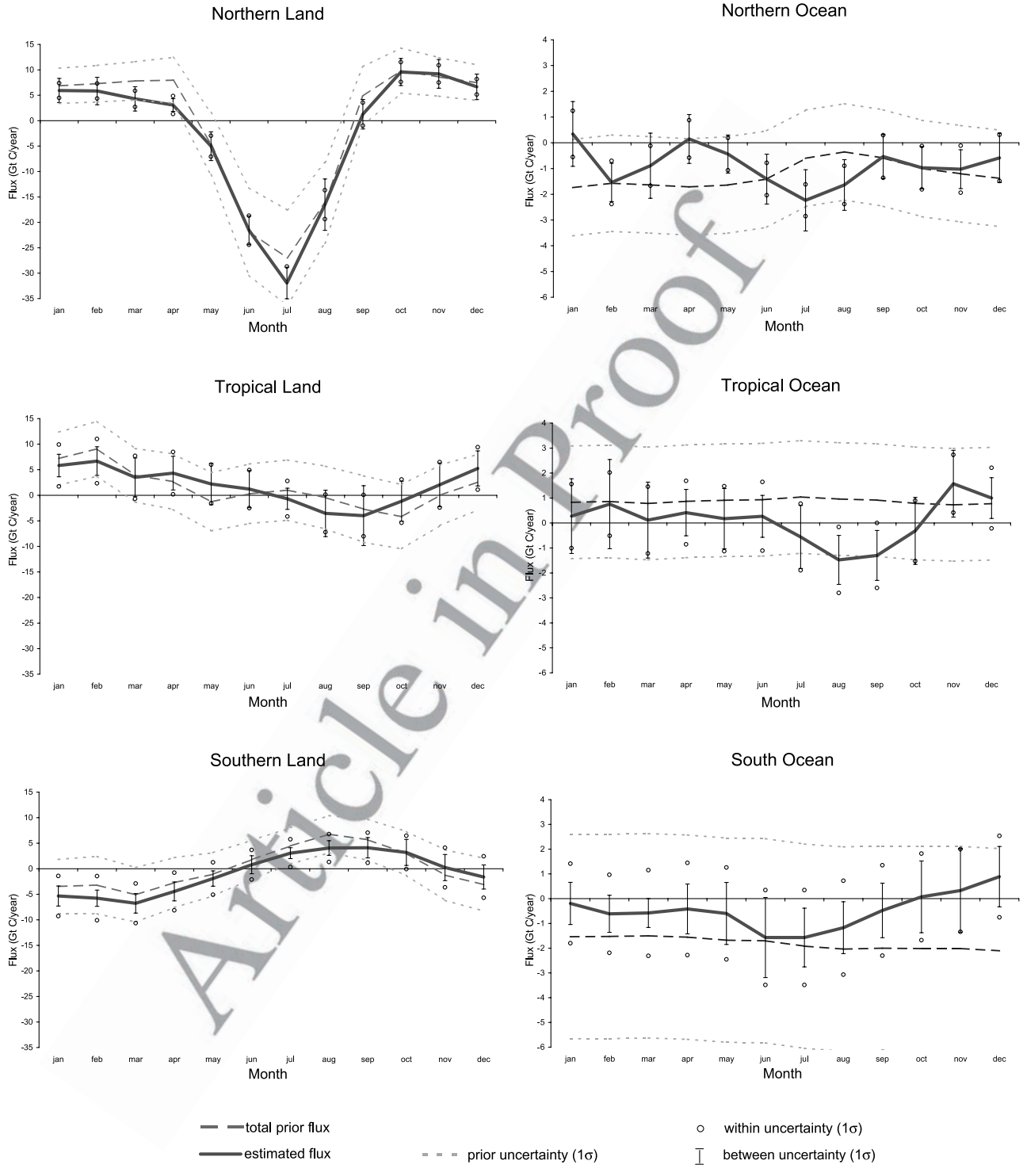

Figure 3. Model mean estimated flux, prior flux, prior uncertainties, and posterior uncertainties for aggregated land and ocean regions. The fluxes do not include fossil fuel emissions. Different scales are used for the land and ocean regions.

net uptake in the 1992 to 1996 time period (assuming the prior model was correctly capturing the long-term seasonality of this region). Only M:MACCM2 places the maximum net uptake in August although July has nearly the same level of net uptake. The two African land regions and Tropical Asia show some significant departures from the prior flux but due to a lack of observational constraint the flux estimates are unreliable. Australasia exhibits departures from the prior estimate in the austral fall changing from a net source to a net sink in April.

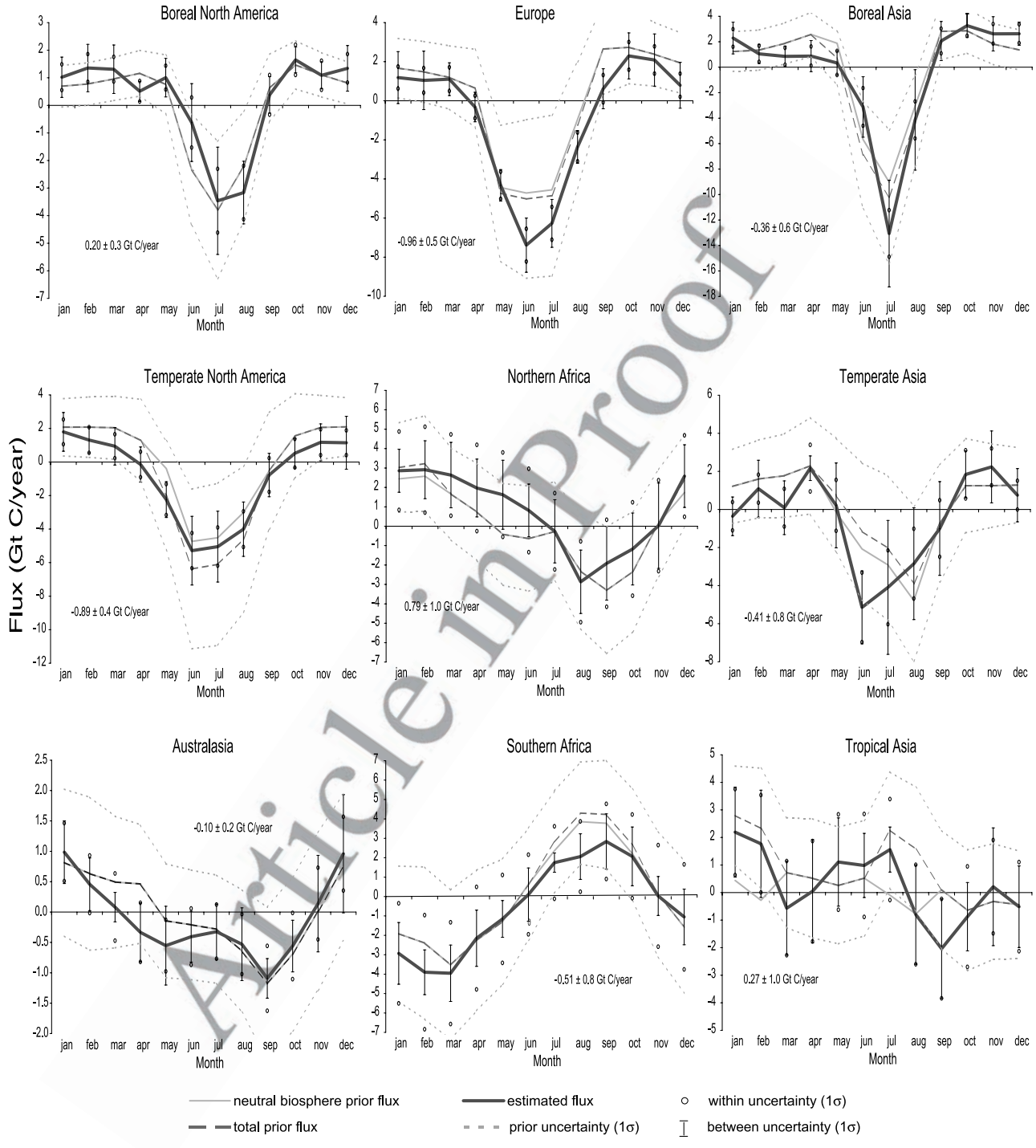

Figure 4. Model mean estimated flux, total prior flux, neutral biosphere prior flux, prior uncertainties, and posterior uncertainties for selected land regions. Numerical estimate of annual mean flux and total uncertainty is provided in each figure. Note that the vertical scale varies. The fluxes do not include fossil fuel emissions.

[32] Disaggregation of selected ocean regions is shown in Figure 5. In many cases, greater seasonality in ocean exchange is implied in the inverse results than was present in the prior ocean flux.

[33] All of the northern ocean regions exhibit heightened seasonality with both the North Pacific and the North Atlantic showing seasonality that is somewhat out of phase with the prior ocean exchange. As mentioned in the discussion of Figure 3, the estimated seasonality has similarities to the adjacent terrestrial seasonal cycle and may be an indication that terrestrial flux is being incorrectly allocated to neighboring ocean regions. In the case of the

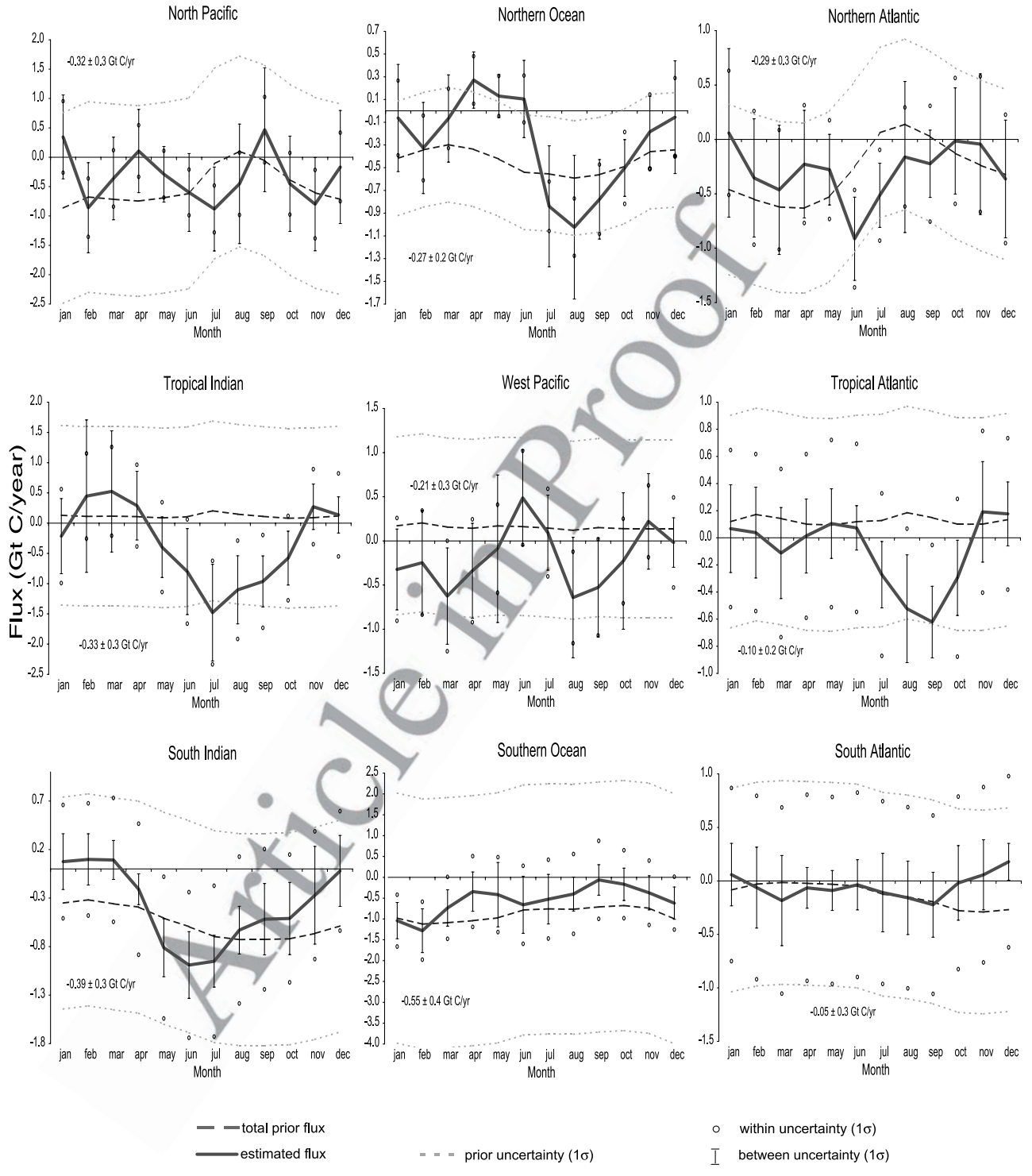

Figure 5. Model mean estimated flux, total prior flux, prior uncertainties, and posterior uncertainties for selected ocean regions. Numerical estimate of annual mean flux and total uncertainty is provided in each figure. Note that the vertical scale varies. The fluxes do not include fossil fuel emissions.

Southern Ocean region, the fall and spring exchange estimated here suggests less uptake than the prior flux. This may explain the discrepancy between the annual mean estimates of ocean flux derived from ΔpCO_2 measurements and those estimated with the inverse estimate [*Gurney et al.*, 2002]. The greatest differences between the prior and estimated flux occur during the austral fall and spring months. Ocean CO_2 measurements are typically only taken during the summer months. Recent ocean measurements taken during January and August 2000 in the Indian

Antarctic sector of the Southern Ocean support this hypothesis. These measurements showed seasonal variations in pCO_2 values south of 50°S that indicateCO_2 uptake in summer and emission in winter [*Metzl et al.*, 2001]. Furthermore, a 1D biogeochemical simulation performed in the same study for all months in the year 2000 showed a seasonality similar to that found here. If the seasonality exhibited in this work is true for other parts of the Southern Ocean, this would reduce the Southern Ocean ΔpCO_2-based uptake estimate, which is currently determined predominantly by summer measurements.

[34] All the tropical ocean regions shown in Figure 5 exhibit greater uptake during the July to September months compared to the prior flux estimate. A small annual mean net uptake is estimated in these ocean regions in contrast to the small annual mean sources of the prior flux estimate. In the case of the tropical Indian Ocean, the annual mean uptake is driven by the Seychelles observations. Removal of this station from the inversion changes this region from an annual mean net sink to an annual mean net source (+0.7 ± 0.4 Gt C/year). The total annual mean tropical ocean flux is estimated as approximately neutral due to the greater net emission from the East Pacific region (0.66 ± 0.3 Gt C/year).

[35] In both the land and oceanic regions the relative magnitude of the two uncertainty measures is strongly dependent upon the number of observing sites and the amount of error they are assigned. This difference is most evident when comparing the tropical regions, where observations are sparse, and the northern extratropical regions where observations are much more common. The within uncertainty is large in the tropical regions compared to the uncertainty due to model spread. Conversely, the within error is relatively small in the northern extratropics compared to the model spread. The increase in model spread in regions with greater observational constraint is largely due to the fact that the differences in model transport are more often quantified where observations exist.

3.2.2. Sensitivity to Prior Flux Uncertainties

[36] One can vary the prior flux uncertainty to further explore the level to which the prior flux is influencing the inversion results. This has been accomplished by increasing the prior flux uncertainties to 2, 5, and 10 times the levels used in the control case inversion. Figure 6a shows the results of this sensitivity test for a few selected regions. Regions for which observations provide constraint show little change as the prior flux uncertainty is increased. However, regions where data is sparse (tropical land and South Atlantic) show considerable sensitivity to the prior uncertainty. This confirms the limited confidence that should be placed on the tropical land and certain ocean regions suggested by the flux uncertainties presented in Figures 3, 4, and 5. Because these regions have very little data constraint, they tend to be constrained by the prior and prior uncertainty level unless required to compensate for changes in those regions with data constraint such as the northern land and many of the ocean regions. This compensation is a direct result of the requirement to maintain the global mass balance defined by the atmospheric growth rate. This is most obvious in the case of the Tropical and South Atlantic Ocean regions where large anti-correlated fluxes observed.

[37] Figure 6a also shows an extreme sensitivity test in which the background biosphere exchange amplitude has been reduced to 50% of that used in the control case in all months. This further confirms the data constraint evident in the northern extratropical regions and the limited confidence that accompany the tropical land and certain ocean regions.

[38] In order to test the possibility that terrestrial seasonality is "leaking" into the estimated fluxes for the northern oceanic regions, the inversion was run with reduced (factor of 4) prior uncertainties for the North Pacific, Northern Ocean, and North Atlantic regions. These ocean regions are then strongly constrained to mimic the prior flux seasonality. Figure 6b shows the resulting fluxes and difference for the summation of the northern land regions (Boreal and Temperate North America, Boreal and Temperate Asia, Europe). As shown in Figure 6b, the suppression of the heightened seasonality for the northern ocean regions is shifted to the adjacent land regions and follows the terrestrial seasonal cycle quite closely. The magnitude of the flux difference is small compared to the northern land seasonal fluxes, so this has little impact on the estimated fluxes for land. Though not conclusive, the result of this test is consistent with leakage of land fluxes into the adjacent ocean regions. Though not performed in the TransCom 3 experiment, inclusion of carbon isotope or O_2/N_2 values would more conclusively test this hypothesis.

3.2.3. Predicted CO_2

[39] Figure 7a shows the difference between the model mean predicted CO_2 concentration and the observed CO_2 at all stations and months. The largest mismatches occur for Hungary (HUN: 16.7°E, 47°N) in winter, which is likely due to the difficulty of matching concentrations at a site with large observed variability not expected to be captured by the global scale transport models used in this study. Fortunately, this station has large "data uncertainty" (1.4 to 4.0 ppm), so models are only weakly required to match the observed concentration. When the mismatches are scaled by their assigned uncertainty, a different picture emerges. This quantity, the station by station contribution to the cost function or "χ^2 per station," is formally expressed as

$$\chi_i^2 = \frac{\left(D_i^s - D_i^o\right)^2}{\sigma_i^2}, \tag{5}$$

where D_i^s is the simulated concentration at station i and D_i^o is the observed concentration at station i with uncertainty σ_I [*Peylin et al.*, 2002]. Values much greater than 1 indicate that the difference between the predicted and observed concentration at that station is much greater than the uncertainty assumed in the inversion. This suggests that the uncertainty assigned to these stations is too small and, hence, they may be influencing the inversion result more than is warranted.

[40] Figure 7b shows the annual mean of these values against station latitude. One station in particular, Cape Rama India (CRI: 73.8°E, 15.1°N) shows an annual mean χ_i^2 value of 3.4, indicating that the mismatch between the

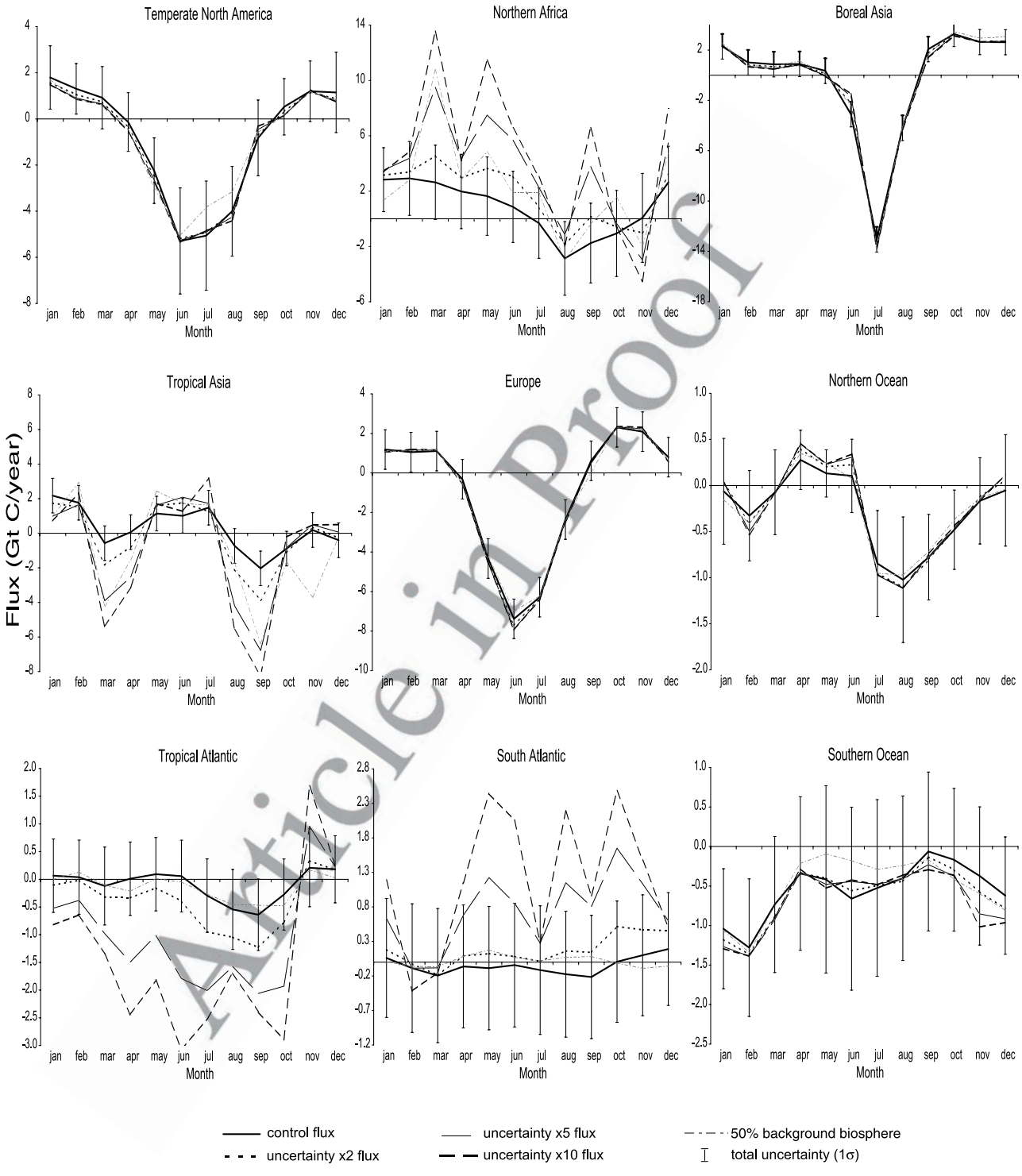

Figure 6a. Model mean control flux, and estimated fluxes with prior uncertainties scaled by factors of 2, 5, and 10 for selected land and ocean regions. Also shown are the results for a case in which the background biosphere exchange is reduced to 50% of that used in the control run. The total uncertainty (between and within uncertainty) for the control case is provided. Note that the vertical scale varies.

predicted and observed CO_2 concentration is almost twice the assigned uncertainty. Upon closer examination, this is primarily due to the χ_i^2 value in the month of February (14.7), which is due to a combination of low assigned uncertainty (0.8 ppm) and relatively large mismatches (model mean of 2.8 ppm). Other stations with two or more months exceeding a χ_i^2 value of 4 are Guam (GMI: 144.8°E, 13.4°N, December, January, March), Izana,

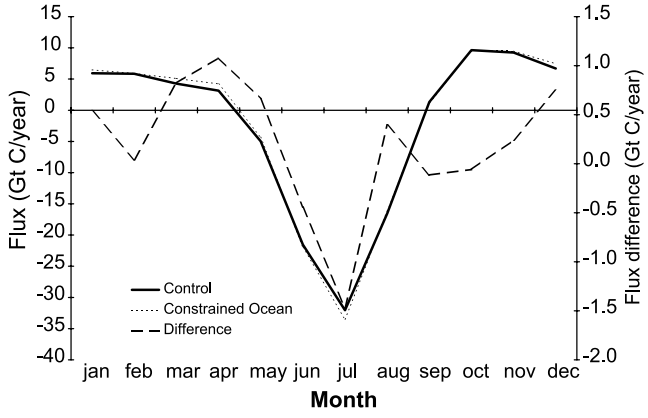

Figure 6b. Estimated fluxes for the control case, the case in which prior uncertainties for the North Pacific, Northern Ocean, and North Atlantic are reduced by a factor of 4, and the difference. The fluxes represent the sum of the Boreal North America, Temperate North America, Boreal Asia, Temperate Asia, and Europe regions.

Canary Islands (IZO: 16.5°W, 28.3°N, June, July), Utah, United States (UTA: 113.7°W, 39.9°N, January, February), Colorado, United States, 5000 m (CARR: 104.8°W, 40.9°N, March, April), Plateau Rosa, Italy (PRS: 7.7°E, 49.3°N, June, July), and Hungary (December, January). Sensitivity tests of the annual mean inversion found similar results for Guam and Cape Rama India [*Law et al.*, 2003].

[41] By the same token, χ_i^2 values much less than one indicate stations for which the assigned uncertainty may be too large and should, therefore, contribute more to the total χ^2 value. Stations for which the annual mean χ_i^2 value is less than 0.25 (indicating mismatches $^1/_2$ the assigned uncertainty) include Bass Strait, Tasmania (AIA: 144.3°E, 40.5°S), South Pole (SPO: 24.8°W, 90°S), Halley Bay, Antarctica (HBA: 25.5°W, 75.7°S), Syowa Station, Antarctica (SYO: 39.6°E, 69°S), Mawson Station, Antarctica (MAA: 62.9°W, 67.6°S), and Palmer Station, Antarctica (PSA: 64°W, 64.9°S). All of these stations are in the southern high latitudes.

[42] In order to confirm that these stations are either providing too much or too little weight to the inversion, a number of tests have been performed. In the first, the stations with largeχ_i^2 values are removed from the inversion. In the second, the stations with small χ_i^2 values are adjusted such that their uncertainty is reduced by a factor of 2. In the last test, both of these changes are made. The results are shown in Figure 8 The tropical regions show the most significant changes, and independent tests (not shown) indicate that these are due primarily to the removal of the Guam and Cape Rama India stations. Reduction of the uncertainty associated with the southern high latitude stations had a negligible impact on the regional fluxes except for some small changes in the South Indian Ocean region.

[43] Given the much greater number of observing sites over the northern extratropics, the removal of a few sites has little impact on the fluxes in those regions. However, the removal of Guam and Cape Rama, India, constitute a considerable reduction in observational constraint in the tropics and hence, lead to changes in those regions primarily.

4. Discussion

4.1. Comparison to Annual Mean Inversion

[44] Table 1 presents the model mean, annual mean carbon flux estimates for each of the land and ocean regions considered in this study. In addition, the model mean flux estimates from the previously published annual mean inversion are included for comparison. The two studies show considerable agreement in all regions with the exception of Northern Africa. The current study estimates an annual mean release from this region (0.79 ± 1.0 Gt C/year) compared to the previous study which estimated no net flux (0.01 ± 1.3 Gt C/year). However, given the large amount of uncertainty associated with the estimates for this region, the change lies within the uncertainty. Since the global total atmospheric growth rate is identical in the two studies, the difference in Northern Africa must be compensated for elsewhere. This occurs equally across the Tropical Asia and Australasia regions, both of which are also estimated with considerable uncertainty. Examination of the aggregated land and ocean totals indicates that the differences between the two studies reflect compensatory fluxes between the Tropical and Southern land and ocean regions, respectively.

[45] In the northern extratropical regions, the current study estimates a slightly larger annual mean net uptake in Europe but produces less uptake in Temperate and Boreal Asia. However, each of these differences is well within the estimated uncertainty.

[46] The consistency between the annual mean inversion and the annual mean calculated from the seasonal inversion is consistent with a recent study exploring various aspects of the CO_2 inversion problem [*Peylin et al.*, 2002]. In their 17-region inversion, which studied results from three models, the authors found regional model mean differences no larger than 0.5 Gt C/year.

4.2. Posterior Flux Amplitude

[47] As suggested in section 3.1, the posterior flux seasonality for the northern land, in particular, will reflect adjustments to the background responses such that the total predicted CO_2 seasonal cycle best matches the observed CO_2 seasonal cycle. Figure 9a ($r^2 = 0.7$) shows the model-specific relationship between the estimated northern land flux amplitude and the northern extratropical background concentration amplitude (the values in Figure 2 legend). As expected, those models which generated relatively weak seasonality when driven by the background fluxes (UCI, JMA, TM2, UCB), generate estimated northern land flux amplitudes that are generally the largest among the 12 models. Models which generated strong seasonality in response to the background fluxes (MATCH:NCEP, NIRE, TM3, GCTM) require less seasonal adjustment in order to match the CO_2 observations over the northern extratropics.

[48] A similar relationship is evident when these indices are considered in conjunction with the annual mean estimated northern land flux. Figure 9b ($r^2 = 0.6$) shows the model-specific relationship between the northern extratrop-

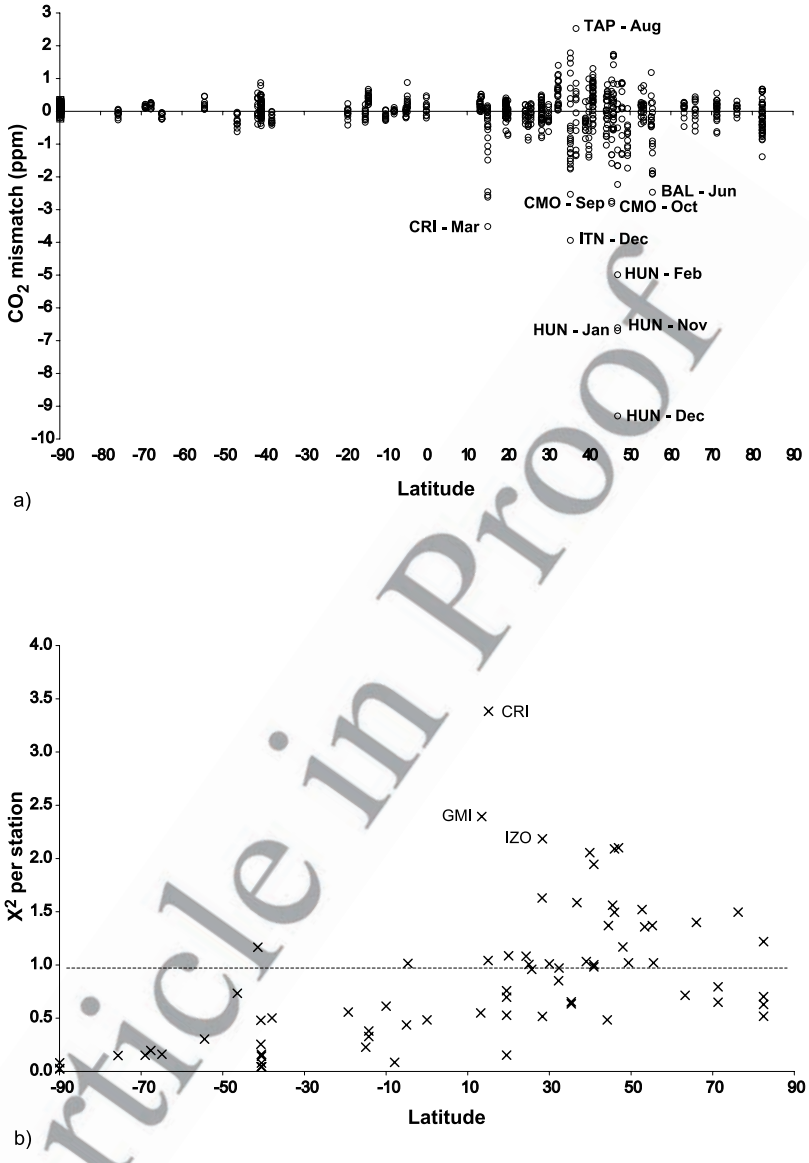

Figure 7. (a) Difference between the model mean predicted CO_2 concentration and the observed. The model mean dramatically underestimates winter concentrations at Hungary. (b) Model/Annual mean of the χ^2 per station values. Largest values are noted for Cape Rama India (CRI), Guam (GMI), and Izana Observatory (IZO).

ical background concentration amplitude and the estimated annual mean northern land flux. Most of the models which generated weak seasonality in response to the background fluxes (UCI, JMA, TM2) and required more seasonal flux adjustment also infer the smallest annual mean uptake in the northern land regions. The relationships exhibit some scatter. For example, UCB which was one of the models with a weak background response amplitude requires a relatively large northern land sink. This may be due to the strong background response to winter emissions but a relatively weak response to summer uptake (see Figure 1a).

[49] In previous work, the annual mean northern land flux correlated with the strength of the model rectifier and the distribution of the models follows closely the distribution found in Figure 9 [*Gurney et al.*, 2003]. Hence models which respond vigorously to the background fluxes, simulate strong annual mean rectifiers, require less seasonal flux adjustment and require the largest northern land sink to best match observed CO_2.

4.3. Mechanistic Implications of the Inverse Estimates

[50] Consistent with a variety of other studies, a large northern extratropical land sink (-2.5 ± 1.2 Gt C/year) is evident in the results presented here [*Tans et al.*, 1990; *Ciais et al.*, 1995; *Fan et al.*, 1998; *Bousquet et al.*, 1999; *Kaminski et al.*, 1999; *Pacala et al.*, 2001; *Baker*, 2001; *Peylin et al.*, 2002]. Our annual mean uptake is greater in Temperate North America (-0.90 ± 0.5 Gt C/year) and Europe (-0.98 ± 0.4 Gt C/year), with less uptake in Temperate Asia (-0.43 ± 0.7 Gt C/year) and Boreal Asia

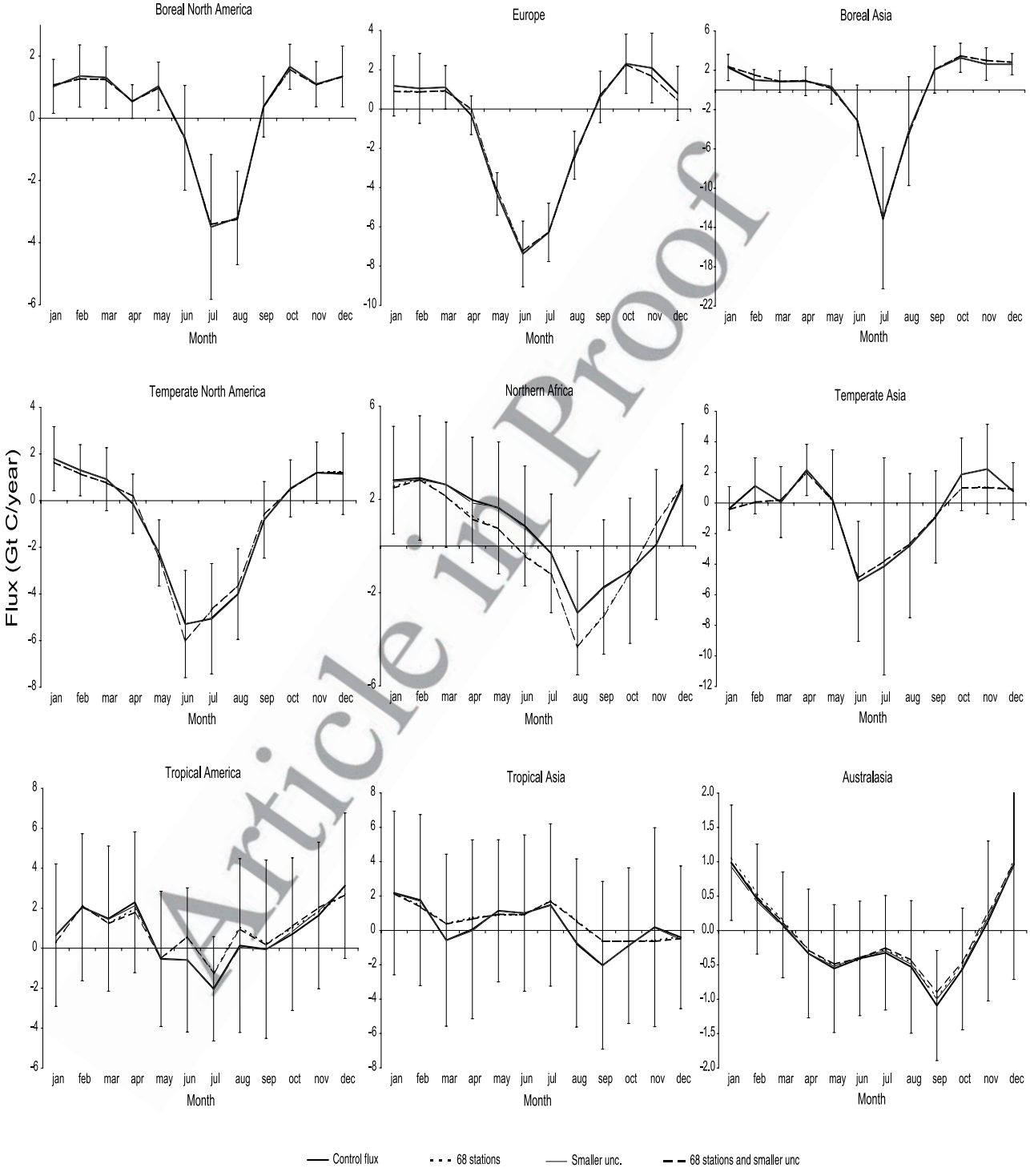

Figure 8a. Station sensitivity for selected land regions. Estimated flux for the control inversion (75 stations), an inversion with 68 stations (removed CRI, GMI, IZO, UTA, Carr 5000m, PRS, and HUN), the control inversion with halved uncertainty on six southern stations (Bass Strait, SPO, HBA, SYO, MAA, and PSA), and an inversion with the combination of these two station adjustments. Note that the vertical scale varies. The fluxes do not include fossil fuel emissions.

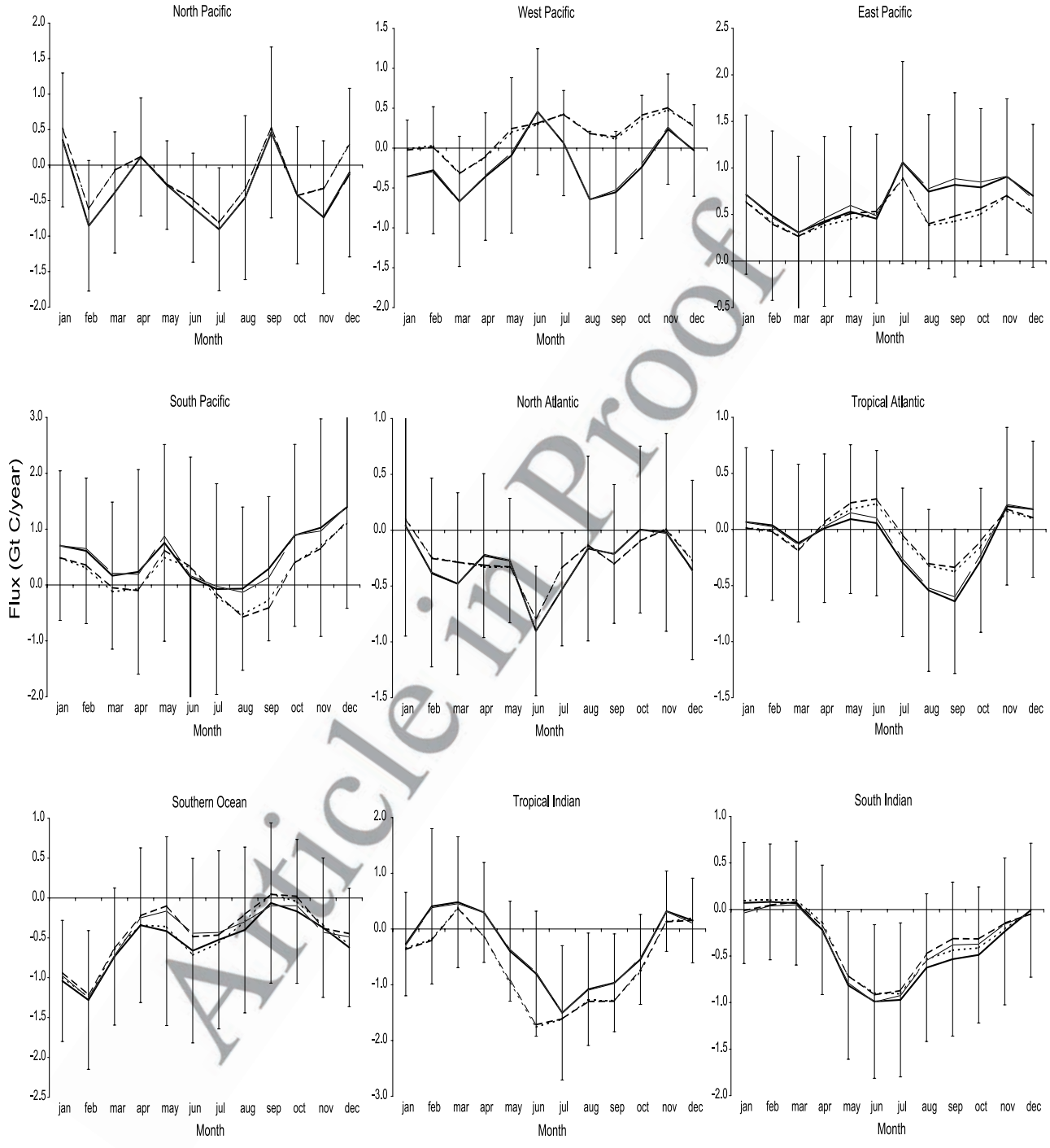

Figure 8b. As in Figure 8a but for selected ocean regions.

(-0.39 ± 0.7 Gt C/year). A number of different hypotheses have been proffered to explain this residual uptake. These include fertilization by Nitrogen or CO_2 itself, changes in temperature and precipitation, and alterations in land-use [*Houghton et al.*, 1998; *Schimel et al.*, 1996; *Prentice et al.*, 2001]. Though the flux estimates in Figures 3, 4, and 5 cannot explicitly test these hypotheses, the broad features in the northern land regions may provide some useful additions to the current evidence supporting the various proposed uptake mechanisms. Both Boreal Asia and Europe show greater uptake or lessened respiration at the height of the growing season when compared to the seasonally balanced prior flux. Even when additional uptake as estimated by inventory studies is included, the peak European uptake is significantly greater than the prior flux. One possible explanation of this is the use of air temperature rather than soil temperature in the CASA model used to generate the prior flux estimates. This would tend to increase the level of heterotrophic respiration and hence offset the net uptake over the growing season. This is further suggested by the

t1.1 **Table 1.** Annual Model Mean Flux Estimates, Uncertainties, and Results From Previously Published Annual Mean Inversion Study

t1.2 Region	Mean Estimated Flux, Gt C/year	"Within" Uncertainty, Gt C/year	"Between" Uncertainty, Gt C/year	*Gurney et al.* [2002] Inversion,[a] C/year	Flux Difference, Gt C/year
t1.3 Boreal North America	0.20	0.18	0.28	0.28	−0.08
t1.4 Temperate North America	−0.89	0.22	0.32	−0.82	−0.07
t1.5 Tropical America	0.74	0.73	0.77	0.67	0.07
t1.6 South America	−0.24	0.64	0.61	−0.12	−0.12
t1.7 Northern Africa	0.79	0.54	0.85	−0.01	0.78
t1.8 Southern Africa	−0.51	0.58	0.60	−0.29	−0.22
t1.9 Boreal Asia	−0.36	0.23	0.51	−0.60	0.23
t1.10 Temperate Asia	−0.41	0.34	0.74	−0.42	0.01
t1.11 Tropical Asia	0.27	0.45	0.94	0.42	−0.15
t1.12 Australasia	−0.10	0.14	0.15	−0.15	0.05
t1.13 Europe	−0.96	0.18	0.43	−0.61	−0.35
t1.14 North Pacific	−0.32	0.14	0.28	−0.25	−0.06
t1.15 West Pacific	−0.21	0.15	0.27	−0.15	−0.05
t1.16 East Pacific	0.66	0.18	0.27	0.63	0.03
t1.17 South Pacific	0.51	0.29	0.49	0.49	0.01
t1.18 Northern Ocean	−0.27	0.08	0.17	−0.30	0.02
t1.19 North Atlantic	−0.29	0.15	0.30	−0.45	0.16
t1.20 Tropical Atlantic	−0.10	0.18	0.16	−0.05	−0.05
t1.21 South Atlantic	−0.05	0.24	0.07	−0.04	−0.01
t1.22 Southern Ocean	−0.55	0.17	0.33	−0.47	−0.08
t1.23 Tropical Indian Ocean	−0.33	0.19	0.26	−0.34	−0.01
t1.24 South Indian Ocean	−0.39	0.19	0.22	−0.24	−0.15
t1.26 Northern land	−2.42	0.30	1.09	−2.16	−0.26
t1.27 Tropical land	1.80	0.78	1.65	1.10	0.70
t1.28 Southern land	−0.85	0.70	0.94	−0.56	−0.29
t1.29 Northern ocean	−0.88	0.24	0.51	−1.00	0.12
t1.30 Tropical ocean	0.03	0.37	0.41	0.09	−0.06
t1.31 South ocean	−0.49	0.39	0.51	−0.26	−0.22
t1.33 Total Land	−1.46	0.62	0.75	−1.62	0.16
t1.34 Total Ocean	−1.34	0.62	0.75	−1.18	−0.16
t1.36 Global Total	−2.81	0.01	0.00	12.80	−0.00

t1.37 [a]This reflects an annual mean inversion without the Darwin observing station.

difference in many of these northern land regions during the winter. Europe, Boreal Asia, Temperate North America, and Temperate Asia all contain months where the estimated flux is lower than the prior value, suggesting less winter respiration than the prior model. Differences in peak growing season uptake could also be due to errors in the NPP estimated in the prior model which are primarily driven by NDVI measurements [*Potter et al.*, 1993]. This is also relevant for the considerable mismatch of peak uptake in the Temperate Asian region. Many of the models in this study place the maximum uptake in June, whereas the prior model placed the maximum in August. This difference in peak uptake suggests that the June CO_2 concentration, driven primarily by the background biosphere exchange, is too high relative to observations and hence a large sink is required to reduce this mismatch.

[51] Because the Temperate Asian region spans latitudes from roughly 15°N to 45°N and has only a few CO_2 observing sites, the difference may be due to poor regional representation in the inverse estimate [*Kaminski et al.*, 2001; *Engelen et al.*, 2002]. Such "representation error" is further suggested by performing the inversion without the Ulann Uul Mongolia (UUM: 111.10°E, 44.5°N), Tae-ahn Peninsula (TAP: 126.13°E, 36.73°N), and Ryori Japan (RYO: 141.83°E, 39.03°N) CO_2 observing stations. Removal of these stations results in a more even distribution of uptake across the June to August timeframe. The seasonality of these three influential stations within and downwind of the Temperate Asian region are likely not representative of the region as a whole. Hence the background biospheric exchange generates CO_2 levels that reflect the whole region while the inverted fluxes are driven by a small spatially biased sample of atmospheric CO_2 as measured by these influential stations. Subdivision of the Temperate Asia region may result in a less biased posterior flux estimate but would likely increase the posterior uncertainty. The motivation for limiting the number of inverted regions is the reduction of random error and the need to limit the computation burden of the forward model simulations. This trade-off between random error and bias is further discussed in recent work [*Baker*, 2001].

[52] This source of error in the inversion set-up itself is one source of potential bias that is very likely present in undersampled regions. The other primary source of error in the inversion approach is error due to transport. TransCom was initially devised to explore that magnitude of the transport error. However, only the random component (the between uncertainty estimates) can be quantified here. In considering the model mean flux estimates, this error may be minimized through the use of the model average. However, all models may contain the same transport biases and therefore result in biased flux estimates.

[53] Both the boreal regions show a slight delay in the onset of growing season uptake relative to the prior model.

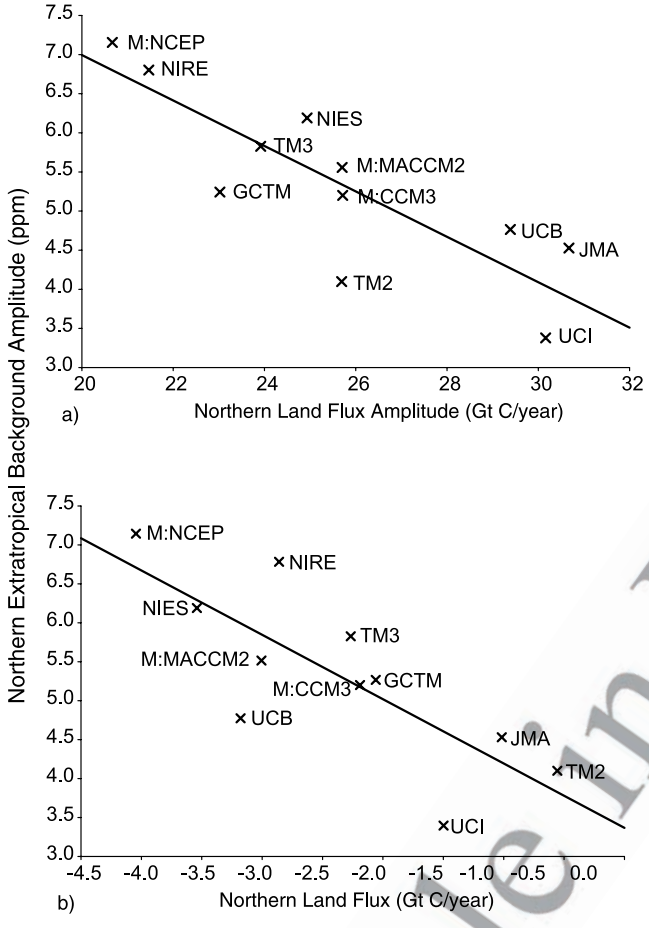

Figure 9. (a) Estimated Northern land flux amplitude (October through March minus June through August) versus the northern extratropical background (fossil plus neutral bio plus background ocean) response amplitude (r^2 = 0.75). (b) Northern land flux versus the northern extratropical background response amplitude (r^2 = 0.62).

As suggested by other work, this may be the result of earlier Spring thaw, resulting in an imbalance of respiration over photosynthesis [*Goulden et al.*, 1998]. In the month of June, this would require a 50% and 38% increase in the prior model respiration flux in order to match the estimated flux for the Boreal North American and Boreal Asian regions, respectively.

5. Conclusions

[54] With the participation of 12 atmospheric tracer transport models, a control case has been constructed to characterize the seasonal sources and sinks of carbon as another step in the TransCom atmospheric CO_2 inversion experiment. In order to construct this control inversion, decisions regarding prior fluxes, flux uncertainties, observational data and observational data uncertainties have been made.

[55] As found in recent TransCom work, the model responses to the background tracers provide a first indication of model to model differences. In the current experiment, the amplitude of the background flux response was inversely related to the amplitude of the estimated northern land flux. Furthermore, those models that exhibit a weak response amplitude to the background flux are among the models with the smallest northern land sink. This relationship is consistent with earlier TransCom results showing the relationship between models that tend to rectify seasonal exchange with the biosphere and the annual mean estimated net uptake over the northern land.

[56] For the northern land regions, the model mean results show deviations from the prior flux in both the growing season and during winter months. Most notable are the significantly greater uptake during the height of the growing season over Europe compared to the prior model. Temperate North America and Boreal Asia exhibit less emission during some winter months, while a 2-month discrepancy exists regarding the timing of peak uptake in Temperate Asia.

[57] The northern oceans show heightened seasonality that may be due to misallocation of terrestrial flux to adjacent oceanic regions. As with the earlier annual mean inversion results, the Southern Ocean region exhibits less carbon uptake than ΔpCO_2 measurements would suggest. There is general agreement between the ΔpCO_2-based prior flux and the fluxes estimated here for Austral summer, but significant departures during fall and spring months occur suggesting that the timing of ΔpCO_2 observations may be, in part, responsible for the discrepancy.

[58] Owing to limited CO_2 observations, tropical regions, particularly over land, show considerable uncertainty and may contain unrealistic seasonal swings in flux due to unconstrained adjustments to maintain the global mass balance constraint. These regions are far more sensitive to prior flux uncertainties than the northern extratropics which show insensitivity to this aspect of the inversion set-up.

[59] The timing of the differences between the prior model and the estimated fluxes suggest that respiration may play an important role in either errors in the prior model or real changes in the winter flux for the northern extratropical land regions. In particular, changes in the timing of increased springtime respiration versus photosynthesis may explain the lessened net spring uptake in Boreal North America and Boreal Asia.

[60] Biases caused by transport error across all models or representation error are potential limitations to this method. However, only random errors are characterized in this study. Furthermore, interpretation is somewhat limited by examination of a single 5-year mean and the use of the single station network used here. Though we have tested the model mean inversion result to some aspects of the inversion set-up, this is not exhaustive, and future work will test further elements, in particular those related to station choices and uncertainties. Finally, interannual variations in seasonality, which may give further mechanistic insight, have not been explored in this study.

[61] Further results from the TransCom experiment are forthcoming. In particular, results are expected from an interannual inversion, model to model comparisons, and a comparison of inverse results using different inversion approaches. These constitute the last primary elements of the TransCom 3 intercomparison and should shed further

light on the sources and sinks of carbon and the sources of uncertainty in making these inverse estimates.

[62] **Acknowledgments.** This work was made possible through support from the National Science Foundation (OCE-9900310), the National Oceanic and Atmospheric Administration (NA67RJ0152, Amend 30), and the International Geosphere Biosphere Program/Global Analysis, Interpretation, and Modeling Project. S. Fan and J. Sarmiento acknowledge support from NOAA's Office of Global Programs for the Carbon Modeling Consortium.

References

Andres, R. J., G. Marland, I. Fung, and E. Matthews (1996), A 1° × 1° distribution of carbon dioxide emissions from fossil fuel consumption and cement manufacture, 1950–1990, *Global Biogeochem. Cycles*, *10*(3), 419–429.

Baker, D. F. (2001), Sources and sinks of atmospheric CO_2 estimated from batch least-squares inversions of CO_2 concentration measurements, Ph.D. dissertation, Princeton Univ., Princeton, N. J.

Bousquet, P., P. Ciais, P. Peylin, M. Ramonet, and P. Monfrey (1999), Inverse modeling of annual atmospheric CO_2 sources and sinks: 1. Method and control inversion, *J. Geophys. Res.*, *104*(D21), 26,161–26,178.

Bousquet, P., P. Peylin, P. Ciais, C. Le Quéré, P. Friedlingstein, and P. Tans (2000), Regional changes in carbon dioxide fluxes of land and oceans since 1980, *Science*, *290*, 1342–1346.

Ciais, P., P. P. Tans, M. Troliier, J. W. C. White, and R. J. Francey (1995), A large Northern Hemisphere terrestrial CO_2 sink indicated by the $^{13}C/^{12}C$ ratio of atmospheric CO_2, *Science*, *269*, 1098–1102.

Denning, A. S., M. Holzer, K. R. Gurney, M. Heimann, R. M. Law, P. J. Rayner, I. Y. Fung, S. Fan, S. Taguchi, P. Friedlingstein, Y. Balkanski, J. Taylor, M. Maiss, and I. Levin (1999), Three-dimensional transport and concentration of SF6: A model intercomparison study (TransCom 2), *Tellus, Ser. B*, *51*, 266–297.

Engelen, R. J., A. S. Denning, and K. R. Gurney (2002), On error estimation in atmospheric CO_2 inversions, *J. Geophys. Res.*, *107*(D22), 4635, doi:10.1029/2002JD002195.

Enting, I. (2002), *Inverse Problems in Atmospheric Constituent Transport*, Cambridge Univ. Press, New York.

Enting, I. G., C. M. Trudinger, and R. J. Francey (1995), A synthesis inversion of the concentration and $\delta^{13}C$ of atmospheric CO_2, *Tellus, Ser. B*, *47*, 35–52.

Fan, S., M. Gloor, J. Mahlman, S. Pacala, J. Sarmiento, T. Takahashi, and P. Tans (1998), A large terrestrial carbon sink in North America implied by atmospheric and oceanic carbon dioxide data and models, *Science*, *282*, 442–446.

GLOBALVIEW-CO_2 (2000), Cooperative Atmospheric Data Integration Project—Carbon Dioxide [CD-ROM], NOAA Clim. Model. and Diag. Lab., Boulder, Colo.

Goulden, M. L., et al. (1998), Sensitivity of boreal forest carbon balance to soil thaw, *Science*, *279*, 214–217.

Gurney, K., R. Law, P. Rayner, and A. S. Denning (2000), TransCom 3 experimental protocol, Pap. 707, Dept. of Atmos. Sci., Colo. State Univ. (Available at http://transcom.colostate.edu/TransCom_3/transcom_3.html)

Gurney, K. R., et al. (2002), Towards robust regional estimates of CO_2 sources and sinks using atmospheric transport models, *Nature*, *415*, 626–630.

Gurney, K. R., et al. (2003), Transcom 3 CO_2 Inversion Intercomparison: 1. Annual mean control results and sensitivity to transport and prior flux information, *Tellus, Ser. B*, *55*, 555–579.

Houghton, R. A., E. A. Davidson, and G. M. Woodwell (1998), Missing sinks, feedbacks, and understanding the role of terrestrial ecosystems in the global carbon balance, *Global Biogeochem. Cycles*, *12*(1), 25–34.

Kaminski, T., M. Heimann, and R. Giering (1999), A coarse grid three-dimensional global inverse model of the atmospheric transport: 2. Inversion of the transport of CO_2 in the 1980s, *J. Geophys. Res.*, *104*(D15), 18,555–18,581.

Kaminski, T., P. J. Rayner, M. Heimann, and I. G. Enting (2001), On aggregation errors in atmospheric transport inversion, *J. Geophys. Res.*, *106*(D5), 4703–4715.

Law, R. M., et al. (1996), tions in modeled atmospheric transport of carbon dioxide and the consequences for CO_2 inversions, *Global Biogeochem. Cycles*, *10*(4), 783–796.

Law, R. M., Y.-H. Chen, K. R. Gurney, and TransCom 3 modelers (2003), TransCom 3 CO_2 inversion intercomparison: 2. Sensitivity of annual mean results to data choices, *Tellus, Ser. B*, *55*, 580–595.

Metzl, N., C. Brunet, A. Jabaud-Jan, A. Poisson, and B. Schauer (2001), Summer and winter air-sea CO_2 fluxes in the Southern Ocean, paper presented at Sixth International Carbon Dioxide Conference, Organizing Comm. of 6th Int. Carbon Dioxide Conf., Sendai, Japan.

Pacala, S. W., et al. (2001), Convergence of land- and atmosphere-based U.S. carbon sink estimates, *Science*, *292*, 2316–2320.

Peylin, P., D. Baker, J. Sarmiento, P. Ciais, and P. Bousquet (2002), Influence of transport uncertainty on annual mean and seasonal inversions of atmospheric CO_2 data, *J. Geophys. Res.*, *107*(D19),4385, doi:10.1029/2001JD000857.

Potter, C. S., J. T. Randerson, C. B. Field, P. A. Matson, P. M. Vitousek, H. A. Mooney, and S. A. Klooster (1993), Terrestrial ecosystem production: A process model based on global satellite and surface data, *Global Biogeochem. Cycles*, *7*(4), 811–841.

Prentice, I. C., G. Farquhar, M. Fashm, M. Goulden, M. Heimann, V. Jaramillo, H. Kheshgi, C. Le Quéré, and R. J. Scholes (2001), The carbon cycle and atmospheric carbon dioxide, in *Climate Change 2001: The Scientific Basis, Contribution of Working Group I to the Third Assessment Report of the Intergovernmental Panel on Climate Change*, edited by J. T. Houghton et al., pp. 183–237, Cambridge Univ. Press, New York.

Randerson, J. T., M. V. Thompson, T. J. Conway, I. Y. Fung, and C. B. Field (1997), The contribution of terrestrial sources and sinks to trends in the seasonal cycle of atmospheric carbon dioxide, *Global Biogeochem. Cycles*, *11*, 535–560.

Rayner, P. J., I. G. Enting, R. J. Francey, and R. L. Langenfelds (1999), Reconstructing the recent carbon cycle from atmospheric CO_2, $\delta^{13}C$ and O_2/N_2 observations, *Tellus, Ser. B*, *51*, 213–232.

Rödenbeck, C., S. Houweling, M. Gloor, and M. Heimann (2003), Time-dependent atmospheric CO_2 inversions based on interannually varying tracer transport, *Tellus, Ser. B*, *55*, 488–497.

Schimel, D., D. Alves, I. Enting, M. Heimann, F. Joos, D. Raynaud, and T. Wigley (1996), CO_2 and the carbon cycle, in *Climate Change 1995: The Science of Climate Change*, *Contribution of WG1 to the Second Assessment Report of the IPCC*, edited by J. T. Houghton et al., pp. 65–86, Cambridge Univ. Press, New York.

Takahashi, T., R. H. Wanninkhof, R. A. Feely, R. F. Weiss, D. W. Chipman, N. Bates, J. Olafsson, C. Sabine, and S. C. Sutherland (1999). Net sea-air CO_2 flux over the global oceans: An improved estimate based on the sea–air pCO_2 difference, paper presented at 2nd CO_2 in Oceans Symposium, Cent. for Global Environ. Res. Natl. Inst. for Environ. Stud., Tsukuba, Japan.

Tans, P. P., I. Y. Fung, and T. Takahashi (1990), Observational constraints on the global atmospheric CO_2 budget, *Science*, *247*, 1431–1438.

Tarantola, A. (1987), The least-squares (12-norm) criterion, in *Inverse Problem Theory: Methods for Data Fitting and Parameter Estimation*, chap. 4, pp. 187–287, Elsevier Sci., New York.

D. Baker, National Center for Atmospheric Research (NCAR), Boulder, CO 80303, USA.

P. Bousquet, P. Ciais, and P. Peylin, Laboratoire des Sciences du Climat et de l'Environment (LSCE), F-91198 Gif-sur-Yvette Cedex, France.

L. Bruhwiler, National Oceanic and Atmospheric Administration (NOAA), Climate Monitoring and Diagnostics Laboratory, 326 Broadway R/CG1, Boulder, CO 80303, USA.

Y.-H. Chen, Department of Earth, Atmospheric, and Planetary Science, Massachusetts Institute of Technology (MIT), Cambridge, MA 02141, USA.

S. Denning and K. R. Gurney, Department of Atmospheric Science, Colorado State University, Fort Collins, CO 80523, USA. (denning@atmos.colostate.edu; keving@atmos.colostate.edu)

I. Y. Fung and J. John, Center for Atmospheric Sciences, McCone Hall, University of California, Berkeley, Berkeley, CA 94720-4767, USA.

M. Heimann, Max-Planck-Institute fur Biogeochemie, D-07701 Jena, Germany.

R. Law and P. Rayner, CSIRO Atmospheric Research, PMB 1, Aspendale, Victoria 3165, Australia. (rachel.law@csiro.au; peter.rayner@csiro.au)

T. Maki, Quality Assurance Section, Atmospheric Environment Division, Observations Department, Japan Meteorological Agency, 1-3-4 Otemachi, Chiyoda-ku, Tokyo 100-8122, Japan.

S. Maksyutov, Institute for Global Change Research, Frontier Research System for Global Change, Yokohama 236-0001, Japan.

B. C. Pak and M. Prather, Earth System Science, University of California, Irvine, CA 92697-3100, USA. (bpak@halo.ps.uci.edu)

S. Taguchi, National Institute of Advanced Industrial Science and Technology, 16-1 Onogawa Tsukuba, Ibaraki 305-8569, Japan.

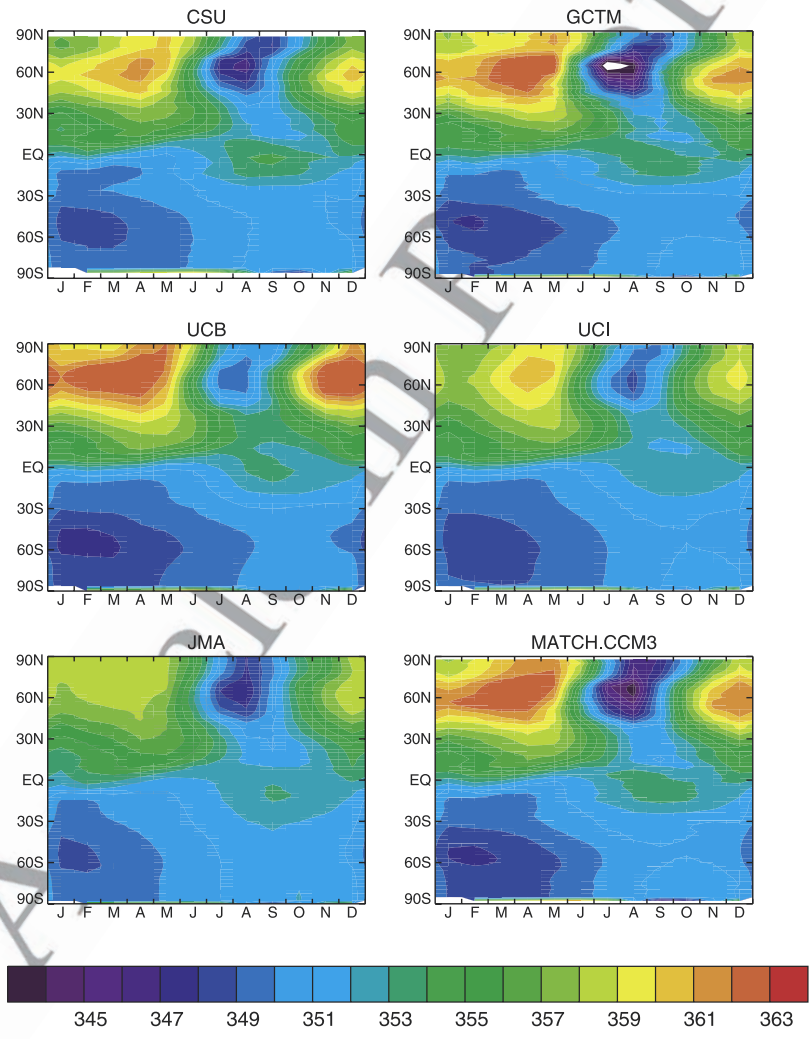

Figure 1. Zonal mean monthly predicted concentration driven by the background fluxes (fossil fuel, seasonally balanced biosphere exchange, ocean exchange) for each of the participating tracer transport models.

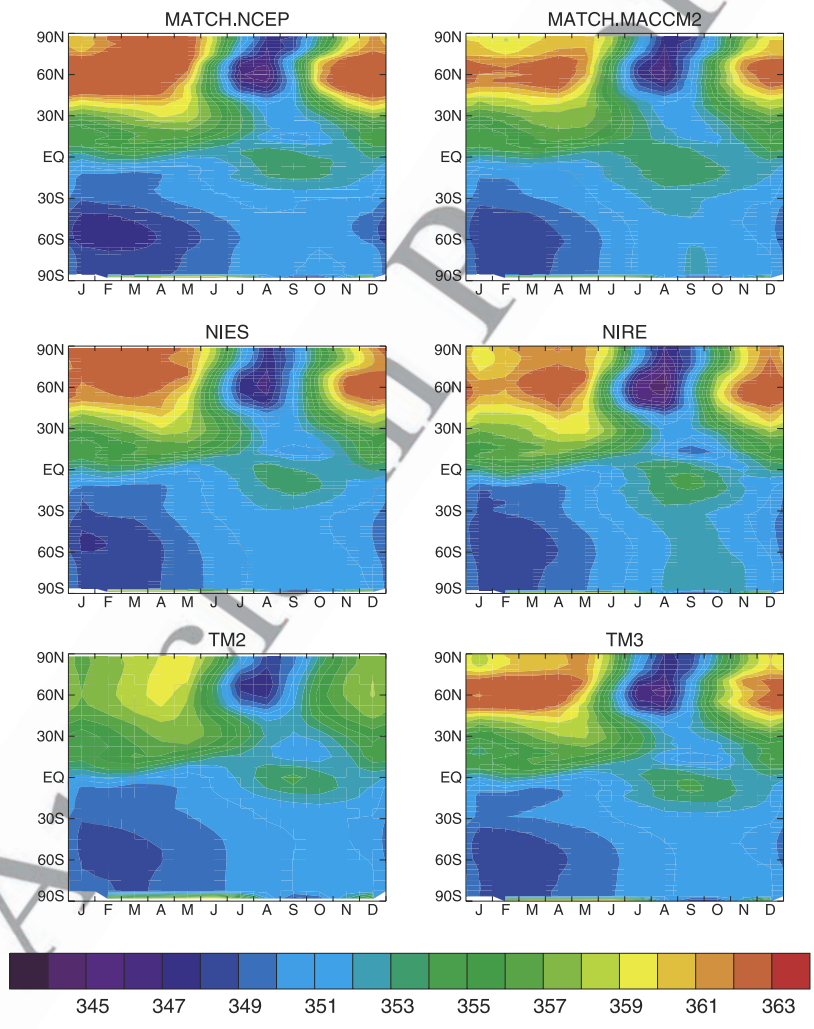

Figure 1. (continued)

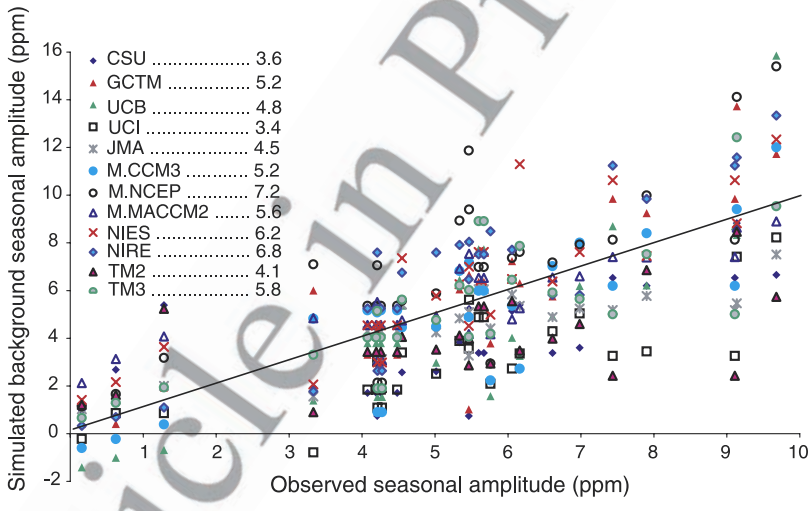

Figure 2. Simulated background seasonal amplitude versus the observed amplitude at stations north of 35°N. Amplitude is defined as the mean October-March concentration minus the mean June-August concentration. The station average simulated values are provided in the legend. The observed station average is 5.6 ppm. A one-to-one line is included.

4.1 Introduction

The TransCom 3 interannual CO_2 inversion builds upon the annual mean and seasonal inversion methods by extending the time domain to include multi-year fluxes. Examination of the interannual fluxes allows one to both compute time-average fluxes with lower uncertainty, ascertain regional trends in carbon exchange, and examine the interannual variability for mechanistic explanations. Analysis of the multi-model results allows for an investigation of the tranport error and can lead to more robust results than an inversion performed with a single model.

Interannual CO_2 inversions have been performed by other investigators starting with *Rayner et al.* in 1999.[1] In that study, the authors used the GISS tracer transport model and two CO_2 observing networks of 12 and 25 stations to infer fluxes for 26 regions (12 ocean, 14 land) spanning the 1980 to 1996 time period. They also utilized observations of the $\delta^{13}C$ and atmospheric oxygen as an aid in separating the ocean from land exchange.

Bousquet and colleagues (2000) performed an interannual inversion using the TM2 tracer transport model and 67 CO_2 observing sites across the time period 1980 to 1998. In that study, which returned fluxes for 19 regions (11 ocean and 8 land), the authors focused solely on the interannual variability (time-mean exchange was removed) by showing that quantification of the interannual variability is far less error prone than the estimation of absolute carbon exchange. The primary reason for this is the magnitude of the CO_2 observations themselves. Absolute flux estimation relies on spatial CO_2 concentration gradients of a few tenths of a ppm whereas the temporal variability exhibits time gradients on the order of a few ppm.

Baker (2001) performed interannual CO_2 inversions with the GCTM model for a similar time period and explored a variety of sensitivity cases including spatial discretization, prior flux values and their uncertainties, and different CO_2 observing networks. A major focus of this study was to explore the impact of different forms of regularization as a way to reduce the estimated flux uncertainties and spurious variability.

Finally, *Rödenbeck* and colleagues (2003b) performed an interannual CO_2 inversion study using the TM3 tracer transport model and five different station networks, ranging in size from 11 to 35 stations. The period examined extended from 1980 to 2000 and the authors discretized the spatial domain into 8º latitude x 10º longitude surface boxes. To accomplish the task of building the response functions for such a dense spatiotemporal domain, the authors utilized an adjoint formulation of the transport model. Unlike all previous interannual CO_2 inversions, this study employed transport winds that varied from year to year based on reanalyzed meteorological observations. A number of sensitivities were examined including spatial aggregation, priors, prior uncertainties, and station choices.

This chapter will cover many of the basics forged in the preceding studies. However, unlike the interannual CO_2 inversions that have come before, this study has the added of advantage of the inclusion of 13 tracer transport models which fortuitously include all the models in the preceding studies. This allows one to quantify the contribution different transport model physics make to the overall flux uncertainty. Furthermore, the sensitivity of the model mean can be tested against many of the axes of sensitivity that have been explored in previous TransCom 3 studies. What I will show is the model mean estimated carbon fluxes are more robust to a variety of inversion set-up choices than would any individual model.

This chapter will begin with the perfunctory treatment of the inversion set-up. Because a number of different time periods and CO_2 observing networks are employed, these are reviewed in some detail. Model mean results will be presented with emphasis on characterizing the two key uncertainty measures generated

[1] There are two other 3D time-dependent studies that were published at roughly the same time (*Law*, 1999; *Dargaville and Simmonds*, 1999). These studies utilized the "mass-balance" inverse approach which is generally considered less reliable than the synthesis batch approach that is used here and in most recent CO_2 inversions. The reason follows from the fact that mass-balance inversion must generate observed CO_2 concentrations in every surface gridcell of the globe. This is performed by an interpolation procedure from fairly sparse monitoring locations. Therefore, errors in the interpolation scheme are directly aliased into the estimated fluxes.

with the model mean. Sensitivity to the prior flux uncertainty, CO_2 observing network, and particular stations will be explored and comparison of long-term means to other studies will be made. The last section in this chapter will present preliminary results exploring linkages to large-scale variability in the atmosphere. This is not meant to be exhaustive but an initial glimpse at work that is slated for the future.

An important caveat in the current study is the fact that none of the transport models involved used interannually varying winds based on true or reanalyzed meteorological observations. The fluxes estimated here are based on winds that repeat over the time period examined. This is a limitation of the initial TransCom experimental protocol and was constructed this way to make the experiment accessible to as many modeling groups as possible. Though utilization of time varying winds has become more common in the last couple of years, it still presents a computational and logistical barrier to many involved in tracer transport modeling.

4.2 Methods

As with all of the TransCom 3 inversion work, the foundations of the inversion used in this interannual experiment are based on the Bayesian synthesis method (*Tarantola*, 1987; *Enting et al.*, 2002). A detailed description of the formalism employed and references to source material is given in previous work for the annual mean TransCom inversion (*Gurney et al.*, 2003). The method used here is the same except that monthly mean CO_2 observations are used for a number of contiguous years rather than annual average CO_2 values composited to a single year. As will be discussed later, different station networks have been chosen to represent different spans of time. The longest time period for which fluxes are estimated is 1980 to 2000.

The forward simulations completed by all the participating modeling groups are identical to those used in the seasonal inversion (*Gurney et al.*, 2004). Details concerning these simulations can be found in that paper or in the TransCom 3 experimental protocol (*Gurney et al.*, 2000). In the case of offline models, a single year of analyzed winds were repeated. In the case of online models, model generated winds were run representing climatological mean conditions and, thus, do not correspond to real transport variability.

One additional model, PCTM, was included in the interannual inversion experiment that was not present in either the annual mean or seasonal inversion. Completion of the forward simulations were not available at the time the analysis on those experiments was being completed. However, annual mean and seasonal results have been generated from the PCTM submission and this model does not appear to be an outlier. As a result, 13 different sets of model output were analyzed in the interannual inversion presented here.

4.2.1 Inversion set-up and observational data

The background fluxes used in this inversion are identical to those used in the seasonal case with one exception. The fossil fuel background flux was used in such a way that the total global growth in fossil fuel emissions was accounted for by scaling the 1990 and/or 1995 emissions maps each year. Prior to 1991, only the 1990 emissions map was used. After 1994, only the 1995 emissions map was used. In between, a weighted average of the two was constructed such that a smooth transition between the two spatial patterns occurred. For the remaining two background fluxes, the neutral biosphere and global oceanic exchange, the same flux patterns were repeated each year.

Prior estimates of the fluxes in each of the 264 region/month flux combinations were determined from independent estimates of terrestrial and oceanic exchange. The land region prior flux estimates incorporate results from recent inventory studies and are identical to the annual mean values used in the annual mean inversion (*Gurney et al.,* 2003). Where more than one estimate for a given region was considered, a mid-point of the estimate spread was used. Because the land region prior fluxes are only available as annual mean values, these were distributed evenly over those months considered the most likely to capture the emission or uptake implied by the prior flux. The ocean region prior flux estimates were prescribed as zero for each month. These priors were used each year of the interannual time period and contained no interannual variation of their own.

The prior flux uncertainty is important for keeping the estimated fluxes within biogeochemically realistic bounds. For land regions in a given month we chose the combination of the uncertainties employed in our annual mean control case (*Gurney et al.,* 2002), and 30% each of NPP and respiration provided by the CASA model of net ecosystem production (*Randerson et al.*, 1997). Since it is unlikely that a given region/month flux adjustment would exceed these values, this provides a reasonable, ecologically relevant upper bound. The prior ocean uncertainties were the product of the annual mean uncertainty values used in the annual mean control inversion and the square root of twelve. This recognized that the variability of the interannual fluxes will require a looser prior than the annual mean inversion experiment. The factor of root twelve was chosen as this represents the conversion between an annual uncertainty and a constant monthly uncertainty assuming no autocorrelation between errors.

The CO_2 observational data were derived from the GLOBALVIEW-2002 dataset (*GLOBALVIEW-CO2*, 2002). GLOBALVIEW is a data product that interpolates CO_2 measurements to a common time interval. Gaps in the data are filled by extrapolation from marine boundary layer measurements. Because many of the stations within the observational dataset have been initiated/retired at various times over the last twenty years and significant gaps exist, a number of different station networks were constructed in this experiment and used to create independent interannual flux estimates. Table A4.1 (Appendix) contains details of the six different networks created.

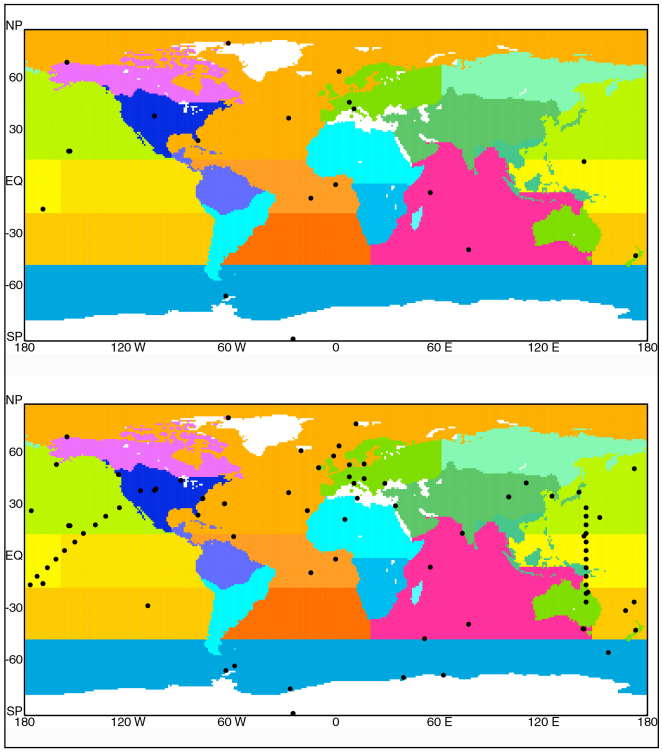

Figure 4.1. Locations of the stations for the a) smallest (23) and b) largest (114) CO_2 observational networks.

Two criteria were employed to arrive at the network choices. First, in order to be included in a network, a station could not have more than a certain number of contiguous years in which the proportion of real to total data falls below 67%.[2] For networks spanning more than one decade, a station could not have more than three contiguous years under this criteria. For the decade length network, this number falls to no more than two. For the five and seven year networks, this falls to no more than one. Second, the multi-year mean percentage of non-missing data in the years that qualified under the first criteria had to exceed 67%. The combination of these two criteria naturally led to the networks represented in table A4.1 (see appendix). The smallest network spanning the 1980 to 2000 time period contained 23 stations while the longest, spanning the 1995 to 2000 time period, contained 114. The 23 station and 114 station networks are shown in figure 4.1.

The uncertainty attached to each data value, *C(D)* in equation 3 of *Gurney et al.*, 2004, was derived from the monthly residual standard deviation (RSD) of individual observations around a smoothed time series as given by GLOBALVIEW. This choice was based on the assumption that the distribution of RSD (higher RSD values for northern and continental sites and lower RSD values for southern hemisphere oceanic sites) reflects the high-frequency variations in transport and regional flux that large-scale transport models are unable to accurately simulate. GLOBALVIEW provides monthly RSD values averaged over 1979-2002 and annual RSD values for each separate year. To obtain monthly values

[2] This value was chosen somewhat arbitrarily. The value appeared to be a natural cut-off when viewing the statistics on all the stations.

for a given time period, the monthly RSD values were scaled by the ratio of the annual RSD values to the 1979-2002 mean annual RSD value.

Direct use of the RSD values for the data uncertainty results in a total reduced χ^2 that is much smaller than unity (*Tarantola,* 1987 pg. 212). This indicates that the predicted concentrations fit the data much better than the uncertainty assigned to the data itself and that the uncertainty should be reduced. The aim is to scale the RSD such that the inversion produces a total χ^2 of 1.0. The details are as follows: the RSD was divided by $(\beta * P)^{0.5}$ where P is the proportion of real data in the record and β is chosen to satisfy our total χ^2 criteria for the particular network. The values for β are provided in table A4.1 (appendix).

4.3 Results

4.3.1 Model Mean

Figure 4.2 shows the model mean interannual inversion results for all the land (part a) and ocean (part b) regions. Included in each of the panels are the results for the six different networks chosen following the criteria described in the last section. The fluxes have been deseasonalized using a 12 month trapezoidal running mean as follows:

$$D_r(t) = \frac{0.5}{12} F_r(t-6) + \frac{1}{12} \sum_{t-6}^{t+6} F_r(t_i) + \frac{0.5}{12} F_r(t+6) \tag{4.1}$$

where $D_r(t)$ is the deseasonalized flux for a particular region, r, for a particular month, t, and $F_r(t)$ is the original flux.

Also included in figure 4.2 are the "within" and "between" uncertainties described in equations 1 and 2 of *Gurney et al.*, 2004. The errors presented in figure 4.2 are associated with the 23 station network only. In order to compute the deseasonalized within model uncertainty, the posterior covariance matrix must be operated on by a deseasonalization operator. This is done as follows:

$$\mathbf{Q} = \mathbf{OPO}^T \tag{4.2}$$

where **Q** represents the deseasonalized posterior covariance matrix for an individual region and model, **O** represents the matrix form of the 12 month trapezoidal running mean, and **P** is the posterior covariance matrix for an individual region and model. Equation 1 of *Gurney et al.*, 2004 is then applied to the diagonal of **Q** so that the within uncertainty can now be written as

$$\overline{\mathbf{C}(\vec{S})} = \sqrt{\sum_{n=1}^{N_{models}} Tr(\mathbf{Q}_n)^2 \Big/ N_{models}} \tag{4.3}$$

The between uncertainty is the spread across the models of the deseasonalized fluxes and is therefore computed as in *Gurney et al.*, 2004 except the flux, in the current case, is the deseasonalized rather than the fully seasonal flux.

As was seen with the annual and seasonal inversion, the relative magnitude of the within and between uncertainties primarily reflect the availability and distribution of CO_2 observations.[3] In those regions for which CO_2 observing stations are neither within or downwind of a region, the within uncertainty is larger

[3] Prior uncertainties can also influence this balance if the prior uncertainty bounds constrict a data driven solution.

than the between uncertainty.[4] On land, the tropics and southern extratropics show larger within than between uncertainty because these regions have few nearby CO_2 observing sites, particularly true for the small 23 station network. In the ocean, the Tropical Indian, East Pacific and the southern extratropical ocean regions (except the Southern Ocean) all have limited nearby CO_2 observations and thus have within uncertainties that tend to be larger than the between. In those regions where CO_2 observations are more prevalent, the between uncertainty tends to be larger (e.g. northern extratropics on land). As the number of observation locations increases in a region, the differences between model concentration response to fluxes from that region are better observed and hence, more easily distinguished. As the number of observing locations decline or are not in the proximity to a regional flux, the different model responses, as seen by the nearest station, are smoothed out relative to one another and hence, are more difficult to distinguish.

[4] "Downwind" is an admittedly subjective term. A quantitative estimate of the power of a station to constrain a particular region can be examined through the "influence" function which incorporates both the basis function response at a particular station and its assigned uncertainty.

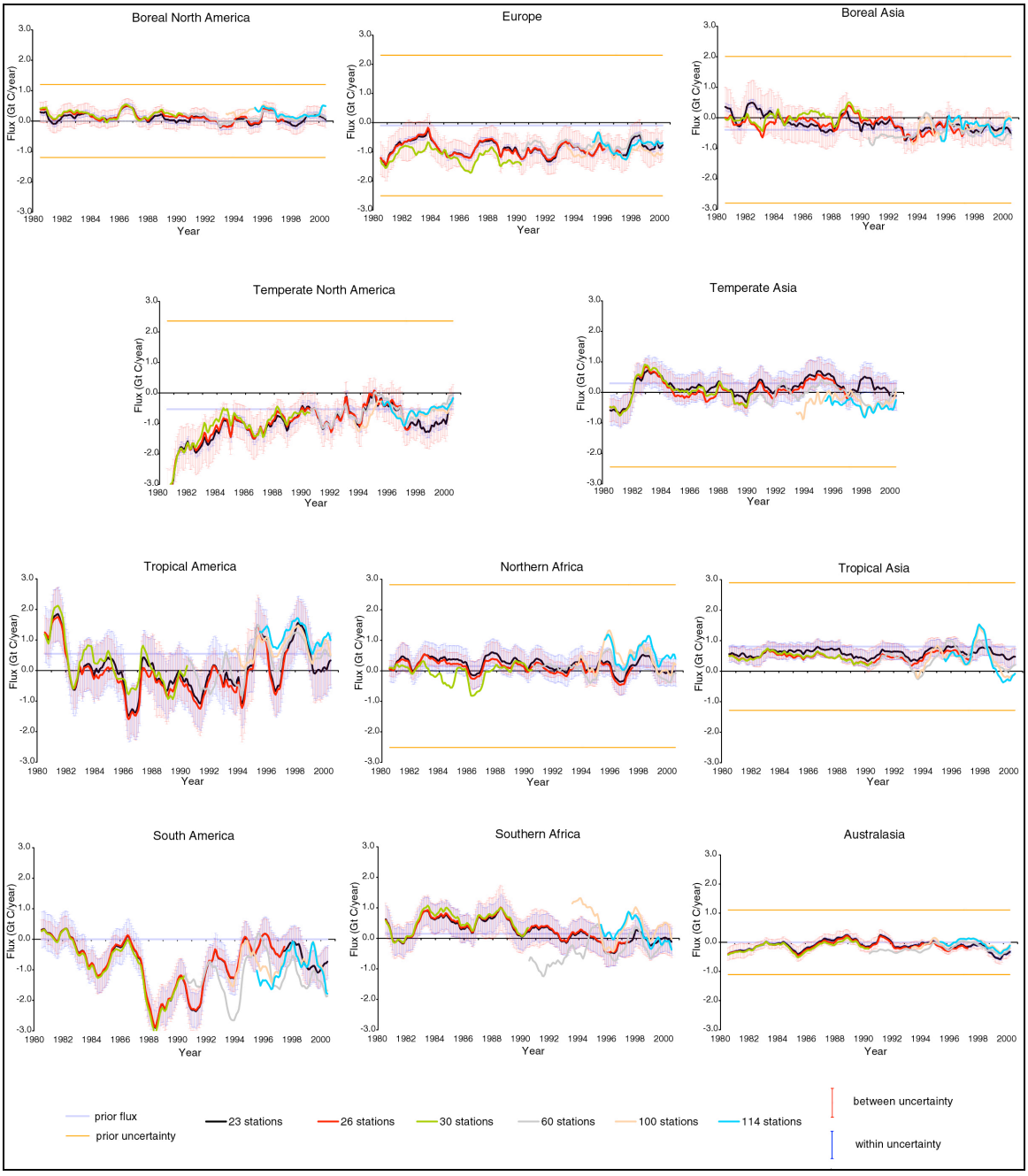

Figure 4.2a. Model mean, deseasonalized, land-based interannual flux estimates (Gt C/year) for the six CO_2 observation networks. The 1σ within and between uncertainty estimates are based on the 23 station network only. Note that all the vertical scales are identical.

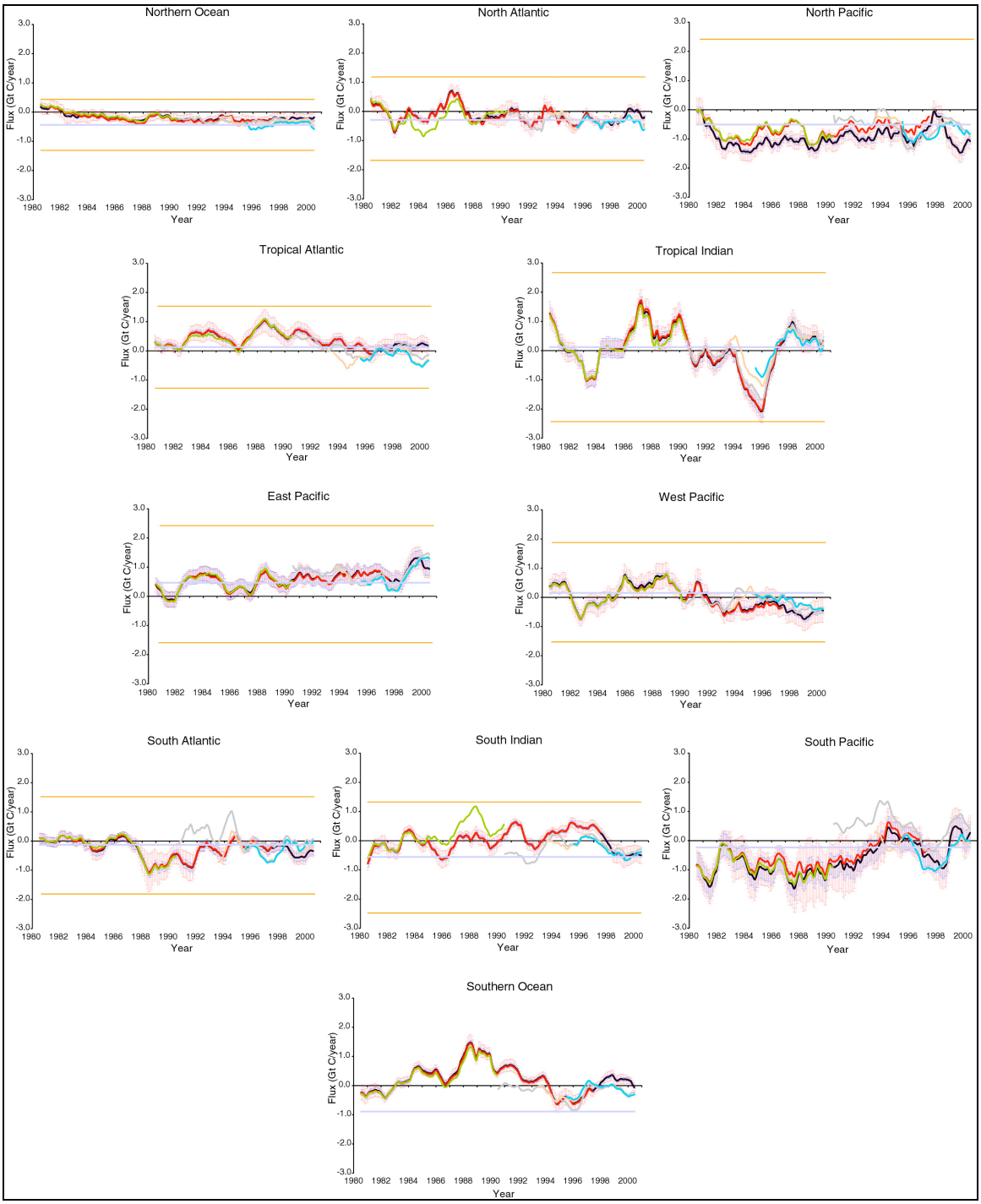

Figure 4.2b. As in figure 4.2a but for the ocean regions.

The relationships between the two measures of uncertainty presented here and the observational location/density can also be examined across the six different networks. Figure 4.3 shows the between and within uncertainty for land and ocean aggregated regions. As the network size increases, the between uncertainty increases while the within uncertainty does not. This is a product of the fact that as stations are added to the observing network, the differences between the models are better observed. The decline of the within uncertainty reflects the fact that there are simply more observing locations to constrain the final flux esimtates. The model spread is also consistently larger over the land regions than over the ocean. This is due to the fact that CO_2 gradients over land are larger and more dependent upon differences in transport out of the PBL.

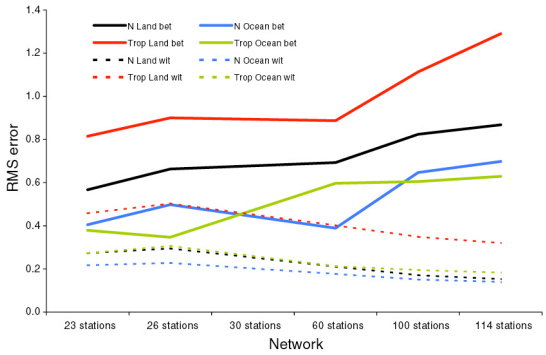

Figure 4.3. Error as a function of aggregated region and station network size.

For many of the TransCom land and ocean regions, the fluxes estimated by the different station networks are consistent in both the long-term mean and interannual fluxes. This is not surprising given that many of the networks contain a large number of overlapping or common stations. Two deviations from this general cross-network consistency occur. First, there are many cases in which regional fluxes exhibit consistent interannual variability but contain long-term mean offsets. Examples of this are the Northern Africa and Tropical America regions.

The second form of deviation is noted by the presence of significant discrepancies between networks not only in long-term mean offsets but in the interannual variation as well. Examples of this are evident in the Southern Africa, Tropical Asia, and South Pacific regions. Most of these examples are in regions with traditionally few observing sites. Hence, as the network density increases, these regions may gain their first, and sometimes only, nearby observing site. For example, the addition of four stations to the 26 station network causes nearly a 1.0 GtC/year shift to the South Indian Ocean region in the late 1980s. The Amsterdam Island station (AMS: 37.95º N, 77.53º E) is one of these four additional stations and lies directly within the South Indian Ocean region. However, previous measurements were being made at AMS by the Laboratoire des Sciences du Climat et de l'Environement (LSCE) laboratory. The 30 station network contains an additional measurement stream at this location, performed by the NOAA Climate Monitoring and Diagnostics Laboratory (NOAA CMDL). The CO_2 measurements from these two different laboratories at this location show an offset of 0.5 ppm for the period 1985 to 1989. This offset is responsibe for the different flux estimates as the network is enlarged to 30 stations.[5]

In the Temperate North American region, the larger networks exhibit consistent interannual variability but suggest roughly 0.5 Gt C/year less uptake in the late 1990s. The 60 station network includes a number of stations that could potentially generate the changes in the late 1990s. As will be discussed in more detail in section *4.3.3.2*, influential stations are not always proximal to a given region. In this example, lessened uptake in the late 1990s as estimated for the 60 station network is caused primarily by Mt. Waliguan Baseline Observatory, China (WLG: 36.27º N, 100.92º E) and Tenerife, Canary Islands (IZO: 28.30º N, 16.48º W).

The between uncertainty displayed in figure 4.2 for the 23 station network is somewhat misleading when interpretation is focused on the interannual variability. As shown in figure 4.4a, and similar to the cross-network behaviour, the spread among the models for a single network is generally driven by a long-term mean offset. The interannual signal, however, is often more consistent across the models. Much of this is likely due to the fact that interannually varying transport is not included in the forward simulations. Differences among the models is then primarily due to different underlying transport algorithms and the different wind datasets chosen by the modelers (which repeat each year). Therefore, the primary force

[5] Inversion results show that the 26 station inversion and the 30 station inversion without the AMS_00D0 are nearly identical in the Southern Indian Ocean region.

driving the interannual variability in the inversion is the temporal variation in the observed CO_2 concentration.[6] Though this simplifies the intermodel comparison, it regrettably limits the biogeochemical interpretation of the results (discussed later).

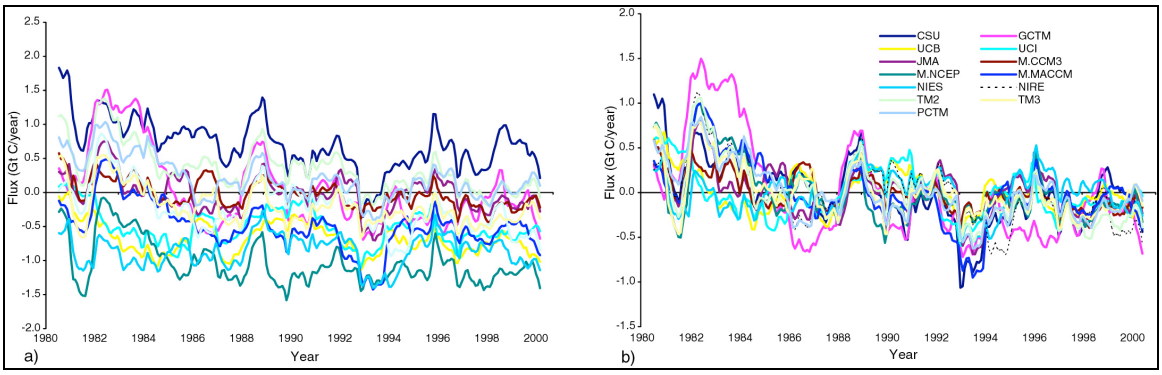

Figure 4.4. Deseasonalized, individual model fluxes for the Boreal Asia region. a) Original, unadjusted fluxes. b) Fluxes with offset from model mean removed.

Figure 4.4b shows an example of this phenomenon for the Boreal Asia region when the individual long-term model offsets are removed. Removal of these offsets for the individual models provides an alternative measure of the model spread when the focus is interannual variability. Figure 4.5 presents the individual regional results when these individual model offsets are corrected for.

[6] This is not strictly true for the online models which can exhibit interannual variation from one year to the next if they are run forward continuously from a single initial condition. In the current study, only two of 13 models are online models.

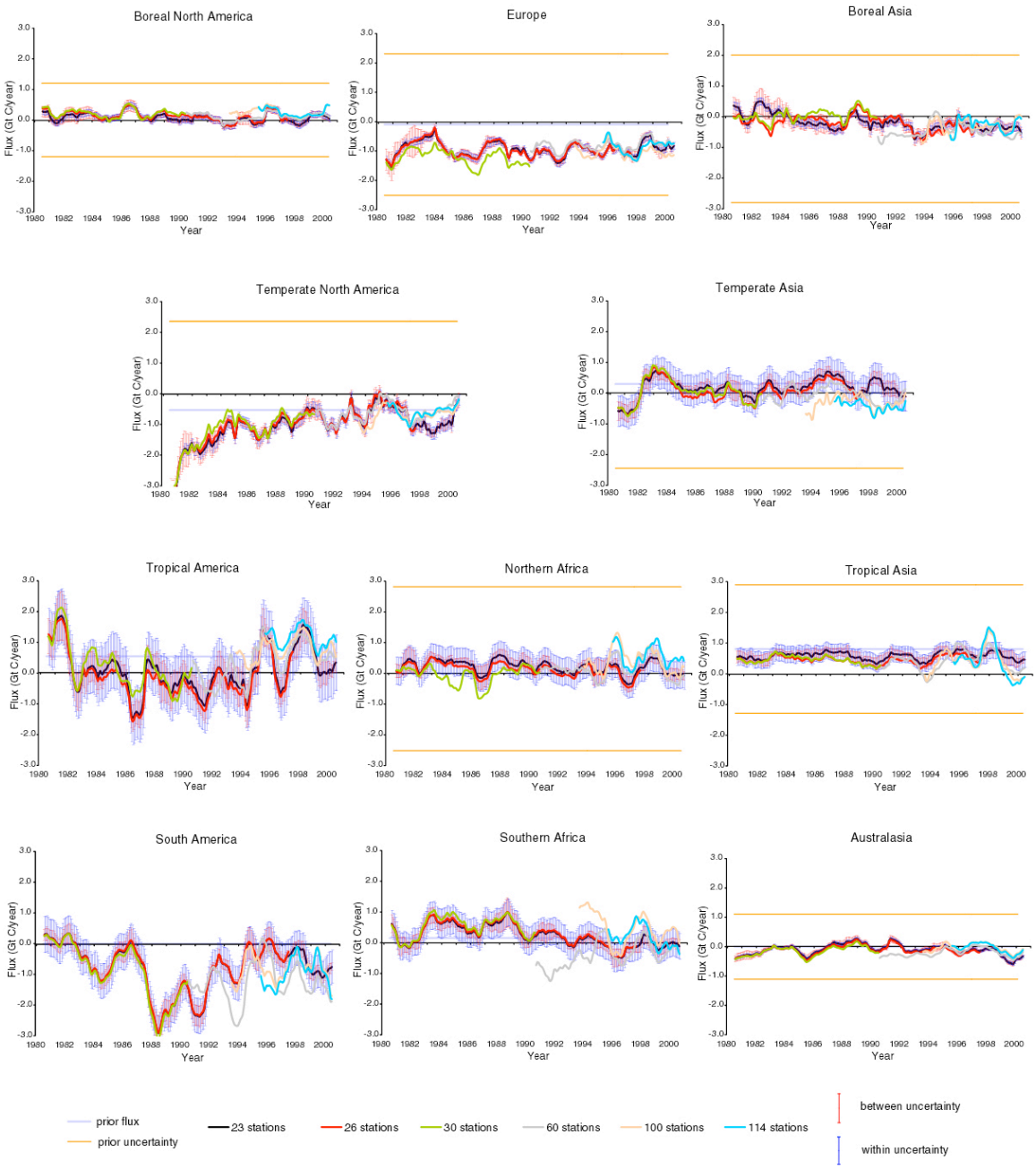

Figure 4.5a. As in figure 4.2a except the individual model long-term mean offsets around the model mean has been removed.

The result is a considerable reduction in the between uncertainty (red error bars). Regions where the data constraint is limited now contrast sharply with those regions less limited by CO_2 observations. Also noticeable are time periods not corrected by the long-term mean differences. For example, the early 1980s in the Europe region shows larger model spread than during the remainder of the 21 year time span. The same phenomenon occurs in the late 1980s in the Tropical and South Atlantic regions.

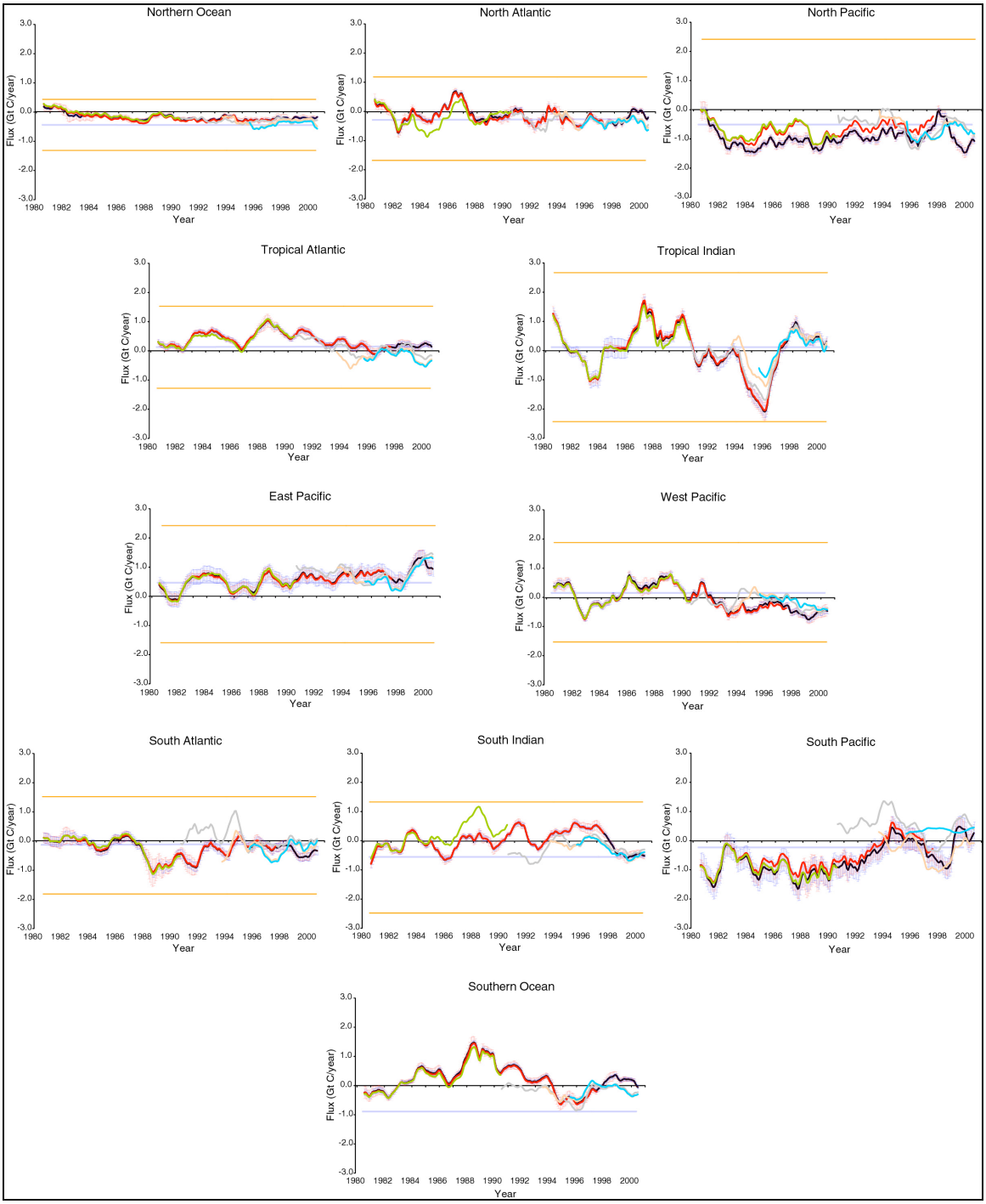

Figure 4.5b. As in figure 4.5a but for the ocean regions.

Turning to the fluxes themselves, the interannual variability on land is greater than that in the ocean regions. This can more easily be seen in figure 4.6 where the individual regions have been aggregated into latitude bands and global totals for land and ocean. The mean variance on land for the two decade period is 1.7 Gt C/year versus 0.9 Gt C/year for the oceans (figure 4.6c). This result is also somewhat dependent upon the network chosen for the analysis (and the relative prior uncertainty – discussed later). As the network density increases, the ratio of land variability to that of the ocean increases to nearly a factor of three for the 114 station network. However, this may not be due to station density *per se*, but the physical processes at work over the particular time period the larger network spans. The relative land/ocean

variability is consistent with the results of some recent inversion studies (*Rayner et al.*, 1999; *Baker*, 2000; *Rödenbeck et al.*, 2003b; *Bousquet et al.*, 2000; *LeQuere et al.*, 2003).

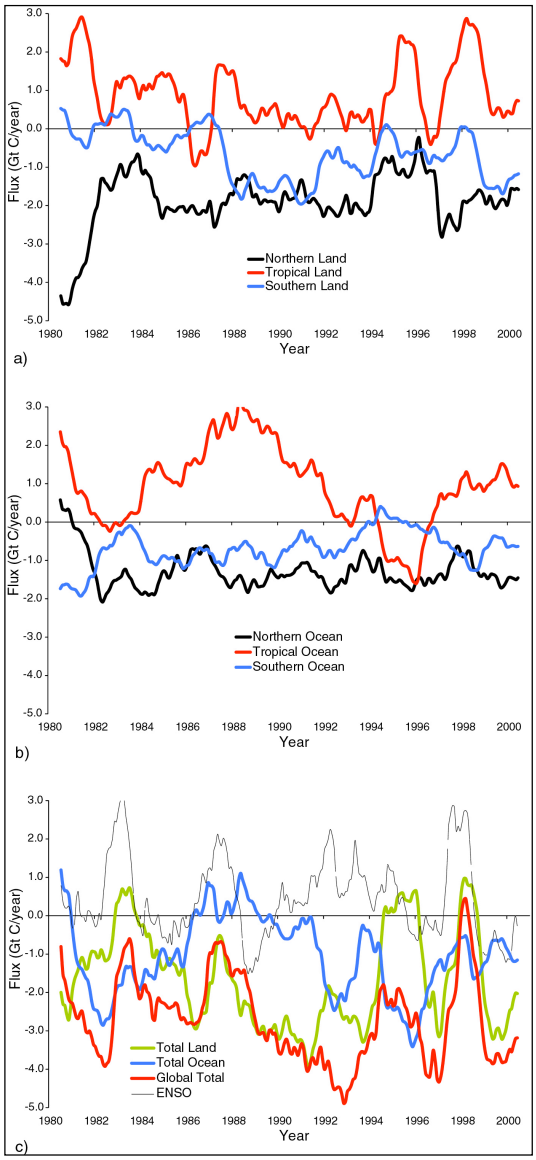

Figure 4.6. Regionally aggregated, deseasonalized carbon fluxes from the inversion using the 23 station network. a) Land, b) ocean, c) totals.

When examined as broad latitudinal bands, the variability on land is larger in the tropics than the northern extratropics (figure 4.6a). However, examination at the regional level in figure 4.5 indicates that the overall variability on land is driven by the Tropical, South, and Temperate American regions. The regions responsible for most of the oceanic variability are the southern and tropical ocean regions (figure 4.6b). At the regional level, the greatest amount of variability comes from the Tropical Indian, South Pacific and Southern Ocean regions.

A number of the regions shift over time from source to sink and vice-versa. For example, Boreal Asia appears to be going from a weak source in the 1980s to a weak sink in the 1990s though the long-term offsets due to the different networks in the 1990s make this interpretation uncertain. Temperate North America shows signs of a weakening sink over the two decade time period. In the oceans, the West Pacific appears to be trending from source to sink since the mod-1980s whereas the South Pacific shows the opposite behaviour.

Many of the regions exhibit large swings in carbon exchange that are often coherent across multiple regions. The total global carbon exchange variation shows a strong correlation to the El Niño-Southern Oscillation (ENSO) timing, as has been noted by many other investigators (*Bousquet et al., 2000; Keeling et al.*, 1995; *Rayner et al.*, 1999b*; Rödenbeck et al.*, 2003b). This can best be seen in figure 4.6c which includes the Multivariate ENSO index (*Wolter and Timlin*, 1993; *Wolter and Timlin*, 1998). The land carbon exchange tends to lag somewhat behind the peak of the ENSO index and responds by turning from sink to source or a lessened sink. Furthermore, the influence of the 1982 El Chichon and June 1991 Pinatubo eruptions can be seen, in the case of Pinatubo, as a gradual strengthening of the global sink in the early 1990s, confounding the ENSO event of the early 1990s. This has been attributed to NPP stimulation from the increase in diffuse to direct radiation resulting from the aerosol loading in the atmosphere (*Gu et al.*, 2003).

The total ocean is a sink for most of the two decades with the exception of the late 1980s where it became a weak source. This was driven solely by the tropical oceans. At the regional scale, this shift was driven by the Tropical Indian and Tropical Atlantic oceans. As will be discussed later, the outgassing from the Tropical Indian Ocean in the mid- to late-1980s is dependent upon the presence of the Seychelles CO_2 monitoring station which has been considered somewhat unreliable due to instrument and location changes (*Tom Conway, personal communication*).

Almost all of the global variations appear to be forced by carbon exchange on land which in turn is driven primarily by the tropical land aggregated region. Similarly, the majority of the global ocean variation is

driven by the tropical ocean aggregated region. Finally, the global ocean and global land exhibit anticorrelated variations with few exceptions. Further exploration of the biogeochemical implications of the interannual variations are performed in later sections.

4.3.3 Model Mean Sensitivity

In the annual mean and seasonal inversion results, the sensitivity of the model mean was tested against some of the key elements of the inversion set-up. In particular, the prior fluxes and their uncertainties were altered and two of the background fluxes removed in order to determine whether or not the estimated fluxes were overly constrained or otherwise influenced by the choice of the prior flux structure. Furthermore, the choice of CO_2 observing network, the assigned observational uncertainty, and model sampling procedures were also explored for the annual mean case (Law et al., 2003).

A similar suite of sensitivity tests have been performed for the interannual CO_2 inversion presented here. However, unlike the annual mean and seasonal inversion cases, some aspects of the inversion set-up are expected in advance to have little influence on the interannual variability though they will likely influence the characterization of long-term mean carbon exchange. For example, the two background fluxes that were tested in the annual mean and seasonal inversions, the neutral biosphere and global ocean fluxes, contain no interannual variability. These fluxes are merely repeated each year.

The collection of CO_2 observing stations that comprise the six different networks outlined here do have a significant impact on both the interannual variability and the long-term mean carbon exchange. This section will take a closer look at three components of the interannual inversion set-up: prior uncertainties, particular stations, and station network sensitivity.

4.3.3.1 loosening the prior uncertainties

Figure 4.7 shows the regional carbon exchange estimates from the 23 station network when the prior uncertainties have been increased by factors of 2 and 5. The largest changes occur in the tropical and southern land and ocean regions, precisely those regions where CO_2 observations are limited or lacking. Even in these regions, the phasing of the interannual variability changes little. The primary impact of loosening the prior flux uncertainties is on the long-term mean carbon exchange. For example, regions such as the East Pacific, West Pacific, Tropical Atlantic, and the South Atlantic exhibit increases in the amplitude of the interannual variability as the prior uncertainties increase. In some regions, such as South America and Southern Africa, the loosening of the prior uncertainty results in a dampening of the interannual amplitude. However, as was found with the annual mean and seasonal inversions, many of these shifts in the long-term mean exchange are compensating dipole behaviour.

Figure 4.8 provides evidence for this by generating a couple of groupings composed of the least constrained regions.[7] These groupings, which are referred to as "TrAmPac", "Atlantis", and "Indian Ocean" are nearly immune to the dipole behaviour evident in their constituent parts. As opposed to simple grouping into latitude bands, a technique often used in inversion studies, these groups represent a more accurate representation of the smallest scale that can be reliably interpreted in the tropical and southern latitudes. This is a very useful outcome of increasing the prior uncertainties.

The particular groupings discovered with the 23 station network may not be required or may change with a different station network. The same procedure as that outlined above was performed for the larger station networks. While compensatory dipole behaviour occurred for all networks, the extent was greatly diminished and scaled roughly with the network size. Unlike the results for the 23 station network, the larger networks did not exhibit changes that would significantly alter either the long-term mean or the interannual variability. A couple of exceptions are worth noting. The 60 station network exhibited some sensitivity to the prior uncertainty values for the Tropical Indian and Southern Africa regions. However, this sensitivity was confined to periodic differences of no more than 0.5 Gt C/year.

[7] These were guided by examination of the posterior covariance matrix. Large off-diagonal negative values indicate regions that exhibit compensatory dipole behaviour.

This exercise indicates that in those regions where observations provide a greater constraint, the prior uncertainty is having little influence upon the model mean carbon exchange. These regions appear to be robust to this particular aspect of the inversion set-up. Regions with little observational constraint are not robust to changes in the prior uncertainty but groupings of these regions are when the groups can be adequately identified. Furthermore, the composition of the groups are dependent upon the suite of CO_2 observing sites included in the inversion.[8]

This last point raises questions about the interpretability of the interannual variability of the individual regions that are not observationally constrained. As was noted in both the annual mean and seasonal inversion, estimates in these regions are uncertain. However, examination of figure 4.8 indicates that both the long-term mean and the interannual variability may be reliable when the these unconstrained regions are grouped correctly.

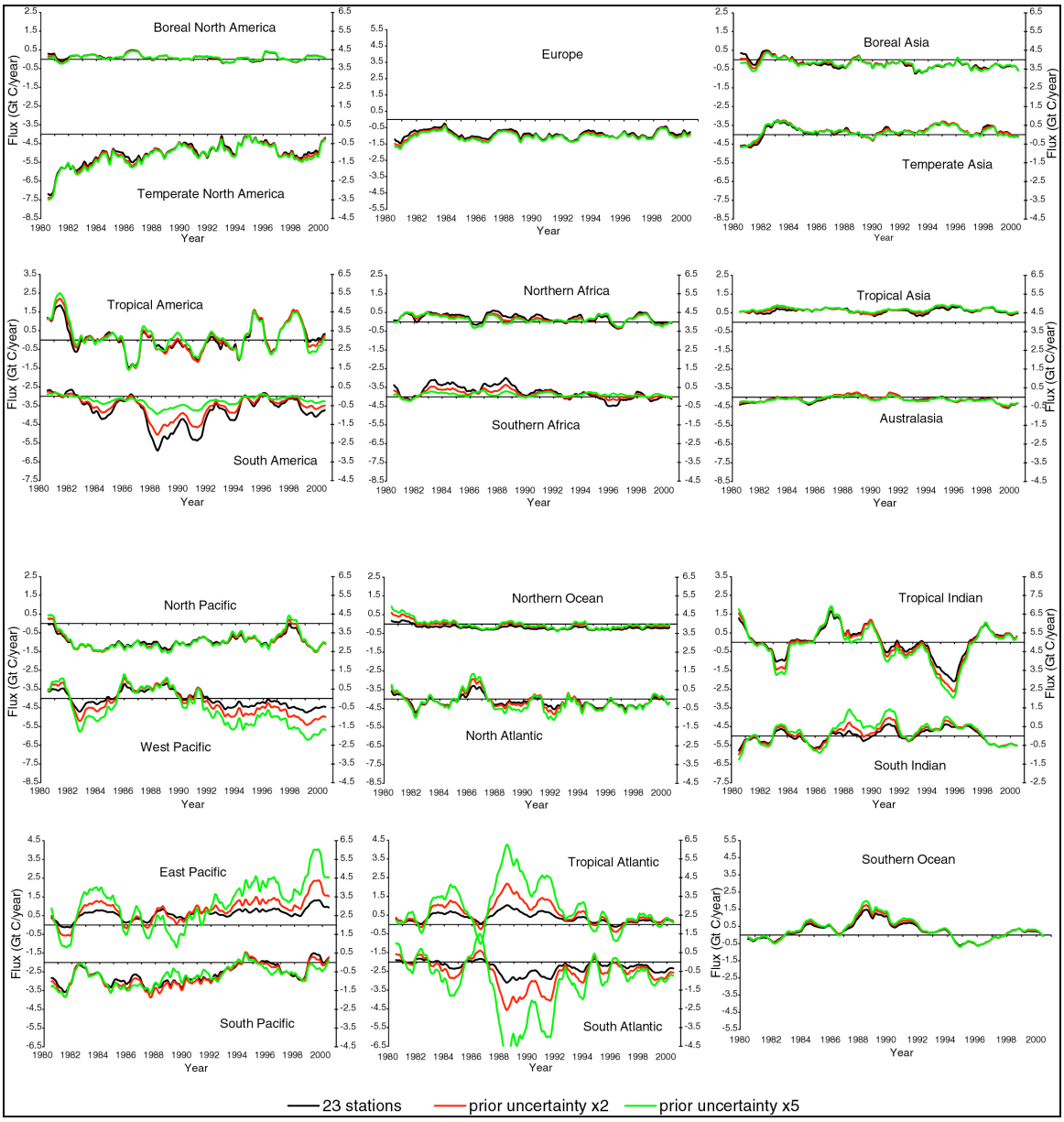

[8] The group composition may also be sensitive to the transport model used, a point that will be considered in future work.

Figure 4.7. Estimated deseasonalized fluxes for land and ocean regions as the prior uncertainty is loosened by 2x and 5x, respectively.

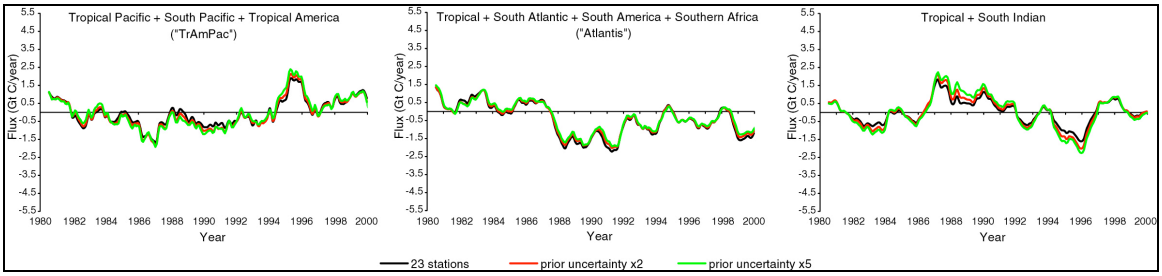

Figure 4.8. Estimated deseasonalized fluxes for three groupings of land and ocean regions as the prior uncertainty is loosened by 2x and 5x, respectively.

4.3.3.2 sensitivity to particular stations

As has been alluded throughout this chapter thus far, individual stations are often responsible for shifts in net carbon exchange between the six networks examined in this study. This is primarily due to the onset of a data constraint for a particular region when moving from one of the smaller station networks to one of the larger. As will be shown, these shifts often occur for the regions with the least overall data constraint in this study. This is evident when examining figure 4.5; the well-constrained regions tend to exhibit few changes in net carbon exchange due to the particular station network employed (e.g., Europe).

This section will examine instances of significant shift in regional net exchange when using one station network versus another and attempt to isolate the station or stations primarily responsible for causing the estimated change. The method employed is straighforward. Stations are added or removed from particular networks and the impact on the estimated fluxes is examined for changes. In some cases this is performed for individual stations, in others, groups of stations are added or removed from particular networks.

Figure 4.5a indicates that the Temperate North America region exhibits weakened uptake in the 1997 to 2000 period when moving from the 23/26 networks to the 60/100/114 station networks. In this instance, station influence was ascertained by removing stations from the 60 station network and examining the resulting changes in net carbon exchange. Three stations, Mt. Waliguan, China (WLG: 36.27º N, 100.92º E), Shemya Island (SHM: 52.72º N, 174.10º E), and Tenerife, Canary Islands (IZO: 28.30º N, 16.48º W) are primarily responsible for the weakened uptake in the target period. Removal of these stations from the 60 station network causes the uptake to increase towards the value estimated using the 23 or 26 station networks.

While IZO can be considered a "downwind" station and hence, influence directly the net carbon exchange, the influence of WLG is more subtle. The only other region influenced by the removal of WLG from the 60 station network is the Temperate Asia region. In that region, the removal of WLG causes the uptake in the 1997 to 2000 period to shift to a source. This shift brings the Temperate Asia region during this period very close to the values estimated using the 23/26 station networks. So, a possible explanation for the influence of the WLG station is that the addition of this particular station causes the Temperate Asia region to move from a source to a sink causing an equal but opposite influence on the Temperate North America region.

In the mid-1990s, the Temperate Asia region goes from a weak source to sink as the network is enlarged from 60 to 100 and 114 stations. Influential in this greater uptake is the addition of Ulann Uul, Mongolia (UUM: 44.45º N, 110.10º E). The addition of this and, as mentioned in the last paragraph, the WLG station causes the Temperate Asia region to change from a 0.5 Gt C/year source to a 0.5 Gt C/year sink in the late 1990s.

In addition to influencing the Temperate North America region, the IZO station has an equally significant impact on the Northern Africa region. When IZO is dropped from the 60 station network, the Northern Africa region exhibits a source decrease of roughly 0.5 Gt C/year in the 1997 to 1999 time period. After

1999, dropping IZO weakens the net uptake to near neutrality (a change of roughly 0.5 Gt C/year). So, the introduction of concentration data at the IZO station causes a weakened sink in Temperate North America and a greater source in Northern Africa over the 1997 to 2000 time period.

In the early 1990s, the Southern Africa region changes from a weak source to a sink of roughly -1.0 Gt C/year when the network is expanded to 60 stations. The most influential stations in this instance are the additions of Crozet, France (CRZ: 46.45º S, 51.85º W) and Ragged Point, Barbados (RPB: 13.17º N, 59.43º W). The addition of CRZ and RPB cause the shift from source to sink in the 1990 to 1992 time period followed by CRZ dominating the source to sink shift in the 1992 to 1995 time period. Increasing the station network to 100 stations causes greater emissions in the 1994/95 time period. This increase is due to the addition of the Bass Strait aircraft sampling (AIA: 40.53º S, 144.30º E).

The South American region is a net sink during the decade of the 1990s. However, expanding the station network from 23/26 to 60 stations and more intensifies this uptake, particularly in the 1992 to 1995 time period. As with the impact on the Southern Africa region, the addition of CRZ is responsible for the enhanced uptake. The CRZ station further influences a shift in the South Atlantic ocean region moving the South Atlantic from a sink to a source in the early 1990s.

Finally, the addition of CRZ in the 60 station network influences the South Pacific region by changing it from a relatively large sink (about -1.0 Gt C/year) to a moderate source (~0.5 Gt C/year) in the early to mid-1990s. CRZ is not the only station responsible for this shift, equally important in this case are the Pacific shiptrack measurements (POCS) and Cape Grim, Tasmania (CGO: 40.68º S, 144.68º E) station measurements.

When the 60 station network is expanded to 100 stations, the South Pacific carbon exchange returns to the temporal pattern of the smaller 23/26 station networks. This return is due primarily to the inclusion of the Easter Island station (EIC: 29.15º S, 109.43º W). Finally, increasing the network again to a total of 114 stations causes the South Pacific to change from a -1 Gt C/year sink in the late-1990s to a weak source.

In summary, the CRZ station influences four regions in the southern hemisphere; Southern Africa, South Atlantic, South Pacific and South America. In the two land regions, the addition of CRZ generates greater uptake. However, in the South Atlantic and South Pacific regions, the opposite impact occurs, changing the South Atlantic from a weak sink to a source and the South Pacific from a ~1.0 Gt C/year sink to a ~0.5 Gt C/year source in the early 1990s.

The South Indian ocean region shows changes when the 23/26 station network is expanded to 30 stations. As was explained in section *4.3.1*, this is due to the addition of a second laboratory measuring CO_2 concentrations at the Amsterdam Island location (AMS: 37.95º N, 77.53º E). An adjacent region, the Tropical Indian ocean region is relatively unaffected by the addition of this additional measurement at AMS. However, the Tropical Indian ocean region is sensitive to the presence of the Mahe Island, Seychelles station (SEY: 4.67º S, 55.17º E) accounting for nearly all the IAV seen in figure 4.5b.

The final region examined in this section is the Tropical Asia land region. Most noticeable is the enhanced source centered around 1998 when going from the 23/26/60 station networks to the 100/114 station networks. As was alluded to previously, this dramatic increase in CO_2 emissions is very likely due to biomass burning observed at the surface and through remote sensing (*Schimel and Baker, 2002*). The addition of the Japan Airlines samples (WPON) which monitors CO_2 concentrations bewteen Tokyo and Syndey at altitudes of 8000 to 13000 meters, is primarily responsible for the greater estimated emissions in the Tropical Asia region for 1998.

The addition of observing sites as the CO_2 observing network expanded over time does not simply confirm the net exchanges estimated with the smaller station networks but adds observational constraint to regions that typically had very little. In doing so, large shifts in multi-year mean net exchanges occur and often occur in tandem longitudinally. For example, the Temperate North America, Temperate Asia, and Northern Africa regions were all influenced by the addition of WLG and IZO to the smallest station networks (i.e., 23 and 26 stations). The Southern Africa, South Atlantic, and South America regions were influenced in

tandem by the addition of CRZ to the small networks. What is perhaps most surprising about the influence of these stations is that many of the large shifts seen in the estimated fluxes when considering one network versus another are due to a small subset of stations, many of which are not proximal to the region influenced. These longitudinal teleconnections are likely due to the fact that the global growth rate and the meridional gradient in CO_2 is well-quantified and therefore reflected in the constraint placed on the regional fluxes.

An important question emerges in the context of the foregoing analysis: Are the estimated flux shifts that emerge with a few of the key added stations more representative of the true fluxes than without these additions? All else being equal, increasing the number of observing sites would lead one to expect more realistic and perhaps more accurate flux estimates. However, one may want place greater scrutiny on such influential stations given their obvious importance. Particular stations that exhibit CO_2 time series inconsistent with other records may be an indication of spurious behaviour due to recording errors or other alternations to the measurement procedure. Such errors can manifest themselves as shifts in regional estimated uptake, particularly when the station in question is the only or one of a small number of stations influencing a particular basis function region. Alternatively, the flux shifts witnessed in the foregoing analysis may be a reflection of better observational constraint and hence, may better represent the true fluxes.

An analysis of the particular stations highlighted in this section has not been performed. As such, there is no conclusive answer to the question of how much confidence can be placed on the shifts in estimated flux that occur as the station network is expanded. However, with the subset of stations identified, future work can efficiently determine which stations, if any, may be giving rise to spurious flux shifts.

4.3.3.3 sensitivity to station network

The discussion in the preceding section and examination of figures 4.2 and 4.5 indicate that the model mean is sensitive to the particular station network employed in the CO_2 inversion. Because the different networks contain a subset of non-common stations, flux estimates change to reflect the additional data constraint provided by the different stations. If one were to consider the changes to estimated fluxes with differing networks but were to consider an individual model, the way in which the fluxes would change as the station composition were altered is a function of the model responses at the various stations. Therefore, different networks would cause different flux alterations across models in addition to across station networks.

Figure 4.9 shows the Temperate North America deseasonalized interannual flux estimates for the six station networks. Panel a) shows the result for the UCB model while panel b) shows the result for the MATCH:NCEP model.[9] Though many of the broad features are the same, the models show differences in the way their fluxes respond to the change in station network.

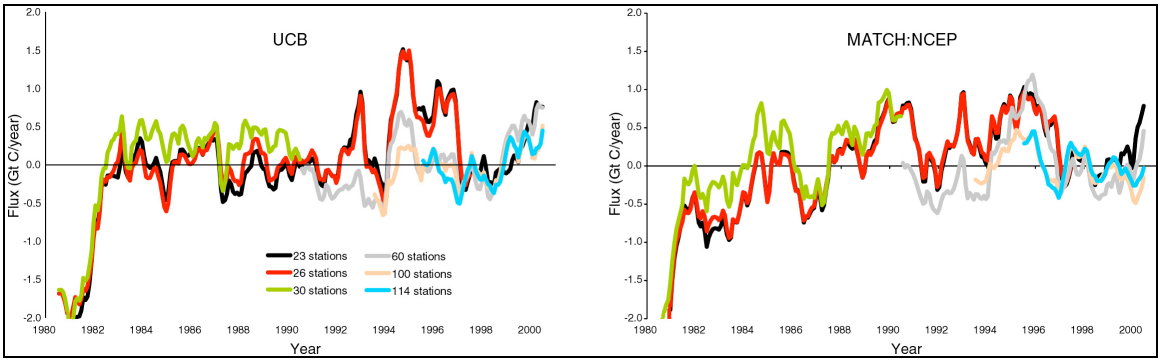

Figure 4.9. Deseasonalized interannual flux estimates for all six networks and for model a) UCB, and b) MATCH:NCEP.

[9] These models were chosen at random from the 13 model ensemble. A description of all the models in the interannual experiment is found in *Gurney et al.*, 2004.

In order to compare the interannual flux sensitivity to different station networks of the model mean versus individual models, a measure of across network variance is computed. Two different time periods are considered: the decade of the 1980s and the 1995 to 2000 time period. In the first, 3 different networks can be used to compute a variance at each timestep. In the second time period, 4 networks can be used to characterize a variance. This variance has been calculated at each monthly timestep for each of the two periods, for each of the models, and for the model mean flux. The time series of variance for the model mean can be reduced to a long-term, model mean by taking the RMS error of the timeseries. The same computation can be completed for each of the 13 models. Finally, the individual model errors can be reduced to an average individual model variance by taking the RMS error of the individual model long-term RMS values. The result is a representation of the error due to the different networks as experienced by the model mean and the individual models. This error has been computed for each land region and for the two time periods specified.

Figure 4.10 shows a comparison of these two error metrics. For all regions, the model mean exhibits less sensitivity to changing station networks in comparison to individual models. The figure also shows which regions are most sensitive to the changing station network composition. The pattern reflects a combination of which regions experienced the addition of nearby stations and whether or not those regions were already under some data constraint.

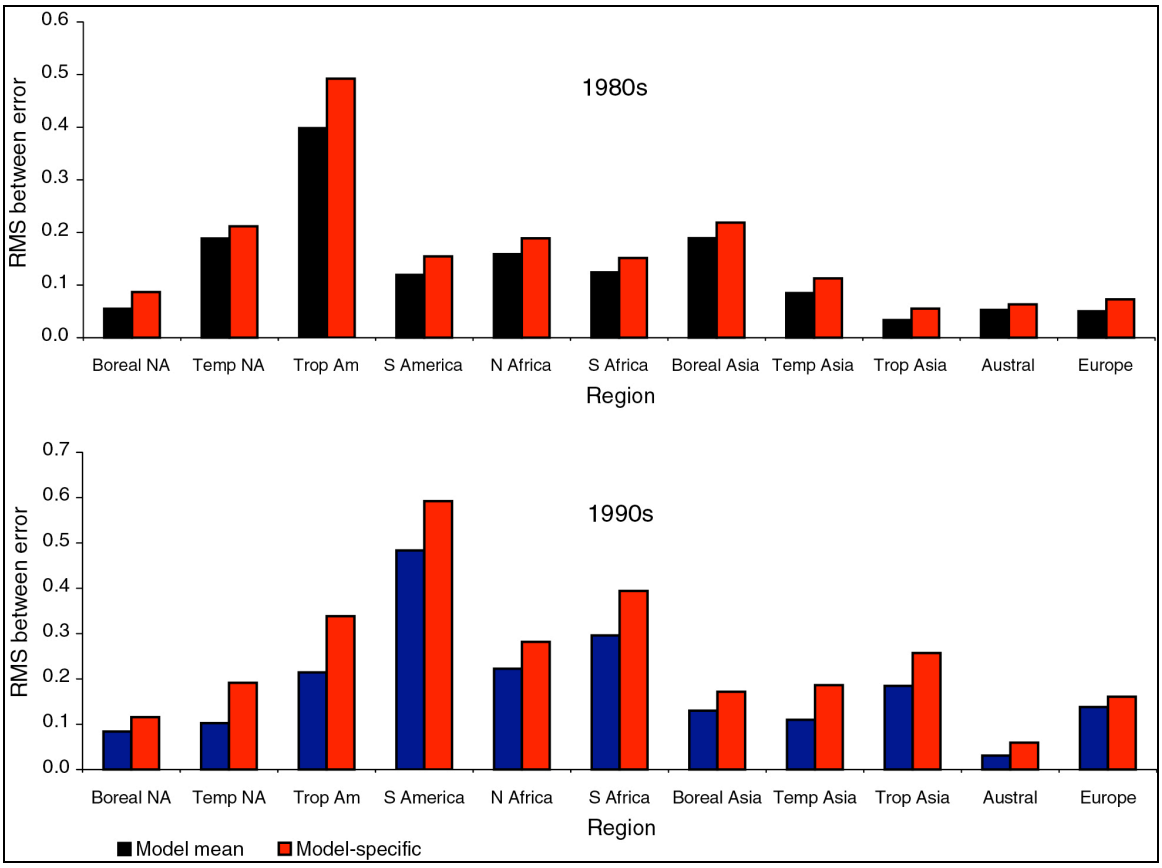

Figure 4.10. Comparison of the RMS between uncertainty due to network composition for two different time periods. The different color bars represent the model mean sensitivity and the model-specific sensitivity.

4.4 Discussion

4.4.1 Reduction to annual means/comparisons

Time averaging of the interannual inversion results allows one to compare results across the TransCom 3 levels in addition to comparing to other time averaged studies. Figure 4.11 shows the regional 1992 to 1996

mean carbon exchange across the different levels of the TransCom 3 experiment[10]. For the interannual inversion, the same 75 stations used in the annual mean and seasonal inversions are included and the uncertainty values are identical to those used in the seasonal inversion case. This makes for a more precise comparison[11].

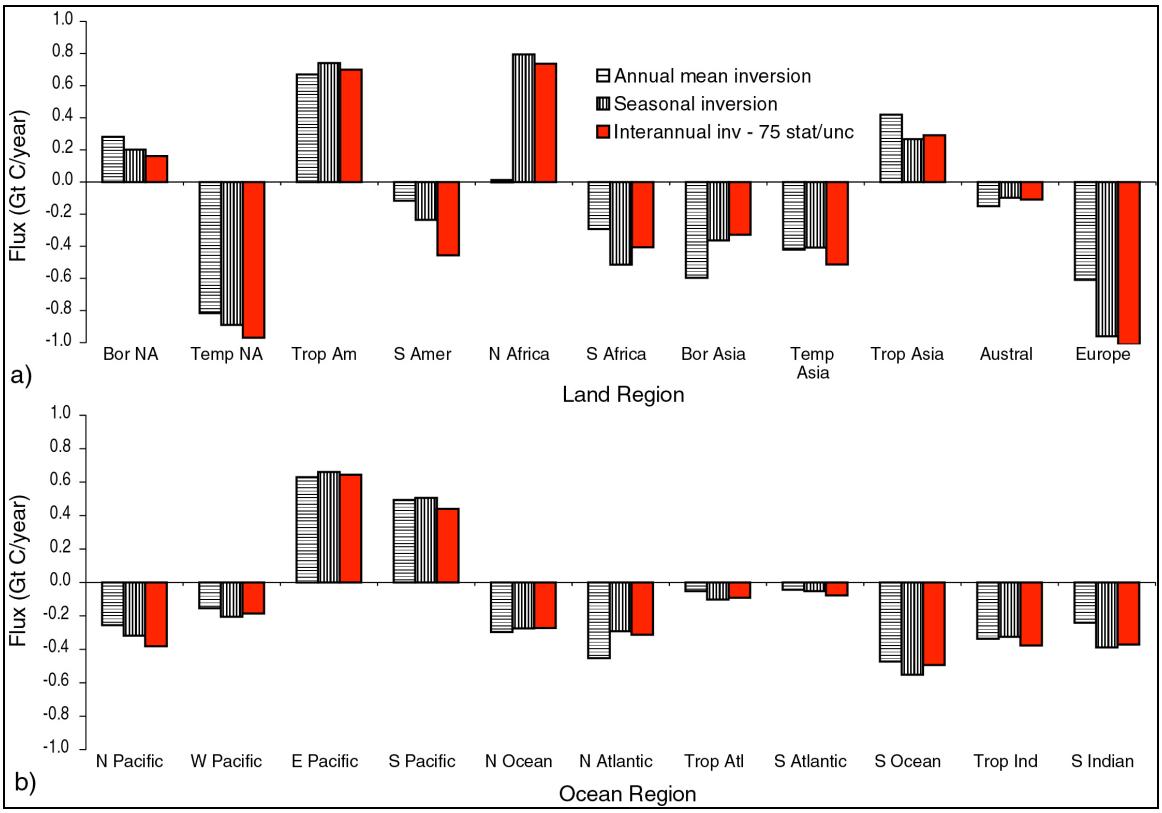

Figure 4.11. Model mean carbon exchange for the 1992 to 1996 time period across different inversion methods. a) land regions, b) ocean regions.

With the exception of North Africa, the annual mean, seasonal and interannual inversion using the 75 station network arrive at similar time-averaged carbon exchange values. Both the northern ocean regions and the Southern Ocean region exhibit uptake of roughly comparable levels. The general consistency across the three methods is heartening and suggests that the possibility of bias due to temporal representivity error is not particularly acute for this time period (*Engelen et al.*, 2003; *Peylin et al.*, 2003).

As was commented on in both the annual and seasonal inversions, carbon uptake is comparable in Temperate North America (-0.8±0.7, -0.9±0.4, -0.97±0.3 Gt C/year) and Europe (-0.6±0.6, -1.0±0.5, -1.0±0.3 Gt C/year) during this time period at slightly less than 1 Gt C/year with Temperate Asia (-0.4±0.9, -0.4±0.8, -0.5±0.6 Gt C/year) approximately half that value.[12] Except for the South Pacific, both the northern and southern ocean regions are sinks to atmospheric CO_2. The tropical ocean regions in this time period are predominantly shown as sinks with the exception of the East Pacific, contrary to what is expected from purely temperature related arguments. For the 75 station network, the West Pacific ocean region is relatively well-constrained by the Pacific Ocean ship data. However, the three other tropical ocean regions (West Pacific and Tropical Atlantic and Indian) have far fewer nearby observing sites.

[10] Table A4.2 provides all the fluxes and uncertainties associated with figure 4.11.

[11] The comparison remains imperfect however. The priors and prior uncertainties in the three inversions are not identical. Furthermore, the data uncertainties in the seasonal inversion were constructed to match the values in the annual mean inversion when annualized assuming independent errors. This assumption is likely not reflective of the real world.

[12] The values provided are for the annual, seasonal and 75 station interannual inversion, respectively. All uncertainties are "total" 1σ error values which incorporate both the within and between uncertainty measures.

Examination of the 1995 to 2000 time average allows one to examine the behaviour across four of the interannual inversion station networks more readily than can be achieved through examination of figures 4.2 and 4.5. Figure 4.12 shows these results for the land, ocean, and grouped regions identified in section *4.3.3.1*.[13]

As with the cross-level comparison of figure 4.11, there is a general consistency across the four networks for this time period. Part of this is due to the fact that the regions for which the greatest amount of cross-network disagreement occurred (see figures 4.2 and 4.5) have been combined into the three grouped regions displayed at the right of figure 4.12.

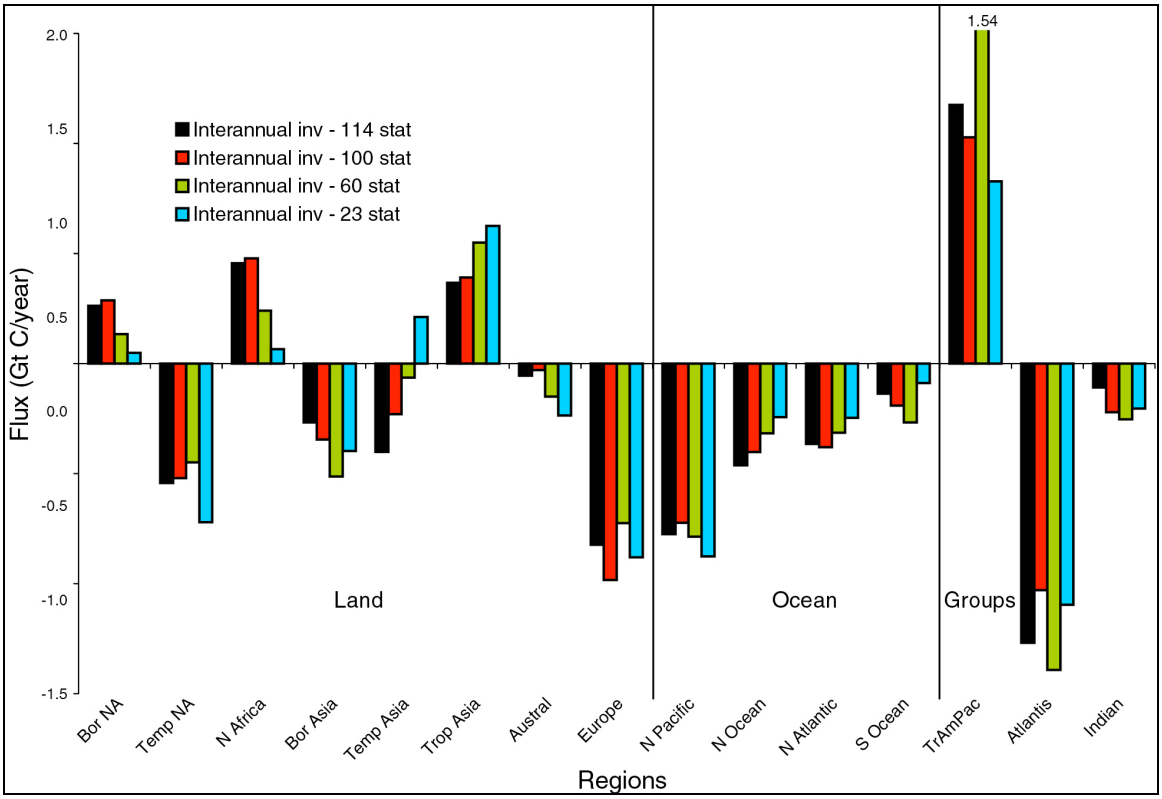

Figure 4.12. Model mean, time-averaged carbon exchange for the 1995 to 2000 time period across different CO_2 observation station networks.

This time period shows a diminishment of the uptake in Temperate North America compared to the 1992 to 1996 time period though the 23 station network has the least amount of change from the preceding five year time period. As was noted in section *4.3.3.2*, three stations in particular, WLG, SHM and IZO, were influential in weakening the uptake in the late 1990s.

Temperate Asia exhibits the largest shift across the four networks, going from a source for the 23 station network, to an increasing sink in the larger networks. As was discussed in section *4.3.3.2*, the 1990s brought the first CO_2 observing stations to Asia. In particular, the 60 station network gained the addition of Tae-ahn Peninsula, Korea (TAP: 36.73° N, 126.13° E) and the Mount Waliguan Observatory, China (WLG: 36.27° N, 100.92° E) at the eastern end of the Temperate Asian region. The addition of these two stations to the 60 station network is responsible for the shift in carbon exchange. The 100 station network further gained observing sites in Minamitorishima, Japan (24.30° N, 153.97° E) and Ulaan Uul, Mongolia (44.45° N, 111.10° E). The latter station was responsible for the increasing sink in the late 1990s.

[13] Table A4.3 in the appendix provides all the fluxes and uncertainties.

The Northern Africa region exhibits the opposite behaviour, going from near-neutral exchange in the 23 station network to a ~0.5 Gt C/year source in the 100 station network. As was mentioned previously, the first shift is due to the inclusion of CRZ in the 60 station network while the second is due the inclusion of the AIA aircraft sampling in the 100 station network.

If the 23 station network is excluded from the comparison, all 11 land and 11 ocean regions can be compared.[14] Figure 4.13 shows the 1995 to 2000 mean carbon exchange for all regions and for the three largest station networks used in this study.[15]

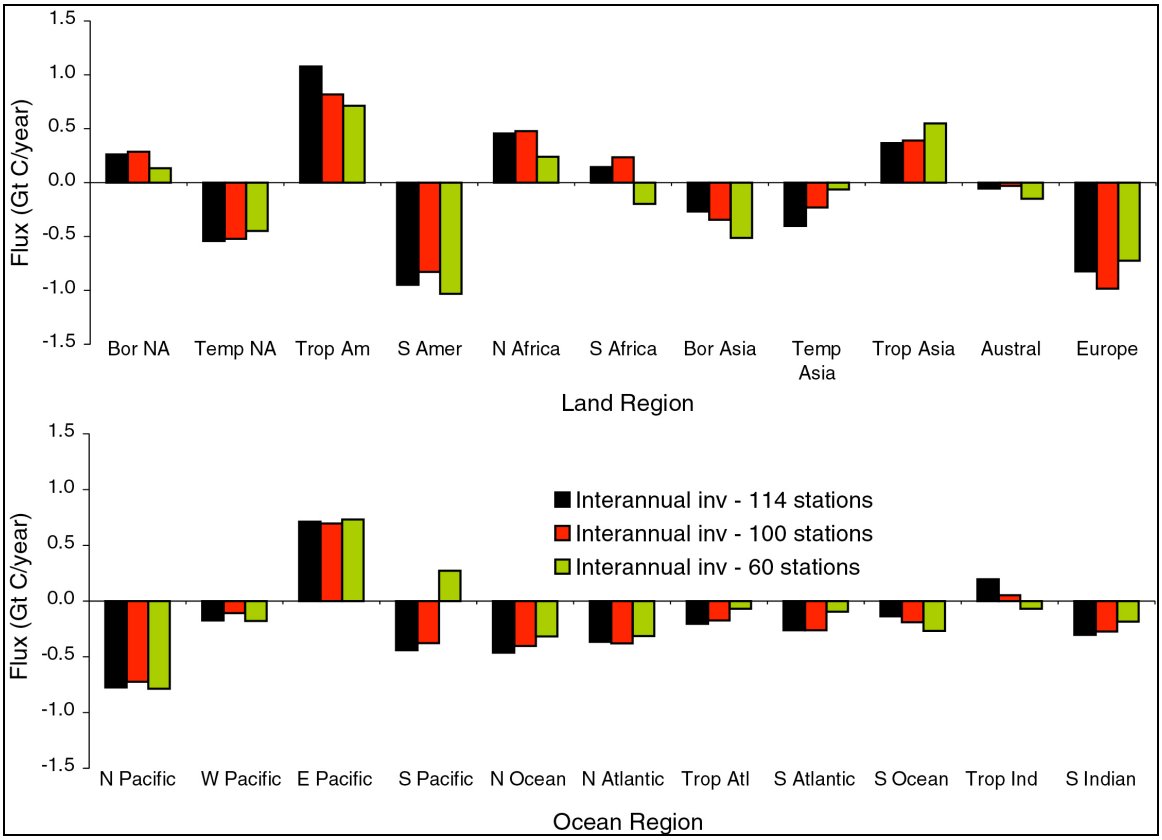

Figure 4.13. Model mean, time-averaged carbon exchange for the 1995 to 2000 time period across different CO_2 observation station networks. All 11 land and 11 ocean regions are separately estimated.

With the exception of a few regions, this time period shows considerable consistency in terms of both the direction and magnitude of the carbon exchange. As was mentioned previously, the Southern Africa and Tropical Indian ocean regions in the 60 station network are observationally unconstrained. In both these regions, the 60 station network estimates a flux that is opposite in sign to either the 100 or 114 station networks In the case of the Tropical Indian ocean, the addition of CO_2 monitoring at Cape Rama, India (CRI: 15.08° N, 73.84° E) accounts for the change from a weak sink to a weak source. The South Pacific region also changes from a source to sink between the 60 station network and the two larger networks. As discussed in section *4.3.3.2*, this is due to the addition of the CO_2 observing site at Easter Island (EIC: 29.15º S, 109.43º W) in the 100 station network. For example, the 1995 to 2000 mean carbon exchange for the 100 station network without EIC is +0.14 Gt C/year as opposed to –0.38 Gt C/year with EIC.

With the full spatial resolution intact, a number of features persist. Europe remains a sink nearly twice the size of Temperate North America. The combination of Boreal and Temperate Asia is roughly in between

[14] This relates to the logic of *section 4.3.3.1* in which certain regional groupings were considered more robust than certain individual regions.
[15] Table A4.4 in the appendix provides all the fluxes and uncertainties.

Temperate North America and Europe in terms of uptake. South America is estimated as a sink while Tropical America is a source of similar magnitude.

In the oceans, the only two regions that are estimated as carbon sources to the atmosphere are the East Pacific and the Tropical Indian ocean. The other two tropical oceans, West Pacific and Tropical Atlantic are some of the weaker sinks. In the case of the West Pacific, the weak sink may reflect the presence of the very strong ENSO event within the averaging time period.

In the annual and seasonal TransCom 3 inversions, the fluxes estimated for the Southern Ocean region were consistently half of the uptake estimates derived from ΔpCO2 measurements (*Gurney et al.*, 2002; *Gurney et al.*, 2003; *Gurney et al.*, 2004). Similar magnitudes are estimated here. However, recent updates to the ocean ΔpCO2 estimates bring these two results into agreement (*Takahashi et al*., 2002).[16] The fluxes computed from the ΔPCO_2 measurements are representative of the year 1995. For the Southern Ocean the updated carbon exchange based on the ΔpCO_2 measurements come to –0.35 to –0.45 Gt C/year depending upon which flux formulation is used. The Southern Ocean region time-mean flux estimate for the 1992 to 1996 time period when averaged over all the TransCom 3 models and the levels/networks represented in figure 4.12 is –0.41± 0.17 Gt C/year.

Finally, table 4.1 presents the total land and ocean results from this study alongside two separate revisions to IPCC estimates for the decade of the 1980s and 1990s. The interannual inversion results from this study are represented by the 23, 30, 60 and 100 station networks. The primary difference between the two IPCC revisions comes in the decade of the 1990s where the *Plattner et al,*. (2002) revisions come up with more uptake in the oceans at the expense of the land sink.

When considering the decade of the 1980s, the interannual inversion results exhibit slightly less ocean uptake and slightly more land uptake than the IPCC revisions indicate. However, given the uncertainty bounds, the estimates cannot be considered in strict disagreement.

Table 4.1. Estimates of total land and total ocean net carbon exchange for the 1980s and the 1990s as estimated by the current study and other recent integrated sources.

	Ocean				Land			
	80s		90s		80s		90s	
Source	Flux	unc	flux	Unc	Flux	unc	Flux	unc
IPCC 1[a]	-1.8	0.8	-1.9	0.7	-0.3	0.9	-1.2	0.9
IPCC 2[b]	-1.7	0.6	-2.4	0.7	-0.4	0.7	-0.7	0.8
IAV (23)[c]	-1.4	0.8	-2.0	0.9	-0.8	0.9	-1.1	0.9
IAV (30)[c]	-1.2	0.9	NA	NA	-1.0	0.9	NA	NA
IAV (60)[c]	NA	NA	-1.0	1.1	NA	NA	-2.1	1.1
IAV (100)[d]	NA	NA	-1.9	1.3	NA	NA	-0.8	1.3

[a] Estimates taken from *Le Quere et al.*, 2003. *IPCC,* 2001 estimates (*Prentice et al.*, 2001) were adjusted to account for the circulation effect of ocean O_2.

[b] Estimates taken from *Plattner et al.*, 2002. *IPCC*, 2001 estimates (*Prentice et al.*, 2001) were adjusted to account for larger O_2 outgassing.

[c] Inversion estimates have been corrected for river transport between land and ocean. 0.6 Gt C/year has been used (Sarmiento and Sundquist, 1992)

[d] The average for the 1990s includes the years 1993 to 1999. This means that the global total uptake is not identical to the networks that span the entire decade of the 1990s.

For the decade of the 1990s, the interannual inversion estimates for the 23 station and 100 station networks agree fairly well with the IPCC estimates though it must be noted that the 100 station network spans the 1993 to 1999 period and, hence, arrives at a global total uptake (-2.7 Gt C/year) that is somewhat less than that estimated from the entire decade of the 1990s (-3.1 Gt C/year).

[16] Personal communication from Taro Takahashi indicates that the values presented in Takahashi et al., 2002 must be updated using winds at the 10 meter height rather than the 0.995 sigma level of the transport model used in the carbon flux calculation. These corrections are available at: http://www.ldeo.columbia.edu/res/pi/CO2/carbondioxide/text/10m_wind.prn

During the decade of the 1990s, the 60 station network disagrees quite substantially with both the IPCC estimates and the other station networks shown in Table 4.1. For the oceans, the difference is due to the change in the South Pacific and, to a lesser extent, the change in the South Atlantic regions. In the 23 and 100 station networks, the South Pacific ocean region is estimated as a sink of -0.37 Gt C/year and –0.34 Gt C/year, respectively. In the 60 station network, the South Pacific is estimated as a 0.51 Gt C/year source. The explanation was described in section *4.3.3.2* - the inclusion of CRZ, CGO, and the POCS ship measurements in the 60 station network shifts the South Pacific region from a sink to a source. The observations at CRZ are primarily responsible for the shift in the South Atlantic region from a –0.3 Gt C/year sink to a 0.1 Gt C/year source. When the network grows to 100 stations, the EIC observing site is primarily responsible for the South Pacific region returning to a –0.34 Gt C/year sink during this time period.

On land, the extra uptake estimated for the 60 station network when compared to the 23 station network is found in both the South America and Southern Africa regions. As was discussed in *section 4.3.3.2*, the South America region shifts from a –0.7 Gt C/year sink during the 1990s to a –1.2 Gt C/year sink due primarily to the inclusion of the CRZ station in the 60 station network. The Southern Africa region is also strongly influenced by the inclusion of CRZ in the 60 station network in addition to RPB. The return to larger ocean uptake and smaller land uptake with the 100 station network rests primarily with these same regions and is mostly due to the inclusion of the aircraft sampling at Bass Strait (AIA: 40.53º S, 144.30º E).

The dramatic difference in the land and ocean totals for the network comprised of 60 stations compared to either independent estimates or other networks is troubling, primarily because the changes are due to a small number of unconstrained regions altered by a very small number of observing sites. It leaves open the question of whether or not the average 1990s flux estimate as produced by this study is or is not consistent with the IPCC estimates. As was indicated in *section 4.3.3.2*, examination of these particularly influential stations for potential errors is warranted. Though not attempted in this study, examination of the observational record of CRZ could greatly illuminate whether or not the flux estimate for the 60 station network are inconsistent with the other networks used here due to observational errors.

4.4.2 Comparison to recent inverse work

Though often using different observing sites, inversion methodology and transport models, other interannual inversion studies may provide some insightful contrasts or confirm some of the more robust results in this study. Rather than exhaustively culling results from all recent interannual inversions, I will focus attention on the most recent, and perhaps most thorough, interannual inversion study by Christian Rödenbeck and colleagues at the Max Planck Institute in Jena, Germany (*Rödenbeck et al.*, 2003b).

Rödenbeck et al. used one transport model but included a number of CO_2 observing networks that span overlapping time periods. *Rödenbeck et al.* imposed strict guidelines regarding which station records would be used in the CO_2 inversion. This resulted in five networks ranging in size from 11 to 35 stations. The 11 station network spans the 1982 to 2000 time period, the 16 station network began in 1986, the 19 station network began in 1990, the 26 station network began in 1993, and the 35 station network began in 1996.

Another important distinction, one that has been mentioned previously, is the use of reanalyzed time-dependent winds. *Rödenbeck et al.* use time-dependent winds but the model mean results presented here do not. Some studies have concluded that interannually varying transport is a negligible contribution to the interannual variations in atmospheric CO_2 and hence, inverse flux estimates (*Dargaville et al.*, 2000). Others have come to quite different conclusions, suggesting that fixed-year transport causes random errors as large as the posterior estimation error (*Rödenbeck et al,* 2003a). However, the random errors introduced by fixed-year transport were predominantly in the northern extratropics.

In the current study, different models employed different fixed-year winds. This may reduce the possibility of bias that might have occurred had all modelers used the same fixed-year transport. However, the mixture of fixed-year winds is very likely a contributor to the between model uncertainty presented throughout this chapter thus far. Fundamentally, this may be viewed as a trade-off between bias and random error. Using a single transport model with interannually varying winds may reduce the random error but could result in

biased transport due to the single representation of transport physics. The use of many models, each of which is using a single fixed-year wind dataset, may reduce the bias due to varying transport physics but increase the random estimation error. Of course, there is no quantitative way to know how much bias is eliminated through various representations of transport physics and the use of different fixed-year winds. However, to the extent that these do cause random error, they are captured in the between uncertainty measure.

Figure 4.14 shows the land and ocean total deseasonalized carbon exchange from *Rödenbeck et al.*adjacent to the results found in this study. The carbon exchange for the total land is similar with four distinct maxima coincident with the 1982/83, 1987/88, 1995, and 1998 ENSO warm phase peaks. However, the magnitude of the peaks differ somewhat between the two studies. *Rödenbeck et al.* show the 1987/88 land peak as nearing 1 Gt C/year while the results here show lessened uptake relative to the adjacent years but remaining a sink rather than a source. The period of maximum land uptake during the early 1990s are consistent between the two studies, particularly if one overlooks the 60 station network. Preceding sections have indicated that this network may be unrepresentative of the actual fluxes because a few regions were dramatically altered by the addition of a very few stations. The land maxima and minima in the mid- to late-1990s are also consistent between the two studies. However, the maximum emission (roughly 3 Gt C/year) in 1998 is consistent when only the two largest networks are considered.

The total ocean exchange shows far more differences. From 1986 to 1989, the total ocean flux was slightly positive here but *Rödenbeck et al.* maintain a weak sink over that period. The weak emission for the global ocean in this study is primarily driven by the tropical oceans which increase their carbon emissions up to approximately 3 Gt C/year in the late 1980s. Furthermore, the 1985 peak found in *Rödenbeck et al.* is found in none of the three overlapping networks in this study. The overall peak to peak variability in the 1990s is greater in this study though this conclusion is somewhat dependent upon which network is considered. As with the land total, the 60 station network exhibits unrealistic variability and should probably be deemphasized in this comparison. Nonetheless, the peak to peak varaibility in this study is roughly 4 Gt C/year compared to roughly 1.5 Gt C/year in the *Rödenbeck et al.*results.

Both studies exhibit less cross-network agreement in the late-1990s for the total ocean particularly during the lead up to and during the strong 1998 ENSO event.

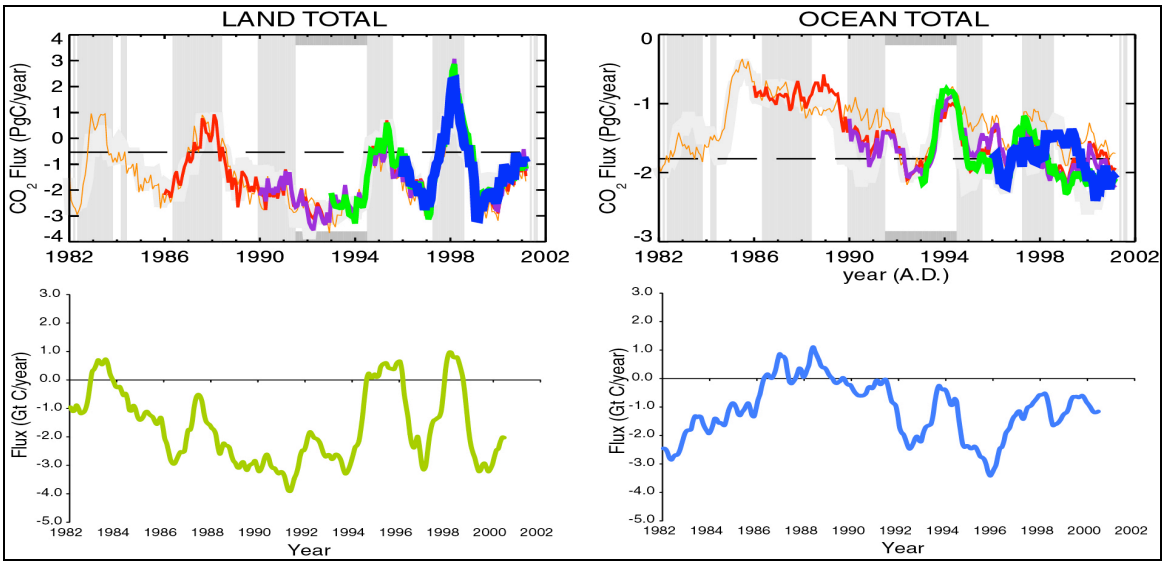

Figure 4.14. Comparison of total land and total ocean fluxes from this study (bottom panels) and *Rödenbeck et al.*, 2003.

Regionally, a number of differences are worth noting. The large spike in carbon emissions centered on the year 1998 and coincident with a strong ENSO warm phase is evident in both studies across the tropical and southern land regions. However, *Rödenbeck et al.* estimate this emission event occuring in both Boreal and

Temperate Asia whereas the current study does not. Long-term mean differences on land include both the Tropical Asia and Europe regions. *Rödenbeck et al.* find a long-term mean source for Europe whereas a significant sink is found here. The opposite occurs for Tropical Asia; *Rödenbeck et al.* estimate a long-term mean sink whereas a source is found here. Finally, the South America region exhibits a large sink in the late 1980s in this study but *Rödenbeck et al.* find near neutral emissions over this same period. As with Tropical Asia, comparisons for the South America region come with considerable uncertainty.

The difference in the long-term mean exchange for Europe is the most striking land contrast. This region is relatively well-observed and has been consistently estimated as a large sink across the different TransCom experiments in addition to many inversion studies.

In the ocean regions, *Rödenbeck et al.* find less interannual variability overall with the exception of the Tropical Indian ocean region. Both studies find a reduced source in the East and South Pacific coincident with the strong 1990 ENSO event.

4.4.3 Biogeochemical implications: El Niño-Southern Oscillation

A number of hypotheses have been proposed to explain the time-dependent behaviour of carbon exchange with the land and oceans (*Conway et al.*, 1994; *Keeling et al.*, 1995; *Braswell et al.*, 1997; *Rayner et al.*, 1999b; *Yang and Wang*, 2000; *Vukicevic et al.*, 2001). Most are tied to known variations in climate which themselves are related to observed modes of variability in the atmosphere. Distinct from interannual variability are phenomena that work on somewhat slower timescales, such as land-use change, or are short infrequent events, such as large fires or volcanic eruptions (*Houghton*, 2000; *van der Werf et al.*, 2003; *Robock*, 2002).

Though a complete exploration of the hypothesized biogeochemical roots of interannual variation in carbon exchange are beyond the scope of this study, an abbreviated investigation into connections with the ENSO cycle provides a glimpse of the potential for future work.

During the onset of an ENSO event, the growth rate of atmospheric CO_2 increases, suggesting lessened uptake/greater emission of carbon by the surface. This has been attributed to lessened emission from the equatorial Pacific due to the higher surface temperatures and reduced upwelling in the tropical eastern Pacific margin (*Feely et al.*, 1999; *Winguth et al.*, 1994). However, it has also been suggested that the carbon exchange with the terrestrial biosphere responds to altered climatic conditions associated with the phasing of ENSO through change in photosynthesis and respiration (*Kindermann et al., 1996, Gerard et al., 1999, Jones et al., 2001; Schaefer et al., 2002*). These alterations can induce acute carbon exchange events such as large fires associated with ENSO-induced drought conditions (*Keeling et al.*, 1995; *Schimel and Baker*, 2002*; van der Werf et al., 2004*). As the ENSO progresses out of the warm phase into the La Niña period, atmospheric CO_2 growth rates decrease suggesting greater uptake/lessened emission by the surface. This has been attributed to increased growth stimulated by greater northern extratropical rainfall and nutrient mobilization in the growing season following the ENSO warm phase (*Braswell et al.*, 1997).

Carbon flux correlation to ENSO has already been noted qualitatively at the scale of total land in this study. Examination of figures 4.2 and 4.5 show that many regions coherently respond to the ENSO timing. Because of the strength of the 1998 ENSO event and the fact that it occurs over the time period with the largest CO_2 observing network used in this study, the late 1990s present a strong case for ENSO/carbon flux correlation analysis. Many of the tropical land and ocean regions exhibit swings in carbon exchange roughly coincident with the 1998 ENSO event. On land, the Tropical Asia, Northern and Southern Africa and America, respectively, show strong potential responses.

In order to quantify the correlation between the regional carbon exchange and ENSO events, each region has been correlated separately to the Multivariate ENSO Index (MEI index) with lags extending one year ahead and behind. The results for the 23 station network are shown in figure 4.15.

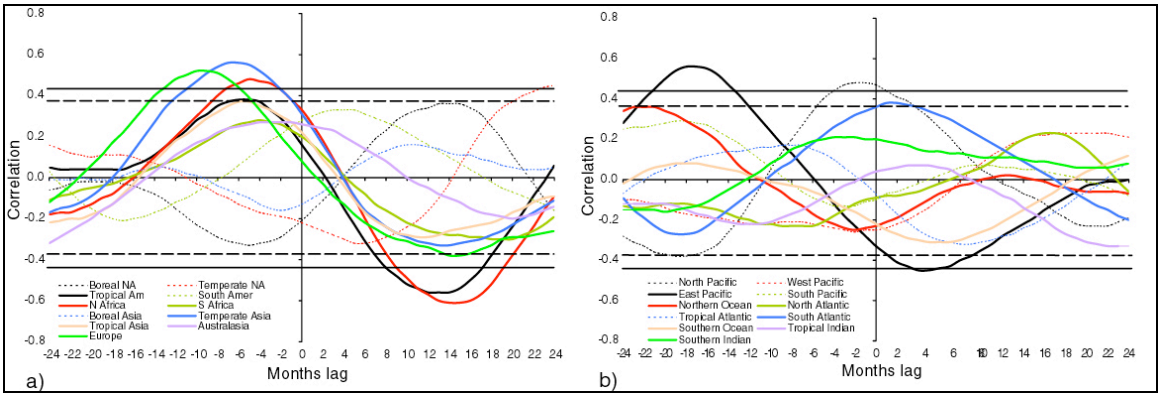

Figure 4.15. Lagged correlation between the MEI ENSO index and the regional carbon exchange for the 23 station network. a) land regions, b) ocean regions. Two-tailed significance (95%) is denoted by the solid horizontal lines. The one-tailed significance level (95%) is denoted by the horizontal dashed line.

On land, positive correlations occur across many regions with lag values of 4 to 10 months. The positive lagged correlation begins with Australasia (~ -3 months) and Southern Africa (~ -4 months) followed by Northern Africa, Tropical Asia, and Tropical America (~ -5 months). Finally, correlation maxima occur for Temperate Asia (~-6 months) and Europe (~-9 months). Using a one-tailed significance test, all of these regions achieve significance (95%) except for the Australasia region. Using a two-tailed significance test, only Northern Africa, Temperate Asia, and Europe achieve significance.[17]

In the oceans, the progression is less clear. The East Pacific shows a significant negative correlation at 4 months ahead of the ENSO index maximum and a significant positive correlation roughly 1.5 years after the ENSO index. The North Pacific exhibits a relationship nearly opposite to the found in the East Pacific. The North Pacific has a significant positive correlation roughly 2 months after the ENSO peak and a significant negative corrrelation 1.5 years after. The only other regions achieving statistical significance are the South Atlantic, Tropical Atlantic, and the Northern Ocean. The South Atlantic has a significant positive correlation 1 month prior while the Tropical Atlantic has a significant negative correlation approximately 8 months prior to the ENSO index maximum, respectively. Finally, the Northern ocean has a significant positive correlation roughly 2 years after the ENSO maximum.

The 23 station network extends from 1980 to 2000 and therefore encompasses multiple ENSO events. However, as has been shown by others, the Mount Pinatubo eruption in June 1991 interrupted the carbon flux response hypothesized to occur as a result of ENSO dynamics. Hence, the resulting correlations will be somewhat compromised by this. Furthermore, the use of all 11 land and 11 ocean regions from the inversion using the 23 station network is prone to greater uncertainty in the tropical land and ocean regions than found with the larger station networks.

The same exercise can be performed with the 114 station network which will focus exclusively on the large 1998 ENSO event and should provide greater confidence regarding tropical fluxes. Figure 4.16 shows these results.

[17] In the case of the 23 station network, a total of 250 monthly values are available. However, these have been reduced to a total of 19 degrees of freedom for calculating the significance.

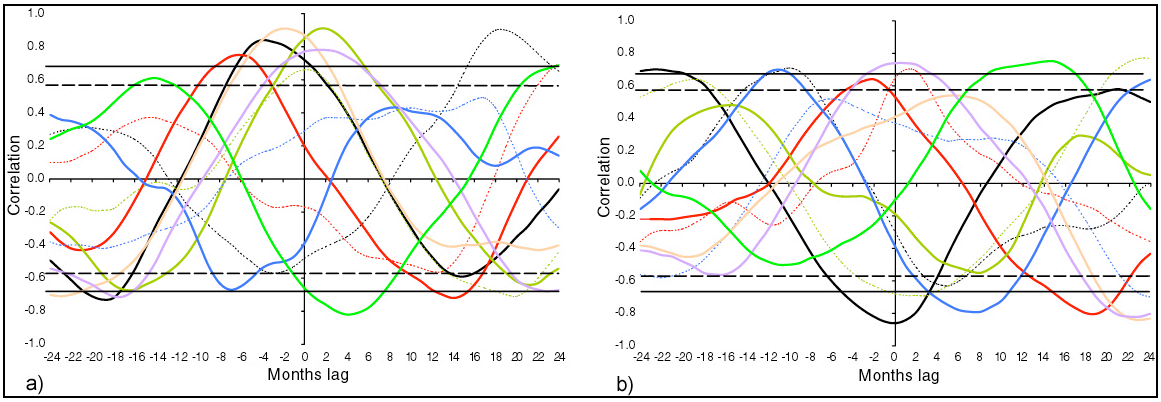

Figure 4.16. Lagged correlation between the MEI ENSO index and the regional carbon exchange for the 114 station network. Legend is identical to figure 4.15. The vertical scale is larger than found in figure 4.15.

The correlation values are larger overall but with a very similar progression of regions and timing. In this case, the Australasia and Southern Africa timing are similar and nearly coincident with the maximum of the ENSO index. Following this are South America and Tropical Asia, lagging the maximum by roughly 1 month. The Tropical America regions follows at approximately 4 months, the Northern African region at roughly 6 months and Europe at 11 months. The Temperate Asia region exhibits a lagged correlation distinctly different from that calculated with the longer 23 station network. Here, the response of Temperate Asia exhibits the same timing but is negatively correlated with the ENSO index rather than positively related. All of the regions described achieved significance for the one-tailed test and all but Europe and the South America region achieved significance with the two-tailed test.

In the oceans, the East and North Pacific regions show similar behaviour to that found for the 23 station network. In this shorter timespan, the significant negative correlation in the East Pacific is coincident with the maximum of the ENSO index as opposed to the approximate 5 month lead in the 23 station network. The North Pacific exhibits a significant positive correlation roughly 10 months after the ENSO maximum compared to only 3 months when using the 23 station network. As with the smaller network, both the Northern Ocean and the South Atlantic regions exhibit significant positive correlations, 12 months and 4 months after the ENSO maximum, timing quite different from that found with the smaller network. Othe regions exhibiting significant relationships are the Tropical Indian (coincident with the ENSO maximum), the West Pacific (preceding by ~2 months), and the South Pacific (lagging by ~18 months) regions.

Though not a conclusive analysis, the progression of correlations on land is somewhat consistent with hypotheses regarding the terrestrial response to ENSO events. A recent study by researchers at the Hadley Centre in the United Kingdom attempted to isolate the underlying mechanisms between ENSO and carbon exchange on land (*Jones et al., 2001*). In that study, the "HadCM3LC" coupled ocean-atmosphere GCM with an interactive carbon cycle is run in an effort to simulate the observed CO_2 and ENSO variations. Having achieved reasonable correspondence between the model simulation and observations, the authors examine the mechanisms linking ENSO and the response of the carbon cycle.

The Hadley Centre research shows positive correlations between the ENSO warm phase peak and land to atmosphere fluxes in Amazonia, Tropical Asia, and Australia. In these three regions, a combination of higher temperatures and lower precipitation cause a reduction in GPP and an increase in respiration. In Amazonia, the temperature is the larger influence while in Tropical Asia and Australia, the lessened precipitation is the larger factor. In Tropical Africa a similar positive correlation occurs but is induced solely by the increase in temperature and the subsequent increase in soil respiration. Much of North America shows a negative correlation with the ENSO warm phase. The authors attribute this to a wetter and cooler climate which yields large increases in GPP.

The timing of the correlations noted in figure 4.15 and 4.16 are particularly intriguing and suggest a migration in the response from the tropical regions to the northern extratropics months later. The mechanisms driving the northern extratropical land regions is less clear from the lagged correlation values.

The lag may be due to the seasonality of the northern extratropical land regions. Since theENSO index maxima tend to occur during the northern Winter months, the response in the northern extratropics may manifest itself during the following growing season, roughly 6 months later. This would explain the roughly 6 and 9 month lag associated with the positive correlations found in Temperate Asia and Europe, respectively.

4.5 Conclusions

This chapter has presented interannual carbon exchange results from the TransCom 3 experiment. The interannual fluxes and uncertainties from the 13 models that participated in this experiment constitute an enormous amount of computational output. Rather than analyze the individual model results, the current chapter has focused on analyzing the model mean fluxes and the two critical uncertainties that can be derived from the model ensemble. Sensitivity to CO_2 observing networks, their composition, and prior flux uncertainties have been explored and related to how they influence the long-term mean fluxes and the interannual variability. The long-term means and variations have been compared to a number of different studies and an initial look taken at a key biogeochemical driver of carbon flux interannual variations.

As with the annual mean and seasonal inversions, an important distinction between this and other studies is the availability of a suite of transport models from which one can calculate a model mean. This, like the previous TransCom work, results in the model mean being relatively robust to a number of the factors that are typically associated with uncertainty in CO_2 inversions.

Firstly, the individual model results indicate that though the long-term means diverge, the interannual variability is consistent across the individual models. This occurs in spite of the different fixed-year winds used to drive the various models and their different transport physics. Because TransCom was constructed to attempt to quantify the error in CO_2 inversion due to transport, this result allows us to not only compute an uncertainty associated with the transport but better characterize the transport spread in the interannual signal. As a result, the total error estimates contained in the interannual results are reduced, providing much more confidence in the interannual fluxes.

As with many other aspects of the interannual inversion results, interpretation of the two fundamental uncertainty indices, the within or random error and the between or model spread, are tied to the observational network employed. As the observational network becomes more dense, particularly over land, the within error is reduced but the model spread increases. This increase in the model spread is greater over land than over the ocean regions. In other words, as more observing locations are included in the inversion, the differences between the models are better seen by the observing network and this is more acutely true over land where the source gradients are typically larger due to the influence of the fossil fuel source and biosphere exchange.

The prior uncertainty bounds have been considered by many as a critical component in forming the posterior fluxes. This is often the case where either the uncertainties are too small or a particular basis function region is unconstrained by data. If both occur, the posterior flux will mirror the prior. If uncertainties are large and no observational constraint present, posterior fluxes typically generate compensatory dipole behaviour across the unconstrained regions.

In the current study the question of how much influence is being imparted by the prior must be within the context of which of the six station networks one is considering. In the smallest network constructed here, loosening the prior uncertainty causes many of the tropical land and ocean regions to exhibit compensatory dipole behaviour. However, the advantage to the exercise is that it assists in identifying those regions that can be combined in order to construct a grouped region that does reflect some observational constraint. For the small network employed here, this allowed for the identification of three grouped regions.

As the station network is progressively increased between 60 and 114 stations, the loosening of the priors has less and less influence on the posterior flux. Though some small shifts occur in the long-term mean carbon exchange, the interannual variability is preserved.

The next measure of robustness regards the sensitivity of the model mean to the different observing networks constructed. I have generated a measure of cross-network error by computing an RMS error for two different time periods, the 1980s and the 1995 to 2000 time period. By comparing the individual model error due to the different networks to the model mean error to the different networks, one can assess whether or not the model mean is a more robust estimate of carbon exchange when different networks are used. For the TransCom results, the model mean is consistently less sensitive to the station network composition than any individual model.

The last sensitivity test performed here is less about robustness and more about explaining which stations cause some of the more noticeable shifts from one overlapping network to another. In some cases, stations are added to regions with few pre-existing stations and can thus alter carbon exchange via the new and sizeable influence they impart. In other cases, new stations are added to a region that contradict or conflict with the flux determination of pre-existing stations. Three stations were found to cause sizeable shifts in the regional flux estimation when they entered the observing network: CRZ, WLG, and IZO. In the case of CRZ, the South America and Southern Africa regions exhibit increased uptake while the South Pacific and South Atlantic regions exhibit lessened uptake or a greater source in the early 1990s. The addition of WLG and IZO cause shifts during the mid-1990s in three land regions: Temperate North America, Temperate Asia and Northern Africa. In this instance, Temperate North America exhibits weakened uptake, Temperate Asia changes from a sink to source, and Northern Africa exhibits a weakened source. Except for the Temperate North American region, the influence is expressed in regions which had little or no observational constraint prior to the addition of the noted stations.

Reduction of the interannual results to long-term means indicates that the TransCom 3 inversion results are relatively robust to temporal truncation or the degrees of freedom allowed in the time domain. Further evidence for robustness across network composition is provided by comparing the long-term mean exchange.

Comparison of the long-term means for land and ocean separately with independently-derived efforts such as those summarized in the IPCC reports indicates some convergence at the large scale. For the decade of the 1980s, the ocean was the dominant sink relative to the land though the inverse results presented here would conclude that the relative sinks strength is not as large as that summarized by the IPCC. For the decade of the 1990s, much closer agreement is evident. However, it is clear that the station network comprised of 60 stations is possibly an outlier among the networks constructed in this study. This was confirmed in the section aimed at examining the influence of individual stations and was found to be due to the addition of the CRZ station.

The relationship of the regional carbon exchange estimates to the El Niño-Southern Oscillation index has been explored. The results indicate that significant heightened carbon emissions travel in both time and space from the Tropical Pacific ENSO peak value. The spatial progression starts in the tropics with nearly coincident carbon emission events and migrates to the extratropics roughly a year later. The results are broadly consistent with existing hypotheses concerning the linkage between ENSO and carbon exchange.

Comparison to a recent independent atmospheric inversion study confirms the difficulty in estimating the long-term sources and sinks compared to the interannual variations. At the scale of total ocean and total land, both the long-term means and the interannual variability exhibit consistency. However, examination at the regional scale shows large differences in the long-term mean exchange thought the broad features of the interannual variability remain comparable.

Like all inversion studies, this one is subject to potential bias. The following is a list of these potential caveats:

- Even with a large number of tracer transport models, there is the possibility that features of their transport physics are all biased in the same way. For example, they could all include too much interhemispheric transport or too little convection in particular locations.

- The use of fixed spatial distribution patterns or "footprints" for the regional basis functions and the background fluxes can give rise to "spatial representation error". This has been discussed both in previous TransCom papers and in *Engelen et al.* (2000).

- Sampling in global tracer transport models and sampling in the real world are unquestionably different. Transport models cannot capture subgrid homogeneity in atmospheric CO_2 which may be reflected in CO_2 measurements. Though efforts are made to measure CO_2 in ways that make them somewhat representative of large air masses, this process is imperfect and may contain bias.

Analysis of the interannual TransCom results is only beginning. In addition to analysis of the model-to-model differences, a variety of interesting tasks remain to be pursued with the model mean:

- Comparison to global biogeochemical modeling studies

- Sensitivity to the removal of the neutral biosphere and the background ocean exchange.

- Comparison to eddy flux carbon exchange at existing measurement towers.

- Full investigation of linkages to model of climate variability including the Arctic Oscillation, temperature and precipitation anomalies, fire, land-use change and other contributors to interannual variability in regional carbon exchange.

Beyond the TransCom experiment itself, the future of atmospheric carbon inversions is moving in a variety of directions. Though adequate when coupled to observations that represent monthly means and observational networks of 100 stations, the synthesis inversion approach will be far too cumbersome as CO_2 measurements move to continuous monitoring and attain densities afforded by remote sensing strategies. The advent of such measurement strategies requires different methodological tools.

The first of these is the use of the adjoint of transport models. The advantage of the adjoint is the reduced computational burden when constructing the response functions for a particular transport model. Traditional forward-running response function approaches must run a separate simulation for each basis function region, time-averaging period, and observing location. An adjoint model, in contrast, must be run separately for each observational location only. The response at every gridcell and timestep is available for each observing location as a result. Of course, as the number of observing locations increases, the cost of simulation does so as well. However, the benefit is that the response at each model gridcell and at the timestep of the transport model is available for use within an inversion.

Though the adjoint-derived response function can be used with a synthesis inversion approach, there are advantages to incorporating the adjoint of atmospheric transport with a data assimilation scheme. An assimilation scheme can incorporate observations into the optimization procedure as they are taken, allowing for greater flexibility in the use of continuous observations. Both, an increase in continuous monitoring and satellite CO_2 measurements are part of future plans in carbon cycle research.

Of course, in order to make use of continuous monitoring at the surface and satellite snapshots of concentrations along orbital tracks, the onus is shifted to improvements in transport modeling. Off-line, course resolution models, such as most in the TransCom experiment are probably not suited for the future assimilation effort. Transport models run at resolutions below 1 degree with timesteps that allow for the characterization of the diurnal cycle are essential. Realistic simulation of the planetary boundary layer and realistic sub-grid vertical transport are essential.

The TransCom experiment has met success in a number of ways, sometimes exceeding the original expectations. The magnitude of transport error in relation to other sources of error in the CO_2 inversion technique has been well-quantified and explored. Furthermore, TransCom has generated flux estimates that are robust to many aspect of the inversion, providing a considerable amount of confidence in the estimates

themselves. Like all intercomparison efforts, the TransCom experiment cannot be farily compared with "state-of-the-art" efforts that individual groups or laboratories must continue to work on. Nevertheless, certain problems can only be solved through collective efforts and rely on the individual groups and laboratories to continue to push the boundaries individually on CO_2 inverse research.

References

Baker, D.F. *Sources and Sinks of Atmospheric CO_2 Estimated from Batch Least-Squares Inversions of CO_2 Concentration Measurements*. PhD Dissertation, Princeton University, 293 pp. (2001).

Bousquet, P., P. Peylin, P. Ciais, C. Le Quéré, P. Friedlingstein, and P. Tans, Regional changes in carbon dioxide fluxes of land and oceans since 1980, *Science*, *290*, 1342-1346, 2000.

Braswell, B.H., Schimel, D.S., Linder, E. and Moore, B. The response of global terrestrial ecosystems to interannual temperature variability, *Science*, 278, 870-872, 1997.

Conway, T.J., Tans, P.P., Waterman, L.S. and Thoning, K.W. Evidence for interannual variability of the carbon-cycle from the National Oceanic and Atmospheric Administration/Climate Monitoring and Diagnostics Laboratory global air-sampling network, *J. Geophys. Res.* D99, 22831-22855, 1994.

Dargaville, R.J., and Simmonds, I. Calculating CO_2 fluxes by data assimilation coupled to a three dimensional mass balance inversion, in *Inverse Methods in Global Biogeochemical Cycles*, Geophys. Monograph. Ser., vol 114, Ed. By P. Kasibhatla et al., 255-264, AGU, Washington DC, 1999.

Dargaville, R.J., Law, R.M., and Pribac, F. Implications of interannual variability in atmospheric circulation on modeled CO_2 concentrations and sources estimates, *Global Biogeochemical Cycles*, 14 (3), 931-943, 2000.

Engelen, R.J., A. Scott Denning, K.R. Gurney, and TransCom 3 modelers, "On Error Estimation in Atmospheric CO_2 Inversions," *Journal of Geophysical Research*, **107** (D22), 4635, 2002.

Enting, I. 2002. *Inverse Problems in Atmospheric Constituent Transport*. Cambridge University Press: Cambridge, U.K.

Feely, R., Wahihkhof, R., Takahashi, T., and Tans, P. Influence of el nino on the equatorial pacific contribution to atmospheric CO_2 accumulation, *Nature*, 398, 597-601, 1999.

Gerard, J.C., Nemry, B., Francois, L.M., and Warnant, P. The interannual change of atmospheric CO_2: contribution of subtropical ecosystems?, *Geophys. Res. Lett.*, **26** (2), 243-246, 1999.

GLOBALVIEW-CO_2, Cooperative Atmospheric Data Integration Project - Carbon Dioxide, CD-ROM, NOAA CMDL, Boulder, Colorado, 2002.

Gu , L., Baldocchi, D.D, Wofsy, S.C, Munger, J.W., Urbanski, S.P, and Boden T.A. Response of a deciduous forest to the mount Pinatubo eruption: Enhanced photosynthesis, *Science*, 299, 2035-2038, 2003.

Gurney, K., R. Law, P. Rayner, and A.S. Denning, TransCom 3 Experimental Protocol, Department of Atmospheric Science, Colorado State University, USA, Paper No. 707, http://transcom.colostate.edu/TransCom_3/transcom_3.html, 2000.

Gurney, K.R., R.M. Law, A.S. Denning, P.J. Rayner, D. Baker, P. Bousquet, L. Bruhwiler, Y.H. Chen, P. Ciais, S. Fan, I.Y. Fung, M. Gloor, M. Heimann, K. Higuchi, J. John, T. Maki, S. Maksyutov, P. Peylin, M. Prather, B.C. Pak, J. Sarmiento, S. Taguchi, T. Takahashi, C.W. Yuen, Towards robust regional estimates of CO_2 sources and sinks using atmospheric transport models, *Nature, 415*, 626-630, 2002.

Gurney, K.R., R.M. Law, A.S. Denning, P.J. Rayner, D. Baker, P. Bousquet, L. Bruhwiler, Y.H. Chen, P. Ciais, S. Fan, I.Y. Fung, M. Gloor, M. Heimann, K. Higuchi, J. John, T. Kowalczyk, E. Maki, S. Maksyutov, K. Masarie, P. Peylin, M. Prather, B.C. Pak, J. Randerson, J. Sarmiento, S. Taguchi, T.

Takahashi, C.W. Yuen, Transcom 3 CO_2 Inversion Intercomparison: 1. Annual mean control results and sensitivity to transport and prior flux information, *Tellus*, *55B***,** 555-579, 2003.

Gurney, K.R., R.M. Law, A.S. Denning, P.J. Rayner, B. Pak, and the TransCom 3 L2 modelers, "Transcom 3 Inversion Intercomparison: Control results for the estimation of seasonal carbon sources and sinks," accepted to *Global Biogeochemical Cycles*, 2004.

Houghton, R.A. Interannual variability in the global carbon cycle, *J. Geophys. Res.*, 105 (D15), 20,121-20,130, 2000.

Jones, C.D., Collins, M., Cox, P.M., and Spall, S.A. The carbon cycle response to ENSO: A coupled clijate-carbon cycle model study, *J. Clim.*, **14**, 4113-4129, 2001.

Keeling, C.D, Whorf, T.P., Wahlen, M, and Vanderplicht, J. Interannual extremes in the rate of rise of atmospheric carbon-dioxide since 1980, *Nature*, 375, 666-670, 1995.

Kindermann, J., Wurth, G., Kohlmaier, G., and Badeck, F-W. Interannual variation of carbon exchange fluxes in terrestrial ecosystems, *Global Biogeochemical Cycles*, **10** (4), 737-755, 1996.

Law, R.M. CO_2 sources from a mass-balance inversion: sensitivity to the surface constraint, *Tellus*, 51B, 254-265, 1999.

Law, R., Y.H. Chen, K.R. Gurney, P. Rayner, A.S. Denning, and TransCom 3 modelers, "TransCom3 CO_2 inversion intercomparison: 2. Sensitivity of annual mean results to data choices," *Tellus*, 55B (2), 512-521, 2003.

Le Quere, C., O. Aumont, L. Bopp, P. Bousquet, P. Ciais, R. Francey, M. Heimann, C.D. Keeling, R.F. Keeling, H. Kheshgi, P. Peylin, S.C. Piper, I.C. Prentice, and P.J. Rayner, Two decades of ocean CO_2 sink and variability, *Tellus*, 55B, 6490656, 2003.

Peylin, P. Baker, D., Sarmiento, J., Ciais, P., and Bousquet, P. Influence of transport uncertainty on annual mean and seasonal inversions of atmospheric CO_2 data, *J. Geophys. Res.*, 107, 10.1029/2001JD000857, 2002.

Plattner, G.-K., F. Joos, T.F. Stocker, Revision of the global carbon budget due to changing air-sea oxygen fluxes, *Global Biogeochemical Cycles*, 16(4), 1096 (doi: 10.1029/2001GB001746), 2002.

Prentice, I.C., G.D. Farquhar, M.J.R. Fasham et al. The Carbon cycle and atmospheric carbon dioxide. In: Climate Change 2001: The Scientific Basis. Contribution of Working Group I to the Third Assessment Report of the Intergovernmental Panel on Climate Change (eds Houghton J.T., Y. Ding, D.J. Griggs et al.), pp. 183-237. Cambridge Unviersity Press, Cambridge, UK, 2001.

Rayner, P. J., I.G. Enting, R.J. Francey, and R.L. Langenfelds, Reconstructing the recent carbon cycle from atmospheric CO_2, $\delta^{13}C$ and O_2/N_2 observations, *Tellus*, *51B*, 213-232, 1999a.

Rayner, P.J. and Law, R.M. The relationship between tropical CO_2 fluxes and the El Nino-Southern Oscillation, *Geophysical Research Letters*, 26 (4), 493-496 1999b.

Robock, A. Pinatubo eruption: The climatic aftermath, *Science*, 295, 1242-1244, 2002.

Rodenbeck, C. Houweling, S., Gloor, M. and Heimann, M. Time-dependent atmospheric CO_2 inversions based on interannually varying tracer transport, *Tellus* B55, 488-497, 2003.

Rödenbeck, C. S. Houweling, M. Gloor, and M. Heimann, CO_2 flux history 1982-2001 inferred from atmospheric data using a global inversion of atmospheric transport, *Atmos. Chem. Phys. Discuss., 3*, 2575-2659, 2003b.

Sarmiento J.L. and Sundquist, E.T. Revised budget for the oceanic uptake of anthropogenic carbon dioxide, *Nature*, 356, 589-593, 1992.

Schaefer, K., Denning, A.S., Suits, N., Kaduk, J., Baker, I., Los, S., and Prihodko, L. Effect of climate on interannual variability of terrestrial CO_2 fluxes, *Global Biogeochemical Cycles*, **16** (4), 1102, doi:10.1029/202GB001928, 2002.

Schimel, D. and Baker, D., The Wildfire Factor, *Nature*, **420**, 29-30, 2002.

Takahashi, T., Sutherland, S. C., Sweeney, C., Poisson, A., Metzl, N., Tillbrook, B., Bates, N., Wanninkhof, R., Feely, R. A., Sabine, C., Olafsson, J. and Nojiri, Y. (2002). Global sea-air CO2 flux based on climatological surface ocean pCO2, and seasonal biological and temperature effects, *Deep-Sea Res. II*, 49, 1601-1622.

Tarantola, A. 1987. Chapter 4 in: *Inverse Problem Theory: Methods for Data Fitting and Parameter Estimation*, Elsevier, Amsterdam.

van der Werf, G, Randerson, J.T., Collatz, G.J., Giglio, L., Kasibhatla, P.S., Arellano, A.F., Olsen, S.C., and Kasischke, E.S., Continental-scale partitioning of fire emissions during the 1997 to 2001 El Nino/La Nina Period. *Science*, **303**, 73-76, 2004.

Vukicevic, T., Braswell, B.H., and Schimel, D. A diagnostic study of temperature controls on global terrestrial carbon exchange, *Tellus* B53, 150-170, 2001.

Yang, X. and Wang, M.X. Monsoon ecosystems control on atmospheric CO_2 interannual variability: infered from a significant positive correlation between year-to-year changes in land precipitation and atmospheric CO_2 growth rate, *Geophysical Research Letters*, 27 (11), 1671-1674, 2000.

Winguth, A.M.E., Heimann, H., Kurz, K.D., Maier-Reimer, E., Mikolajewicz, U. and Segschneider, J. El Nino-Southern Oscillation related fluctuations of marine carbon cycle, *Global Biogeochemical Cycles*, 8, 39-63, 1994.

Wolter, K., and M.S. Timlin, 1993: Monitoring ENSO in COADS with a seasonally adjusted principal component index. *Proc. of the 17th Climate Diagnostics Workshop*, Norman, OK, NOAA/N MC/CAC, NSSL, Oklahoma Clim. Survey, CIMMS and the School of Meteor., Univ. of Oklahoma, 52-57. Data: http://www.cdc.noaa.gov/~kew/MEI/mei.html#ref_wt1

Wolter, K., and M.S. Timlin, 1998: Measuring the strength of ENSO - how does 1997/98 rank? *Weather*, **53**, 315-324.

Appendix

Table A4.1 Station listing for the six CO_2 observing networks used in the interannual inversion. Time period and the values for β are shown.

23 stations: 1980 - 2000	26 stations: 1980 - 1997	30 stations: 1980 - 1990	60 stations: 1990 - 2000	100 stations: 1993 - 2000	114 stations: 1995 - 2000
β = 2	β = 2	β = 2	β = 1	β = 0.8	β = 1
alt_06D0	alt_06D0	alt_06D0	alt_00D0	aia005_02D2	aia005_02D2
asc_00D0	ams_11C0	ams_00D0	alt_06D0	aia015_02D2	aia015_02D2
ams_11C0	asc_00D0	ams_11C0	alt_02D0	aia025_02D2	aia025_02D2
azr_00D0	azr_00D0	asc_00D0	alt_04D0	aia035_02D2	aia035_02D2
bhd_15C0	bhd_15C0	avi_00D0	ams_11C0	aia045_02D2	aia045_02D2
brw_00C0	brw_00C0	azr_00D0	asc_00D0	aia055_02D2	aia055_02D2
brw_00D0	brw_00D0	bhd_15C0	azr_00D0	aia065_02D2	aia065_02D2
cmn_17C0	cba_00D0	brw_00C0	bhd_15C0	alt_00D0	alt_00D0
gmi_00D0	cmn_17C0	brw_00D0	bme_00D0	alt_06D0	alt_06D0
key_00D0	cmo_00D0	cba_00D0	bmw_00D0	alt_02D0	alt_02D0
kum_00D0	gmi_00D0	cmn_17C0	brw_00C0	alt_04D0	alt_04D0
mlo_00C0	key_00D0	cmo_00D0	brw_00D0	ams_11C0	ams_11C0
mlo_00D0	kum_00D0	gmi_00D0	cfa_02D0	asc_00D0	asc_00D0
nwr_00D0	mbc_00D0	key_00D0	cgo_00D0	azr_00D0	ask_00D0
psa_00D0	mlo_00C0	kum_00D0	cgo_02D0	bal_00D0	azr_00D0
sch_23C0	mlo_00D0	mbc_00D0	cgo_04D0	bhd_15C0	bal_00D0
Sey_00D0	nwr_00D0	mlo_00C0	cmn_17C0	bme_00D0	bhd_15C0
smo_00C0	psa_00D0	mlo_00D0	crz_00D0	bmw_00D0	bme_00D0
smo_00D0	sch_23C0	nwr_00D0	gmi_00D0	brw_00C0	bmw_00D0
spo_00C0	sey_00D0	psa_00D0	hba_00D0	brw_00D0	brw_00C0
spo_00D0	smo_00C0	sbl_06D0	izo_00D0	car030_00D2	brw_00D0
stm_00D0	smo_00D0	sch_23C0	izo_27C0	car040_00D2	bsc_00D0
stmebc_00D0	spo_00C0	sey_00D0	key_00D0	car050_00D2	car030_00D2
	spo_00D0	smo_00C0	kum_00D0	car060_00D2	car040_00D2
	stm_00D0	smo_00D0	maa_02D0	cfa_02D0	car050_00D2
	stmebc_00D0	spo_00C0	mhd_00D0	cgo_00D0	car060_00D2
		spo_00D0	mid_00D0	cgo_02D0	cba_04D0
		stm_00D0	mlo_00C0	cgo_04D0	cfa_02D0
		stmebc_00D0	mlo_00D0	cmn_17C0	cgo_00D0
		wes_23C0	mlo_02D0	cri_02D0	cgo_02D0
			mqa_02D0	crz_00D0	cgo_04D0
			nwr_00D0	eic_00D0	cmn_17C0
			poc000_00D1	esp_02D0	cri_02D0
			pocn05_00D1	esp_06D0	crz_00D0
			pocn10_00D1	gmi_00D0	eic_00D0
			pocn15_00D1	hba_00D0	esp_02D0
			pocn20_00D1	hun_00D0	esp_06D0
			pocn25_00D1	ice_00D0	gmi_00D0
			pocn30_00D1	itn051_00C3	hba_00D0
			pocs05_00D1	itn496_00C3	hun_00D0
			pocs10_00D1	itn_00D0	ice_00D0
			pocs15_00D1	izo_00D0	itn051_00C3
			pocs25_00D1	izo_27C0	itn496_00C3
			pocs30_00D1	jbn_29C0	itn_00D0
			psa_00D0	key_00D0	izo_00D0
			rpb_00D0	kum_00D0	izo_27C0
			ryo_19C0	kum_04D0	jbn_29C0
			sch_23C0	maa_02D0	key_00D0
			sey_00D0	mhd_00D0	kum_04D0
			shm_00D0	mhdcbc_11C0	kum_00D0
			smo_00C0	mhdrbc_11C0	lef030_00C3
			smo_00D0	mid_00D0	lef396_00C3
			spo_00C0	mlo_00C0	lef_00D0
			spo_00D0	mlo_00D0	lmp_28D0
			spo_02D0	mlo_02D0	maa_02D0
			stm_00D0	mnm_19C0	mhd_00D0
			stmebc_00D0	mqa_02D0	mhdcbc_11C0
			syo_00D0	nwr_00D0	mhdrbc_11C0
			tap_00D0	poc000_00D1	mid_00D0
			wlg_00D0	pocn05_00D1	mlo_00C0
				pocn10_00D1	mlo_00D0
				pocn15_00D1	mlo_02D0
				pocn20_00D1	mnm_19C0
				pocn25_00D1	mqa_02D0
				pocn30_00D1	nwr_00D0
				pocs05_00D1	poc000_00D1
				pocs10_00D1	pocn05_00D1
				pocs15_00D1	pocn10_00D1
				pocs25_00D1	pocn15_00D1
				pocs30_00D1	pocn20_00D1
				psa_00D0	pocn25_00D1
				rpb_00D0	pocn30_00D1
				ryo_19C0	pocs05_00D1
				sch_23C0	pocs10_00D1
				sey_00D0	pocs15_00D1
				shm_00D0	pocs25_00D1
				sis_02D0	pocs30_00D1
				smo_00C0	psa_00D0

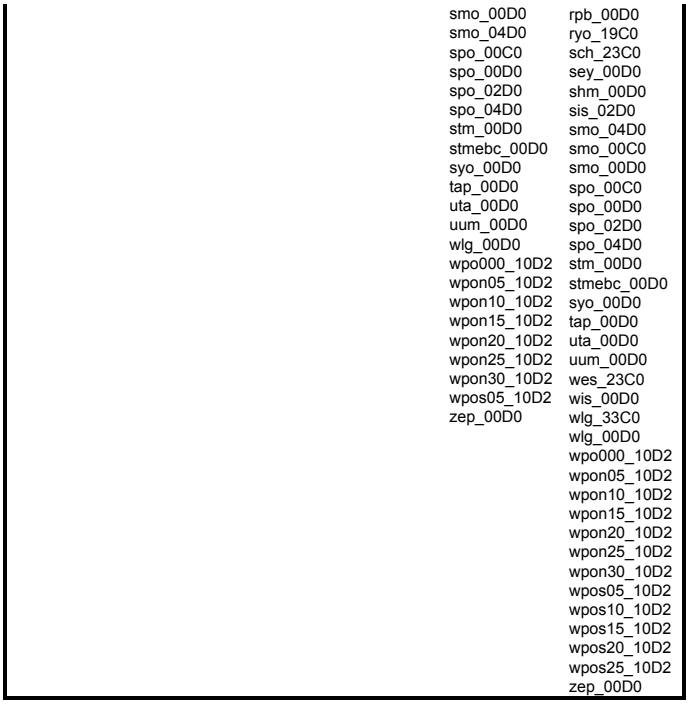

Table A4.2 Fluxes and uncertainties associated with figure 4.11 (Gt C/year)

Region	92-96 AM inv		92-96 Cyclo inv		92-96 75 stat/unc	
	flux	tot unc	flux	tot unc	flux	tot unc
Bor N America	0.28	0.47	0.20	0.33	0.16	0.28
Temp N America	-0.82	0.66	-0.89	0.39	-0.97	0.30
Tropical America	0.67	1.18	0.74	1.06	0.70	0.72
S America	-0.12	1.01	-0.24	0.88	-0.46	0.86
Northern Africa	0.01	1.30	0.79	1.01	0.74	0.81
Southern Africa	-0.29	1.01	-0.51	0.83	-0.41	0.64
Boreal Asia	-0.60	0.75	-0.36	0.56	-0.33	0.56
Temperate Asia	-0.42	0.93	-0.41	0.81	-0.51	0.74
Tropical Asia	0.42	0.86	0.27	1.04	0.29	0.92
Australasia	-0.15	0.33	-0.10	0.21	-0.11	0.15
Europe	-0.61	0.56	-0.96	0.47	-1.01	0.41
N Pacific	-0.25	0.45	-0.32	0.31	-0.38	0.29
W Pacific	-0.15	0.40	-0.21	0.31	-0.19	0.27
E Pacific	0.63	0.41	0.66	0.33	0.64	0.27
S Pacific	0.49	0.66	0.51	0.56	0.44	0.50
Northern Ocean	-0.30	0.23	-0.27	0.19	-0.27	0.17
North Atlantic	-0.45	0.42	-0.29	0.33	-0.31	0.29
Tropical Atlantic	-0.05	0.35	-0.10	0.24	-0.09	0.16
South Atlantic	-0.04	0.43	-0.05	0.25	-0.08	0.10
Southern Ocean	-0.47	0.35	-0.55	0.37	-0.49	0.47
Tropical Indian	-0.34	0.48	-0.33	0.32	-0.38	0.27
South Indian	-0.24	0.38	-0.39	0.29	-0.37	0.23

Table A4.3. Fluxes and uncertainties associated with figure 4.12 (Gt C/year)

Region	95-00 23 stat		95-00 60 stat		95-00 100 stat		95-00 114 stat	
	flux	tot unc	flux	tot unc	flux	tot unc	flux	tot unc
Bor N America	0.04	0.26	0.13	0.24	0.29	0.38	0.29	0.40
Temp N America	-0.70	0.52	-0.45	0.42	-0.52	0.35	-0.50	0.31
Northern Africa	0.06	0.40	0.23	0.49	0.45	0.72	0.52	0.93
Boreal Asia	-0.41	0.46	-0.52	0.44	-0.35	0.51	-0.34	0.54
Temperate Asia	0.20	0.39	-0.06	0.56	-0.23	0.42	-0.40	0.48
Tropical Asia	0.63	0.33	0.54	0.43	0.39	0.41	0.38	0.48
Australasia	-0.22	0.14	-0.15	0.13	-0.03	0.15	-0.04	0.15
Europe	-0.82	0.51	-0.72	0.44	-0.98	0.37	-0.80	0.43
North Pacific	-0.87	0.32	-0.79	0.33	-0.73	0.39	-0.74	0.42
Northern Ocean	-0.27	0.15	-0.32	0.15	-0.40	0.18	-0.46	0.22
North Atlantic	-0.25	0.18	-0.36	0.20	-0.38	0.30	-0.41	0.32
Southern Ocean	-0.09	0.18	-0.27	0.20	-0.19	0.22	-0.18	0.21
TrAmPac	0.73	0.48	1.55	0.69	1.03	0.68	1.28	0.75
Atlantis	-0.70	0.40	-1.45	0.74	-1.09	0.87	-1.33	0.97
Indian Ocean	-0.20	0.19	-0.25	0.38	-0.22	0.45	-0.22	0.46

Table A4.3. Fluxes and uncertainties associated with figure 4.13

Region	95-00 60 stat		95-00 100 stat		95-00 114 stat	
	flux	tot unc	flux	tot unc	flux	tot unc
Bor N America	0.13	0.24	0.29	0.38	0.29	0.40
Temp N America	-0.45	0.42	-0.52	0.35	-0.50	0.31
Tropical America	0.69	0.87	0.79	0.81	1.10	0.93
S America	-1.06	0.80	-0.86	0.93	-1.01	0.97
Northern Africa	0.23	0.49	0.45	0.72	0.52	0.93
Southern Africa	-0.21	0.55	0.22	0.69	0.21	0.80
Boreal Asia	-0.52	0.44	-0.35	0.51	-0.34	0.54
Temperate Asia	-0.06	0.56	-0.23	0.42	-0.40	0.48
Tropical Asia	0.54	0.43	0.39	0.41	0.38	0.48
Australasia	-0.15	0.13	-0.03	0.15	-0.04	0.15
Europe	-0.72	0.44	-0.98	0.37	-0.80	0.43
N Pacific	-0.79	0.33	-0.73	0.39	-0.74	0.42
W Pacific	-0.18	0.23	-0.11	0.29	-0.14	0.30
E Pacific	0.74	0.28	0.70	0.30	0.67	0.30
S Pacific	0.28	0.43	-0.38	0.36	-0.37	0.34
Northern Ocean	-0.32	0.15	-0.40	0.18	-0.46	0.22
North Atlantic	-0.36	0.20	-0.38	0.30	-0.41	0.32
Tropical Atlantic	-0.07	0.32	-0.17	0.30	-0.22	0.31
South Atlantic	-0.09	0.34	-0.26	0.31	-0.28	0.31
Southern Ocean	-0.27	0.20	-0.19	0.22	-0.18	0.21
Tropical Indian	-0.07	0.38	0.05	0.35	0.05	0.41
South Indian	-0.18	0.26	-0.27	0.28	-0.27	0.29

5.1 Introduction

The emissions of fossil fuel CO_2 form a key component of atmospheric CO_2 inversions. In the Bayesian synthesis inversion used in the TransCom 3 experiment (Gurney et al. 2002; Gurney et al. 2003; Gurney et al., 2004), the fossil fuel emissions are designated as a "background" or "presubtracted" flux. Fossil fuel emissions are not the only background fluxes specified; two other fluxes are included in this fashion: a neutral biosphere flux and a global oceanic flux.

In the simplest terms, once the background emissions are specified in space and time, the fluxes that are estimated in the inversion process, the "residual" fluxes, represent adjustments to these background fluxes such that the sum of the background and the residual fluxes best match atmospheric CO_2 concentrations observed at particular times and locations. The use of the term "presubtracted" for the background fluxes can best be explained by the following expression denoting the linearly summed components of the atmospheric CO_2 budget.

$$C_{obs} = C_{ff} + C_{oc} + C_{nbio} + \sum_{i=1}^{N} C_{res} \tag{5.1}$$

where C_{obs} represent the observed CO_2 at a particular point in space and time, C_{ff} represents the contribution to the observed CO_2 due to global fossil fuel emissions, C_{oc}, the contribution due to a chosen global oceanic flux, C_{nbio}, the contribution due to a neutral biosphere flux, and C_{res}, the contribution of the residual fluxes from the chosen N discretized regions (see Gurney et al. 2000). An additional term, the oxidation of CO is considered small and is neglected here. This expression is valid for every location in the atmosphere. Rearrangement of this basic budget makes clear the motivation behind the term "presubtracted"; the residual CO_2 can be defined as the difference between the observed CO_2 and the sum of the first three terms on the right-hand side of equation 5.1. Hence, the background fluxes are subtracted from the observations leaving the residual CO_2 concentration as the observational constraint in the inversion.

In practice, the fossil fuel, neutral biosphere, and oceanic fluxes can be adjusted in the inversion process in the same way that the discretized residual fluxes are. However, this is typically not performed in atmospheric CO_2 inversions and these fluxes are provided to the inversion with small uncertainty and hence, are fixed at the values provided. In many ways, this is a convention concerning how the estimated fluxes (the 11 land and 11 oceanic residual fluxes in the T3 experiment) are reported. One could report the sum of all the flux contributions on the right-hand side of equation 1. This is often done for the oceanic fluxes but not traditionally done for the fossil and neutral biosphere fluxes. There are two reasons for this convention.

First, the three presubtracted fluxes are considered well-known. For the fossil fuel background flux, the emissions are considered reliable at the 1º x 1º scale and as annual means. Whether or not this is sufficient for the current trajectory of atmospheric CO_2 inversions is the substance of this chapter, which will I will return to shortly. The neutral biosphere portion of the background fluxes is considered a subset of the total NBP, by definition, while the oceanic fluxes are generally considered a good first guess and represent a combination of model and data products. The second reason relates to the first; the background fluxes are not considered as scientifically interesting as the residual fluxes primarily because the latter constitute the portion of the global carbon budget that is poorly understood.

The fundamental problem with this line of reasoning comes about if the assumed background fluxes are sufficiently different from the true background fluxes, particularly when the spatial and temporal scale of these fluxes are different from those solved for. Were this to occur, these errors would be aliased into the residual fluxes and constitute a bias to the solution (Kaminski et al., 2001; Engelen et al., 2002). For the case of the fossil fuel background flux this arises primarily because the underlying data may not contain the true dynamics in space and time that fossil emissions in the real world reflect.

Therefore, the purpose of the current chapter is to test how much impact more realistic fossil fuel carbon fluxes might have on the series of TransCom 3 results completed in the last few years. Because the TransCom 3 methodology associated with the inclusion of fossil background fluxes is widely found in inverse studies of atmospheric CO_2, the results presented here have wide applicability to atmospheric CO_2 inversions in general.

5.2 Methodology: Annual mean and seasonal inversions

5.2.1 Fossil fuel emissions

Figure 5.1a and 5.1b show global gridded maps of fossil fuel emissions for the years 1990 and 1995 that were used in the TransCom 3 experiment.

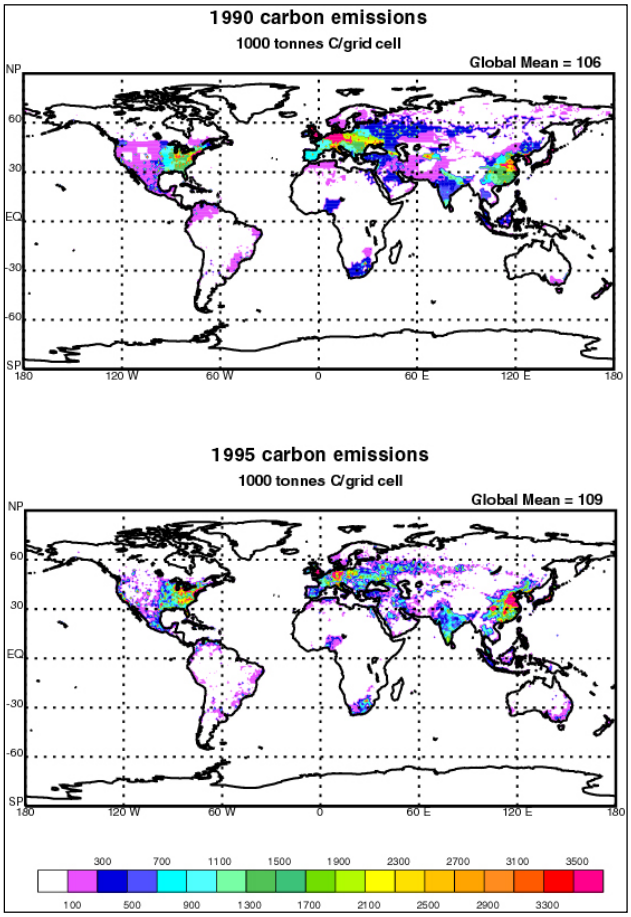

Figure 5.1. Fossil fuel emissions for a) 1990 and b) 1995. Units are 1000 tonnes C/grid cell and the grid cells are dimensioned 1º x 1º.

The 1990 annual mean fossil emissions (1º x 1º) are from Andres et al. (1996) and total 5.812 GtC yr^{-1}. The 1995 annual mean fossil source (1º x 1º) is derived from the data prepared by Brenkert (1998) and totals 6.173 GtC yr^{-1}. The 1990 emissions were constructed from country level emissions of CO_2 due to fossil fuel burning and cement manufacturing which in turn were derived from UN energy statistics (Marland and Rotty, 1984; Boden et al., 1995). The country emissions were allocated to clusters of grid cells (and sub-clusters for 9 countries) based on a political unit data set outlining nation-states (Lerner et al., 1988). The emissions within these grid cell clusters were allocated according to 1984 population density. A number of adjustments were made to account for border issues, land/sea masking, and the maintenance of very small countries. The 1995 fossil fuel emissions were constructed similarly to the 1990 emissions. The primary difference was the use of 1990 population density estimates rather than 1984 (Li, 1996).

These two gridded emissions datasets (or their immediate predecessors) are widely used as background fluxes in atmospheric CO_2 inversions (e.g. Rodenbeck et al., 2003; Peylin et al., 2003; Bousquet et al., 2000;Rayner et al., 1999; Fan et al., 1998). In the TransCom 3 experiment, a combination of the 1990 and 1995 emissions are used to capture some of the temporal shifts that are known to have occurred in fossil emissions during the 1990s. These emission maps are introduced as background fluxes and are fixed.

As mentioned in the introduction, were these emissions to contain errors, these would be aliased into the residual fluxes. Potential errors can come in two forms: 1) errors in the emissions data themselves, and 2) mismatches between the spatiotemporal resolution of the fossil fuel emissions and the residual fluxes.

In the first instance, much care has been taken to accurately account for the fossil fuel emissions around the globe. At the 1º x 1º scale, errors of 6% to 10% are typically quoted (Marland and Rotty, 1984). Though such errors are not insignificant, the more error prone aspect of the emissions data is the way in which emissions are allocated at scales smaller than a country. Emissions do not covary with population density in all cases. For example, California electricity production occurs primarily outside the state. The emissions associated with the in-state consumption occurs at the power generating facilities which may be hundreds to thousands of miles away from the direct consumption of electricity. Highways are another example of potentially low population locations that may have inordinately large emissions.

The second form of error has the potential to be more serious. These two commonly used fossil fuel datasets reflect annual mean emissions and represent only the stated years. Temporal variability at scales smaller (seasonal, diurnal) and larger (interannual) than the annual mean are not represented. Variations at scales smaller than 1º x 1º are also not captured, though such variability is not routinely challenged by atmospheric inversions to date.

A number of atmospheric CO_2 inversions have estimated fluxes at monthly scales (seasonal inversions) and multiyear scales (interannual inversions) and have relied on one or both of the fields introduced above. Furthermore, should fossil fuel emissions exhibit seasonal or diurnal variations that covary with vertical transport in the planetary boundary layer, rectification may occur (Denning et al., 1996). Recent fossil emissions data for the United States and Europe indicate that fossil fuel emissions do exhibit seasonality with greater emissions during winter months and less during summer months (Blasing et al., 2003, Levin et al., 2001). Figure 5.2a shows fossil emissions data for the United States. The long-term monotonic increase and the seasonal variation is evident in the data. Figure 5.2b indicates that the peak-to-peak amplitude varies from 20% to 30% and has exhibited a steady decline over the time period shown.

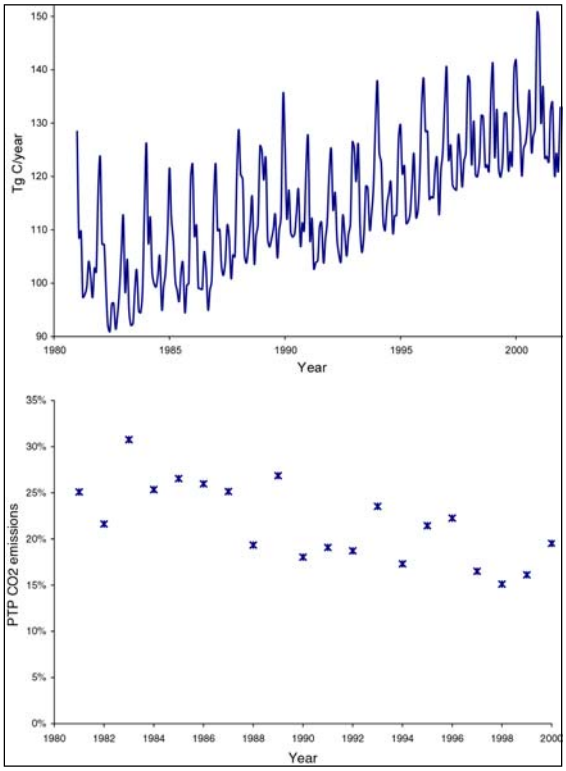

Figure 5.2. a) Total fossil fuel CO_2 emissions for the United States (Tg C/year). B) Peak to peak fossil fuel emissions for the United States.

The decline in the seasonal amplitude is due to the rise of coal combustion in summer months in order to produce greater electricity. This is likely due to the expansion of air-conditioning during the Summer (Blasing et al., 2002; Gregg and Andres, 2003). European researchers have suggested that the equivalent peak-to-peak amplitude for Europe is approximately 40%, slightly higher than that shown for the United States (Levin et al., 2001).

Country tabulations of fossil fuel emissions over the last two decades indicate that the interannual variation in the spatial pattern of emissions has been changing. These are most likely due to geopolitical and economic events (see Nakicenovic et al., 2000). Examples include the demise of the centrally-planned economies of central Europe at the beginning of the 1990s, the dramatic growth in the East-Asian economy, and the fuel shifts that have occurred recently in Western Europe countries.

In the following experiment, I test the sensitivity of the annual, seasonal, and interannual TransCom 3 inversion results to two potential variations in fossil emissions not captured in the standard experiment. I will test the impact of seasonally varying fossil fuel emissions and emissions that vary in space and time over multiyear timescales.

5.2.2 The transport models

In order to fully explore the possible inverse results to more realistic fossil fuel emissions, three different transport models have been used that span key transport characteristics of the TransCom 3 experiment (Gurney et al., 2003). Figure 5.3a shows the annual/zonal mean surface CO_2 concentration of the TransCom 3 models to 1990 fossil fuel emissions. The CO_2 concentration represents the 4th year of a 4 year simulation in which the 1990 fossil fuel emissions (described in last section) are repeated each year.

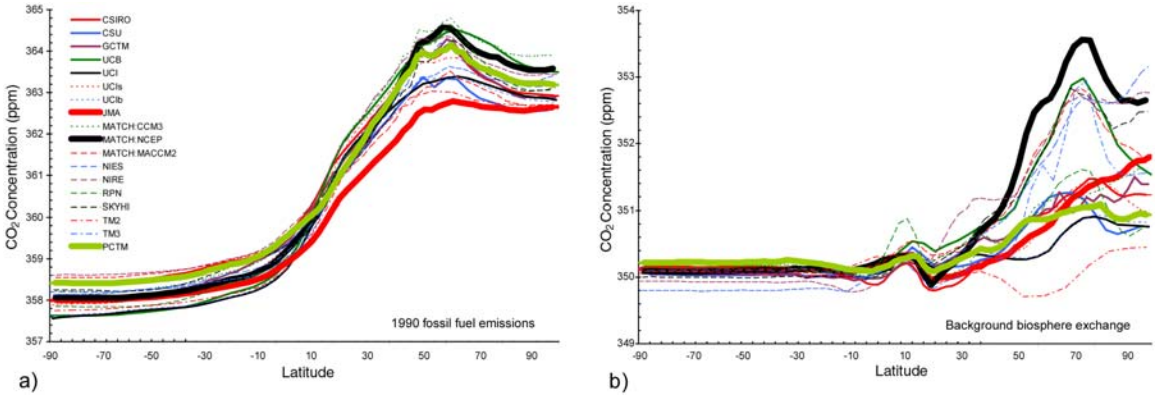

Figure 5.3. a) Annual/zonal mean surface CO_2 concentration (ppm) resulting from 4 years constant emissions of 1990 fossil fuel CO_2 and b) neutral biosphere exchange. The models used in the current study are denoted in bold.

The three models chosen for this study are represented by bold lines: MATCH:NCEP, JMA-CDTM, and PCTM. MATCH:NCEP has the largest concentration maximum over the source regions of the northern hemisphere while JMA-CDTM has the smallest. The PCTM model exhibits a CO_2 concentration maximum that is towards the larger of the 18 models shown though not as large as the MATCH:NCEP model. The magnitude of the interhemispheric gradient provides a useful index of how vigorously the various models transport CO_2 horizontally and vertically. (Denning et al., 1999).

Figure 5.3b shows the annual/zonal mean surface CO_2 concentration of the TransCom 3 models to the neutral biosphere flux generated from the Carnegie Ames Stanford Approach model (Randerson et al., 1997). As with the fossil fuel emissions, MATCH:NCEP has one of the larger CO_2 concentration maxima while JMA-CDTM is among the models with the smallest. In contrast to the fossil fuel emissions, PCTM has a concentration maximum towards the smaller of the models shown. The relative magnitude of the northern extratropical CO_2 maximum (coincident with the strongly seasonal biosphere exchange) provides a reasonable indication of how strongly the models exhibit seasonal rectification. In this case, it is not only the vigor with which the model transports CO_2 out of the boundary layer but whether or not the vertical transport and planetary boundary layer (PBL) mixing depth have seasonal variation that is anticorrelated with the biosphere exchange itself (Heimann et al., 1986; Keeling et al., 1989; Denning et al., 1995). Though possessing considerable "trapping" of the aseasonal fossil fuel emissions, PCTM appears to contain vertical transport and PBL mixing that has weak seasonality or is more in phase with the biosphere exchange.

Given the importance of these two responses to diagnosing the overall transport characteristics of tracer transport models, the three models chosen do a good job at spanning the spread available to the TransCom 3 experiment.

5.2.3 Hypothesized seasonal fossil fuel emissions

In order to test the impact that seasonal fossil fuel emissions might have on inverse results, a series of hypothesized seasonal fossil fuel emissions maps were generated. These emissions were created by taking the existing TransCom 3 fossil fuel emissions and adding seasonal variation. This was done at every grid cell according to:

$$F^{n}_{i,j,m} = F^{o}_{i,j,m} + A_k F^{o}_{i,j,m} \sin\theta_j \cos\left(\frac{2\pi(m-1)}{12}\right) \quad (5.2)$$

where $F^{n}_{i,j,m}$ is the new flux at grid cell with longitude index *i*, latitude index *j*, and month index *m*. $F^{o}_{i,j,m}$ is the original flux. A_k is the amplitude factor (AF) that represents the percent increase in the original fossil emissions. Nine different AFs were chosen creating nine different seasonal fossil fuel emissions maps. These included AFs of 0% (the aseasonal "base case"), 10%, 20%, etc. up to 80%. This AF is modified by both a latitude and time (month) dependence. The former is represented by θ_j which is the latitude in radians. The latter is represented by the expression within the cosine term and causes a maxima to occur in January and a minima to occur in July.

Figure 5.4 shows an idealized example with an AF of 20% and a base emission level of 100. This shows that the emissions reach a maximum at 90º North, decreasing as the latitude decreases, and ultimately changing sign in the southern hemisphere. It is important to note that given the 80% amplitude modification case, the January emissions are roughly three times larger than the July emissions at 40º North. For the 50% amplitude modification case, this gives a January/July ratio of roughly 2. As indicated previously, limited data for the US and Europe indicate peak to peak amplitudes at roughly 40º N are on the order of 20% to 30%. In this formulation, that would correspond most closely to an AF of 30%.

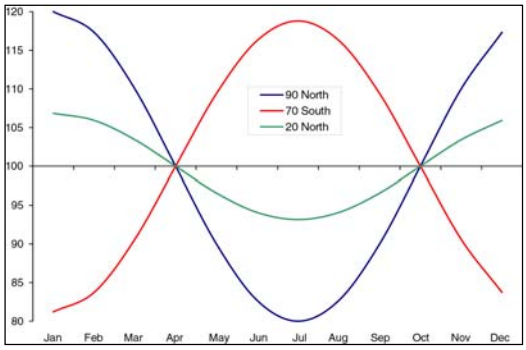

Figure 5.4. Seasonal fossil fuel emissions example with an amplitude factor of 20% and a base level of 100 units.

5.2.4 Interannually varying emissions

In order to capture realistic interannual variations in fossil fuel emissions at the scale of the basis function regions (see figure 1, Supplementary information in Gurney et al., 2002 for a basis function map), annual tabulations of fossil fuel emissions at the country level have been utilized (Marland et al., 2003). Because the gridded fossil fuel emissions introduced in section 5.2.1 are only available for the years 1990 and 1995, country level data is necessary to capture the spatiotemporal changes in emissions over many years.

Each country in the country level fossil fuel emissions tabulation was assigned to one of the 11 TransCom 3 land regions. For each region and year (1979 to 2000) a fraction of the annual global total emissions was generated. The 1990 fossil fuel emissions map, described in section 5.2.1 was similarly regionalized into the 11 TransCom land regions. The 11 regional fossil fuel emissions maps were run though the PCTM model as individual components of the background fossil fuel flux. In this way, CO_2 concentration resulting from this flux at all the observing stations were generated from each of the regions, independently. The CO_2 concentration associated with a given regional fossil fuel emissions pattern can then be scaled each year to reflect the spatiotemporal changes evident in the country level data. This can be seen by redrafting equation 5.1.

$$C_{obs}(t) = \sum_{i=1}^{11} \alpha_i(t) C^{i}_{ff} + C_{oc} + C_{nbio} + \sum_{i=1}^{22} C_{res}(t) \quad (5.3)$$

where α_i represents the fraction for a given region, *i,* in a given year, *t*, and C^{i}_{ff} represents the fossil fuel emissions for a given region and year. This model run will be referred to as the "perturbed" interannual run.

A base case run for this interannual experiment was constructed by running the global 1990 emissions map (no regionalization) for each year but allowing the global total emissions to change according to the global sum of the country level emissions. This is a simpler interannual background construction than was used in the previous chapter. Because flux differences are the target of this investigation, this is considered sufficient. This model run will be referred to as the "base" interannual run.

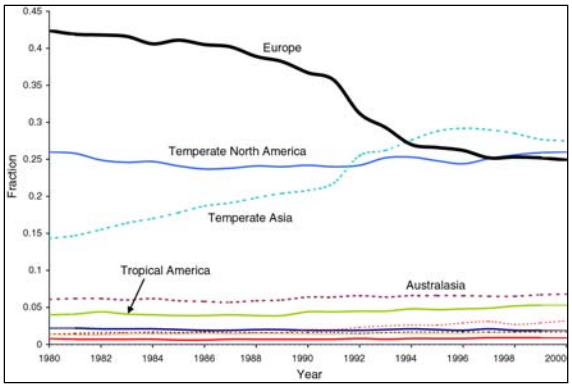

Figure 5.5. Regional fossil fuel emissions as a fraction of the yearly global total.

Two important caveats must be mentioned. First, the forward simulations were run with the PCTM model only. The impact to the interannual inversion from realistic interannually varying fossil fuel emissions was considered less dependent on individual model transport and more a reflection of the changing surface emissions. However, efforts are underway to duplicate the effort performed here with both the MATCH:NCEP and JMA-CDTM models.

The other caveat is the admission that the spatial distribution within the individual TransCom 3 regions remains fixed at the 1990 level. Therefore, the results will only address changes that cause fossil fuel emissions to shift from one region to another but do not reflect changes that occur within regions. The implications of this will be discussed later.

The timeseries of the regional fractions are shown in figure 5.5. Europe and Temperate Asia show the greatest changes over this time period. Europe experienced declines of over 35% in the late 1980s and early 1990s. Temperate Asia shows increasing emissions throughout the period with some leveling off starting in the mid-1990s. Absolute emissions in Temperate North America grew at a rate nearly comparable to the global total hence, it's fractional share remained fairly constant.

5.3 Results

5.3.1 Annual mean inversion

Nine seasonal fossil emissions maps were constructed following the procedure described in section 4.2.3 and run through the three models. Figure 5.6a shows the annual/zonal mean CO_2 concentration for four of the nine AF cases. Figure 5.6b shows a difference plot of the 30% and base AF cases for each of the models. The model with the largest rectifier (MATCH:NCEP) exhibits the greatest sensitivity to the fossil seasonality. PCTM has the next largest CO_2 concentration difference followed by the JMA-CDTM model.

The other feature to note is the absolute magnitude of the increase in northern extratropical concentration as the fossil seasonality is increased. For the MATCH:NCEP model, the maximum concentration difference in the northern extratropics of figure 5.6b is roughly 0.4 ppm. If

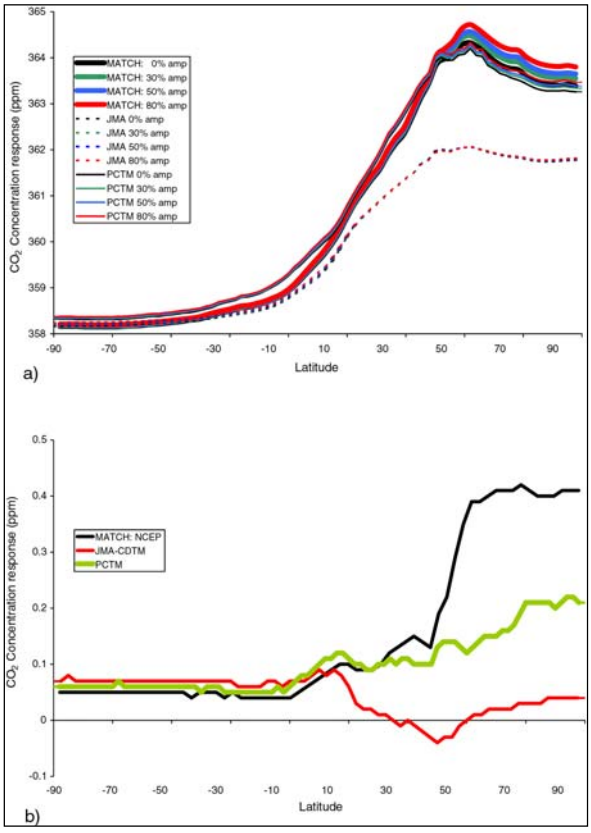

Figure 5.6. a) Annual/zonal mean surface CO_2 concentration resulting from seasonal fossil fuel emissions for four of the nine AFs (including the base case). b) CO_2 concentration difference between the 80% and base AF cases.

one considers the more realistic AF case of 30%, the maximum concentration difference of about 0.15 ppm.

This suggests very small amounts of rectification when one compares this to the CO_2 concentration maximum from the neutral biosphere exchange of over 3.7 ppm. The expectation is that the residual fluxes will be little influenced by the annual mean rectification of the seasonal fossil fuel emissions.

Table 5.1 shows the residual fluxes for all 22 TransCom 3 land and ocean regions. The CO_2 observing stations used, their associated uncertainty and the prior flux information was all identical to that used in the control TransCom 3 annual mean inversion (Gurney et al., 2002). The only difference was that the current inversion used only the 1990 fossil fuel emissions rather than a mixture of 1990 and 1995. This was done for simplicity since the focus here is on the difference when seasonality is included in the emissions.

The table provides the base case and the flux difference for the 30% AF case. As expected the changes are very small compared to the magnitude of the residual fluxes in the base case run. This result leads to the first important conclusion concerning the impact of seasonal fossil fuel emissions: there is no fossil fuel rectification of any significance.

Table 5.1. Annual mean, regional inverse flux estimates (Gt C/year) for the base AF case and the change in flux (Gt C/year) for an inversion run with the 30% AF. Results are shown for all three models.

	JMA		M:NCEP		PCTM	
Region	base	change	base	change	base	Change
Boreal N America	0.24	-0.01	-0.08	0.01	-0.08	0.02
Temp N America	-0.92	0.04	-0.68	-0.01	-0.92	0.01
Trop America	0.54	-0.01	0.40	-0.01	0.06	-0.02
South America	0.21	0.00	-1.04	0.00	-0.43	0.03
Northern Africa	-0.59	0.00	0.53	0.07	0.04	-0.08
Southern Africa	-0.17	0.01	-1.16	0.00	-0.08	0.01
Boreal Asia	-0.65	-0.03	-1.39	-0.07	0.25	-0.03
Temperate Asia	0.46	0.01	-0.13	0.05	-0.48	0.08
Tropical Asia	0.51	-0.02	1.43	0.04	0.04	-0.02
Australasia	0.13	0.00	0.08	0.00	-0.11	0.00
Europe	-0.38	0.04	-1.04	-0.04	-1.05	0.00
N Pacific	0.31	0.00	0.70	0.01	0.53	-0.01
W Pacific	-0.25	-0.01	-0.09	0.00	-0.26	0.01
E Pacific	0.09	-0.01	0.09	-0.02	0.03	0.00
S Pacific	0.47	0.00	0.33	0.01	0.85	0.00
Northern Ocean	0.23	0.00	0.27	0.00	0.38	0.00
N Atlantic	-0.08	0.00	0.20	-0.01	0.26	0.00
Tropical Atlantic	-0.13	0.00	-0.11	0.00	0.00	0.01
S Atlantic	0.12	0.00	0.06	0.00	0.19	0.01
Southern Ocean	0.16	0.00	0.74	0.00	0.39	-0.01
Trop Indian Ocean	-0.51	-0.01	0.00	-0.02	-0.68	0.01
S Indian Ocean	-0.16	0.00	0.55	0.00	0.27	0.00

5.3.2. Seasonal inversion

Though the influence on the annual mean inversion is small, the impact may be larger on the seasonal inversion. The concern for the seasonal inversion is not rectification, but straightforward bias in the monthly mean residual fluxes.

An initial glimpse at how the monthly estimated fluxes might respond to a seasonal fossil emissions field is shown in Figure 5.7a. This figure shows the monthly mean CO_2 concentration response (full CO_2

concentration without initial condition of 350 ppm) at three northern stations; Hungary (HUN: 46.95ºN, 16.65ºE), Mauna Loa (MLO: 19.53ºN, 155.58ºW), and North Carolina (ITN: 35.35ºN, 77.38ºW). Hungary represents the station with the largest response due to its proximity to fossil fuel sources. North Carolina had the largest response of the North American stations while Mauna Loa was typical of background, oceanic stations.

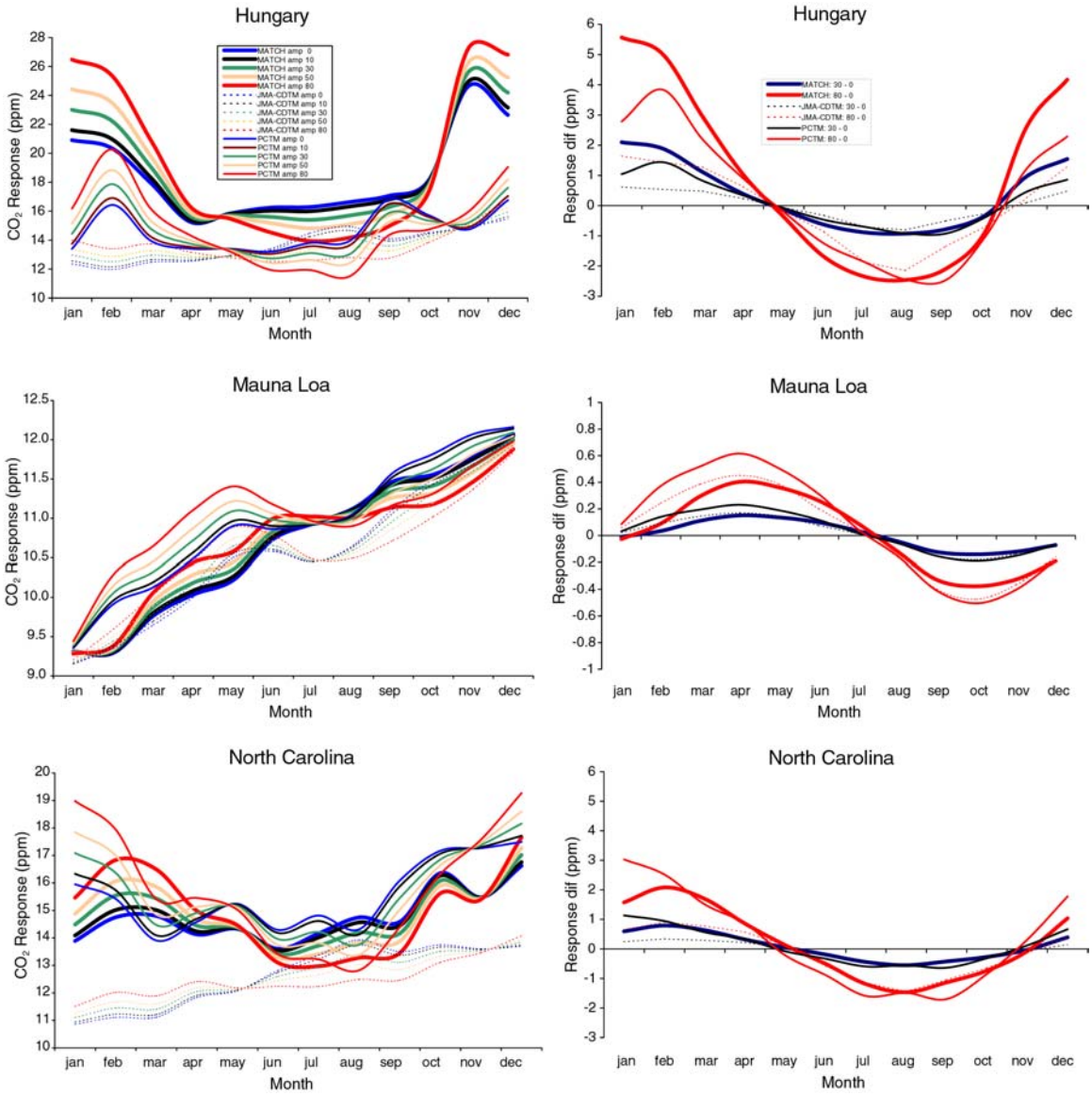

Figure 5.7. a) CO_2 concentration response at three stations reflecting seasonal fossil fuel emissions. Five AFs for each of the three models are shown. b) CO_2 concentration response difference between the 80% AF and the base case and the 30% AF and the base case.

The first item to note is that both the underlying transport and the seasonality of the fossil fuel emissions itself contribute to the total seasonality of the response. The seasonality of the base AF case combined with previous TransCom 3 results suggests that both the MATCH and the PCTM models have less vertical and horizontal mixing in Winter compared to JMA-CDTM. Examination of the 30% versus the base AF cases indicates that the contributions due to the seasonality of mixing and the seasonal emissions are comparable for the MATCH and PCTM models. For the JMA-CDTM model, the emissions seasonality dominates due to the fact that the JMA-CDTM model has little transport seasonality.

Figure 5.7b shows the same three stations but reflects the difference between the base AF case and the 30% and 80% AF cases, respectively. Over the two land-based stations, both MATCH and PCTM respond vigorously to the fossil seasonality while JMA-CDTM shows a much weaker response.

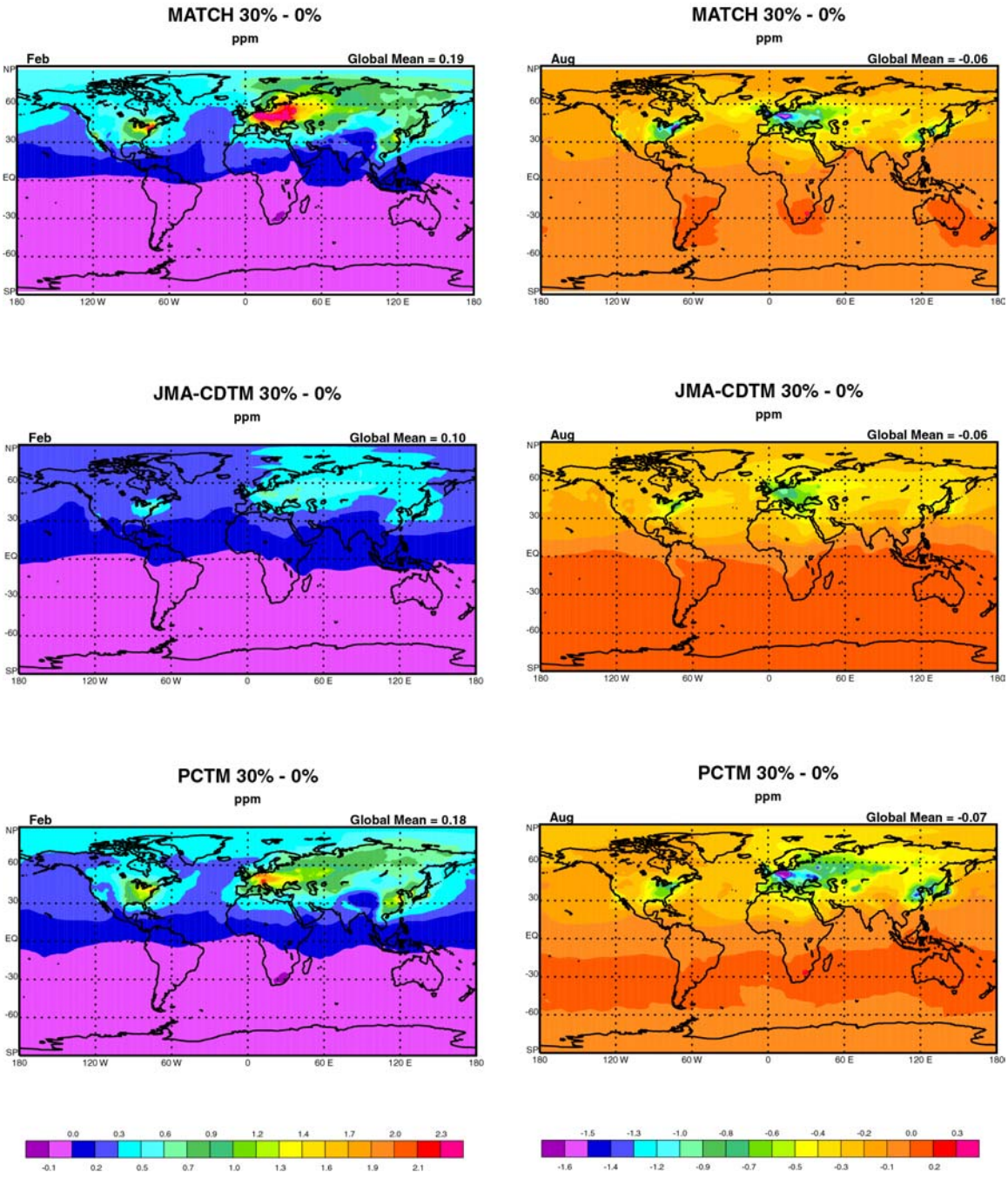

Figure 5.8. Global surface CO_2 concentration response (ppm) for the months of February and August. Maps represent the difference between the 30% and base AF fossil fuel emissions cases.

Figure 5.8 shows similar information but for the entire global surface and for the months of February and August. The MATCH and PCTM models exhibit much greater sensitivity to the seasonal emission at all times of the year than JMA-CDTM. However, MATCH has a much more vigorous response in the Winter compared to PCTM but PCTM appears to have a somewhat more vigorous Summer response, particularly

in Eurasia. This suggests that PCTM is mixing more in the Winter than MATCH but mixing less in the Summer. This may partly explain why PCTM traps non-seasonal fossil to the same extent as MATCH but has a relatively weak rectifier (see figures 5.3a and 5.3b).

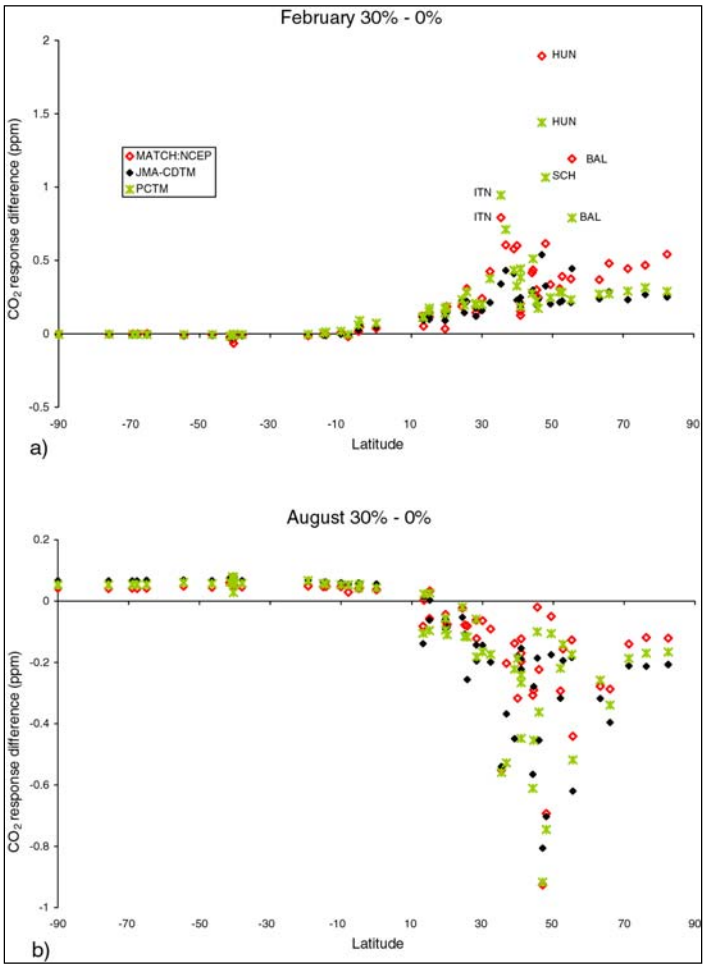

Figure 5.9. CO_2 concentration response difference at all of the observation stations for the month of a) February and b) August. The values represent the difference between the 30% and base AF fossil fuel emissions cases.

Examination of the February and August response relative to the base case at all the stations included in the inversion is shown in Figure 5.9.

Since the station locations are where the observations influence the residual fluxes, these differences will give a good indication of how the regional residual fluxes will likely turn out. In February, the ordering of the response is similar to what is seen in Figure 5.8, MATCH and PCTM respond most vigorously to the seasonal emissions with JMA-CDTM showing a weak response. However, August shows all three models responding similarly to the emissions suggesting that at the stations, summertime mixing is comparable. This is somewhat different from the interpretation one might come away with after looking at figure 5.8. This highlights the importance of examining responses at the stations rather than at every surface model grid cell.

As with the annual mean inversion, all nine fossil fuel emission cases were included in a series of seasonal inversions. Details on the inversion methodology and the construction of the regional response functions can be found in Gurney et al., 2004.

Figure 5.10 shows results for the Temperate North American and European regions for all three of the models and for base, 30% and 80% AF cases. Note that the results are deseasonalized.

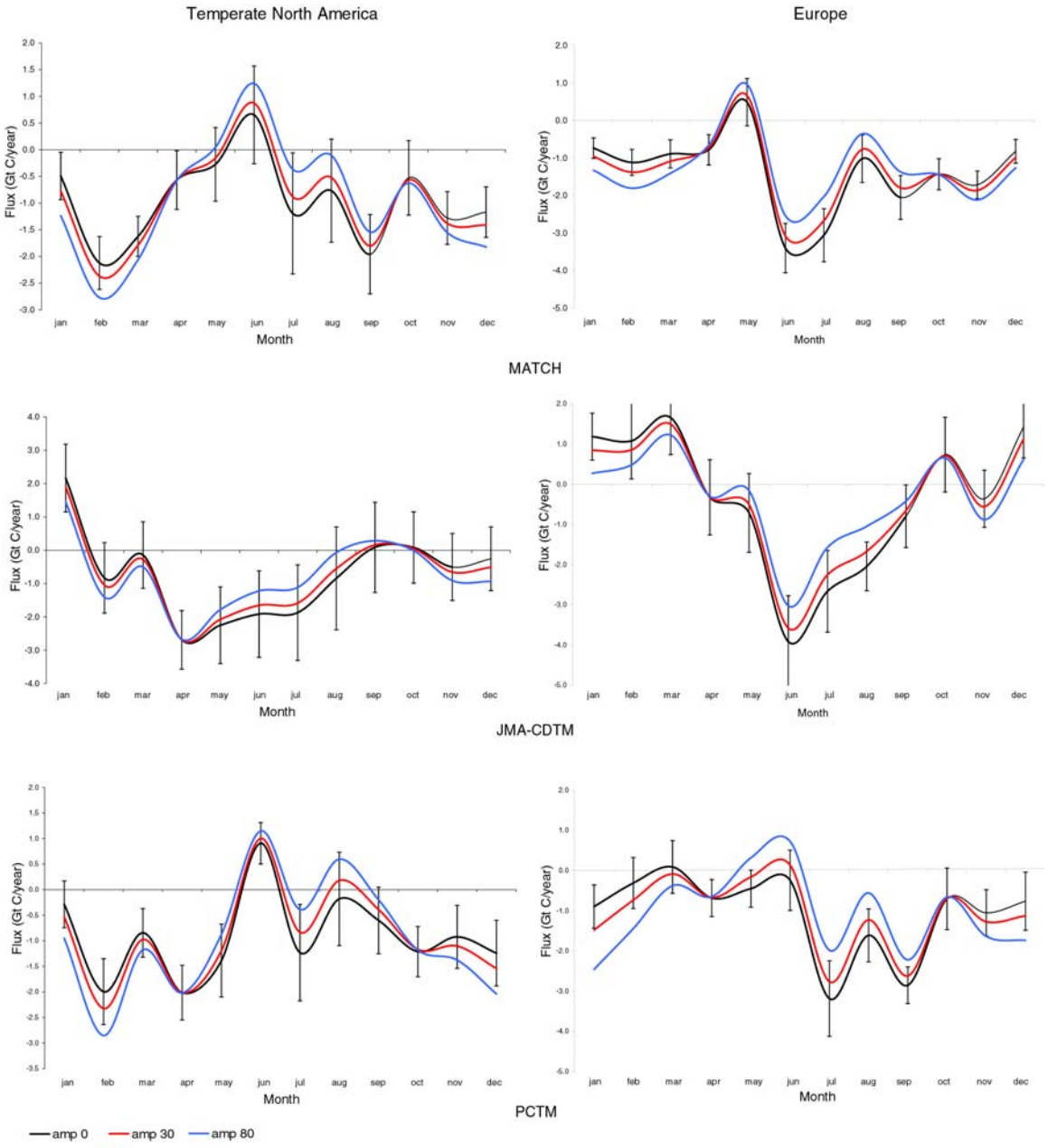

Figure 5.10. Monthly mean inverse flux estimates for the Temperate North American and European land regions. Inverse flux estimates are shown for three fossil fuel AF cases (base, 30%, and 80%) and all three transport models.

Both the MATCH and PCTM models require lessened respiration outside of the growing season while the JMA model requires little adjustment during the Winter months. All models require greater uptake during the growing season in Europe while only JMA requires greater uptake in Temperate North America. Figure 5.11 shows the residual seasonal fluxes for all northern extratropical land regions as the difference between the 30% and base AF cases.

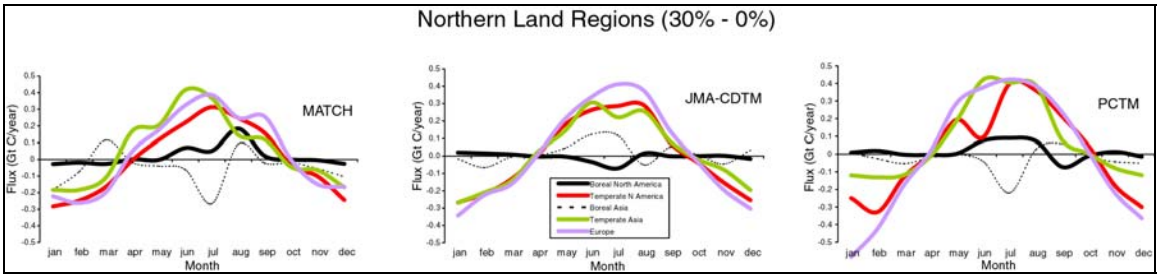

Figure 5.11. Estimated regional fluxes for each month and each model represented as the difference between the 30% and the base AF cases. All northern extratropical regions are shown.

All three models exhibit the same overall behaviour. During the winter months, respiration fluxes are lessened due the greater amount of fossil CO_2 generated during these months near the surface. During the summer months, less uptake is required to counter the lessened fossil fuel CO_2.

What is somewhat surprising is that the seasonal fossil emissions require changes to the northern land fluxes that are of very similar magnitude for all three models. The response differences in figure 5.9 would have suggested that JMA-CDTM would require the smallest flux adjustment as the fossil fuel seasonality increases, particularly in the Winter. The likely explanation for this is the fact that the stations where the response differences are the greatest in figure 5.9, are stations for which the "data uncertainty" is very large and hence, have a proportionately smaller influence on the inversion results. For example, the three stations exhibiting the largest response difference for the MATCH:NCEP model in figure 5.9a are HUN, BAL, and ITN. These stations also have the three largest uncertainty values. If one were to weight the response differences in figure 5.9a by the associated station uncertainty ($1/\sigma^2$), the result would be as shown in figure 5.12.

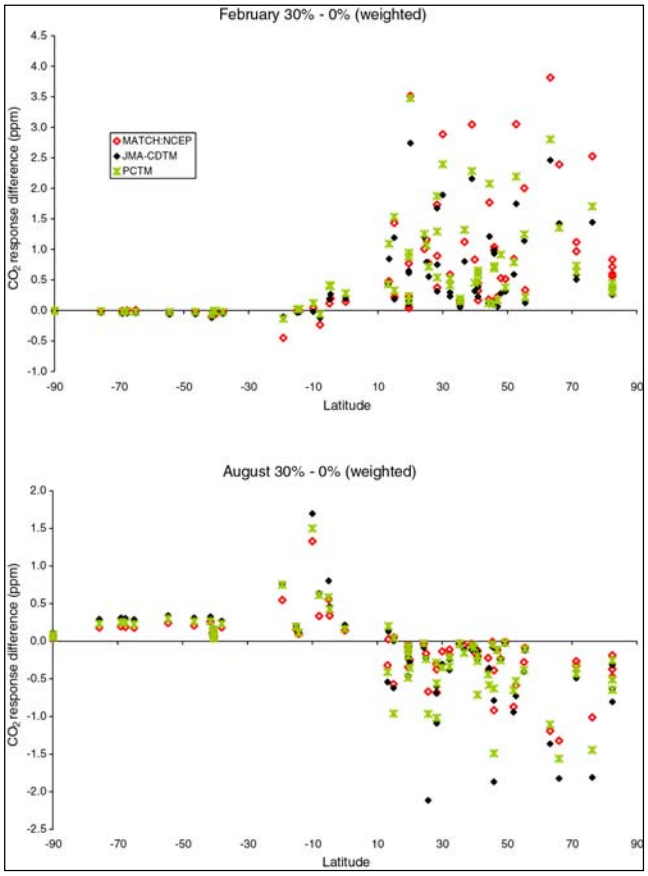

Figure 5.12. As in figure 5.9 except the response values have been weighted by the inverse square of the "data uncertainty".

Unlike the annual mean inversion, fossil fuel seasonality has profound implications for the seasonal inversion. The residual fluxes estimated for the northern extratropical land regions are substantially altered when fossil fuel seasonality is included in the background flux.

The residual fluxes estimated for these land regions are typically interpreted as alterations of regional biosphere exchange, either through land-use change or regional scale fluctuations of temperature or precipitation (Gurney et al., 2003).

As shown in figures 5.10 and 5.11, the potential bias to the residual fluxes caused by the misspecification of the fossil fuel background flux can cause biases of up to 50% at the height of the growing season, seriously undermining previous

interpretation of seasonal inverse results. Clearly, a more accurate portrayal of fossil fuel seasonality is required in order to interpret seasonal atmospheric CO_2 inversions.

5.3.3. Interannual inversion

Methodological details regarding the interannual inversion were discussed in detail in the previous chapter. The important differences to note when comparing the interannual inversion to the seasonal or annual mean inversion relate to the CO_2 observational station network chosen. The annual mean and the seasonal inversion utilized an average of CO_2 observations for the years 1992 to 1996. Given the criteria detailed in Gurney et al., 2002, this led to a network comprised of 75 CO_2 observing stations.

Like the multi-model inversions described in the previous chapter, a number of different networks have been used that span different time periods. The longest time period for which stations meet the TransCom criteria, spans 1980 to 2000. Over this time period, 21 stations qualify as continuously operating. The shortest qualifying network is comprised of 117 stations and spans the 1995 to 2000 time period. These are the networks and time periods that I will examine in conducting the interannual fossil fuel sensitivity experiment.

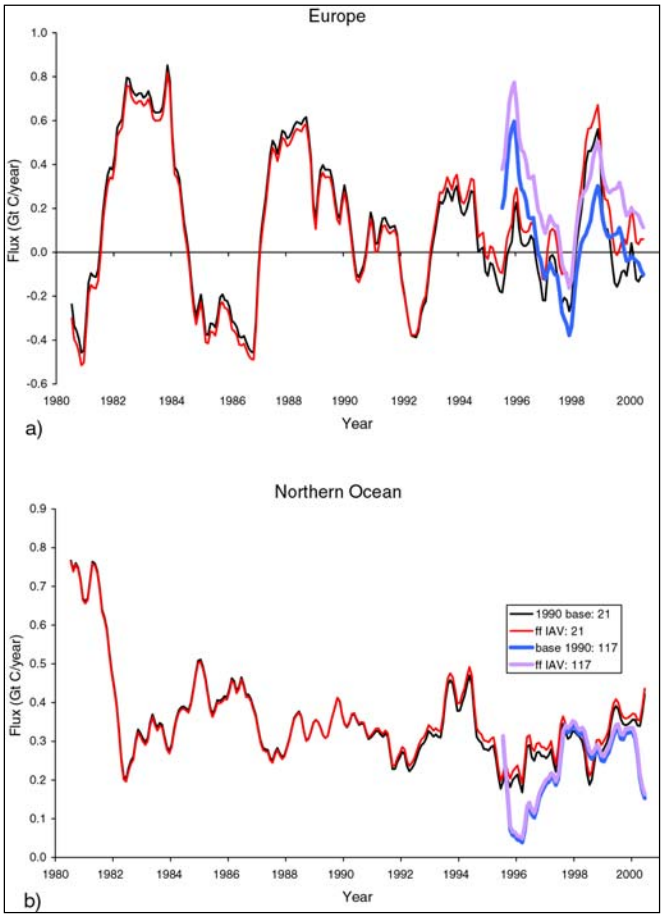

Figure 5.13. The impact of spatiotemporal changes on residual fluxes for two regions. The base interannual inversion results (black) and the perturbed interannual inversion results (red) are shown for the a) European region, and the b) Northern Ocean region. The heavy lines denote the 21 station network while the light lines denote the 117 station network.

Figure 5.13 shows the impact of including large-scale regional shifts in the interannual inversion for the most effected regions. Overall, the interannual variability is little changed owing to the smooth nature of the regional shifts (see figure 5.5). The primary impact is a shift in the long-term mean values.

Both the European and adjacent Northern Ocean region are effected by the shifting fossil fuel spatial pattern. Both the 21 and 117 station networks show an increase in the European residual flux starting in the mid-1990s owing to the fact that the share of European fossil fuel emissions declines (see figure 5.5).

The Northern Ocean region shows a similar feature though the adjustment is less dramatic. This is due to the fact that the model response for the Northern Ocean and the European region are not completely orthogonal. Hence, some of the impact of the changing European fossil fuel emissions are attributed to the Northern Ocean region.

Figure 5.14 shows difference plots for these two regions and the two different stations networks used. As mentioned in the previous chapter, the increasing number of CO_2 observational stations later in the GlobalView database were added primarily in the northern extratropical land regions. This appears to cause a shift in the adjustment between the two regions shown. As the number of European stations increase, the residual flux is more correctly attributed to the European region and less to the Northern ocean region. This is seen by the increase in the difference

flux for the European region utilizing 117 stations and a decrease in the difference flux over the Northern Ocean.

It is important to note that the interannual results influence interpretation of the annual means tested in section 5.3.1. For example, the 1996 to 2000 mean difference for the European region (117 station network) is roughly 0.2 Gt C/year. This represents over a 25% change in the calculated five year average for this region in the last chapter.

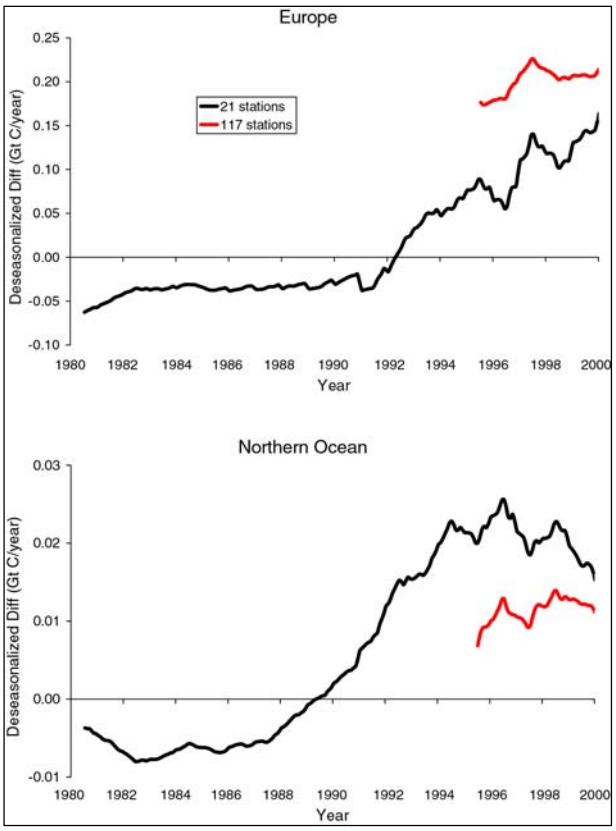

Figure 5.14. The deseasonalized flux difference (Gt C/year) between the base interannual run and the perturbation run for a) Europe and b) the Northern Ocean. Both the 21 and 117 station network results are shown.

5.4 Discussion and Conclusions

Overall, the greatest impact of attempting to simulate more realistic fossil fuel emissions within the TransCom 3 atmospheric CO_2 inversions is on the interpretation of the seasonal fluxes. Recent data of fossil fuel consumption in both the United Stated and Europe indicate that fossil fuel emissions, do indeed, have a seasonal cycle with peak to peak amplitudes that range from 20% to 30%. It is likely that fossil fuel use in the remainder of the industrial and industrializing countries also varies over the year though sub-tropical latitudes may be less likely to exhibit to such variations.

The combination of atmospheric transport trapping the greater fossil fuel emissions in the winter months and the fact that CO_2 observations are primarily at the surface results in significant changes to the estimated regional fluxes that result from atmospheric CO_2 inversions. For the TransCom 3 seasonal inversion, biases of up to 50% at the height of the growing season were found in regions where fossil fuel emissions are a large portion of the surface CO_2 emissions.

This potential bias appears to less dependent upon model transport than first thought. This is primarily due to the fact that the stations near the seasonal fossil source regions are stations that in the TransCom 3 inversion set-up, have large associated data uncertainty. Such stations leverage much less influence on the inverse minimization than those with relatively small data uncertainty. As models are run at higher resolution with analyzed winds (and therefore able to simulate point locations better) the sensitivity of the residual fluxes to transport differences will likely increase.

A couple of important caveats should be mentioned regarding the hypothesized seasonal fossil fuel emissions. First, real fossil fuel emissions are very likely not as smooth as those hypothesized here. The United States emissions data shown in figure 5.2a exhibit structure not captured by equation 5.2. The phasing may also be somewhat shifted in general and as a function of latitude or region. Finally, the real emissions appear to have an amplitude that exhibits interannual variability in addition to the broad amplitude decline over time.

It is possible that fossil fuel emissions exhibit a diurnal cycle owing to the fact that transportation, lighting, heating and some industrial/commercial processes vary between night and day. This will vary somewhat by latitude but also by longitude. Though purely speculative, this may have an added impact when inversion move to solving for residual fluxes at sub-daily temporal resolution.

Fossil fuel seasonality appears to have little impact on the annual mean inversion. This is consistent with what one might expect from a basic numerical argument. If one considers the Temperate North American region, the peak to peak span of the total biospheric flux is roughly 7 GtC/year. This should be compared to a peak to peak span of roughly 0.5 GtC/year for fossil fuel emissions, assuming a 30% AF. Based on the span of emissions alone, one would not expect significant rectification. However, this comparison of flux extremes represents a regional integral. Given the strong heterogeneity of fossil fuel emissions, one might expect that areas proximal to fossil fuel source regions could have flux spans that rival locations with active biospheric exchange. Were station locations also proximal to these intense fossil fuel emitting locations, fossil fuel rectification may occur and be observed. This is where the results of the annual mean experiment performed here are useful. One important caveat to the annual mean results are the fact that the basis function regions are very large relative to the extent of fossil fuel source regions. Inversions that attempt to resolve basis functions at much finer scales may contain grid cells for which the seasonality of fossil emissions are on par with biospheric exchange.

Annual mean inverse results are sensitive to more realistic fossil fuel emissions insofar as they represent an average of years for which realistic spatiotemporal fossil fuel emissions were not simulated. As demonstrated in section 5.3.3, consideration of the shifting fossil fuel emissions in Europe throughout the 1990s led to a reduction in the 5 year average net uptake of over 25% compared to an inversion run with a fixed fossil fuel spatial pattern.

The year to year variability of residual fluxes in a time dependent inversion appear little affected by the inclusion of realistic shifts in the fossil fuel spatial pattern. An important caveat to this conclusion is the limited way the spatiotemporal changes were accounted for in the current study. Spatiotemporal changes at scales smaller than the large basis function regions of the TransCom 3 project may alter the interannual variability of residual fluxes. This may not only pertain to between country emission shifts but within country shifts.

As atmospheric CO_2 inversions solve for fluxes at smaller and smaller spatial and temporal scales, realistic spatiotemporal fossil fuel emissions are required. Furthermore, the problem of displaced energy consumption and production vis a vis CO_2 emissions will be critical.

Fortunately, there is no need to completely reinvent the wheel. A large community of researchers work on detailed energy production and consumption though the focus is not on CO_2 emissions. Oftentimes, the emphasis is on emissions of other more short-lived but directly hazardous pollutants. However, there is an extremely useful collaboration to be made between the inverse modeling community and the energy modeling community, particularly as the inverse approach further reduces the spatiotemporal scale of their estimated carbon fluxes.

References

Andres, R.J., Marland, G., Fungi, I., & Matthews, E. distribution of carbon dioxide emissions from fossil fuel consumption and cement manufacture, 1950-1990. *Global Biogeochem. Cycles* **10**, 419-429 (1996).

Brenkert, A.L. Carbon dioxide emission estimates from fossil-fuel burning, hydraulic cement production, and gas flaring for 1995 on a one degree grid cell basis, (http://cdiac.esd.ornl.gov/ndps/ndp058a.html), 1998.

Blasing, T.J., C.T. Broniak, and G. Marland,. Preliminary estimates of the annual cycle of fossil fuel emissions from the USA. Carbon Dioxide Information Analysis Center, Oak Ridge National Laboratory, March, 2003.

Blasing, T.J., Broniak, C.T., and Marland, G. Refinements in the spatial and temporal resolultion of fossil-fuel CO_2 emissions data, *Eos Trans. AGU, 83*(47), Fall Meet. Suppl., Abstract GC72B-0212, 2002.

Bousquet, P., P. Peylin, P. Ciais, C. Le Quéré, P. Friedlingstein, and P. Tans, Regional changes in carbon dioxide fluxes of land and oceans since 1980, *Science*, *290*, 1342-1346, 2000.

Denning, A.S., Fung, I.Y. & Randall, D.A. Latitudinal gradient of atmospheric CO_2 due to seasonal exchange with land biota. *Nature* **376**, 240-243 (1995).

Denning, S. *et al.* Three-dimensional transport and concentration of SF_6: A model intercomparison study (Transcom 2). *Tellus* **51B**, 266-297 (1999).

Engelen, R.J., A.S. Denning, and K.R. Gurney, On error estimation in atmospheric CO_2 inversions, *J. Geophys. Res.*, *107*(D22)**,** 4635, doi: 10.1029/2002JD002195, 2002.

Fan, S., M. Gloor, J. Mahlman, S. Pacala, J. Sarmiento, T. Takahashi, and P. Tans, A Large Terrestrial Carbon Sink in North America Implied by Atmospheric and Oceanic Carbon Dioxide Data and Models, *Science*, *282*, 442-446, 1998.

Gregg, J.S. and Andres, R.J. A method for impriving temporal and spatial resolution of carbon dioxide emissions, *Eos Trans. AGU, 84*(46), Fall Meet. Suppl., Abstract B42A-0936, 2003.

Gurney, K., R. Law, P. Rayner, and A.S. Denning, TransCom 3 Experimental Protocol, Department of Atmospheric Science, Colorado State University, USA, Paper No. 707, http://transcom.colostate.edu/TransCom_3/transcom_3.html, 2000.

Gurney, K.R., R.M. Law, A.S. Denning, P.J. Rayner, D. Baker, P. Bousquet, L. Bruhwiler, Y.H. Chen, P. Ciais, S. Fan, I.Y. Fung, M. Gloor, M. Heimann, K. Higuchi, J. John, T. Maki, S. Maksyutov, P. Peylin, M. Prather, B.C. Pak, J. Sarmiento, S. Taguchi, T. Takahashi, C.W. Yuen, Towards robust regional estimates of CO_2 sources and sinks using atmospheric transport models, *Nature, 415*, 626-630, 2002.

Gurney, K.R., R.M. Law, A.S. Denning, P.J. Rayner, D. Baker, P. Bousquet, L. Bruhwiler, Y.H. Chen, P. Ciais, S. Fan, I.Y. Fung, M. Gloor, M. Heimann, K. Higuchi, J. John, T. Kowalczyk, E. Maki, S. Maksyutov, K. Masarie, P. Peylin, M. Prather, B.C. Pak, J. Randerson, J. Sarmiento, S. Taguchi, T. Takahashi, C.W. Yuen, Transcom 3 CO_2 Inversion Intercomparison: 1. Annual mean control results and sensitivity to transport and prior flux information, *Tellus*, *55B***,** 555-579, 2003.

Gurney, K.R., R.M. Law, A.S. Denning, P.J. Rayner, B. Pak, and the TransCom 3 L2 modelers, "Transcom 3 Inversion Intercomparison: Control results for the estimation of seasonal carbon sources and sinks," accepted to *Global Biogeochemical Cycles*, 2003.

Heimann, M., Keeling, C.D., and Fung, I.Y. in *The Changing Carbon Cycle: A Global Analysis* (eds Trabalka, J.R. and Reichle, D.E.) 16-49, Springer, New York, 1986.

Kaminski, T., Rayner P.J., Heimann M. & Enting I.G. On aggregation errors in atmospheric transport inversions. *J. Geophys. Res.*, **106**, 4703-4715 (2001).

Keeling, C.D., Piper, S.C. and Heimann, M. in *Aspects of Climate Variability in the Pacific and Western Americas* (ed. Peterson, D.H.) 305-363, Geophys. Monograph 55, American Geophysical Union, Washington DC, 1989.

Lerner, J. Matthews, E. and Fung, I. Methane emissions from animals: A global high-resolution database, Global Biogeochemical Cycles, 2, 139-156, 1988.

Levin, I, Kromer, B., and Schmidt, M. Regional fossil fuel CO_2 fluxes quantified by atmospheric observations: an approach to verification of the Kyoto Protocol. Paper presented at Sixth International Carbon Dioxide Conference, Sendai, Japan, 62-65, 2001.

Li, Y.-F. McMillan, A., and Scholtz, M.T. Global HCH usage with 1 degrees x 1 degrees longitude/latitude resolution, Environmental Science & Technology, 30, 3523-3533, 1996.

Marland G. and Rotty R.M. Carbon dioxide emissions from fossil fuels: a procedure for estimation and results for 1950-1982, *Tellus*, 36B, 232-261, 1984.

Marland, G. Boden, T.A. and Andres, R.J. Global, Regional, and National Annual CO_2 Emissions from Fossil-Fuel Burning, Cement Production, and Gas Flaring: 1751-2000 (revised August 2003), NDP-030, Oak Ridge, USA, 2003.

Nakicenovic, N., Alcamo, J., Davis, G., de Vries, B., Fenham, J., Gaffin, S. Gregory, K., Grubler, A., Jung, T.-Y., Kram, T., Lebre La Rovere, E., Michaelis, L., Mori, S., Morita, T., Pepper, W., Pitcher, H., Price, L., Riahli, K., Roehrl, A., Rogner, H.-H., Sankovski, A., Schlesinger, M., Shukla, P., Smith, S., Swart, R., van Rooijen, S., Victor, N., Dadi, Z. *Special Report on Emissions Scenarios*, Intergovernmental Panel on Climate Change, Cambridge University Press, Cambridge, UK, 2000.

Peylin, P., D. Baker, J. Sarmiento, P. Ciais, and P. Bousquet, Influence of transport uncertainty on annual mean and seasonal inversions of atmospheric CO_2 data, *J. Geophys. Res.*, *107*(D19), 4385, doi: 10.1029/2001JD000857, 2002.

Randerson, J.T., Thompson, M.V., Conway, T.J., Fung, I.Y. and Field, C.B. 1997. The contribution of terrestrial sources and sinks to trends in the seasonal cycle of atmospheric carbon dioxide. *Global Biogeochem. Cycles,* **11**, 535-560.

Rayner, P. J., I.G. Enting, R.J. Francey, and R.L. Langenfelds, Reconstructing the recent carbon cycle from atmospheric CO_2, $\delta^{13}C$ and O_2/N_2 observations, *Tellus*, *51B*, 213-232, 1999.

Rödenbeck, C. S. Houweling, M. Gloor, and M. Heimann, CO_2 flux history 1982-2001 inferred from atmospheric data using a global inversion of atmospheric transport, , *Atmos. Chem. Phys. Discuss., 3*, 2575-2659, 2003.